SONOCHEMICAL REMEDIATION OF MERCURY FROM CONTAMINATED SEDIMENTS

DISSERTATION

Presented in Partial Fulfillment of the Requirements for the Degree Doctor of Philosophy

in the Graduate School of The Ohio State University

By

Ziqi He, B.S., M.S.

*****

The Ohio State University

2006

Dissertation Committee:

Professor Linda K. Weavers, Advisor

Professor Harold W. Walker

Professor John J. Lenhart

Professor Jerry M. Bigham

Professor Richard T. Sayre

Approved by:

_____

Advisor

Civil Engineering Graduate Program

ABSTRACT

In Ohio, Lake Erie and its bordering watersheds have been contaminated with PCBs, Hg, and other heavy metals. Contaminated sediments, especially Hg-laden sediments, result in fish consumption advisories, which adversely affect sport and commercial fishing industries. Existing remediation options to deal with metal-contaminated sediments such as capping and dredging followed by *ex situ* treatments including washing, thermal extraction and bioremediation have their individual limitations. For example, with capping Hg is not removed and may pose a future risk. *Ex situ* treatments following dredging require costly excavation and treatment are lengthy due to slow and/or irreversible desorption.

In this study, the development of sonochemistry as an alternative remediation technology of Hg contaminated sediments was investigated. Experiments were conducted in model (Al_2O_3 and HgS) and field-contaminated sediments (certified PACS-2 marine sediments from NRC) to fundamentally and mechanistically understand how ultrasound will work with Hg and metal contaminated sediments.

Ultrasound was able to enhance Hg release from model and real sediments. In the Al_2O_3 system doped with Hg(II), ultrasound enhanced initial Hg(II) release at pH 4.0 compared to hydrodynamic mixing suggesting that ultrasound accelerated desorption.

The desorption of Hg(II) by sonication at 2 min was higher than that expected based on the Hg(II) sorption curve indicating that ultrasound altered the chemical equilibrium of Hg(II). With cinnabar (HgS), ultrasonic release of Hg from HgS occurred through oxidizing S into sulfur oxidation products (S_{ox}) including $S_2O_3^{2-}$, SO_3^{2-} and SO_4^{2-}. To validate the ability of ultrasound to release Hg, Hg release from PACS-2 marine sediments was examined and ultrasonic acceleration of Hg release compared to mechanical shaking was also observed.

Experimental factors including sonication power intensity and reaction time were observed to affect Hg desorption. The higher the power intensity of sonication, the higher the desorption of Hg(II). Although ultrasound enhanced initial Hg desorption, decreases in Hg desorption occurred with prolonged sonication. To understand the mechanisms of ultrasonic desorption of Hg, ultrasonic effects on the changes in particle properties were determined for Al_2O_3 and HgS systems. Ultrasound dramatically reduced Al_2O_3 particle size, changed surface morphology and decreased the point of zero charge (PZC). Hg(II) occlusion by aluminum hydroxide re-precipitates was proposed as the primary reason for Hg(II) resorption with longer sonication times. Unlike with Al_2O_3, ultrasound significantly reduced cinnabar particle size and increased surface area, leading to higher Hg(II) adsorption on the HgS surface. In addition, sonication increased the cinnabar surface isoeletric point (IEP), indicating adsorption of Hg(II) and/or mineral phase transformation from cinnabar to metacinnabar. These observations suggested that caution should be taken with the duration of sonication when applying this technology to remediation of sediments to avoid or reduce re-association of desorbed Hg(II) with sediments.

Besides ultrasonic factors, the effects of sediment matrix parameters including pH, chloride, and organic matter were examined. Results showed that low pH conditions and the presence of Cl^- facilitated sonolytic release of Hg(II) from Al_2O_3 in the absence of organic matter, whereas the desorption of humic acid from Al_2O_3 dictated the release of Hg(II). The influence of organic matter was also observed with HgS. Dissolved humic acid enhanced HgS dissolution, released more Hg(II) into aqueous solution, and affected S_{ox} formed by ultrasound due to the synergistic effects of ultrasound and humic acid. In PACS-2 marine sediment, the difference in Hg release between pH 4 and 8 was attributed to the difference of dissolved natural organic matter under the two pH conditions.

Furthermore, the ability of ultrasound to release a series of metals with different binding strengths and water exchange rates was investigated in Al_2O_3 and PACS-2 marine sediment. Results showed that sonication was able to enhance Hg(II), Pb(II), Ni(II) and Cr(III) desorption from Al_2O_3. However, longer sonication times led to a decrease in Hg(II) and Pb(II) desorption while Ni(II) and Cr(III) desorption continued to increase due to differences in their water exchange rates which determine the resorption rates. The release patterns and efficiencies of metals from PACS-2 were different for various metals and at different pH conditions likely due to the differences in their affinity to different sediment compositions, metal speciation and oxidation state, and the effects of organic matter in sediment.

Finally, observing that ultrasound enhanced Hg desorption, the application of ultrasound combined with biomass sorption for the removal of Hg from sediments was investigated. A transgenic *C. reinhardtii* (2AMT-2) expressing a plasmamembrane-anchored metallothionein polymer was tested to quickly uptake Hg(II) from aqueous

phase due to its higher binding capacity and broader pH range than wild type alga. The combined technique of ultrasound and 2AMT-2 was effective to remove Hg from solids and sediments, especially from Al_2O_3 and HgS with no natural organic matter. An implication of the results is that the application of ultrasound combined with biomass (transgenic *C. reinhardtii*) has the potential for *in-situ* Hg removal from contaminated sediments or *ex-situ* Hg removal from dredged sediments under certain conditions.

Dedicated to my parents,
my wife Lan,
and my daughter Amber

ACKNOWLEDGMENTS

First of all, I would like to express my sincere gratitude to my advisor, Dr. Linda K. Weavers, for her understanding, encouragement, guidance and surport during my study and research. Especially, she gave me the opportunity to work on a new remediation technology, many great ideas during my research, and invaluable suggestions in course work. I have benefited from her as how to be a good researcher and instructor. I also thank her for precious advice and help in my career pursuit.

I would like to acknowledge Dr. Harold W. Walker, Dr. John J. Lenhart, Dr. Jerry M. Bigham, Dr. Patrick G. Hatcher and Dr. Richard T. Sayre for serving as my committee in my candidate exam and final defense and for their valuable comments and suggestions. Thanks are also given to Dr. Yu-ping Chin and Dr. Samuel J. Traina for their help in my research and manuscripts.

Special thanks are given to Dr. Jerry M. Bigham and Sandy Jones for the wonderful course, SS750 Soil Mineralogy, and the flexibility and help in using freeze drying, XRD, carbon content, and EGME and BET surface analyses. I thank Dr. Danold Golightly for help in ICP-OES measurements and understanding lab rules and his availability to answer all kinds of questions. Thanks are also due to Ashish Deshmukh and William C. Hockaday for their help in NMR measuremnt and spectra analysis, Dr.

Yu-ping Chin for the help in HPSEC operation, Dr. Berry Lyons for discussion and reference on Hg sediment sampling, Sreenivas Bhattiprolu for the help with SEM measurements, Lisa Hommel for XPS scan and spectra analysis, Dr. Prabir K. Dutta and Pamatha Payra for the use of untracentrifuge, Douglus Beak and Dr. Libby Dayton and Shane Whitacre for using microwave digestion, Zoee Gokhale and Dr. Richard Sayre's current group for the help with algae inoculation and Yu Sik Hwang for FTIR analysis.

Many thanks to former and current labmates: Mustafa Bob, Aaron Frim, Mikko Lamminen, Panuwat Taerakul, Jason Cheng, Dong Chen, Ping Sun, Liang-Hiong Chia, Limei Yang, Eric Onderak, Xueming Tang, June Ju Lee, Yusik Hwang, Yaning Yang, Maggie Pee, Laura Jacobs, Vibhash Vaidya, Sindhu Tatimatla, Dawn Deojay, Mike Scullion, and Krishnakumar Raman for their friendship and the wonderful time we had together in lab and office and GROUP MEETING. Specifically, I am thankful to Dong Chen for the good work in our collaborated DOM study and understanding during difficult times, Panuwat Taerakul for teaching me how to operate CVAAS and Jason Cheng for his help with Autotitrator and IC operation and maintenance. Thanks are also given to undergraduate students, Erin Lamb and Douglas J Schaffer, for working on my project and helping me with my English.

This study was supported by NOAA/Ohio Sea Grant College Program and the NSF Environmental Molecular Science Institute (EMSI) at The Ohio State University.

Last but not least, I would like to dedicate this work to my parents, brother and sisters for their unconditional support and understanding. Special thanks to my wife, Lan, for her love, support, encouragements and accompany. Thank my daughter, Amber, for cheering me up when I am not in a good mood.

VITA

August 14, 1974 …… Born – LinYi, China

1998 …… B.S., Water Supply and Sewer Engineering, Xi'an University of Architecture and Technology, China

2001 …….....… M.S., Environmental Engineering, Xi'an University of Architecture and Technology, China

2001 – Present ……. Graduate Research Associate, The Ohio State University

PUBLICATIONS

Research Publication

1. Z. He, S. J. Traina, J. M. Bigham, and L. K. Weavers. Sonolytic desorption of mercury from aluminum oxide. *Environmental Science & Technology,* 2005, *39(4)*, 1037-1044.

2. D. Chen, Z. He, L. K. Weavers, Y. Chin, H. W. Walker, and P. G. Hatcher. Sonochemical reaction of dissolved organic matter. *Research on Chemical Intermediates*, 2004, *30(7/8)*, 735-753.

3. J. Wang, X. Wang, and Z. He. Characteristics of membrane fouling by turbidity and humic substances. *Mo Kexue Yu Jishu.* 2002, *22(1)*, 24-28.

FIELDS OF STUDY

Major Field: Civil Engineering

TABLE OF CONTENTS

Page

ABSTRACT ii

DEDICATION ..... ……vi

ACKNOWLEDGMENTS vii

VITA ix

LIST OF TABLES xvi

LIST OF FIGURES xviiii

CHAPTERS

1. INTRODUCTION AND BACKGROUND 1

1.1 Mercury Sources and Contaminated Sediment 1

1.2 Mercury in Aquatic Systems 2

1.3 Sediment Control Technologies 9

1.3.1 In Situ Capping 9

1.3.2 Dredging Followed by ex situ Treatment 10

1.4 Ultrasound and Its Application 13

1.4.1 Cavitation and Thermal and Chemical Effects 13

1.4.2 Physical and Mechanical Effects 16

1.4.3 Application of Ultrasound in Environmental Remediation 17

1.5 Transgenic *Chlamydomonas reinhardtii* 19

1.6 Objectives and organization of the dissertation 20

2. SONOLYTIC DESORPTION OF MERCURY FROM ALUMINUM OXIDE 25

2.1 Abstract 25

2.2 Introduction 26

2.3 Materials and Methods 29

2.3.1 Materials 29

2.3.2 Sorption and sample preparation 30

2.3.3 Desorption 30

2.3.4 Measurement and characterization 32

2.4 Results and Discussion 33

2.4.1 Sonication effects on the desorption of Hg(II) 33

2.4.2 Sonication effects on alumina particles 36

2.4.3 Mechanism for reduced Hg(II) desorption 41

3. SONOLYTIC DESORPTION OF MERCURY FROM ALUMINUM OXIDE: EFFECTS OF pH, CHLORIDE AND ORGANIC MATTER 52

3.1 Abstract 52

3.2 Introduction 53

3.3 Materials and Methods 55

3.3.1 Materials 55

3.3.2 Experimental procedure and analyses 56

3.4 Results and Discussion 57

3.4.1 Hg(II) adsorption curves 57

3.4.2 The effect of pH on the desorption of Hg(II) 60

3.4.3 The effect of chloride on the desorption of Hg(II) 62

3.4.4 The effect of organic matter on the desorption of Hg(II) 63

4. RELEASE OF MERCURY FROM CINNABAR (α-HgS) BY SONOCHEMICAL DISSOLUTION 73

4.1 Abstract 73

4.2 Introduction 74

4.3 Experimental Section 76

4.3.1 Materials and Procedure 76

4.3.2 Analyses and characterization 78

4.4 Results and Discussion 78

4.4.1 Sonochemical dissolution of cinnabar based on S_{ox} products 78

4.4.2 Ultrasonic release of mercury 83

4.4.3 Ultrasonic effects on cinnabar particles 84

4.4.4 Effects of humic acid 86

5. SONOLYTIC RELEASE OF METALS (Hg, Pb, Ni, Cr) FROM ALUMINUM OXIDE AND MARINE SEDIMENT 95

5.1 Abstract 95

5.2 Introduction 96

5.3 Experimental Section 98

5.3.1 Materials 98

5.3.2 Experimental procedures 98

5.4 Results and Discussion 101

5.4.1 Sonolytic desorption of metals from Al_2O_3 101

5.4.2 Sonolytic release of metals from PACS-2 marine sediment..... 105

6. REMOVAL OF MERCURY FROM SEDIMENT BY ULTRASOUND COMBINED WITH BIOMASS (TRANSGENIC CHLAMYDOMONAS REINHARDTII) 120

6.1 Abstract 120

6.2 Introduction 121

6.3 Materials and Methods 123

6.3.1 Algae cell growth and harvest..... 123

6.3.2 Hg(II) binding to algal cells 124

6.3.3 Experimental procedures 124

6.3.4 Analyses 126

6.4 Results and Discussion 126

6.4.1 Binding of aqueous Hg(II) to algal cells 126

6.4.2 Removal of Hg(II) from Al_2O_3 and HgS by ultrasound combined with 2AMT-2..... 128

6.4.3 Removal of Hg from PACS-2 marine sediment by ultrasound combined with 2AMT-2 132

7. CONCLUSIONS AND FUTURE WORK..... 142

7.1 Conclusions 142

7.2 Future Studies 146

APPENDIX

A. SONOCHEMICAL REACTIONS OF DISSOLVED ORGANIC MATTER 149

A.1 Abstract..... 149

A.2 Introduction 150

A.3 Methodology 152

A.3.1 Preparation of DOM 152

A.3.2 Ultrasonic Units 152

A.3.3 Experimental Conditions 153

A.3.4 Sample Analysis 154

A.4 Results 155

A.4.1 Initial Characterization of Aldrich and Pahokee Peat DOM 155

A.4.2 TOC Reduction of DOM 157

A.4.3 Changes in $Color_{465}$ 157

A.4.4 SUVA Changes to DOM 158

A.4.5 ^{13}C NMR Changes to DOM 158

A.4.6 Molecular Weight Changes to DOM 159

A.4.7 Total Acidity Measurement of DOM 161

A.5 Discussion 161

A.5.1 Ultrasonic Factors Affecting Sonochemical Reactions of DOM 161

A.5.2 Alterations to DOM through Sonication 164

A.5.3 Implications for Use of Sonolysis in Environmental Applications 166

BIBLIOGRAPHY 186

LIST OF TABLES

Table Page

Table2.1 Surface Area (SA)† under 36 W cm^{-2} Sonication 44

Table 4.1 Dissolution rates of cinnabar based on S_{ox} production within 3 hr sonication . 89

Table 4.2 •OH and SO_4^{2-} production rates within 1 hr sonication 90

Table 5.1 Metal water exchange rate constants 110

Table A. 1 Comparison of the initial characteristics of Aldrich and Pahokee peat DOM. 169

Table A. 2 Comparison of the aromaticity of DOM as a result of sonication. 170

Table A. 3 Molecular weight of DOM before and after 4 hours of sonication..... 171

Table A. 4 Acidity of DOM before and after 4 hours of sonication. 172

LIST OF FIGURES

Figure Page

Figure 1.1 Mercury cycle in aquatic ecosystems 23

Figure 1.2 Three reaction zones in cavitation process 24

Figure 2.1 Desorption of Hg(II) from alumina particles (pH = 4.0, T = 20 °C, I = 0.1M, [particle] = 33 g L^{-1}, $[Hg(II)]_{initial\ on\ particle}$ = 5.0 μmol g^{-1}, D_0 = 110 μm). Figure inset: pH dependent Hg(II) sorption curve. 45

Figure 2.2 Hg(II) distribution with 36 W cm^{-2} sonication. Hg desorbed into the aqueous phase and remaining on the solid phase with sonication time were measured independently. The mass balance was determined by $Hg(II)_{mass\ balance} = Hg(II)_{in\ aqueous\ phase} + Hg(II)_{in\ solid\ phase}$. 46

Figure 2.3 Particle size distribution with time by ultrasound (pH = 4.0, T = 20 °C, I = 0.1 M, [particle] = 33 g L^{-1}, sonication power 36 W cm^{-2}, D_0 = 110 μm). 47

Figure 2.4 SEM images of particle morphology (a) before sonication, (b) after 60 min sonication at power 36 W cm^{-2}. 48

Figure 2.5 Aluminum concentration in supernatant with sonication and hydrodynamic mixing (pH = 4.0, I = 0.1 M, [particle] = 33 g L^{-1}, sonication power 36 W cm^{-2}). .. 49

Figure 2.6 XPS spectra of Hg 4f before and after 60 min sonication (pH = 4.0, T = 20 °C, I = 0.1 M, [particle] = 33 g L^{-1}, $[Hg(II)]_{initial\ on\ particle}$ = 5.0 μmol g^{-1}, sonication power 36 W cm^{-2}). 50

Figure 2.7 Desorption of Hg(II) from pre-sonicated alumina particles (pH = 4.0, I = 0.1M, [particle] = 33 g L^{-1}, $[Hg(II)]_{initial\ on\ particle}$ = 5.0 μmol g^{-1}, D_0 = 5 μm). 51

Figure 3.1 Hg(II) adsorption to alumina particles in the absence and presence of chloride or humic acid (I = 0.1 M, $[Hg(II)]_0$ = 0.75 mM, $[Cl^-]_0$ = 1.5 mM, $[HA]_0$ = 900 mg L^{-1}, [particle] = 133 g L^{-1}, 24 hr equilibrium). 67

Figure 3.2 Humic acid adsorption to alumina particles (I = 0.1 M, $[Hg(II)]_0$ = 0.75 mM, $[HA]_0$ = 900 mg L^{-1}, [particle] = 133 g L^{-1}, 24 hr equilibrium). 68

Figure 3.3 Desorption of Hg(II) from alumina particles (pH = 4.0, T = 20 °C, I = 0.1 M, [particle] = 33 g L^{-1}, $[Hg(II)]_{initial\ on\ particle}$ = 5.0 μmol g^{-1}, sonication intensity 36 W cm^{-2}). 69

Figure 3.4 Desorption of Hg(II) from alumina particles in the presence of chloride (pH = 4.0, T = 20 °C, I = 0.1 M, $[Cl^-]_0$ = 1.5 mM, [particle] = 33 g L^{-1}, $[Hg(II)]_{initial\ on\ particle}$ = 5.0 μmol g^{-1}, sonication intensity 36 W cm^{-2}). 70

Figure 3.5 The desorption of Hg(II) from alumina particles laden with humic acid (pH = 8.0, T = 20 °C, I = 0.1 M, [particle] = 33 g L^{-1}, $[Hg(II)]_{initial\ on\ particle}$ = 5.0 μmol g^{-1}, $[HA]_{initial\ on\ particle}$ = 5.5 mg C g^{-1}, sonication intensity 36 W cm^{-2}). 71

Figure 3.6 The desorption of humic acid from alumina particles (pH = 8.0, T = 20 °C, I = 0.1 M, [particle] = 33 g L^{-1}, $[Hg(II)]_{initial\ on\ particle}$ = 5.0 μmol g^{-1}, $[HA]_{initial\ on\ particle}$ = 5.5 mg C g^{-1}, sonication intensity 36 W cm^{-2}). 72

Figure 4.1 S_{ox} produced during sonication at three cinnabar concentrations (pH = 4.0, T = 20 °C, I = 0.01 M, sonication intensity 18 W cm^{-2}). Figure inset: dissolved Hg(II) formed during sonication at three cinnabar concentrations. 91

Figure 4.2 Cinnabar surface area during sonication (pH = 4.0, T = 20 °C, I = 0.01 M, [cinnabar] = 1.67 g L^{-1}, sonication intensity 18 W cm^{-2}). Figure inset: Hg(II) adsorbed on cinnabar (a) normalized Hg(II) content equivalent to S_{ox} based on initial surface area, (b) maximum Hg(II) adsorption capacity (7.5 μM m^{-2}), (c) normalized Hg(II) content equivalent to S_{ox} correcting for surface area increases. 92

Figure 4.3 SEM images (a) before sonication, (b) after 3 hr sonication (pH = 4.0, T = 20 °C, I = 0.01 M, [cinnabar] = 1.67 g L^{-1}, sonication intensity 18 W cm^{-2}). 93

Figure 4.4 Dissolved Hg(II) formed (a) and S_{ox} produced (b) in the presence of humic acid (pH = 4.0, T = 20 °C, I = 0.01 M, [cinnabar] = 1.67 g L^{-1}, [HA] = 8.5 mg C L^{-1}, sonication intensity 18 W cm^{-2}). 94

Figure 5.1 Desorption of Hg(II) from alumina particles (pH = 4.0, T = 20 °C, I = 0.1 M, [particle] = 33 g L^{-1}, $[Hg(II)]_{initial\ on\ particle}$ = 5.0 μmol g^{-1}, sonication intensity = 36 W cm^{-2}). Figure inset: pH dependent Hg(II) sorption curve. 111

Figure 5.2 Desorption of Pb(II) from alumina particles (pH = 3.0, T = 20 °C, I = 0.1 M, [particle] = 33 g L^{-1}, $[Pb(II)]_{initial\ on\ particle}$ = 30 μmol g^{-1}, sonication intensity = 36 W cm^{-2}). Figure inset: pH dependent Pb(II) sorption curve. 112

Figure 5.3 Desorption of Ni(II) from alumina particles (pH = 4.0, T = 20 °C, I = 0.1 M, [particle] = 33 g L^{-1}, $[Ni(II)]_{initial\ on\ particle}$ = 8.6 μmol g^{-1}, sonication intensity = 36 W cm^{-2}). Figure inset: pH dependent Ni(II) sorption curve. 113

Figure 5.4 Desorption of Cr(III) from alumina particles (pH = 3.0, T = 20 °C, I = 0.1 M, [particle] = 33 g L^{-1}, $[Hg(II)]_{initial\ on\ particle}$ = 50 μmol g^{-1}, sonication intensity = 36 W cm^{-2}). Figure inset: pH dependent Cr(III) sorption curve. 114

Figure 5.5 Release of Hg from PACS-2 marine sediment (T = 20 °C, I = 0.1 M $NaNO_3$, [particle] = 33 g L^{-1}, $[Hg]_{certified}$ = 3.04 ± 0.20 mg kg^{-1}, sonication intensity 36 W cm^{-2}). 115

Figure 5.6 Release of Pb from PACS-2 marine sediment (T = 20 °C, I = 0.1 M $NaNO_3$, [particle] = 33 g L^{-1}, $[Pb]_{certified}$ = 183 ± 8 mg kg^{-1}, sonication intensity 36 W cm^{-2}). 116

Figure 5.7 Release of Ni from PACS-2 marine sediment (T = 20 °C, I = 0.1 M $NaNO_3$, [particle] = 33 g L^{-1}, $[Ni]_{certified}$ = 39.5 ± 2.3 mg kg^{-1}, sonication intensity 36 W cm^{-2}). 117

Figure 5.8 Release of Cr from PACS-2 marine sediment (T = 20 °C, I = 0.1 M $NaNO_3$, [particle] = 33 g L^{-1}, $[Cr]_{certified}$ = 90.7 ± 4.6 mg kg^{-1}, sonication intensity 36 W cm^{-2}). 118

Figure 5.9 Dissolved organic matter released from PACS-2 marine sediment (T = 20 °C, I = 0.1 M $NaNO_3$, [particle] = 33 g L^{-1}, sonication intensity 36 W cm^{-2})..... 119

Figure 6.1 Binding of Hg(II) to transgenic (2AMT-2) and wild type (CC2137) of *C. reinhardtii* cells (pH = 6.0, I = 0.01 M $NaNO_3$, 1 mL of 5.0 A_{750nm} of cells in 30 mL solution with various Hg concentrations after sorption for 136

Figure 6.2 Hg(II) uptake kinetics by 2AMT-2 cells (pH = 6.0, I = 0.01 M $NaNO_3$, 1 mL of 6.4 A_{750nm} of cells in 30 mL with initial 1.33 μM Hg solution) 137

Figure 6.3 Removal of Hg(II) from Al_2O_3 with time (pH = 5.0, T = 20 °C, I = 0.01 M $NaNO_3$, [particle] = 16.7g L^{-1}, $[Hg(II)]_{initial\ on\ particle}$ = 5.0 μmol g^{-1}, 4 ml of 200 A_{750nm} of transgenic cells, sonication intensity 20 W cm^{-2})..... 138

Figure 6.4 Release of Hg(II) from cinnabar by ultrasound and 2AMT-2 cells (pH = 4.0, T = 20 °C, I = 0.01 M $NaNO_3$, [cinnabar] = 0.0333 g L^{-1}, 4 ml of 200 A_{750nm} of transgenic cells, sonication intensity 20 W cm^{-2}, measured Hg(II) on algal cells by digestion was calculated as dissolved Hg(II)). 139

Figure 6.5 Removal of Hg from PACS-2 marine sediment with time (T = 20 °C, I = 0.01 M $NaNO_3$, [particle] = 8.3 g L^{-1}, $[Hg]_{certified}$ = 3.04 ± 0.20 mg kg^{-1}, 4 ml of 200 A_{750nm} of transgenic cells, sonication intensity 20 W cm^{-2})..... 140

Figure 6.6 Dissolved organic matter released from PACS-2 marine sediment by sonication (T = 20 °C, I = 0.01 M $NaNO_3$, [particle] = 8.3 g L^{-1}, $[Hg]_{certified}$ = 3.04 ± 0.20 mg kg^{-1}, sonication intensity 20 W cm^{-2})..... 141

Figure A.1 TOC reduction of Aldrich DOM with sonication under different ultrasonic frequencies and energy densities. 173

Figure A.2 TOC reduction of Pahokee peat DOM with sonication under different ultrasonic frequencies and energy densities..... 174

Figure A.3 $Color_{465}$ loss of Aldrich DOM with sonication under different ultrasonic frequencies and energy densities. 175

Figure A.4 $Color_{465}$ loss of Pahokee peat DOM with sonication under different ultrasonic frequencies and energy densities. 176

Figure A.5 SUVA at 254 nm decrease of Aldrich DOM with sonication under different ultrasonic frequencies and energy densities..... 177

Figure A.6 SUVA at 254 nm decrease of Pahokee peat DOM with sonication under different ultrasonic frequencies and energy densities..... 178

Figure A.7 SUVA at 280 nm of Aldrich DOM decrease with sonication under different ultrasonic frequencies and energy densities. 179

Figure A.8 SUVA at 280 nm decrease of Pahokee peat DOM with sonication under different ultrasonic frequencies and energy densities. 180

Figure A.9 ^{13}C NMR spectra of Aldrich DOM before and after 4 hours of sonication. Y-axis represents relatively intensity. 181

Figure A.10 ^{13}C NMR spectra of Pahokee peat DOM before and after 4 hours of sonication. Y-axis represents relatively intensity. 182

Figure A.11 HPSEC spectra of Aldrich DOM before and after 4 hours of sonication... 183

Figure A.12 HPSEC spectra of Pahokee peat DOM before and after 4 hours of sonication. 184

Figure A.13 The formation of H_2O_2 with sonication under different ultrasonic frequencies and energy densities. 185

CHAPTER 1

INTRODUCTION AND BACKGROUND

1.1 Mercury Sources and Contaminated Sediment

Mercury, as a pervasive and highly toxic pollutant that accumulates in organisms, is one of the most intriguing global environmental pollution concerns. As a result, it is probably the most studied of all trace elements in the environment. Since the last decade of the 20th century, environmental scientists, legislators, and the public have become aware of mercury pollution in the global environment.

Natural mercury sources include: (1) degassing from mercury mineral deposits and the oceans, (2) volcanic emissions, and (3) forest fires (*1,2,3*). The anthropogenic sources of mercury mostly result from: (1) solid waste (e.g. batteries, thermometers), (2) coal and oil combustion, (3) metallurgical processes (iron, lead, and zinc), (4) production of mercury and gold, and (5) degassing from mercury contaminated aquatic and terrestrial systems (through reduction of Hg(II) to Hg(0)) (*4,5,6*). Anthropogenic mercury sources account for 10-30% of the annual mercury emission (*4*) and have been estimated to triple the concentration of Hg in the atmosphere during the last century (*7*). The majority (95%) of mercury enters the atmosphere as Hg(0), which is oxidized primarily

by O_3 to divalent Hg(II) via gas phase reactions. Once oxidized, Hg(II) will precipitate and deposit in surface terrestrial and aquatic systems.

Anthropogenic point sources and atmospheric deposition have posed serious problems for aquatic systems. USEPA reported that in Ohio, Lake Erie and bordering watersheds have received serious sediment contamination and are contaminated with polychlorinated biphenyls (PCBs), mercury, and other heavy metals (*8*), resulting in fish consumption advisories, which adversely affect sport and commercial fishing industries.

The ecological and toxicological effects of mercury are strongly dependent on the chemical species present. Besides elemental mercury, Hg(0), the major forms of mercury found in the environment are ionic mercury Hg(II) and organic mercury, particularly methylmercury. Among them, methylmercury, which affects the central nervous system, is the most toxic and bioaccumulative form and has been banned as a pollutant since the 1970s. Methylmercury predominately occurs in the environment by methylation of divalent inorganic Hg(II) in aqueous systems through biotic processes mediated by sulfate-reducing bacteria (*4*).

1.2 Mercury in Aquatic Systems

As shown in Figure 1.1, mercury may undergo several different biogeochemical processes in aquatic systems including (*9*): volatilization/deposition at the water-air interface driven by oxidation/reduction reactions, sedimentation/resuspension through adsorption/desorption and precipitation/dissolution, methylation/demethylation, and bioaccumulation and biomagnification (*4,10,11,12*).

Deposition/volatilization

Atmospheric Hg(II) deposition and runoff are the major pathways for Hg to enter aquatic systems. The main loss mechanism of Hg in aquatic systems is volatilization or gas evasion through reduction reactions (*13*). Reduction of Hg(II) to Hg(0) may occur through bacterial action and photoreduction, with the bacterial route predominant in high Hg waters. Some bacteria contain a series of genes known as the *mer* operon, directing the bacteria to produce an enzyme called merA, which converts Hg(II) to Hg(0). In the low picomolar Hg concentrations, reduction of Hg(II) seems to be affected chiefly by photochemical processes with three possible mechanisms: (i) direct photoreduction of Hg(II); (ii) photoreduction of Fe, Mn, or humic acids which further reduces Hg(II) and (iii) photocatalysis of bacterial reduction of Hg(II). However, it has been known that all these processes are affected by the presence of Hg complexing ligands especially DOC and chloride.

Sedimentation/resuspension

In most aquatic systems, the net Hg deposition is greater than volatilization. The majority of aquatic Hg is exported to the sediments through adsorption or sedimentation. Partition coefficients have been calculated for the relative affinity of Hg(II) and methylmercury for sediment over water on the order of 100,000 ml/g sediment (*14*), indicating a strong preference for Hg(II) and methylmercury to remain bound to bottom sediment. About 98% of Hg added to the bulk water of an aquatic system was associated with sediments at pH = 4.0 to 4.5 (*4*). Binding to organic matter and inorganic components such as sulfides and metal oxides, and precipitation as HgS are the main

mechanisms for Hg in sediments. This stored Hg in sediment can serve as an important mercury reservoir with sediment-bound mercury resuspending back into the aquatic ecosystem, influencing Hg bioaccumulation and mobility. More details are discussed in the following section on factors affecting Hg behavior in aquatic systems.

Methylation/demethylation

Methylation is a key step in the entrance of mercury into the food chain. Methylation of Hg – the transfer of Hg(II) to methylHg, requires the formation of an alkyl anion group, CH_3^-, a strong base highly unstable in water. Thus, methylation reactions are either the result of microbial activities or photochemical processes. Sulfate-reducing bacteria have been reported to be the dominant role of Hg methylation (*4,15*). It is possible that photochemical reactions involving organic matter such as acetate and humic acids may lead to the formation of methylHg (*13*). Demethylation of organic Hg is an important process taking place in natural waters through biological and photochemical route as well (*13,16*). Nonetheless, a balance of methylation and demethylation is important in maintaining methylHg levels in aquatic systems which determine Hg bioaccumulation and magnification in food chain.

Bioaccumulation and biomagnification

Although microorganisms can uptake all Hg species from both aqueous phase and sediment, the methylHg to total Hg ratios in organisms are much greater than the ratios in aquatic systems, indicating that methylHg is the most bioaccumulative Hg species. Using ^{203}Hg isotope, Wang et al. (*17*) have found that methylHg has faster uptake and higher

bioaccumulation to polychaete than inorganic Hg(II). This is due to the lipid solubility of methylHg and its permeability through cellular membrane of microorganisms (*13*). In fact, the high ratio of methylHg in organisms is attributed to its effective bioaccumulation. Hg(II) diffuses out of organisms readily as it diffuses into phyto- or bacterio-pico-plankton, while methylHg is efficiently retained by microorganisms (*13*). Due to its bioaccumulation, methylHg transfers from low level microorganisms to top level predators, magnifying methylHg in higher levels of the food chain. Bioaccumulation and biomagnifications of Hg result in adversely affects of fish consumption and human health.

In general, all the biogeochemical processes in aquatic systems are dependent on a variety of environmental variables including pH, organic matter, chloride, sulfide, redox conditions, and components of sediment. For example, decrease in pH may stimulate methylHg production at the sediment/water interface. High contents of organic carbon and sulfur in sediment can reduce mercury bioavailability. DOC and chloride have been proved to influence Hg sorption, methylation, bioaccumulation, and redox reactions in aqueous phase (*2*). The environmental factors affecting the behavior of Hg in aquatic systems (*2,4,13,16,18*) as listed below.

Organic Matter

As one of the most important components of sediments, natural organic matter (NOM) is a significant factor affecting Hg speciation and fate. It has been estimated that organic matter can bind up to 95% of the Hg(II) in rivers and lakes (*11*). The responsible

functional groups for Hg binding are reduced thiol (R-SH), disulfide (R-SS-R), disulfane (R-SSH), and carboxyl groups (*19,20,21*). NOM plays a key role in Hg mobility in the environment. NOM, as a dissolved form, may inhibit Hg(II) adsorption to sediments by competition with the sediment surface for Hg(II) ions. However, NOM itself may bind to mineral surfaces, enhancing Hg(II) adsorption through the formation of ternary complexes. In fact, it is the fractionation of NOM (dissolved vs adsorbed) that determines the behavior and distribution of Hg in sediments (*22*). In addition, NOM has been reported to affect Hg methylation (*15*). Furthermore, NOM can influence abiotic reduction of Hg(II). It has been shown that humic substances can reduce Hg(II) in the presence of sunlight (*13,23,24*).

Sulfide

Another important factor is the presence of sulfide (S(-II)), which binds Hg(II) strongly, influencing mercury chemical forms and mobility. HgS has been postulated as one of the largest sinks for Hg in sediments and soils under anaerobic conditions because of its low solubility (*4*). In anoxic environments, both α-HgS (cinnabar) and β-HgS (metacinnabar) are very persistent compared to other Hg species and cannot be dissolved without the presence of other ligands or oxidants. However, oxidation of reduced S(-II) (*25,26,27*) and strong complexes of Hg(II) with many ligands such as polysulfides and dissolved organic matter (DOM) impact the efficiency of HgS in immobilizing Hg (*28,29,30*). Leached aqueous Hg contributes to an increase in Hg availability for methylation and bioaccumulation (*4,13*).

Metal (Hydr)oxides

As discrete particles and/or as coatings on other mineral surfaces in natural systems, metal (hydr)oxides strongly sorb inorganic Hg(II) in water (*31*). Since the most effective Hg binding is controlled by organic matter and sulfide, the adsorption of Hg by metal (hydr)oxides is less important than other metals. However, in low organic matter oxic conditions, metal (hydr)oxides are efficient sinks for Hg because of their chemical properties and physical structure. For example, metal (hydr)oxides have been found to sorb Hg(II) strongly in the absence of organic matter (*32*,*33*,*34*,*35*).

Effect of pH

Since it affects both particle surface charge characteristics and metal speciation (*36*), pH is an important factor controlling Hg(II) sorption and determining Hg mobility (*37*). At low pH, Hg was found to be easy to release (*38*), while others claim that the sorption of Hg on sediment increases at low pH (*39*). In fact, the processes of sorption and desorption of Hg at different pH values depend on the kind of Hg speciation. In the case of organic matter dictating Hg speciation, less desorption of Hg at low pH is attributed to sorption to large amounts of organic matter, whereas low pH favors Hg desorption under conditions of low organic matter. In addition, pH seems to affect Hg reduction and methylation. For example, high pH favors reduction of Hg(II) to Hg(0), inhibiting the available Hg(II) for methylation. Moreover, high pH also favors the processes of demethylation (*16*).

Effect of Chloride

As a strong ligand for Hg(II), chloride (Cl^-) also is an important factor affecting Hg(II) speciation and sorption. Studies have shown that the addition of Cl^- significantly reduced Hg(II) adsorption under acidic conditions and resulted in a shift in the sorption edge (*40,41*). This is due to strong dissolved Hg-Cl_n complexes ($HgCl^+$, HgClOH, $HgCl_2$, $HgCl_3^-$, $HgCl_4^{2-}$). The strong complexes of Hg-Cl_n also reduce Hg methylation by competing with free Hg(II). In marine and estuary sediment, the rate of Hg methylation has been found to be lower than in fresh water sediments (*42*). In addition, the presence of chloride induces oxidation of Hg(0) to Hg(II) due to the strong Hg-Cl_n complexes shifting the reaction of Hg(0) to Hg(II) (*43*). Furthermore, the complex of $HgCl_2$ is the key effect determining cellular uptake of inorganic Hg(II) due to its fair lipid solubility (*13*).

In addition, as discussed above, redox reactions and biologically mediated transformations are important processes in the Hg cycle and speciation in sediments. The key factor determining the concentration of mercury in biota is the methylmercury concentration in water, which is controlled by net methylation and demethylation processes. Complexation and adsorption of the precursor, divalent mercury, by ligands and sediments could inhibit the production of methylmercury. In general, the major fraction of mercury in an aquatic system, inorganic mercury, is stored in sediments, persists and works as a source of methylmercury under different environmental conditions. For example, an increase of mercury desorption from sediments was observed with high Cl^- concentration, low acidity, or high dissolved organic matter (*44,45,46*). Even as a very insoluble and much less leachable Hg species, HgS may be dissolved

through oxidation of reduced S(-II) and ligand exchange reactions (*25*,*27*,*28*). Therefore, the treatment and removal of mercury from sediments are necessary for the control of methylation and bioaccumulation of mercury.

1.3 Sediment Control Technologies

Because Hg cannot be decomposed, in addition to source control, remediation is an option to lower Hg levels in contaminated water systems. There have been many technologies for treating aqueous mercury, including precipitation by sulfide S(-II), adsorption onto granular activated carbon (GAC) or powder activated carbon (PAC), ion exchange using cation resins, membrane filtration, and bacterial reduction of Hg(II) to Hg(0). Most of these technologies have been demonstrated in full-scale treatments (*47*). However, it is difficult to treat sediments and soils because the sorbed contaminants are less accessible to treatment methods than dissolved counterparts.

In general, remediation options to deal with metal contaminated sediments can be categorized as (*48*,*49*): (a) containment or isolation of contaminants through *in-situ* capping or *ex-situ* landfilling; and (b) dredging followed by *ex-situ* treatments to remove contaminants. The commonly used technologies available for treatment of sediment are reviewed and discussed as below.

1.3.1 In Situ Capping

In situ capping involves the placement of a proper covering material over contaminated sediment, thereby reducing the impact of contaminants in aquatic systems (*50*). On a laboratory scale, Moo-Yound et al. (*51*) showed that a mixture of sand and

finer particles can adsorb Hg and reduce Hg leaching to the overlying water. In a field study, a capping layer contained mercury in the original sediment quite well with a few exceptions (*52*). In the review of encapsulation technologies for the management of Hg contaminated wastes (*53*), numerous materials were reported to physically immobilize Hg reducing Hg leaching.

The advantage of *in situ* capping is the relatively low cost. However, *in situ* capping leaves the contamination in place, which will be a future contamination source. For various reasons (advective flows, bioturbation, diffusion, etc.), covered Hg may pass through the capping layer and enter into the overlying water. For example, laboratory experiments have suggested that subaqueous groundwater flows reduce the efficiency of capping significantly (*54*). Therefore, the effectiveness of *in situ* capping is dependent on site characterization such as hydrodynamic flows and geotechnical conditions.

1.3.2 Dredging Followed by ex situ Treatment

Ex situ capping or containment is to dredge and relocate contaminated sediment to other sites near the shore or on the land and isolate the sediment by clean material such as sand at the edges and above to minimize adverse environmental effects. Similar to *in situ* capping, the long-term stability of metals is a major concern. Landfilling is another option for disposal of dredged sediments. However, landfilling can only be used for small volumes and previous dewatering of sediments is a must since landfill facilities cannot handle slurries (*49*).

Besides *ex-situ* capping and landfilling, several types of cleaning techniques may be applicable for the cleanup of dredged metal-contaminated sediments, including washing, thermal extraction, and biological treatments.

Washing

Sediment washing involves the addition of a solution to contaminated sediments to transfer the contaminants from the sediments to the washing solution. This method is appropriate for weakly bound metals in the form of hydroxides, oxides and carbonates. However, in the presence of large amounts of organic compounds or a high fraction of clays, the removal of metals by washing is insignificant. Pretreatment to remove organic matter, mechanical shaking or various additives such as acid, base, surfactants, and chelating agents can increase metal leaching from soils and sediments (*48,55,56*). But the cost and biodegradability of the additives limit these combined processes for washing.

Thermal Extraction

Thermal extraction is utilized to evaporate metals at 800 ^{o}C from sediments. It is primarily applied to Hg contaminated sediments (*48*). In an on-site thermal remediation of Hg-contaminated soils, Chang and Yen (*57*) found that with 700 ^{o}C and 2 hr retention time Hg content in soil decreased from 95 mg kg^{-1} to 1 mg kg^{-1}. However, it requires large quantities of energy to dewater the sediments and combust the remaining wet sediments. Hence this process is very expensive. The cost in Chang and Yen's study (*57*)

is \$834 m^{-3} of soils. In addition, it is controversial for communities where the incinerator will be located due to atmospheric pollution concerns. Appropriate air pollution control systems are needed to minimize air pollution.

Bioremediation

Although microorganisms do not completely destroy metals, they alter metal chemical properties via biosorption and redox reactions and have been applied to bioremediation of metal contaminants (*58*,*59*).

Biosorption is a biological treatment method involving the adsorption of metals to the surface or interior of biomass such as algal or bacterial cells (*60*). Due to surface functional groups such as carboxyl, amine, hydroxyl, and sulfhydryl groups, biomass can adsorb appreciable quantities of positively charged metal ions. Studies have shown that bacteria and algae remove metals (Cd, Co, Cu, Pb, etc.) from aqueous solution (*61*,*62*,*63*). Removal of Hg(II) from water by genetic engineered *E. coli* has indicated the potential application of *E. coli* for Hg contaminated site remediation (*64*). Phycoremediation of heavy metals using transgenic microalgae (*65*) appears to be a very promising route for Hg removal from aquatic environments.

In addition to biosorption, bioremediation can involve microbially mediated redox transformation. For example, a range of bacteria have been found to reduce soluble and toxic U(VI) and Cr(VI) to less mobile and less toxic U(IV) and Cr(III) (*58*). Microbial reduction of Hg(II) to Hg(0) due to *mer* operon has been observed in oxic and anoxic environments (*13*,*66*). After reduction, volatilization of Hg(0) plays an important role in

Hg removal from sediment. Therefore, applying a colony of microorganisms with *mer* operon gene to reduce Hg combined with a technique such as activated carbon to sorb Hg(0) may be an option for remediation of Hg contaminated sediments.

However, due to the strong persistence of Hg in sediment, it may take a long time for heavily contaminated aquatic systems to fully recover. Furthermore, bioremediation may be affected by Hg speciation. For example, complexed Hg(II) ion may be less available to biomass sorption and microbial reduction.

In addition, electrokinetic process and vitrification are alternative technologies for heavy metal contaminated sediments. However, these options are all costly. Overall, dredging is labor intensive and highly expensive. Dredging activities may also cause adverse environmental effects. Subsequent *ex situ* treatment of dredged sediment have limitations including the addition of chemicals and high cost. Moreover, treatment may be highly time consuming due to mixing inefficiencies or slow desorption (*67*). Therefore, more effort should be focused on developing alternative remediation routes for metal-contaminated sediments treatment.

1.4 Ultrasound and Its Application

1.4.1 Cavitation and Thermal and Chemical Effects

The range of human hearing is from about 16 Hz to 16 kHz. Ultrasound is the name given to sound waves having frequencies higher than those to which the human ear can respond (i.e. > 18 kHz). When these waves propagate into liquid media, alternating compression and expansion cycles are produced, causing the media molecules to oscillate

about their mean position. During the compression cycle, the average distance between molecules decreases, while during rarefaction the distance increase. If a sufficiently large negative pressure is applied to the liquid, such that the average distance between molecules exceeds the critical molecular distance necessary to hold the liquid intact, the liquid will break down and cavities will be created – i.e. cavitation bubbles will be formed.

With the passage of ultrasonic waves, a cavity will oscillate in size over many expansion and compression cycles. During such oscillations the amount of gas or vapor that diffuses in or out of the cavity depends on the surface area, which is slightly larger during expansion than during compression. The growing cavitation bubbles can eventually reach a critical size where they cannot efficiently absorb energy from the ultrasonic irradiation and implodes violently. So far, four theories have been proposed to explain the sonochemical events (*68*): (1) hot-spot theory; (2) "electrical" theory; (3) "plasma discharge" theory, and (4) supercritical theory. The "hot-spot" theory suggests that high pressures and temperatures are generated during the violent collapse of the bubble. The "electrical" theory suggests that during bubble formation and collapse, enormous electrical field gradients are generated and these are sufficiently high to cause bond breakage and chemical activity. The "plasma theory" suggests that the formation of microplasmas inside the bubbles inducing chemical activity. The supercritical theory suggests the existence of a layer in the bubble-solution interface where temperature and pressure may be beyond the critical conditions of water and which may have physical properties intermediate between those of a gas and a liquid.

In general, most studies in environmental sonochemistry have adopted the "hot spot" concepts to explain experimental results. This theory considers sonochemistry as a microreactor as schematically shown in Figure 1.2 with three different reaction sites in the presence of air and H_2S (*68,69,70,71*):

(i) The gaseous interiors of collapsing cavities where both temperature and pressure are extremely high (up to and above 5000 K and 500 atmospheres, respectively). Such harsh conditions cause bond breakage and/or dissociation of chemical compounds, by direct pyrolysis of volatile and semi-volatile substances that migrate to the interior of the cavitation bubble. The pyrolysis of H_2S was shown in equation 1.1-1.2. In addition, degradation of H_2S occurs through secondary effects of free radicals •OH and H• pyrolyzed from water as shown in equation 1.3-1.5.

$$H_2S \xrightarrow{)))} \bullet H + \bullet SH \qquad (1.1)$$

$$2 \bullet SH \longrightarrow H_2 + S_2 \qquad (1.2)$$

$$H_2O \xrightarrow{)))} \bullet H + \bullet OH \qquad (1.3)$$

$$\bullet OH + \bullet OH \longrightarrow H_2O_2 \qquad (1.4)$$

$$H_2S + \bullet OH \longrightarrow \bullet SH + H_2O \qquad (1.5)$$

(ii) The interfacial liquid regions between the cavitation bubbles and the bulk solution where a high temperature (ca. 1000-2000 K) with high temperature-gradient exists and most important, the •OH concentration migrating from the interiors of cavitation bubbles is very high in this region (*72*). It has been reported that the majority of degradation takes place in this bubble-bulk interface region, especially

at high solute concentrations. As shown in equation 1.1-1.5 and equation 1.6-1.9, oxidation of H_2S into S oxidation products (Sox) takes place in this region.

$$\bullet H + \bullet H \longrightarrow H_2 \tag{1.5}$$

$$\bullet H + O_2 \longrightarrow \bullet HO_2 \tag{1.6}$$

$$\bullet HO_2 + \bullet H \longrightarrow H_2O_2 \tag{1.7}$$

$$\bullet HO_2 + \bullet HO_2 \longrightarrow H_2O_2 + O_2 \tag{1.8}$$

$$H_2S \xrightarrow{\bullet OH + H_2O_2 + O_2} Sox \tag{1.9}$$

(iii) Lastly, the bulk solution region is at ambient temperature and contains small amounts of •OH radicals that have diffused from the interface may contribute to oxidation and destruction reactions. Oxidation of H_2S may still proceed as shown in equation 1.4-1.9. Many studies have been conducted on the application of ultrasound to degrade the contaminants in water (*73,74,75,76*). Examples include parathion, trichloroethylene, hydroxybenzoic and humic acids, and diverse polychlorinated biphenyls.

1.4.2 Physical and Mechanical Effects

Besides chemical effects, the collapse of cavitation bubbles results in a variety of physical and mechanical effects including shock waves, microjets, microstreaming, acoustic streaming, and microstreamers which play important roles in solid and liquid heterogeneous systems.

Collapse of cavitation bubbles generates high pressure waves up to 10k atm. called shock waves (*77*). Shock waves further cause localized turbulent flows and particle

collisions. Interparticle velocity (3000 m s^{-1}) and collision temperature (3000 K) driven by shock waves were calculated based on metal powder agglomeration in the presence of ultrasound (*69,78*).

When solids, several orders of magnitude larger than the cavitation bubble, are in close proximity to the bubbles, symmetric cavitation is hindered and asymmetric cavitation collapse occurs, leading to the formation of microjets of solvent at a high velocity from 100 to 1000 m/s (*79*) which bombard the solid surface resulting in pitting and erosion.

Cavitation bubble growth and collapse and shock waves result in extremely turbulent flows at the liquid/solid interface, referred to as microstreaming (increasing the rate of mass transfer near the surface). Study has shown that microstreaming plays an important role in ultrasonic cleaning of particle fouled ceramic membrane (*80*).

The absorption of cavitation bubbles by liquid or the movement of cavitation bubbles in liquid causes a flow of the liquid termed acoustic streaming or microstreamer which leads to increased mass transfer (*81*).

According to these physical and mechanical effects, previous studies have shown that ultrasound is able to increase the mass-transfer coefficient (*82*), produce interparticle melting (*77*), enhance dissolution of solids (*83*), change particle size and surface properties (*84*), and modify material structure (*85*).

1.4.3 Application of Ultrasound in Environmental Remediation

The application of ultrasound in environmental remediation may involve any or all of the following: pyrolysis, free radical reactions, improvement of mixing or mass

transfer, promotion of intimate contact between materials, and disturbance of contaminated layers of chemicals.

Sonochemistry, as an advanced oxidation process, has been applied to destroy or accelerate the destruction of liquid-phase contaminants through chemical and thermal effects (*86,87,88,89*). For example, Lu and Weavers demonstrated that sonication was an effective way to degrade 4-chlorobiphenyl from synthetic sediments (*75*). Nagata et al. (*76*) investigated sonochemical decomposition of a series of hydroxybenzoic acids such as monohydroxy-, 3,4-dihydroxy-, 3,4,5-trihydroxybenzoic acids, tannic acid, and reagent and prepared humic acids in water. The decomposition followed first-order kinetics initially, and initial rates were in the range of 1.9-5.1 μM min^{-1} under argon and 1.9-16.4 μM min^{-1} under air. In a combined system of ultrasound and O_3, Weavers et al. (*73*) found that sonolysis and ozonolysis facilitated the degradation of three known organic contaminants, nitrobenzene (NB), 4-nitrophenol (4-NP), and 4-chlorophenol (4-CP). To dissolved organic matter, sonolysis was found to selectively react more with hydrophobic components by •OH radical than the hydrophilic components (*90*). A good example of thermal effect of ultrasound was sonochemical degradation of PFOS and PFOA which was not observed by Fenton reaction (*89*).

According to its physical and mechanical effects, ultrasound has been applied to desorb or accelerate the release of contaminants from soils and sediments. For example, ultrasound rapidly desorbed 4-chlorobiphenyl from synthetic sediments before chemical degradation (*75*). Mecozzi et al. (*91*) demonstrated that ultrasound accelerated humic substance extraction from marine sediment reducing extraction time from 24 hr shaking to 30 min. In the presence of thiourea and H_2SO_4 at 77 ^oC, ultrasound achieved almost

complete silver leaching yield from the solid waste of a silver ore (*92*). In a few minutes of ultrasound assisted extraction with 30% HNO_3, Hg was recovered from soils and sediments with digestion (*93*). Few studies have focused on ultrasonic treatment of metal-contaminated soils and sediments. In the investigation of CuO removal from granular brick by Newman et al. (*94*), 40% removal was found in 30 minutes compared to 6% removal with a conventional shaker. With pretreatments of incineration and size fractionation, as high as 92% removal of Cr from dredged sediments (*95*) and high efficient removal of Pb from soils (*96*) was observed.

Ultrasonic dissolution of metal oxides and metal sulfides has been observed previously (*84*,*97*). Lu et al. (*84*) demonstrated that sonication decreased the particle size of alumina and silica particles following a first-order regime. Dissolved aluminum concentrations 7-20 times higher than that of non-sonicated solutions, generating supersaturated solutions were observed. Sostaric et al. (*97*) found ultrasound-induced dissolution of colloidal CdS through thermal and chemical oxidation of sulfide in CdS.

1.5 Transgenic *Chlamydomonas reinhardtii*

Chlamydomonas reinhardtii (*C. reinhardtii*) is a unicellular, green alga that is found in both soil and fresh water habitats. The cell wall of *C. reinhardtii* contains glycoprotein and pectin layers similar in composition to those in terrestrial plants. The plentiful carboxyl, amine, hydroxyl, and thiol groups have a strong affinity for metal ions. The nature of the bonds between cell functional groups and metal ions can be electrostatic, ionic, or covalent. As inexpensive biomass, algae (living or dead) have an immense capacity to sorb metals such as Cd, Co, Cu, Ag, and Pb and have been applied

to treat wastewaters (*61*,*98*). Advantages of this type of metal–biomass sorption include the low-cost biomass sources and very rapid kinetics coupled with high adsorption capacities. Indeed, recent comparisons have suggested that biosorbents may be cheaper to implement than other commercially available ion exchange resins (*59*,*65*,*99*). Disadvantages include the perceived variation between batches of the biological product, a lack of specificity, and sensitivity to changes in pH. For example, although Adhiya et al. (*62*) demonstrated that freeze dried *C. reinhardtii* cells bound preferentially to Cd compared to Ca, low pH values greatly decreased Cd uptake.

Recent studies have suggested that it may be possible to increase the uptake and specificity of biosorbents using the tools of molecular biology. For example, engineering metal-binding proteins to the cell surface may increase uptake. Metallothionein (MT), a low molecular weight, cysteine-rich metal-binding protein, has been fused to biosorbents to enhance biomass tolerance and binding capacity to metals (*100*). Genetically engineered *E. coli* expressing MT was found to selectively bind Hg(II) over other metals and was resistant to changes in ambient conditions such as pH, ionic strength, and common metal chelators (*64*). Transgenic *C. reinhardtii* expressing MT has been found to bind 2-5 fold more Cd relative to wild type cells (*101*,*102*). Therefore, transgenic *C. reinhardtii* expressing MT is expected to selectively sequester Hg and have a higher metal binding capacity than wild-type *C. reinhardtii*.

1.6 Objectives and organization of the dissertation

Slow desorption following a more rapid release of contaminants from soil is often controlling in the remediation of toxic substances from soils or sediments. This can be

attributed to a number of factors such as aging of sediments, activation energy of sorptive bonds, and mass transfer limitations due to contaminants entering soil particle aggregates and particle micropores. Moreover, organic matter and oxide coatings throughout the aggregates further limit mass transfer through sorbate retardation processes (*67,103*). As described above, ultrasound could increase the mass transfer rate, break up chemical bonds, and affect the surface of sediments. Therefore, ultrasound may provide an alternative technology for sediment remediation by intensively desorbing the contaminants from the sediment and subsequently destroying the contaminants through sonochemical oxidation or removing the contaminants from aqueous phase by other techniques, such as activated carbon adsorption, ion exchange, and bioremediation.

The hypothesis of this study was that ultrasound may effectively accelerate the release of Hg from sediments into aqueous phase through its extreme phenomena (physical, chemical and thermal effects). Once Hg is water-solubilized by ultrasound it then can be recovered from aqueous solution by biomass sorption. As inexpensive biomass, transgenic *C. reinhardtii* was applied as sorption combined with ultrasound due to its plasmamembrane-anchored metallothionein polymer which selectively uptakes Hg with higher binding capacity and pH application range. Overall, the combined system of ultrasound and biomass may provide an alternative technology for Hg contaminated-sediment remediation. Additionally, the effectiveness of this process may be dependent on sonication conditions (power density and duration) and Hg contaminated sediment characteristics such as pH, NOM, Hg speciation.

The overall objective of this research was to investigate fundamentally and mechanistically how ultrasound will work with metal contaminated sediments,

particularly Hg. Specifically, the objectives of this study were: (i) to demonstrate the ability of sonication to release Hg from synthetic and natural sediments; (ii) to characterize the role of sediment matrix parameters including pH, Cl^- and NOM in sonochemical remediation; (iii) to explore the sonochemical desorption mechanisms on the increase of desorption rates; (iv) to determine the ability of sonochemical techniques to treat a series of metals with different binding strengths to sediment particles; (v) to characterize sonochemical reaction of dissolved organic matter; and (vi) to remove and recover Hg from aquatic system by a combined system of ultrasound and biomass sorption.

As a general guide, in addition to the introduction (Chapter 1), this dissertation is composed of 6 chapters and an appendix. Chapter 2 investigates sonochemical desorption of Hg(II) from an aluminum oxide model system. Chapter 3 examines the role of sediment matrix parameters including pH, chloride, and organic matter on sonolytic desorption of Hg(II) from aluminum oxide. Chapter 4 looks at Hg release from cinnabar (HgS) model system by sonochemical dissolution. Chapter 5 demonstrates the ability of sonication to treat an array of metals (Hg, Pb, Ni and Cr) from aluminum oxide and real sediment. Chapter 6 examines the application of ultrasound combined with biomass (transgenic *C. reinhardtii*) to remove Hg from sediments. Finally, Chapter 7 summaries the conclusions of this study and recommendations for future work. In addition, characterization of sonochemical reaction of dissolved organic matter was systematically conducted in the absence of Hg and sediment. Considering that this work is independent of Hg and was a collaborative work with Dr. Dong Chen, it is in the Appendix.

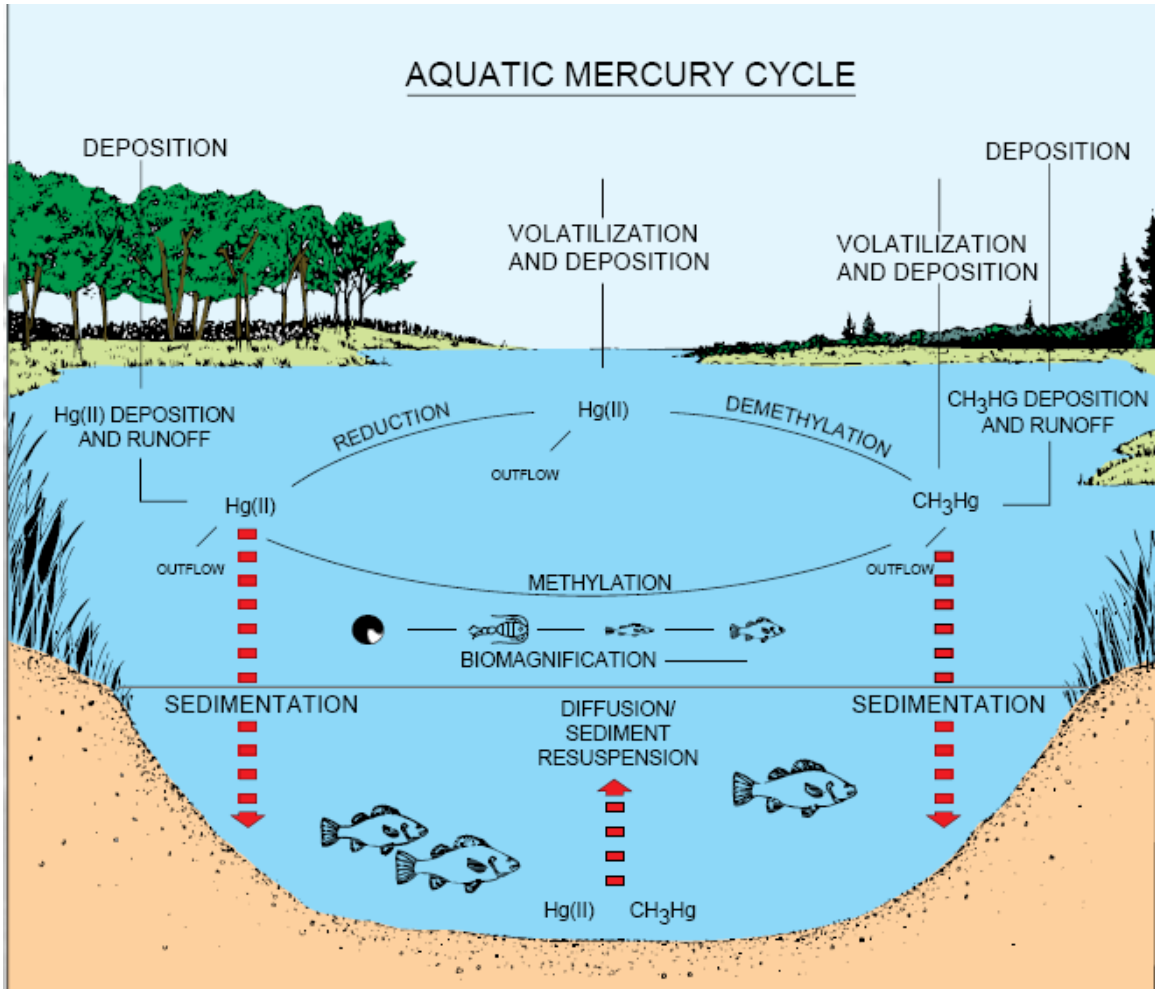

Figure 1.1 Mercury cycle in aquatic ecosystems [9]

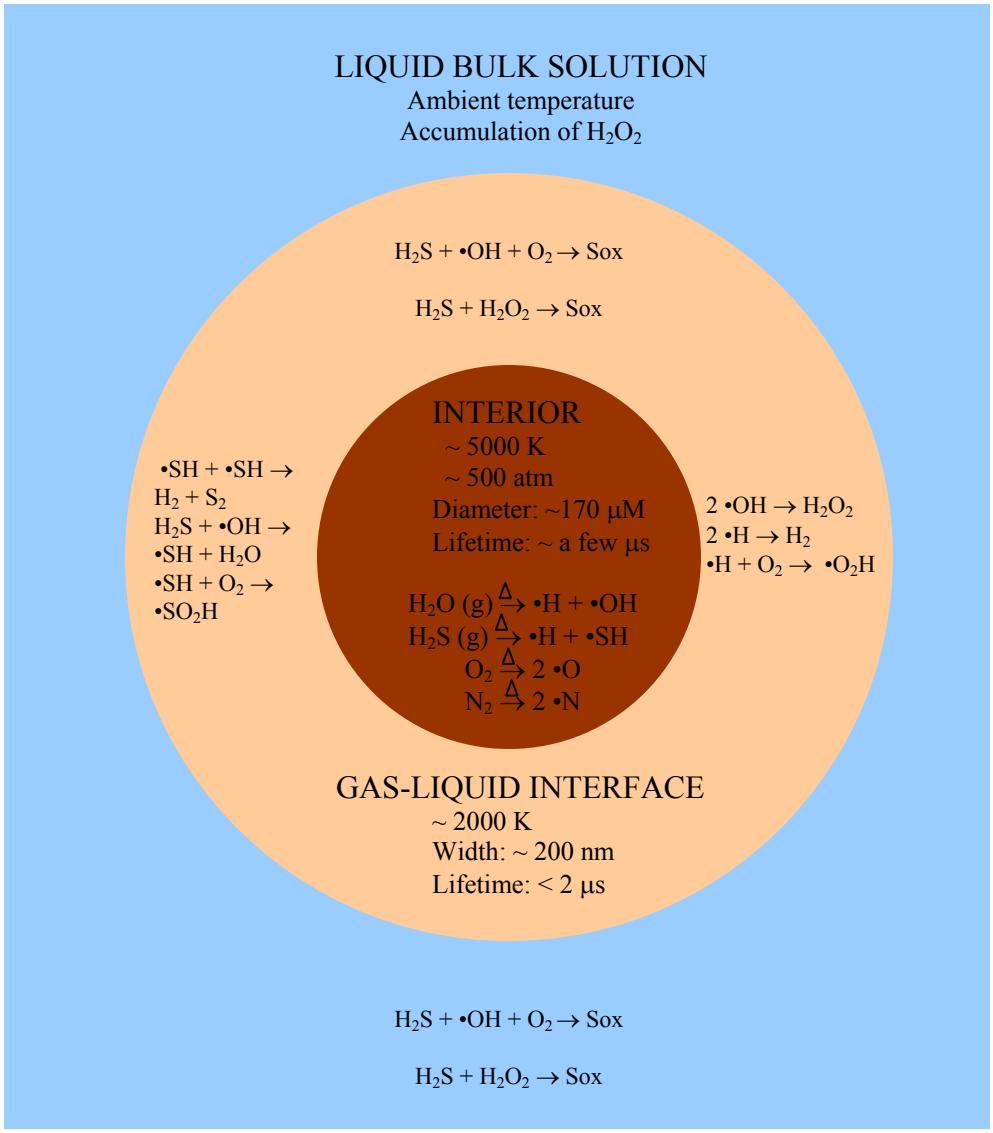

Figure 1.2 Three reaction zones in cavitation process (20 kHz ultrasound)

CHAPTER 2

SONOLYTIC DESORPTION OF MERCURY FROM ALUMINUM OXIDE

(*Environmental Science and Technology*, 2005, 39, 1037-1044)

2.1 Abstract

As discrete particles and/or as coatings on other mineral surfaces in natural systems, aluminum (hydr)oxides are efficient sinks for Hg(II). Ultrasound at 20 kHz was applied to enhance the desorption of Hg(II) from aluminum oxide particles (5.0 μmol Hg g^{-1}). Results showed that at short times ultrasound enhanced Hg(II) release at pH 4.0 compared to both hydrodynamic mixing and that expected based on the Hg(II) sorption curve. The higher the input power of sonication, the higher the desorption of Hg(II). However, with longer times, much less desorption occurred by ultrasound than by hydrodynamic mixing with mass balance measurements demonstrating that the desorbed Hg(II) was resorbed back to the particles. The particles were characterized to explore the mechanism for resorption of Hg(II) by prolonged sonication. No surface area change was observed even though ultrasound dramatically reduced particle size and changed surface morphology. Although a decrease in the point of zero charge (PZC) due to sonication was observed, it was excluded as the primary mechanism for Hg(II) resorption. Hg(II) occlusion by aluminum hydroxide precipitation was supported by X-ray photoelectron

spectroscopy (XPS) results and the formation of solutions supersaturated with Al. Experiments on pre-sonicated particles verified the occlusion theory by ruling out the effects of surface area and PZC.

2.2 Introduction

Mercury may undergo several different biogeochemical processes in aquatic systems including: volatilization and deposition at the water-air interface driven by oxidation/reduction reactions, complexation/decomplexation with ligands, adsorption/desorption to particulate matter and sediments, precipitation/dissolution as metacinnabar (mercuric sulfide), leaching and transport to groundwater, and methylation/demethylation (*4*,*10*,*12*,*19*). The key factor determining the concentration of Hg in biota is the methylmercury concentration in water, which is controlled by net methylation and demethylation processes. Complexation and adsorption of the precursor, Hg(II), by ligands and sediments may inhibit the production of methylmercury (*4*). In fact, the major fraction of Hg in an aqueous system, inorganic Hg, is stored in sediments, and persists as a source of methylmercury under different environmental conditions (*44*). Therefore, the treatment and removal of Hg from sediments are necessary for control of methylation and bioaccumulation. Numerous studies have been conducted to examine Hg(II) sorption and/or release from natural and synthetic particles, including clays (*104*), soils (*46*,*105*, *106*), metal sulfides (*107*,*108*), and metal (hydr)oxides (*32*,*33*,*34*,*35*).

As discrete particles and/or as coatings on other mineral surfaces in natural systems, especially in well-weathered soil and sediments with low natural organic matter, crystalline and amorphous aluminas play significant roles in geology and environmental

sciences (*109*,*110*). Because of their chemical properties and physical structure, aluminum (hydr)oxides are efficient sinks for many contaminants including cations of Pb, Zn, Cd, Sr, and Hg (*32*,*33*,*111*,*112*,*113*). The influence of pH, ionic strength, and ligands (Cl^-, SO_4^{2-}, PO_4^{2-}) on the sorption of Hg(II) by alumina has also been investigated to better understand the Hg(II) sorption process (*22*,*32*). In addition to Hg speciation, surface characteristics (surface area, porosity, pore size distribution as well as PZC) can have a significant impact on adsorption (*110*). Trivedi and Axe (*112*,*114*) have studied the sorption of metal ions to hydrous metal oxides and concluded that intraparticle surface diffusion is an important and rate-limiting step, requiring a lengthy period of time for sorption. Desorption of heavy metals from sediments can be much slower and/or nonreversible (*46*,67). This slow process may lead to long times for the cleanup of dredged metal-contaminated sediments by washing, chemical extraction, thermal extraction, and bioremediation (*48*).

Sonochemical techniques involve the use of sonic or ultrasonic waves to produce an oxidative environment via cavitation bubbles generated during the rarefaction period of sound waves. The formation, growth, and collapse of cavitation bubbles, leading to high local temperatures and pressures, are considered the main mechanism through which chemical reactions occur in sonochemistry. In a homogeneous aqueous system, three different reaction sites have been postulated: (i) The gaseous interiors of collapsing cavities where both temperature and pressure are extremely high (up to and above 5000 K and 1000 atmospheres, respectively) resulting in dissociation of chemical compounds including water (*68*); (ii) The interfacial liquid region between cavitation bubbles and the bulk solution where high temperature (ca. 1000-2000 K) and high temperature gradients

exist; (iii) The bulk solution region at ambient temperature where small amounts of •OH radicals diffusing from the interface may contribute to oxidation and organic contaminant destruction reactions. Studies have been conducted on the application of ultrasound to degrade a variety of contaminants in water (*73*, *74*,*75*,*115*).

Besides chemical effects, the collapse of cavitation bubbles results in a variety of physical and mechanical effects on the surface of solids. When solid particles exist in the vicinity of cavitation bubbles, the collapse may occur symmetrically or asymmetrically depending on the proximity and size of the solids. Symmetric cavitation generates shock waves which result in particle-particle collisions and cause extremely turbulent flow at the liquid/solid interface, referred to as microstreaming (increasing the rate of mass transfer near the surface). When solids are in close proximity to the bubbles, asymmetric collapse occurs, leading to the formation of microjets of solvent which bombard the solid surface resulting in pitting and erosion. Previous studies have shown that ultrasound is able to increase the mass-transfer coefficient (*82*), produce interparticle melting (*77*), enhance dissolution of solids (*83*), change particle size and surface properties (*84*), and modify material structure (*85*).

At present, some investigations have been conducted concerning the effects of ultrasonic desorption and removal of organic components from soil (*75*,*116*,*117*,*118*); however, few studies have focused on ultrasonic treatment of metal-contaminated solids (*94*,*95*). Enhanced release of Cu from brick (*94*) and Cr from dredged sediments (*95*) has been observed. However, Cu on brick was introduced as CuO, not as an adsorbed phase. The study on the removal of Cr from sediments was pretreated with incineration to eliminate organics prior to sonication, which may greatly change Cr bonding with

sediments. Furthermore, the release mechanism and ultrasonic effects on particles have not been explored.

The purpose of this study was to investigate the sonochemical desorption of Hg(II) from aluminum oxide. The specific goals were to demonstrate the ability of sonication to enhance desorption rates compared to conventional mixing, to characterize ultrasound effects on particle properties, and to explore the mechanism for Hg(II) desorption from alumina particles.

2.3 Materials and Methods

2.3.1 Materials

Mercury (II) chloride (certified ACS, Fisher Scientific) was used without further purification. Water used to prepare the solutions was from a Millipore system (R = 18.2 MΩ-cm). Ionic strength and pH were adjusted with NaOH (Reagent ACS, Pellets 97+%, Fisher Scientific), HNO_3 (Trace Metal Grade, Fisher Scientific) and $NaNO_3$ (certified ACS, Fisher Scientific). Custom-Grade standards for Hg (1004 μg/mL, 3.5% HNO_3) and Al (9974 μg/ml, 5% HNO_3) obtained from Inorganic Ventures Inc. were used for cold vapor atomic absorption spectroscopy (CVAAS) and Inductively Coupled Plasma Atomic Emission Spectroscopy (ICP-AES) analysis. Aluminum oxide (adsorption grade Al_2O_3, 80-200 mesh particle size, density 4 g/cm^3) was purchased from Fisher Scientific. The particles had a surface area of 110 m^2 g^{-1} and an average diameter of 110 μm as tested by single-point N_2 Brunauer-Emmett-Teller (BET) surface area analysis, and Malvern Mastersizer particle size analysis. X-ray diffraction (XRD) analysis revealed

very poor crystallinity, mainly including Al_2O_3 (PDF#34-0493) as well as minor amount of boehmite and amorphous alumina phases.

2.3.2 Sorption and sample preparation

Sorption samples were prepared by shaking 15 mL of 0.75 mM Hg(II) stock solution (pH = 2.5, I = 0.1 M) with 2 g alumina particles in 60 mL polypropylene bottles on a rotating shaker at 350 rpm. After 2 hr mixing, the pH was adjusted to 7.0 with 0.1 M HNO_3 or 0.1 M NaOH. After 24 hr the adsorption was observed to reach equilibrium, and the supernatant was separated from the particles by 15 min centrifugation at 1500 rpm. A sample of supernatant was diluted with 5% HNO_3 for storage and CVAAS analysis, and the Hg-laden particles were used for sonication and hydrodynamic mixing desorption experiments. The amount of Hg(II) adsorbed on solids was calculated from the difference between Hg(II) in the stock solution and that remaining in the supernatant solution. The alumina particles were saturated with Hg(II) under the solution conditions in this study based on sorption isotherms.

2.3.3 Desorption

For sonolytic desorption, 2 g of Hg-laden particles were transferred to a glass rosette reactor with 60 mL of 0.1 M ionic strength solution. Batch desorptions were carried out at pH 4.0 controlled with a PHM290 pH-Stat autotitrator (Radiometer Analytical, France) using trace metal grade HNO_3. As shown in the Hg(II) pH dependent sorption curve (inset of Figure 2.1), Hg(II) had a sorption edge from pH 3.0 to pH 5.0. A pH value of 4.0 (15% desorption expected based on pH dependent sorption curve) was

chosen as the desorption condition to demonstrate ultrasonic effects on Hg(II) desorption. A 20 kHz ultrasonic probe system (550 Sonic Dismembrator, Fisher Scientific) was used for sonication experiments at two different power input intensities, 20 W cm^{-2} and 36 W cm^{-2}, as measured by calorimetry (*119*). The probe tip was located near the bottom of the reactor to ensure particles were well mixed throughout the reactor. The reactor was water-jacketed to control the reacting solution temperature at 20.0 ± 0.5 °C by a circulating, constant-temperature bath (Fisher Scientific).

After selected times of sonication, samples were transferred to polypropylene centrifuge bottles and ultracentrifuged for 20 min at 17000 rpm using a centrifuge (Model J2-21, Beckman) to separate the supernatant and particle fractions. An aliquot of the supernatant was diluted with 5% HNO_3 for storage and CVAAS and ICP-AES analysis. The particle pastes were freeze dried for later particle size, surface area, X-ray diffraction (XRD), point of zero charge (PZC), scanning electron microscope (SEM), X-ray photoelectron spectroscopy (XPS), and mass balance analysis. SEM analyses of unaltered Al_2O_3 particles showed similar surface morphology before and after freeze-drying.

For hydrodynamic mixing, 6 g of Hg-laden particles and 180 mL 0.1 M ionic strength solution were transferred to another glass rosette reactor (with the same geometry as the sonication reactor), and mixed by circulation to better control pH compared to conventional shaking or tumbling. A circulation flow rate of 1.2 L min^{-1} was driven by an Economy Drive peristaltic pump with a Model 7518-12 Easy-Load peristaltic pump head (MasterFlex® L/S™, Cole Parmer) and Tygon tubing. This flow rate was arbitrarily chosen due to the difficulty to relate the flow rate to standard shaking conditions. All other conditions, such as pH and temperature, were the same as those

used with sonolytic desorption. The amount of Hg(II) released from the solid was calculated by analysis of the supernatant and by digestion of the solid. Control experiments and selected experiments were performed in duplicate or triplicate to determine the data error and verify reproducibility.

2.3.4 Measurement and characterization

Hg(II) samples were analyzed by CVAAS (SpectrAA 880Z, Varian, Australia) using a 25% $SnCl_2$ (98%, Sigma-Aldrich) and 20% HCl (Trace Metal Grade, Fisher Scientific) reductant solution. Total dissolved Al was analyzed by ICP-AES (Vista Ax, Varian, Australia). Microwave digestion was used in selected experiments to measure Hg(II) on the particles before and after desorption for mass balance analysis. In this procedure, 0.1 g dried solid was dissolved by adding 5 mL HNO_3, 1 mL HCl, and 10 mL HF. Samples were then digested using a nominal 630-watt system at 80% power and 150 psi for 60 min. The completely digested samples were diluted prior to CVAAS analysis.

Particle size analysis, surface area, PZC, XRD, SEM, and XPS were used to characterize particle changes resulting from sonication. Particle size changes were determined by laser light scattering with a Malvern Mastersizer. Specific surface areas were determined using both single-point and multipoint BET N_2 adsorption and desorption isotherms obtained with a surface area analyzer (Micromeritics® FlowSorb 2300). Ethylene glycol monoethyl ether (EGME) (*120*) was also used in this study to measure the specific surface area. Particle surface PZC was measured using potentiometric mass titration (PMT) performed under a N_2 atmosphere following the

procedures of Bourikas et al. (*121*). XRD analyses were conducted with a Philips X-ray diffractometer (Philips Analytical, Natick, MA) using CuKa radiation at 35kV and 20mA. Step-scanned data were collected from 10 to 75° 2θ with a fixed angular increment of 0.05^{o} 2θ and a 3 sec count time. An SEM (Philips XL-30) operated at 12 kV was used to study particle surface morphology changes. Samples were mounted on stainless steel stubs using double-stick carbon tape and sputter-coated with Au. XPS (Kratos Ultra Axis) spectra were obtained using an unmonochromatized Mg Ka (1200 eV) X-ray source, and the pressure in the analytical chamber was in the low 10^{-7} Pa range. Narrow scan spectra of the Hg 4f level were recorded using a fixed pass energy of 22 eV.

2.4 Results and Discussion

2.4.1 Sonication effects on the desorption of Hg(II)

Experiments were conducted to investigate the enhanced effectiveness of ultrasound in desorbing inorganic Hg(II) from particles. Mercury desorption with increasing time under conditions of hydrodynamic mixing and two different sonication powers are shown in Figure 2.1. During short desorption times, release of Hg(II) from alumina particles by sonication was enhanced compared to hydrodynamic mixing. With greater sonication power input, greater initial desorption was observed. After 2 min desorption, 33% and 14% of Hg(II) were released by ultrasound at power intensities of 36 W cm^{-2} and 20 W cm^{-2}, respectively, compared to 8% by hydrodynamic mixing. With longer sonication times, the Hg released by sonication decreased, while desorption by hydrodynamic mixing appeared to approach equilibrium. After 5 min, the release of

Hg(II) at 36 W cm^{-2} sonication began to decrease, and after 30 min, a decrease of Hg(II) released at 20 W cm^{-2} sonication also occurred. At 60 min, much less desorption occurred by sonication (3% and 9% at 36 and 20 W cm^{-2}, respectively) than by hydrodynamic mixing (14%).

The enhanced release of Hg by sonication at short times may be attributed to the extreme conditions generated during the violent collapse of cavitation bubbles. The mechanism by which sonication promotes desorption in a heterogeneous system may be due to an altered chemical equilibrium or improved kinetics of release. Desorption, as an endothermic process, is promoted by energy deposition if bubble collapse occurs in the vicinity of the adsorbent surface. The adsorbed molecules may be released into solution by breaking chemical bonds through shockwaves, microjets and thermal effects from cavitational collapse. With such cavitational events, the available active sites for adsorption and the number of adsorbate molecules in solution will reach a new equilibrium. Equilibrium Hg(II) desorption calculated based on the sorption curve (Figure 2.1) was 15%, whereas Hg(II) desorbed by 36 W cm^{-2} sonication reached 33% at 2 min, indicating that ultrasound altered the chemical equilibrium of Hg(II). Bathen (*122*) found that the thermodynamic equilibrium was shifted to lower sorbed concentrations when investigating the adsorption of fructose on Amberlite resin. The effect was stronger with increasing power. Li et al. (*123*) reported similar results from a phenol and resin system.

Additionally, enhanced desorption may be due to improved mass transfer by ultrasound. Extreme agitation may accelerate mass transfer through intraparticle micropores, which usually is the limiting step for adsorbate molecules to diffuse from

micropore active sites to the bulk solution. For example, both the intrinsic mass transfer coefficient and the effective diffusivity of benzyl chloride through a Na_2S-liquid interfacial film were increased by a factor of 2 ~ 3 in the presence of ultrasound (*124*). The number of cavitational events, the intensity of microstreaming, high-speed microjets and high-pressure shockwaves produced by acoustic cavitation are mostly dependent on the power delivered to the system, explaining why the higher sonication power produced more desorption initially than the lower one (Figure 2.1).

Having observed decreased Hg(II) release with longer sonication times, it was very important to investigate the fate of Hg(II) in this system. It is possible for Hg(II) to volatilize as Hg(0) after certain reduction reactions (*4*); however, sonication control experiments with Hg(II) in the absence of particles did not result in any Hg(II) loss from the system. Next, particles and solution before and after sonication at a power of 36 W cm^{-2} were analyzed to determine the fate of Hg(II) in the system. Hg desorbed into the solution and remaining on the solid phase with sonication time were measured independently. Mass balance analysis of the aqueous and solid phases showed that Hg(II) released at short times re-associated with the solid with continued sonication (Figure2.2). A similar decrease in release as a function of sonication time has also been observed in other studies. For example, decreased diesel removal with long-term sonication from diesel-laden sand was explained as the re-adsorption of oil-water emulsions with an increase of sonication (*118*). Swamy and Narayana (*125*) also found a decreasing trend in the extraction of Cu from oxide ore with prolonged application of ultrasound. They speculated it was due to resorption on hydroxide/oxide surfaces created/exposed by sonication.

Thus, enhanced Hg(II) release at short sonication times is attributed to altered equilibrium conditions and improved mass transfer. The mechanism of reduced Hg(II) desorption observed at longer sonication times in this study will be discussed in more detail in the following sections focusing on the results from sonication at a power of 36 W cm^{-2}.

2.4.2 Sonication effects on alumina particles

To explore reasons for decreased Hg(II) release at longer sonication times, particle characterization experiments were carried out to understand sonication effects on alumina properties. First, changes of particle size were investigated. As shown in Figure 2.3, particle size decreased dramatically with sonication, and the size volume distribution peak of the alumina shifted from 110 μm at the beginning to around 6 μm after 60 min sonication. Lu et al. (*84*) found that sonication decreased particle size following a first-order kinetic regime (calculated from average size loss). An increasing rate of particle size reduction was observed with increasing particle diameter and surface area. The particle size loss in this study was much higher than in their research, even though both their particle size (D_0 = 130 μm) and surface area (SA_0 = 200 m^2 g^{-1}) were bigger than in our study (D_0 = 110 μm, $SA_{0\text{-single-point BET}}$ = 110 m^2 g^{-1}). The difference may be attributed to variations in sonication powers, particle concentrations, and particle composition.

A scanning electron microscope was used to look at the effect of ultrasound on the morphology of particles. Without sonication, the alumina particles, microscopically smooth and macroscopically rough, looked like a random pile of crystallized blocks of various sizes and shapes under the SEM (Figure 2.4). After 60 min sonication, ultrasound

broke down the particles to smaller, rod-like particles and created a microscopically rough and pitted surface morphology. Shockwaves and microjets should be the major mechanisms affecting particle characteristics; however, at 20 kHz sonication, it is not likely that particles smaller than ~150 μm in diameter are impacted by microjet formation (*77*). Thus, microjets were not expected to be the dominant mechanism for particle alterations in this study. On the other hand, shockwaves created by cavitational collapse in the liquid may drive interparticle collisions with a speed of several hundred meters per second, dependent on particle size (*82*). During sonication, the high velocity collisions may 1) break up and/or crack large particles, reducing particle size; 2) fragment particle edges, smoothing particle surfaces macroscopically; and 3) cause small particles to aggregate together, explaining why smaller particles have a lower size reduction rate compared to larger particles. In addition, shockwaves impinge on the particles, generating local surface pitting and microscopic erosion. Based on the dramatic particle size and surface morphology changes observed, an increase of surface area would be intuitively expected. Decreased Hg(II) desorption would be a consequence of newly formed reaction sites resorbing Hg(II) back to the particles.

Next, surface areas were determined by single-point and multipoint BET N_2 measurements. Unexpectedly, there were no obvious increases in surface areas with sonication time, even though results from single-point and multipoint BET N_2 measurements differed slightly (Table 1). At the low temperature of liquid N_2, a fraction of the pores may be closed and not contribute to the measured surface area as hypothesized by Goldberg et al. (*126*). However, the results from room-temperature EGME measurements also showed no surface area changes with sonication (Table 1).

Usually the surface area of a solid is related to the size and morphology of the particles that make up the solid. Amorphous particles may also possess extensive microporosity, which is the most important contributor to surface area and the density of adsorption sites on particles. In this situation, the microporous primary particles within particle aggregates may still be accessible to adsorbate molecules through the continuous mesopores or macropores within the aggregates (*127*). Taking into account the possibility that the alumina particles used in this study possess similar structures and properties to the aggregates mentioned above, it is reasonable for ultrasound to dramatically dissociate the particles, but not substantially increase the surface area. From the observed morphology changes (Figure 2.4), ultrasound did pit and erode the somewhat flat particle surfaces. However, increases in surface area by this effect were clearly insignificant compared to the total primary particle surface area. Therefore, the decrease in Hg(II) desorption with long sonication times cannot be attributed to surface area changes.

Sonication may also induce phase transformations in the solid. For example, Gasnier et al. (*128*) found the formation of corundum (α-Al_2O_3) and bayerite [$Al(OH)_3$] from pure η-Al_2O_3 with sonication (20kHz). The new surface phases formed may have different types of sorption sites and site densities than the original phase; thus, Hg(II) uptake may change without a change of surface area. To investigate possible mineral phase transformations in this study, XRD analyses were conducted to examine the particle mineralogy with sonication time. Compared to the initial data, no pronounced differences were observed (data not shown). Consequently, any phase transformations were limited to a thin film at the particle surfaces, and were undetected by the deep-penetrating X-rays.

Goldberg et al. (*126*) proposed that differences in selenite adsorption on two goethites with similar surface area were probably due to differences in PZC. In our study, ultrasound decreased the PZC of the particles from 9.5 without sonication to 6.8 and 6.5 after 30 and 60 min sonication, respectively; whereas there was almost no change in PZC by hydrodynamic mixing. The potentiometric titration method used in our study does not discriminate PZC differences from different crystal faces of one mineral phase. Therefore, a PZC decrease may arise from phase transformations produced or induced by ultrasound even though XRD did not detect the phase transformations.

Lastly, the aluminum concentration in the supernatant after ultracentrifugation was measured by ICP-AES. The Al concentration in solution increased markedly with time by sonication compared to hydrodynamic mixing (Figure 2.5) and was attributed to the extreme conditions generated by ultrasound. The high temperature in the interfacial region of collapsing cavitation bubbles (2000 K) (*68*) as well as that from interparticle collisions (3000 K) driven by shockwaves (*77*) enhanced the solubility of Al. Moreover, interparticle collisions and particle surface pitting, erosion, impingement and fragmentation by shockwaves and microjets may have generated colloidal particulates from large particles thereby accelerating particle dissolution. The generation of small particles from the mechanical effects of ultrasound (Figure 2.3) may have also resulted in an increased solubility of Al (*129*). Calculations of Al ion activity products (IAP) at pH 4.0 (*109*) revealed that after 15 min sonication, dissolved Al concentrations were greater than the solubility of the most soluble amorphous aluminum (hydr)oxides indicating supersaturated conditions. By contrast, Al concentrations with hydrodynamic mixing were less than the solubility of amorphous aluminum (hydr)oxides. It should also be

noted that after 20 min ultracentrifugation, particles larger than 20 nm were removed. Colloidal particles less than 20 nm in size might have remained in suspension and contributed to the high Al concentration in the supernatant after ultrasound. Any small colloidal particulates would increase the apparent Hg(II) desorbed by measuring Hg(II) adsorbed to colloids in the supernatant. However, the effect was not expected to be significant since the majority of the Hg(II) re-associated with the solid under continued sonication.

It is well known that water reacts with Al_2O_3 to produce Al-hydroxides ($Al(OH)_3$) and Al-oxyhydroxides (AlOOH) (*109*). Near surface corundum (α-Al_2O_3) will readily hydroxylate to a gibbsite-like phase, which has a reported PZC near pH 5 (*130*). In supersaturated Al solutions, a sequence of mineral precipitation has been reported as follows: amorphous aluminum hydroxide → pseudoboehmite → bayerite → gibbsite (*109*). At high Al concentrations, bayerite dominates in this sequence (*33*,*131*). Previous studies by Fourier transform infrared (FTIR) spectroscopy (*33*,*132*,*133*) have found that γ-Al_2O_3 undergoes a surface phase transformation to bayerite, and bayerite has a stronger affinity for Hg(II) (Γ = 0.39-0.44 $\mu mol/m^2$) than γ-Al_2O_3 (Γ = 0.04-0.13 $\mu mol/m^2$) (*33*). In the compilation by Kosmulski (*134*), the average PZC of Al_2O_3 and bayerite were reported as 9.0 and 6.7, respectively. Ultrasound may accelerate phase transformations by increasing the kinetics and enhancing the degree of phase transformation by dissolving particles and creating a supersaturated Al solution, thus decreasing the surface PZC as bayerite forms surficially from Al_2O_3.

With the alumina particles used in this study, we observed large particle size reduction, dramatic changes in surface morphology but no significant changes in surface

area. In addition, the PZC change and supersaturated Al solution conditions observed in this study are consistent with the formation of surface phase bayerite from Al_2O_3.

2.4.3 Mechanism for reduced Hg(II) desorption

From the results and discussion presented above, it appears that the decline in Hg(II) release with sonication was due to a decrease in the PZC induced by ultrasound. To verify this mechanism, XPS was used to detect Hg on the particle surfaces before and after ultrasound. XPS, a widely used surface analytical tool, is particularly effective for obtaining elemental surface concentration and composition information on the nanometer depth scale (*135*). Given near constant surface area before and after ultrasound and the fact that more than 95% of the Hg(II) re-associated with the particles after 60 min sonication, we expected that similar surface Hg(II) coverage existed on the particles before desorption and after 60 min sonication. In fact, the XPS spectra did not give evidence supporting similar Hg(II) coverage before and after ultrasound. There were two Hg 4f peaks before sonication, whereas the Hg 4f signals were not present after 60 min sonication (Figure 2.6). No surface area change and similar amounts of Hg(II) associated with the particles before and after sonication suggest that there was a different Hg(II) spatial distribution induced by ultrasound. Behra et al. (*107*) suggested that the decreased Hg XPS signal on a pyrite (FeS_2) surface was due to burial of Hg at the pyrite – Fe (hydr)oxide interface (from dissolution, oxidation, and precipitation of Fe in pyrite).

The hydrolysis and precipitation of Al from acidic solutions has been shown to produce three general types of species: (i) monomeric aluminum hydroxide complexes $Al(OH)_x(H_2O)_{6-x}^{(3-x)+}$, (ii) polynuclear or polymeric aluminum hydroxide complexes

$Al_p(OH)_q^{(3p-q)+}$ ($1 \leq p \leq 54$), and (iii) micro-crystalline aluminum hydroxide. The relative proportions depend primarily upon the hydrolysis conditions, e.g. pH and Al concentration (*109*). Under the supersaturated Al concentrations observed with sonication in this study (as high as 20 mM), fresh precipitates would be expected to cover the particle surface, occluding sorbed Hg(II). Under similar solution conditions, Parthasarathy and Buffle (*136*) observed the precipitation of 130 Å particles. Therefore, we suggest that with prolonged sonication, most of the Hg(II) was occluded in the deep surface, and was not detectable by XPS whose typical analysis depth is approximately 20-30 Å depending on the surface analyzed and instrument conditions.

To verify an occlusion mechanism for the loss of Hg(II) desorption with longer sonication times, a final set of experiments was performed with pre-sonicated particles. Alumina particles were first sonicated for 1.5 hr with a power of 36 W cm^{-2} using the same conditions as the desorption experiments (pH = 4.0, [particle] = 33 g L^{-1}). Next, the sonicated particles were ultracentrifuged and freeze dried. Control experiments showed similar particle size, surface area, and PZC results as particles used in the Hg(II) desorption experiments after 60 min sonication. Hg(II) sorption and desorption experiments were conducted on the pre-sonicated particles with identical experimental procedures and conditions as on non-presonicated particles. The desorption data and trends with pre-sonicated particles were consistent with those achieved originally (Figure 2.1; Figure 2.7).

These pre–sonication results rule out effects of possible changes in surface reactivities (surface area and PZC) on the reduction in Hg(II) desorption. This combined with the observed changes in Hg(II) spatial distribution on the particles due to sonication

implicates occlusion as the primary mechanism for the reduction in Hg(II) desorption with longer sonication times. Mineral surface phase transformation examination by FTIR and surface molecular-scale studies of Hg(II) adsorption (species and structure) by extended X-ray absorption fine structure (EXAFS) spectroscopy may provide more fundamental information for further understanding this mechanism as these two techniques can be utilized on *in-situ* samples at low adsorption densities.

Acknowledgements

Funding from NOAA/Ohio Sea Grant College Program and the NSF Environmental Molecular Science Institute at The Ohio State University is gratefully acknowledged. The authors thank S. Jones for his help with XRD and BET N_2 measurements.

		Sonication Time (min)						
		0	2	5	15	30	60	180
SA (m^2g^{-1})	Single-point BET	109	106	109	109	108	108	110
	Multi-point BET	122	ND‡	ND‡	120	121	125	ND‡
	EGME	136	151	131	148	150	154	ND‡

† Freeze-dried prior to measurement ‡ Not determined

Table2.1 Surface Area (SA)† under 36 W cm^{-2} Sonication

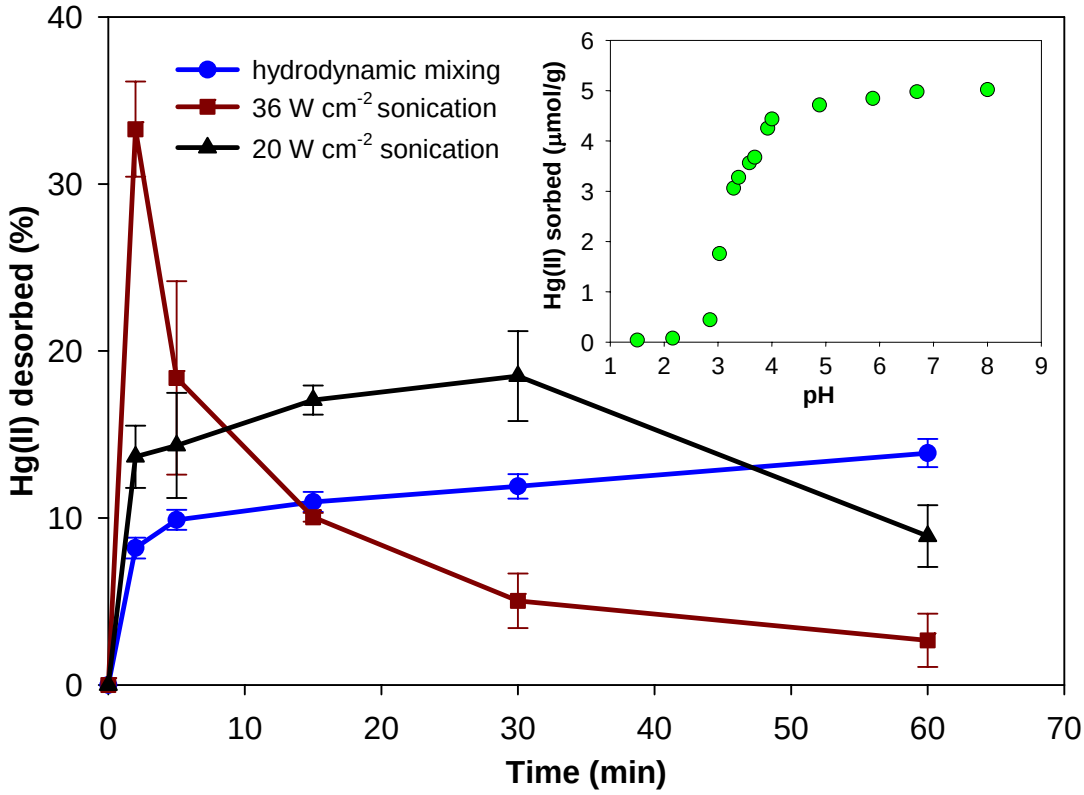

Figure 2.1 Desorption of Hg(II) from alumina particles (pH = 4.0, T = 20 °C, I = 0.1M, [particle] = 33 g L^{-1}, $[Hg(II)]_{initial\ on\ particle}$ = 5.0 μmol g^{-1}, D_0 = 110 μm). Figure inset: pH dependent Hg(II) sorption curve.

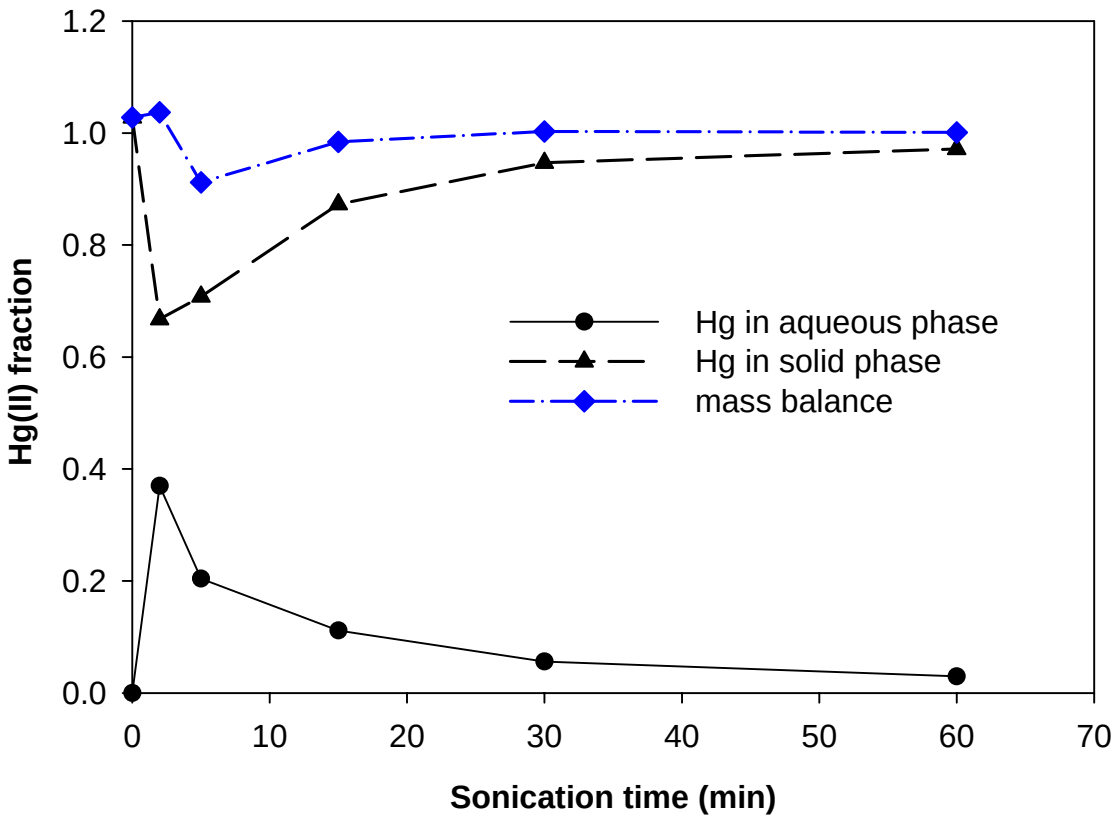

Figure 2.2 Hg(II) distribution with 36 W cm^{-2} sonication. Hg desorbed into the aqueous phase and remaining on the solid phase with sonication time were measured independently. The mass balance was determined by Hg(II)$_{\text{mass balance}}$ = Hg(II)$_{\text{in aqueous phase}}$ + Hg(II)$_{\text{in solid phase}}$.

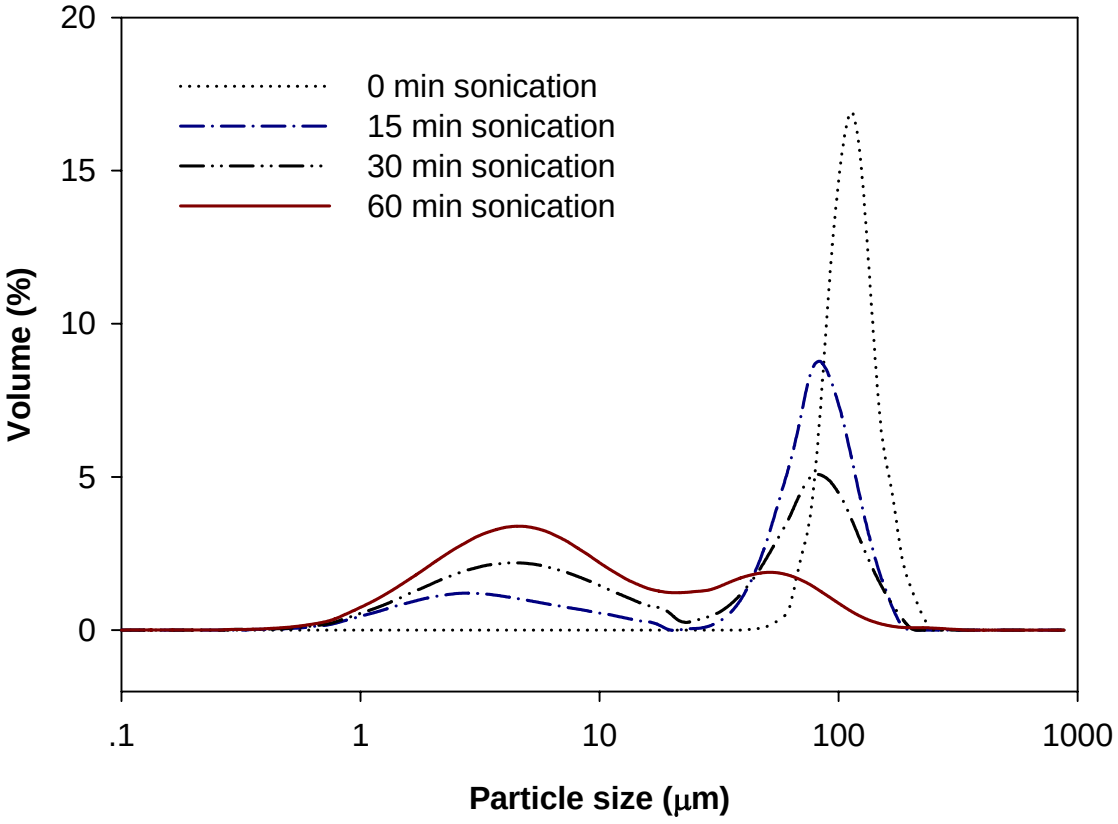

Figure 2.3 Particle size distribution with time by ultrasound (pH = 4.0, T = 20 °C, I = 0.1 M, [particle] = 33 g L^{-1}, sonication power 36 W cm^{-2}, D_0 = 110 μm).

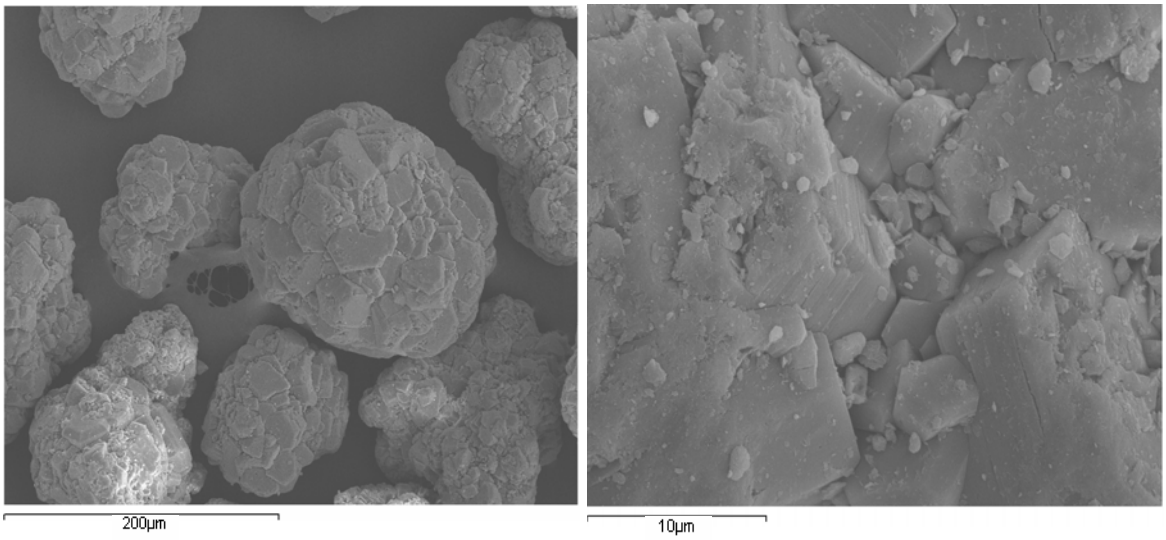

(a)

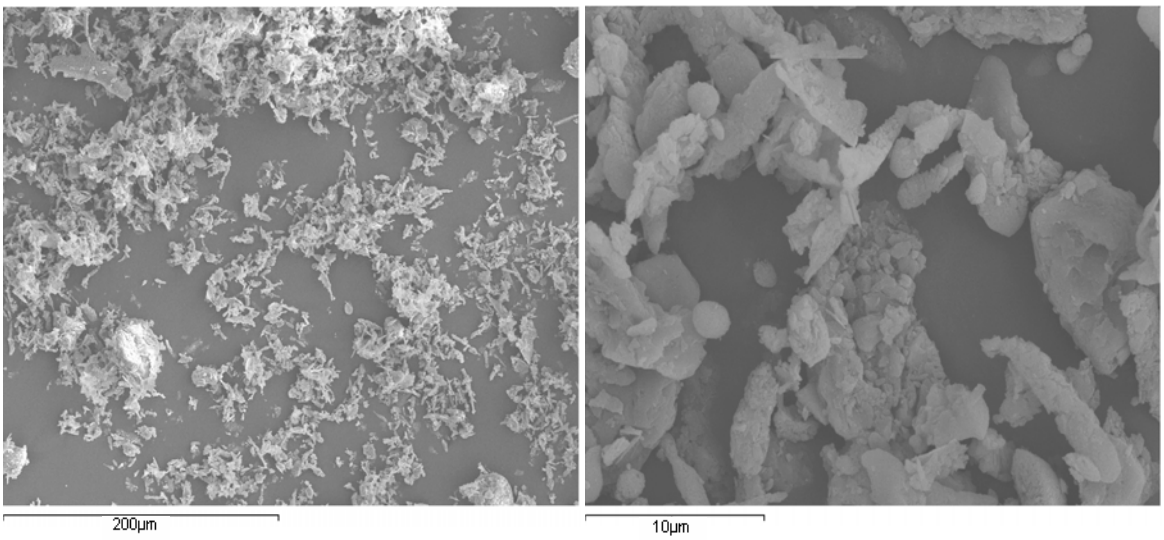

(b)

Figure 2.4 SEM images of particle morphology (a) before sonication, (b) after 60 min sonication at power 36 W cm^{-2}.

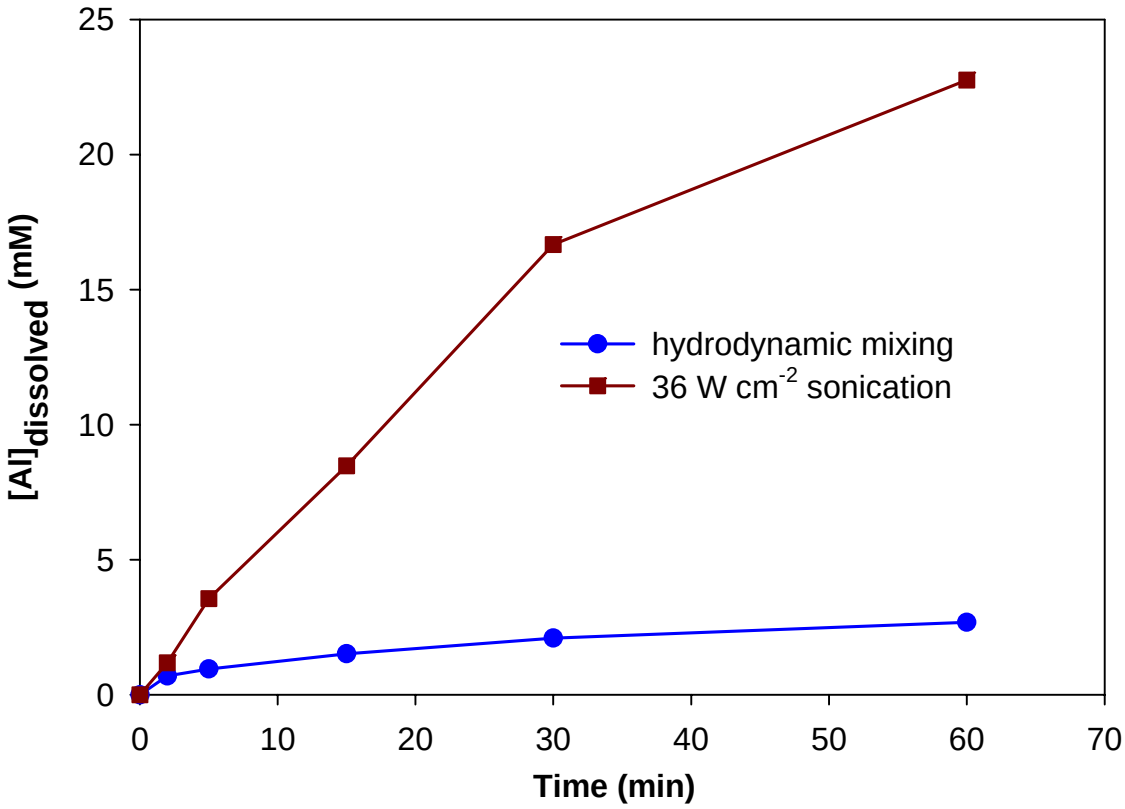

Figure 2.5 Aluminum concentration in supernatant with sonication and hydrodynamic mixing (pH = 4.0, I = 0.1 M, [particle] = 33 g L^{-1}, sonication power 36 W cm^{-2}).

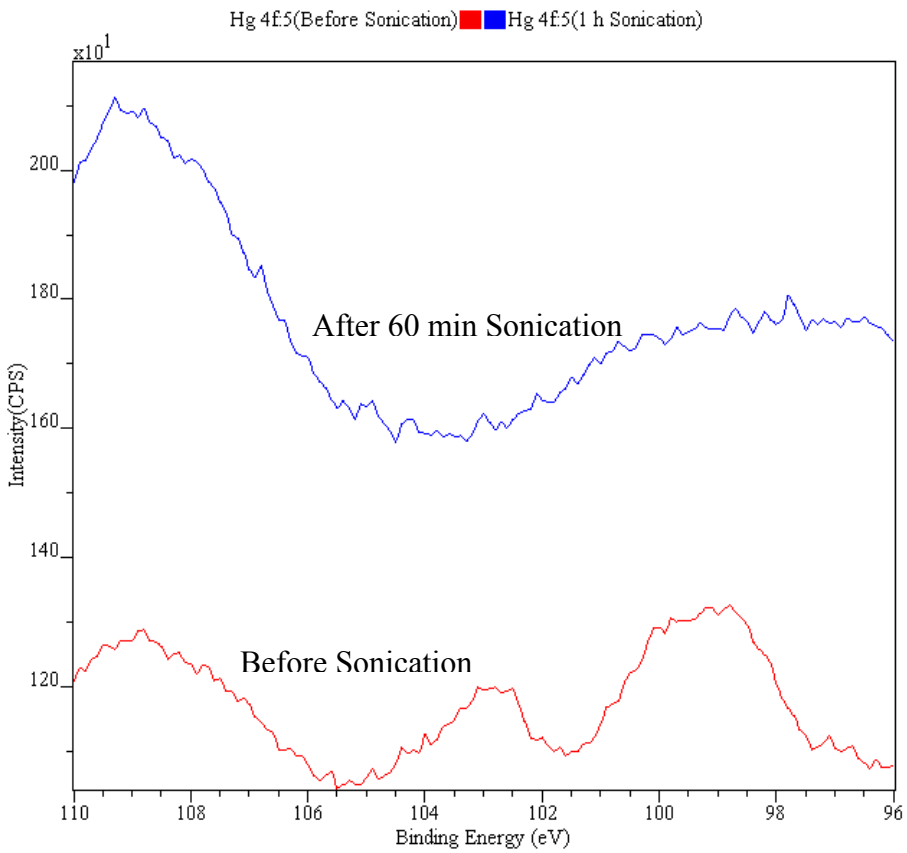

Figure 2.6 XPS spectra of Hg 4f before and after 60 min sonication (pH = 4.0, T = 20 °C, I = 0.1 M, [particle] = 33 g L^{-1}, $[Hg(II)]_{initial\ on\ particle}$ = 5.0 μmol g^{-1}, sonication power 36 W cm^{-2}).

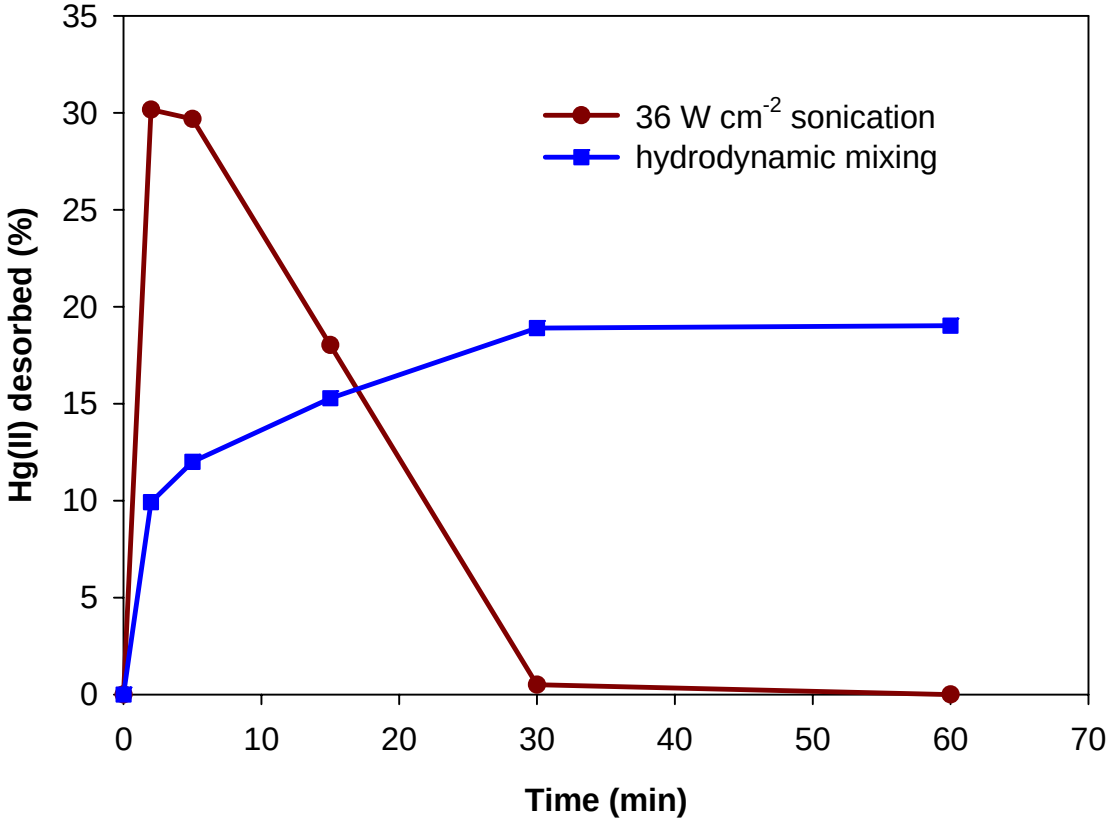

Figure 2.7 Desorption of Hg(II) from pre-sonicated alumina particles (pH = 4.0, I = 0.1M, [particle] = 33 g L^{-1}, $[Hg(II)]_{initial\ on\ particle}$ = 5.0 μmol g^{-1}, D_0 = 5 μm).

CHAPTER 3

SONOLYTIC DESORPTION OF MERCURY FROM ALUMINUM OXIDE: EFFECTS OF pH, CHLORIDE AND ORGANIC MATTER

(Submitted to *Environmental Science and Technology*, May 2006)

3.1 Abstract

The effects of pH, Cl^-, and humic acid (HA) on sonolytic desorption of Hg(II) from aluminum oxide were examined. Results showed that Hg(II) desorption was achieved by lowering the pH from 7 to 4. Ultrasound enhanced the initial Hg(II) release compared to both hydrodynamic mixing and that expected based on the Hg(II) sorption curve. However, longer sonication times led to decreases in Hg(II) desorption due to occlusion by aluminum hydroxide precipitation induced by ultrasound. The presence of Cl^- greatly improved Hg(II) desorption at pH 4 due to the formation of stable nonsorbing $HgCl_2$ complexes at low pH reducing free Hg(II) ion in solution. However, Cl^- did not affect Hg(II) desorption at pH 8 where $Hg(OH)_2$ is the dominant Hg complex rather than $HgCl_2$. Hg(II) desorption from HA-laden Al_2O_3 was dominated by HA. The greater the desorption of HA, the greater the desorption of Hg(II). Ultrasound enhanced initial Hg(II)

release through facilitating HA desorption. However, decreases in Hg(II) desorption were also observed by longer sonication times due to the re-association of desorbed HA back onto Al_2O_3 induced by sonication.

3.2 Introduction

Numerous studies have been conducted to examine Hg(II) sorption and/or release from synthetic and natural particles (*32*,*34*,*105*,*106*). As discrete particles or as coatings on other mineral surfaces in natural systems (*109*), crystalline and amorphous aluminas are efficient sinks for Hg in soil and sediment (*32*,*33*). Axe and Trivedi (*114*) studied the sorption of metal ions to hydrous metal oxides and concluded that intraparticle surface diffusion is an important rate-limiting step, requiring a lengthy period of time for sorption. Desorption of heavy metals from sediments can be much slower or nonreversible (*46*,*67*). This slow process may lead to long times for the cleanup of metal-contaminated sediments by washing, chemical extraction, thermal extraction, and bioremediation (*48*).

As an environmentally benign technology, sonochemistry has been widely explored for remediation (*68*). The mechanisms of sonochemical action are due to thermal, chemical, physical and mechanical effects. Briefly, ultrasound will cause the formation of cavitation bubbles leading to high localized temperatures and pressures (in excess of 5000 K and 500 atm, respectively), which induce chemical reactions resulting in the degradation of organic pollutants (*68*). Studies have been conducted on the application of ultrasound to degrade a variety of contaminants in water (*73*,*75*,*115*).

Besides thermal and chemical effects, the collapse of cavitation bubbles results in a variety of physical and mechanical effects which play an important role in heterogeneous systems. When solid particles exist in the vicinity of cavitation bubbles, the collapse may occur symmetrically or asymmetrically depending on the proximity and size of the solids (*82*). Symmetric cavitation generates shock waves which result in particle-particle collisions and cause extremely turbulent flow at the liquid/solid interface, referred to as microstreaming (increasing the rate of mass transfer near the surface). Asymmetric collapse leads to the formation of microjets of solvent which bombard the solid surface resulting in pitting and erosion. According to these effects, ultrasound has been applied to desorb and leach contaminants from soils and sediments (*75,92,95,137*).

In our previous work, sonolytic desorption of Hg(II) from Al_2O_3 was investigated at pH 4 (*138*). The effects of sonication power and duration of sonication were examined and the kinetics and mechanism of Hg(II) desorption were explored. However, the behavior of Hg in aquatic systems is mainly controlled by adsorption and desorption processes depending on aquatic parameters, particularly OH^-, Cl^-, and organic matter (*4,18*). Since it affects both particle surface charge characteristics and metal speciation (*36*), pH is an important factor controlling Hg(II) sorption determining Hg mobility and methylation (*32,37*). As a strong ligand for Hg(II), chloride (Cl^-) also is an important factor affecting Hg(II) speciation and sorption. Studies have shown that the addition of Cl^- significantly reduced Hg(II) adsorption in acidic conditions and resulted in a shift of sorption edge (*22,40,41*). Another significant factor affecting Hg sorption is natural organic matter (NOM). NOM, as a dissolved form, may inhibit Hg(II) adsorption to

sediments by competition with the sediment surface for Hg(II) ions. However, NOM itself may bind to mineral surfaces, enhancing Hg(II) adsorption through the formation of ternary complexes. In fact, it is the fractionation of NOM (dissolved vs adsorbed) that determines the behavior and distribution of Hg in sediments (*37*).

The purpose of this study was to examine the role of sediment matrix and solution parameters including pH, chloride, and organic matter on sonolytic desorption of Hg(II) from aluminum oxide.

3.3 Materials and Methods

3.3.1 Materials

Mercury (II) nitrate (99.99+%, Sigma-Aldrich) was used without further purification. Ionic strength and pH were adjusted with NaOH (Reagent ACS, Pellets 97+%, Fisher Scientific), HNO_3 (Trace Metal Grade, Fisher Scientific) and $NaNO_3$ (certified ACS, Fisher Scientific). NaCl (certified ACS, Fisher Scientific) was used as a source of Cl^-. Humic acid (HA) was extracted and purified from Pahokee peat following the method of Chen et al. (*115*). Water used to prepare the solutions was from a Millipore system (R = 18.2 MΩ-cm).

Aluminum oxide (adsorption grade Al_2O_3, 80-200 mesh particle size, density 4 g cm^{-3}) was purchased from Fisher Scientific. The particles had a surface area of 110 m^2 g^{-1} and an average diameter of 110 μm as tested by N_2 Brunauer-Emmett-Teller (BET) surface area analysis, and Malvern Mastersizer particle size analysis. X-ray diffraction (XRD) analysis revealed very poor crystallinity, mainly including Al_2O_3 (PDF#34-0493) as well as minor amounts of boehmite and amorphous alumina phases.

3.3.2 Experimental procedure and analyses

Sorption samples were prepared by shaking 15 mL of 0.75 mM Hg(II) stock solution (pH = 2.5, I = 0.1 M) with 2 g alumina particles in 60 mL polypropylene bottles on a rotating shaker at 350 rpm. Different adsorption curves were obtained in DI, 1.5 mM Cl^- or 900 mg L^{-1} humic acid solutions for various pH values. Solution pH was adjusted by manually adding 0.1 M HNO_3 or NaOH. After 24 hr the adsorption was observed to reach equilibrium, and the supernatant was separated from the particles by 15 min centrifugation at 1500 rpm. Samples of supernatant were analyzed for Hg(II) and/or total organic carbon (TOC), and the Hg-laden particles were used for sonolytic and hydrodynamic mixing desorption experiments. The amount of Hg(II) and humic acid adsorbed on solids was calculated from the difference between those in the stock solution and those remaining in the supernatant solution.

For sonolytic desorption experiments, 2 g of Hg-laden particles were transferred to a glass rosette reactor with 60 mL of 0.1 M ionic strength solution. Batch desorptions were carried out at pH 4.0 or pH 8.0 controlled with a PHM290 pH-Stat autotitrator (Radiometer Analytical, France). A 20 kHz ultrasonic probe system (550 Sonic Dismembrator, Fisher Scientific) was used for sonication experiments at a power intensity of 36 W cm^{-2} as measured by calorimetry (*138*). The probe tip was located near the bottom of the reactor to ensure particles were well mixed throughout the reactor. The reactor was water-jacketed to control the reacting solution temperature at 20.0 ± 0.5 °C by a cooling bath.

For comparison purposes, hydrodynamic mixing experiments were conducted in another glass rosette reactor (with the same geometry as the sonication reactor) and mixed by circulation at a flow rate of 1.2 L min^{-1} driven by an Economy Drive peristaltic pump with a Model 7518-12 Easy-Load peristaltic pump head (MasterFlex® L/S™, Cole Parmer) and Tygon tubing. All other conditions, such as solid to liquid ratio, pH and temperature, were the same as those used with sonolytic desorption.

After selected times of desorption, samples were transferred to polypropylene centrifuge bottles and ultracentrifuged for 20 min at 17000 rpm using a centrifuge (Model J2-21, Beckman) to separate the supernatant and particle fractions. The amount of Hg(II) desorbed from the solids was determined by analysis of the supernatant. Control experiments and selected experiments were performed in duplicate or triplicate to determine the data error and verify reproducibility.

Prior to Hg(II) analysis, solution samples were oxidized overnight with 5% BrCl followed by reduction with 30% NH_2OH•HCl. Hg(II) samples were analyzed by cold vapor atomic absorption spectroscopy (CVAAS) (SpectrAA 880Z, Varian, Australia) using a 25% $SnCl_2$ (98%, Sigma-Aldrich) and 20% HCl (Trace Metal Grade, Fisher Scientific) reductant solution. TOC was measured by a Shimadzu TOC-5000A analyzer.

3.4 Results and Discussion

3.4.1 Hg(II) adsorption curves

Before desorption experiments, the effects of pH, Cl^-, and organic matter on Hg(II) adsorption to Al_2O_3 were examined. Figure 3.1 shows the curves of Hg(II) adsorption versus pH with and without the presence of Cl^- or humic acid. Without the

presence of ligands, Hg(II) adsorption has a pH edge from pH 3 to pH 4. Below pH 3, little adsorption occurred, whereas above pH 3, there was a sudden increase in Hg(II) adsorption. This is in agreement with previous studies of Hg(II) adsorption on (hydr)oxides and modeling of this system (*32*,*34*,*40*). However, unlike previous studies (*32*,*34*,*40*), we did not observe a slight decrease of Hg(II) adsorption with a continued increase of pH up to 8. Since the surface potential continued to decrease with increasing pH favoring Hg(II) adsorption, the slight decrease of Hg(II) adsorption with further pH increase was attributed to Hg(II) species transition from $HgOH^+$ to $Hg(OH)_2$ (*40*). Al_2O_3 used in this study consisted of particle aggregates possessing mesopores or macropores as well as micropores as determined by surface area and particle size analyses (*138*). Thus, $Hg(OH)_2$ likely precipitated in mesopores and macropores as well as adsorbing on micropore sites, causing no decreases in Hg(II) adsorption with pH increase. A similar result was observed in an activated carbon system (*139*).

The presence of Cl^- greatly decreased Hg(II) adsorption at low pH shifting the adsorption edge to higher pH values. As shown in Figure 3.1, there was little Hg(II) adsorption below pH 5, whereas a sudden increase in Hg(II) adsorption occurred at pH 6. This higher pH sorption edge compared to without Cl^- was due to the formation of stable, nonsorbing aqueous $HgCl_2$ complexes in solution limiting the amount of available free Hg(II) to adsorb on Al_2O_3 at low pH. At higher pH values, $Hg(OH)_2$ is the dominant Hg(II) species, leading to no Cl^- effect on Hg(II) adsorption. All these observations are consistent with previous studies (*32*,*34*,*40*).

The effect of humic acid on Hg(II) adsorption showed an obvious difference from the effect of Cl^-. At low pH values, HA enhanced Hg(II) adsorption compared to Hg(II)

alone, and the adsorption increased with pH, reaching a maximum at pH 5. At high pH values, a slight decrease in Hg(II) adsorption occurred. At high pH, strong complexes between HA and Hg(II) dominate the Hg species. The effects of organic matter on Hg(II) adsorption to alumina, goethite and soils were found to be dependent on the distribution of organic matter between solid and liquid phases (*140,141,45*). However, previous studies showed that the highest Hg(II) adsorption occurred at low pH, not in the middle of the pH range as observed in this study (pH 5).

To explore this difference, the adsorption of HA as a function of pH was determined by measuring solution TOC. As shown in Figure 3.2, nearly all of the HA was adsorbed below pH 5 and then a significant decline occurred with only 67% adsorption at pH 8.3. The maximum Hg(II) adsorption did not correlate to that of HA adsorption and the extent of the decrease in Hg(II) adsorption at higher pH values was less than the decline in HA adsorption. Therefore, under the conditions in this study, HA affected Hg(II) adsorption, but did not completely dominate Hg(II) adsorption. The high initial Hg(II) to HA ratio of 167 μg Hg mg^{-1} C of HA in our work was much higher than 10 μg of Hg mg^{-1} of DOM due to Hg binding to oxygen functional groups (*19*). Thus, at the Hg(II) to HA ratio in this study, free Hg(II) ions were still available to adsorb to Al_2O_3 in addition to Hg(II)-HA complexes. The free Hg(II) ions in solution obeyed the adsorption curve for Hg(II) without HA, explaining the lack of correlation between Hg(II) adsorption and HA adsorption versus pH values.

3.4.2 The effect of pH on the desorption of Hg(II)

After 5 μmol g^{-1} of Hg(II) was adsorbed on Al_2O_3 at pH 7, 0.1 M of $NaNO_3$ Hg(II)-free solution was replaced to examine the pH effect on Hg(II) desorption. First, the desorption of Hg(II) was conducted at pH 8. Although dissolved Hg(II) was detected, no obvious Hg(II) desorption at pH 8 was observed for either ultrasound or hydrodynamic mixing (data not shown). This result is reasonable based on the pH dependent Hg(II) adsorption curve (Figure 3.1).

Based on Figure 3.1, lowering solution pH will change the adsorption/desorption equilibrium, leading to desorption of mercury. As expected, the desorption of Hg(II) from Al_2O_3 at pH 4 occurred (Figure 3.3). During short desorption times, release of Hg(II) from alumina particles by sonication was enhanced compared to hydrodynamic mixing. After 2 min desorption, 33% of Hg(II) was released by ultrasound compared to 8% by hydrodynamic mixing. With longer sonication times, the Hg released by sonication decreased, while desorption by hydrodynamic mixing appeared to approach equilibrium. At 60 min, much less desorption occurred by sonication (3%) than by hydrodynamic mixing (14%).

Expected Hg(II) desorption at equilibrium at pH 4 based on the adsorption curve (Figure 3.1) is approximately 15%. At 60 min desorption, hydrodynamic mixing approached this equilibrium, suggesting that the Hg(II) adsorption on Al_2O_3 was reversed by lowering pH. This result is in agreement with the work of Gao et al. (*67*) indicating complete desorption of freshly sorbed Cd and Pb occurred by lowering pH. In our work, however, desorption higher than 15% was not achieved due to the equilibrium

desorption/sorption conditions at pH 4. Based on Figure 3.1, we expect that complete desorption would occur at pH < 3.

Sonication enhanced the initial desorption of Hg(II) through the extreme conditions generated by cavitation bubbles. Enhanced desorption may be due to an altered chemical equilibrium and improved kinetics of desorption. Ultrasonic energy may shift the adsorption/desorption equilibrium to a new equilibrium. For example, Bathen (*122*) found that the equilibrium of fructose adsorbed on Amberlite resin was shifted to lower sorbed concentrations by sonication. Li et al. (*123*) also reported similar results for a phenol and resin system. In this study, the desorption of Hg(II) by sonication reached 33% at 2 min, much higher than the expected 15% at pH 4 based on the adsorption curve (Figure 3.1), indicating that ultrasound altered the chemical equilibrium of Hg(II). In addition, ultrasound may enhance the rate of desorption by accelerating mass transfer through intraparticle micropores, often the limiting step for desorption. For example, the intrinsic mass transfer coefficient of benzyl chloride through a Na_2S-liquid interfacial film were increased by a factor of 2 - 3 in the presence of ultrasound (*124*).

The decrease in Hg(II) desorption with prolonged sonication was due to ultrasonic effects on the changes of the surface properties of Al_2O_3 particles. As previously demonstrated (*138*), ultrasound reduced Al_2O_3 particle size and altered surface morphology but did not significantly change surface area. In addition, the particle surface point of zero charge decreased and supersaturated Al solution conditions were observed. Occlusion by aluminum hydroxide precipitation induced by ultrasound was proposed as the primary mechanism for the reduction in Hg(II) desorption with longer sonication times.

3.4.3 The effect of chloride on the desorption of Hg(II)

Hg(II) desorption in the presence of Cl^- (0.5 mM) was not observed at pH 8 (data not shown) because Cl^- did not affect the adsorption/desorption equilibrium of Hg(II) at this pH value. As shown in Figure 3.4, the presence of Cl^- greatly enhanced Hg(II) desorption for both ultrasound and hydrodynamic mixing at pH 4 compared to in its absence (Figure 3.3). For hydrodynamic mixing, 80% of Hg(II) was desorbed at 60 min, much higher than 15% without Cl^- present in solution. For ultrasound, quick initial desorption, 87% at 5 min, occurred compared to 18% without Cl^-. However, similar to Hg(II) without additional ligands, a decrease in Hg(II) desorption with longer sonication times was observed.

The presence of ligands in solution will complex metals reducing free metal ion activity. Complexation with Cl^- acts as a sink for Hg driving more Hg into solution. Gao et al. (*67*) showed that 90% of freshly sorbed Pb and Cd were desorbed from sediment at pH 7-8 using Ethylenediaminetetraacetic acid (EDTA) to sequester aqueous Pb and Cd. In this study, the strong Hg-Cl complexes reduced available free Hg(II) ions in solution and affected the adsorption/desorption equilibrium, subsequently enhancing Hg(II) desorption.

The maximum desorption by hydrodynamic mixing was below 90% as expected based on the adsorption curve (Figure 3.1) indicating that not all the adsorbed Hg(II) was readily desorbed. The reason for this was probably due to the lack of Cl^- to form stable nonsorbing aqueous $HgCl_2$ complexes, the short desorption time, or nonreversible adsorption. Additional experiments with higher Cl^- (15 mM) did not show higher Hg(II) desorption (data not shown). Thus, slow desorption or nonreversible adsorption likely

contributed to this observation. Ultrasound enhanced Hg(II) desorption at short sonication times overcoming slow desorption or nonreversible desorption. However, the observed occlusion by aluminum hydroxide precipitation induced by ultrasound with longer sonication times appeared to obscure complete desorption in the presence of Cl^-.

3.4.4 The effect of organic matter on the desorption of Hg(II)

The behavior of Hg in soil and sediment is primarily controlled by the distribution of natural organic matter between sorbed and dissolved fractions (*37,45,46,142*). Therefore, humic acid (HA) extracted from Pahokee peat was used to simulate the effect of natural organic matter on Hg(II) desorption. 5 μmol g^{-1} Hg(II) and 5.5 mg C g^{-1} of HA were adsorbed on Al_2O_3 at pH 6 (Figure 3.1). Then desorptions of Hg(II) and HA were examined at pH 8 and the results are shown in Figure 3.5 and Figure 3.6.

As shown in Figure 3.5, Hg(II) desorption occurred at pH 8 for both sonication and hydrodynamic mixing although desorption was very low in both cases. Sonication improved the initial Hg(II) desorption. Between 2 and 5 min of desorption, 4% of Hg(II) was released by ultrasound compared to 1% by hydrodynamic mixing. Similar to in the absence of HA, longer sonication times led to decreases in Hg(II) desorption, while desorption by hydrodynamic mixing appeared to approach equilibrium. At 60 min, desorption by sonication (1%) became lower than that by hydrodynamic mixing (2.5%).

Recalling that no Hg(II) desorption was seen at pH 8 without HA, desorption of Hg(II) observed was clearly due to HA. Comparing Figure 3.5 and Figure 3.6, it is obvious that HA desorption has a similar trend and percentage to Hg(II) desorption,

indicating that Hg(II) desorption was controlled by HA behavior. HA may consequently release complexed Hg(II) when it was desorbed from Al_2O_3. Thus, the higher the desorption of HA, the higher the desorption of Hg(II).

Although it is difficult to desorb HA from Al_2O_3 because of the large molecular size and multifunctional groups forming polynuclear surface complexes (*143*), ultrasonic energy enhanced HA desorption. Enhanced initial Hg(II) desorption is attributed to enhanced initial HA desorption by ultrasound. However, decreases in HA desorption also occurred with prolonged sonication (Figure 3.6). The decrease in Hg(II) desorption observed in Figure 3.5 accompanied the decrease in HA desorption. Since HA is an organic compound, one possibility for the decrease in HA desorption with longer sonication is degradation by thermal and chemical effects of ultrasound. However, in a control experiment, no TOC reduction for Pahokee HA was observed with up to 4 hr sonication. Therefore, the decline of HA desorption was not attributed to mineralization caused by ultrasound; rather, HA released at short times re-associated with the solid particles with continued sonication.

The re-association of HA with the particles with longer sonication may be due to a number of different processes. First, as previously demonstrated (*138*), although sonication did not increase particle surface area, ultrasound dramatically broke down particle aggregates to expose intraparticle pores. In fact, the adsorption density of HA in this study (0.05 mg m^{-2}) was much lower than that (2 mg m^{-2}) observed by Ochs et al. (*92*). Thus, some of the exposed surface was not available for HA to adsorb before sonication. Longer sonication may have provided more absorption sites for HA, leading to the resorption of initially desorbed HA. Next, although mineralization of HA was not

observed by sonication, HA functional groups changed due to sonication (*115*). An increase in acidity with increased sonication indicated more carboxylic and phenolic functional groups on HA were produced, leading to higher adsorption of HA to Al_2O_3. Thirdly, besides changing HA functional groups, sonication also decreased the average molecular weight of Pahokee peat humic acid from 4200 Da to 3400 Da (*115*). The small HA molecules generated by ultrasound may have been adsorbed into micropores not available to larger initial HA molecules. Finally, a high molecular weight class (beyond 100000 Da) of humic acid formed by sonication was observed previously (*115,144*). This high molecular weight class of HA is expected to be more easily adsorbed to Al_2O_3 than smaller MW HA.

In addition, supersaturated aluminum solutions were observed after 15 min sonication (*138*). As seen in Figure 3.6, HA desorbed by ultrasound also began to decrease by 15 min sonication. Similar to coagulation in water treatment (*145*), this oversaturation of Al(III) ions produces aluminum hydroxide precipitates, forming "sweep flocs" that enmesh HA. Therefore, the enmeshment of HA induced by supersaturated aluminum solutions caused by ultrasound may be another reason for the decreases in HA desorption with longer sonication times.

In summary, sediment matrix parameters including pH, chloride, and organic matter affected sonolytic desorption of Hg(II) from Al_2O_3. Information obtained in this study will help to understand sonolytic release of Hg from Hg-contaminated particles and provide insight on the application of ultrasound to remediate mercury from sediments. For example, low pH conditions and the presence of Cl^- may facilitate sonolytic release of Hg from sediments; alkaline conditions could favor sonolytic release of Hg from

sediment with high organic matter content. Decreases in Hg(II) desorption occurred with longer sonication times under all conditions due to ultrasonically induced changes in Al_2O_3 properties. This observation suggests that caution should be taken with the duration of sonication when applying this technology to remediation of sediment to avoid re-association of desorbed Hg(II) with sediments.

Acknowledgements

Funding from NOAA/Ohio Sea Grant College Program and the NSF Environmental Molecular Science Institute at The Ohio State University is gratefully acknowledged. The authors thank S. Jones and J. Bigham for their help with XRD and N_2 BET measurements.

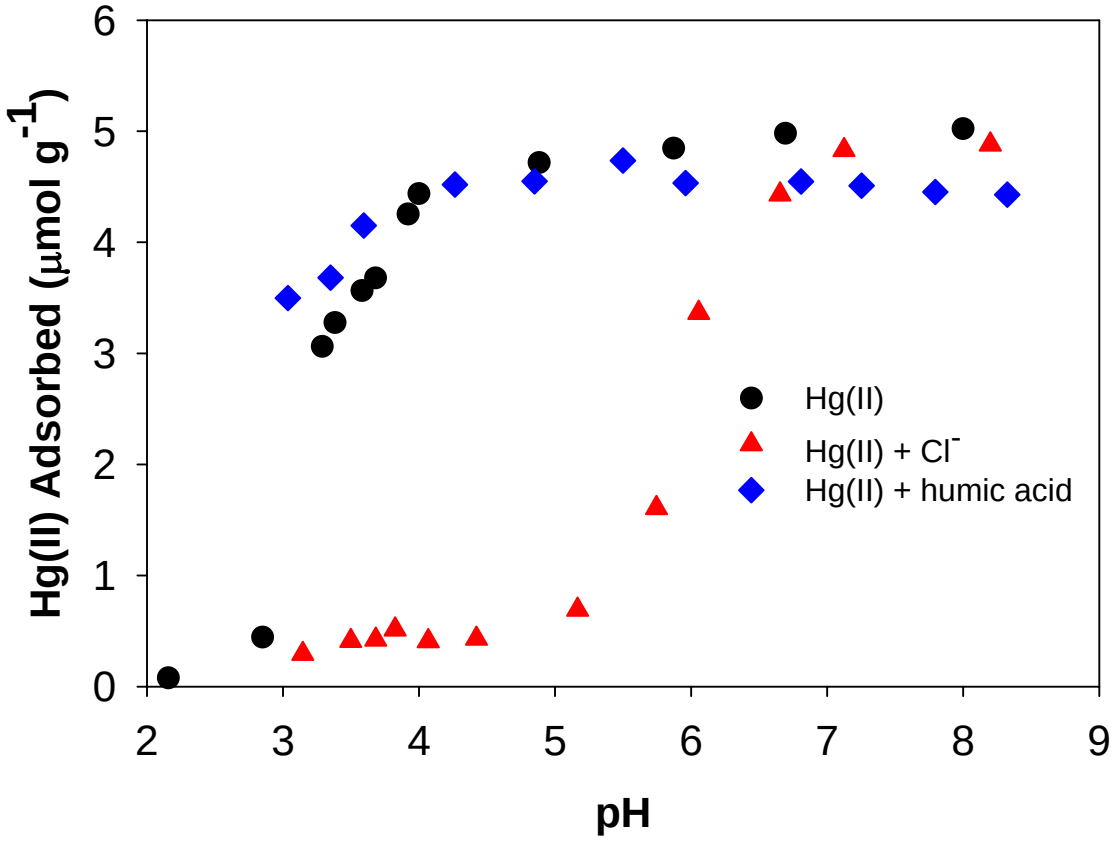

Figure 3.1 Hg(II) adsorption to alumina particles in the absence and presence of chloride or humic acid (I = 0.1 M, $[Hg(II)]_0$ = 0.75 mM, $[Cl^-]_0$ = 1.5 mM, $[HA]_0$ = 900 mg L^{-1}, [particle] = 133 g L^{-1}, 24 hr equilibrium).

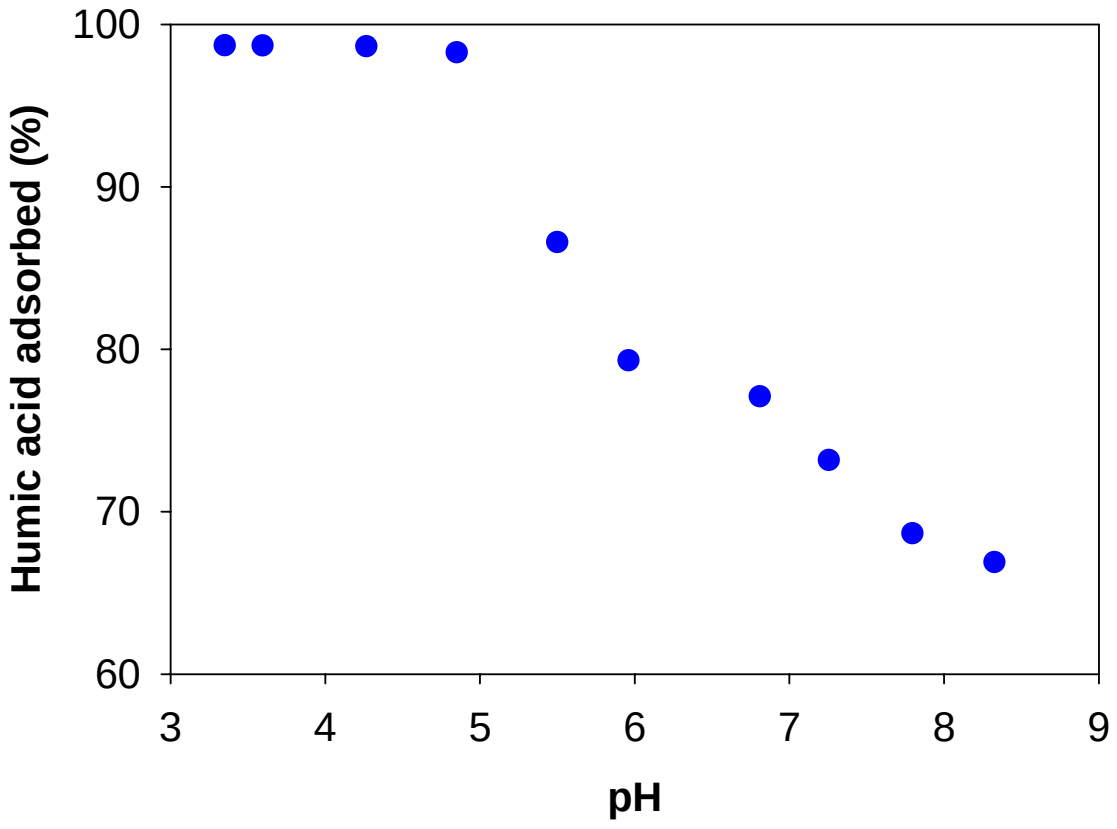

Figure 3.2 Humic acid adsorption to alumina particles (I = 0.1 M, $[Hg(II)]_0$ = 0.75 mM, $[HA]_0$ = 900 mg L^{-1}, [particle] = 133 g L^{-1}, 24 hr equilibrium).

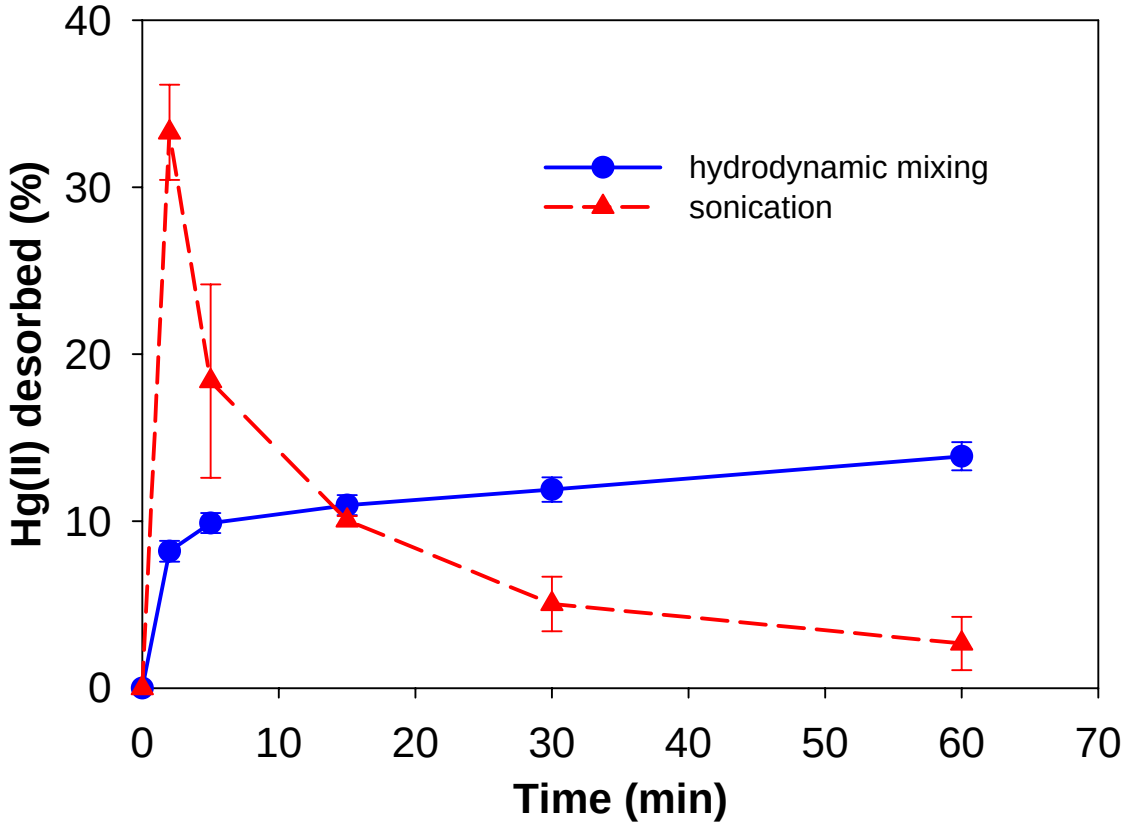

Figure 3.3 Desorption of Hg(II) from alumina particles (pH = 4.0, T = 20 °C, I = 0.1 M, [particle] = 33 g L^{-1}, $[Hg(II)]_{initial\ on\ particle}$ = 5.0 μmol g^{-1}, sonication intensity 36 W cm^{-2}).

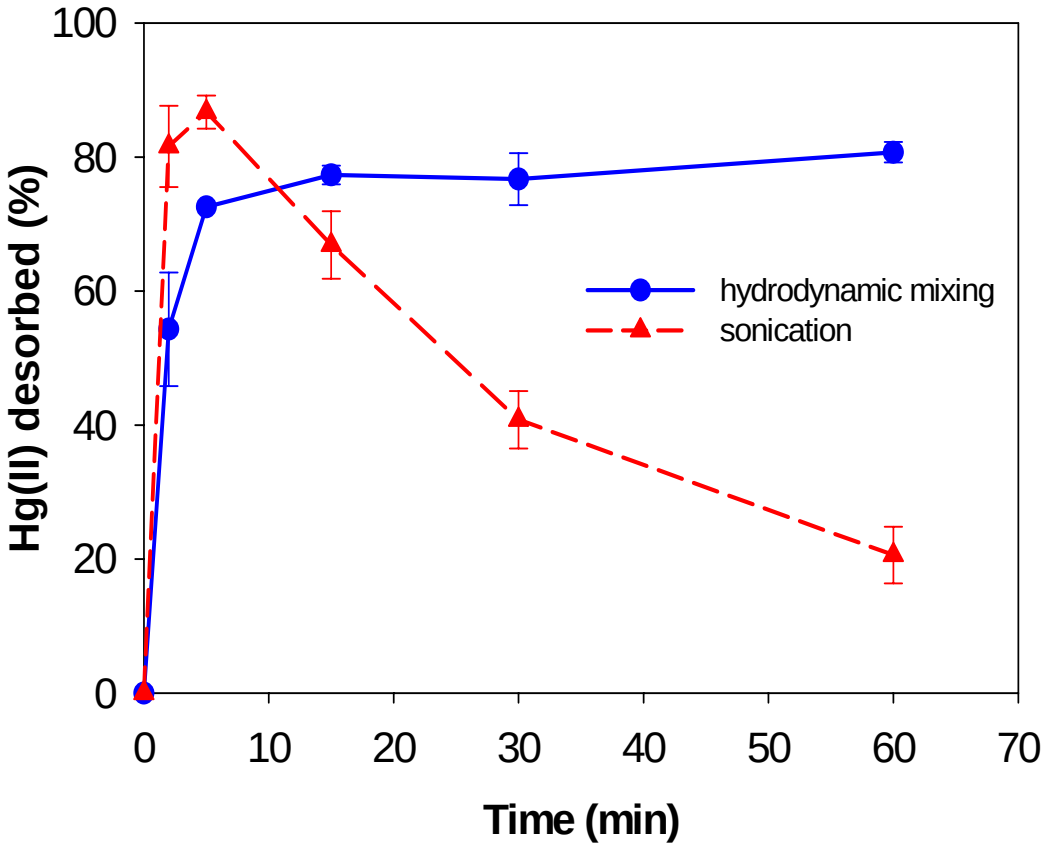

Figure 3.4 Desorption of Hg(II) from alumina particles in the presence of chloride (pH = 4.0, T = 20 °C, I = 0.1 M, $[Cl^-]_0$ = 1.5 mM, [particle] = 33 g L^{-1}, $[Hg(II)]_{initial\ on\ particle}$ = 5.0 μmol g^{-1}, sonication intensity 36 W cm^{-2}).

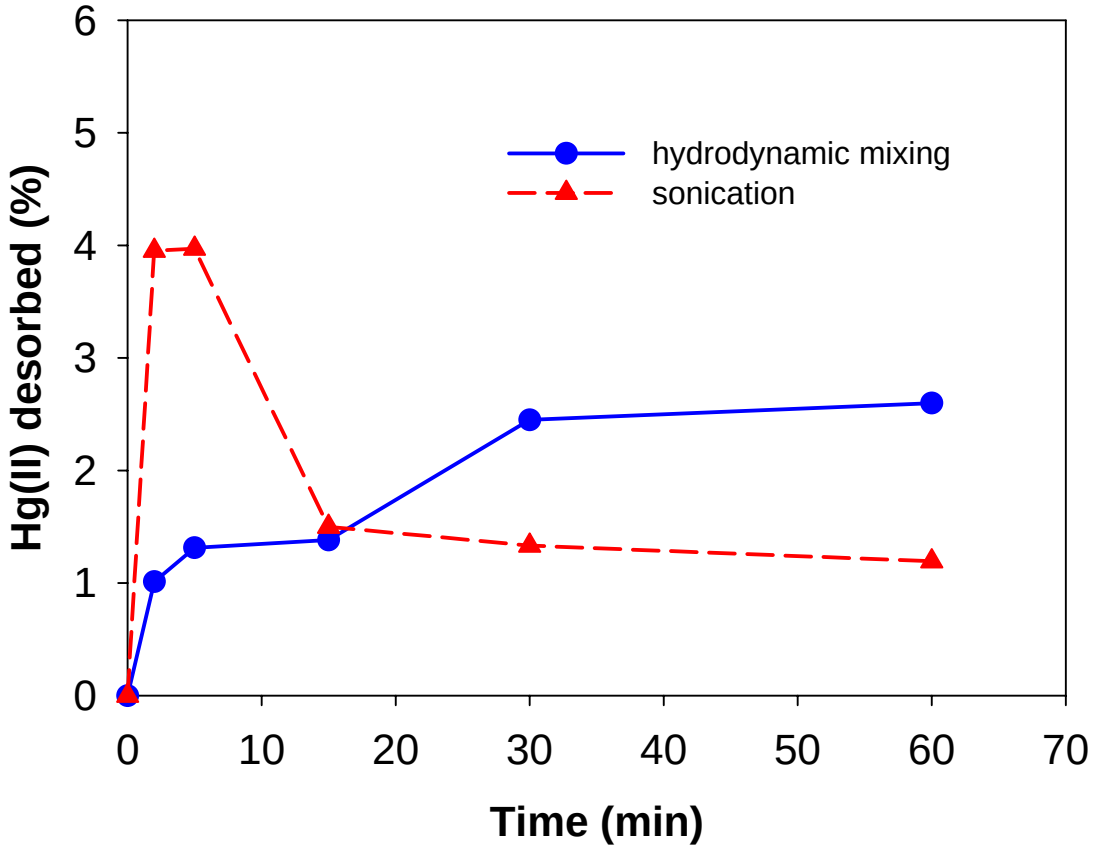

Figure 3.5 The desorption of Hg(II) from alumina particles laden with humic acid (pH = 8.0, T = 20 °C, I = 0.1 M, [particle] = 33 g L^{-1}, $[Hg(II)]_{initial\ on\ particle}$ = 5.0 μmol g^{-1}, $[HA]_{initial\ on\ particle}$ = 5.5 mg C g^{-1}, sonication intensity 36 W cm^{-2}).

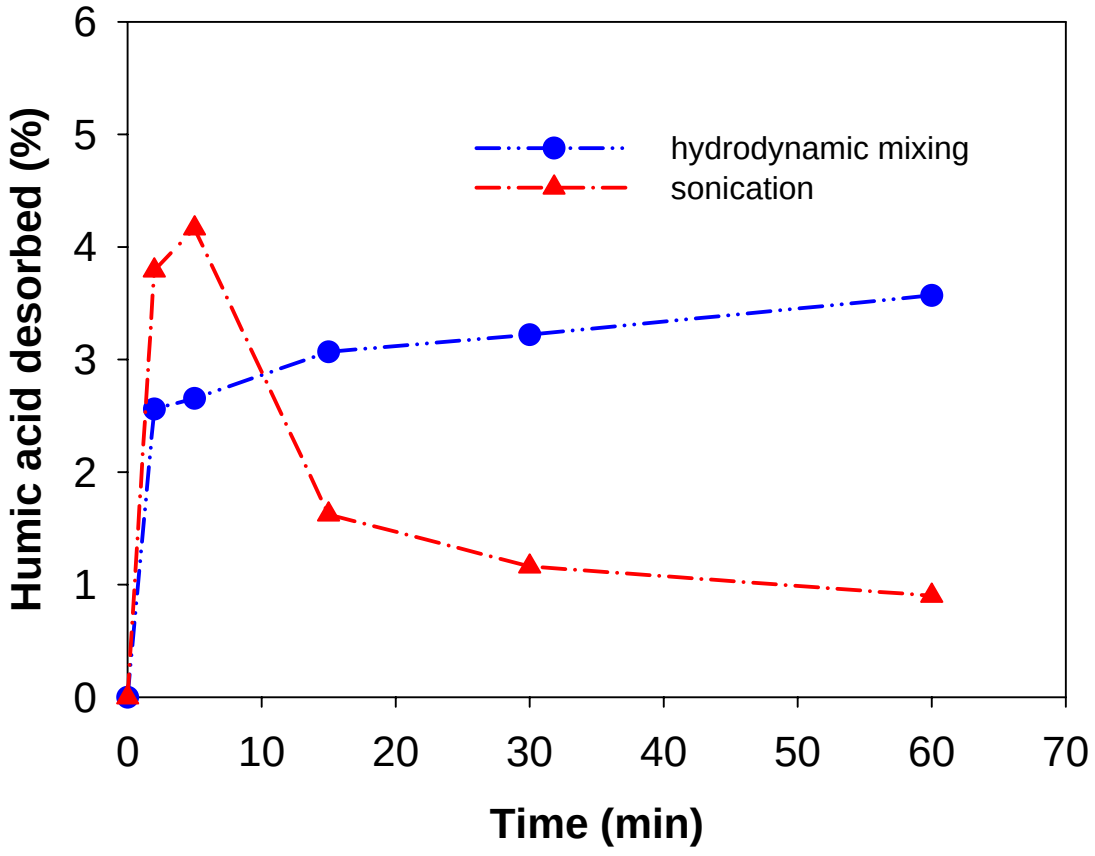

Figure 3.6 The desorption of humic acid from alumina particles (pH = 8.0, T = 20 °C, I = 0.1 M, [particle] = 33 g L^{-1}, $[Hg(II)]_{initial\ on\ particle}$ = 5.0 μmol g^{-1}, $[HA]_{initial\ on\ particle}$ = 5.5 mg C g^{-1}, sonication intensity 36 W cm^{-2}.

CHAPTER 4

RELEASE OF MERCURY FROM CINNABAR (α-HgS) BY SONOCHEMICAL DISSOLUTION

(Submitted to *Environmental Science and Technology*, June 2006)

4.1 Abstract

The application of ultrasound for the dissolution of cinnabar was investigated to determine sulfur oxidation products (S_{ox}) and dissolved Hg(II) released into aqueous solution. Detected S_{ox}, mainly SO_4^{2-}, in the presence of ultrasound suggests that dissolution of cinnabar occurred. Terephthalic acid (TA) used to scavenge •OH showed that •OH was the predominant oxidizing species in initiating the dissolution reaction, but not the only pathway. Hg(II) release rates were much lower than those of S_{ox}. Hg(II) adsorption curves indicated that dissolved Hg(II) adsorbed back onto the remaining cinnabar particles lowering Hg(II) release. Ultrasound significantly reduced cinnabar particle size and increased surface area, leading to higher Hg(II) adsorption. In addition, the cinnabar surface isoeletric point (IEP) increased after sonication, indicating adsorption of Hg(II) and/or mineral phase transformation from cinnabar to metacinnabar. The presence of humic acid (HA) and ultrasound enhanced cinnabar dissolution and

greatly increased the dissolved Hg(II) concentration due to the synergistic effects of ultrasound and HA.

4.2 Introduction

The main precursor of Hg methylation in aquatic systems is soluble inorganic Hg, Hg(II). Scavenging of soluble Hg(II) by sediments may inhibit the production of methylmercury (*4*). The main mechanisms which control Hg distribution in sediments are its strong association with organic matter and sulfur (*4*,*146*). Mercury sulfide (HgS) in sulfidic waters, sediments, and soils has been postulated as one of the largest sinks for Hg (*4*). Both spectroscopic determination and indirect extraction analyses have confirmed that HgS is the major fraction of Hg in sediments (*106*,*146*,*147*).

Cinnabar (red, α-HgS) and metacinnabar (black, β-HgS) are the most common forms of HgS in the natural environment (*146*,*148*). Serving as a natural sink for Hg, HgS is very insoluble and much less leachable compared to other Hg species. However, oxidation of reduced S(-II) (*25*,*26*,*27*) and strong complexes of Hg(II) with many ligands such as polysulfides and dissolved organic matter (DOM) impact the efficiency of HgS in immobilizing Hg (*28*,*29*,*30*). Leached aqueous Hg contributes to an increase in Hg availability for methylation and bioaccumulation (*4*). Therefore, leaching of Hg from HgS is very important for understanding the role of cinnabar in immobilizing Hg.

The mechanisms of sonochemical techniques result from thermal, chemical, and physical phenomena due to the formation of cavitation bubbles (*68*). Inside cavitation bubbles, high temperatures and pressures (in excess of 5000 K and 1000 atm, respectively) (*149*) cause the dissociation of water and volatile compounds by direct

thermolysis, which generates highly reactive species including •OH, H•, HO_2•, and H_2O_2 (*68*,*149*). Relatively high temperatures and concentrated •OH exist at the interfacial region between cavitation bubbles and bulk solution. In bulk solution, secondary chemical reactions occur between surviving reactive species and solute molecules. Physical phenomena (shock waves, microjets, etc.) induced by ultrasound (*149*) play an important role in heterogeneous systems. For example, extremely turbulent flows at the liquid/solid interface increase the mass transfer rate. Shock waves and microjets result in particle size reduction and surface erosion. All these high-energy phenomena may lead to changes in solid surface properties.

Ultrasound has been applied to destroy or accelerate the destruction of pollutants (*71*,*75*,*115*). For example, Kotronarou et al. (*71*) observed rapid oxidation of S(-II) into SO_4^{2-}, SO_3^{2-}, $S_2O_3^{2-}$ by ultrasound. Ultrasound also has been shown to desorb contaminants from soils and sediments (*75*,*95*,*138*) and dissolve metal oxides and metal sulfides (*84*,*97*,*138*). In a system similar to HgS, Sostaric et al. (*97*) found ultrasound-induced dissolution of colloidal CdS. Therefore, ultrasound is expected to cause HgS dissolution and release of Hg.

The purpose of this study was to investigate Hg(II) release from cinnabar by sonochemical dissolution. Cinnabar was chosen in this study because it is the most stable HgS form in the natural environment. In addition, in developing sonication as a means to remediate contaminated sediments, an understanding of Hg release from various possible sediment sorption sites is necessary. The specific goals were to demonstrate ultrasonic oxidation of S in cinnabar, to determine the release of Hg(II) into aqueous phase, and to characterize ultrasonic effects on cinnabar particles. DOM effects on the dissolution of

cinnabar by ultrasound were also examined in this study because of its extensive interaction with Hg in natural waters and sediments and its ability to inhibit reactions with •OH generated from ultrasound (*28*,*29*,*75*,*150*).

4.3 Experimental Section

4.3.1 Materials and Procedure

Cinnabar (99.5%, Fisher Scientific) was used without further purification. X-ray diffraction (XRD) analysis revealed a very crystalline cinnabar phase. The particles had a surface area of 0.90 ± 0.02 $m^2 g^{-1}$ as determined by BET N_2 analysis. Ionic strength and pH were adjusted with NaOH, HNO_3 and/or $NaNO_3$ purchased from Fisher Scientific. Humic acid (HA) was extracted and purified from Pahokee peat following the method of Chen et al. (*115*). Water used to prepare the solutions was from a Millipore system (R = 18.2 MΩ-cm).

For ultrasonic dissolution, cinnabar particles were transferred to a glass rosette reactor with 60 mL of 0.01 M $NaNO_3$ solution with or without 8.5 mg C L^{-1} of HA. Batch reactions were carried out using a 20 kHz ultrasonic probe system (550 Sonic Dismembrator, Fisher Scientific) at a power input intensity of 18 W cm^{-2} measured by calorimetry (*151*). The reacting solution temperature was controlled at 20.0 ± 0.5 °C by a cooling bath. A solution pH of 4 was controlled with a pH-stat autotitrator. For comparison purposes, mechanical shaking experiments were conducted on a rotating shaker at 200 rpm without sonication under the same experimental conditions as those with sonication. After selected reaction times, samples were centrifuged for 15 min at 5000 rpm to separate the supernatant and the particles. Aliquots from supernatant were

used for Hg(II), S(-II), SO_4^{2-}, SO_3^{2-}, $S_2O_3^{2-}$, and total organic carbon (TOC) analyses. Particle pastes were freeze-dried for surface area, XRD, surface IEP, and scanning electron microscope (SEM) analyses. Selected experiments were performed in duplicate or triplicate to determine data error and verify reproducibility.

Hg(II) adsorption onto cinnabar particles was conducted in polyethylene bottles. 0.1 g cinnabar was added to each bottle filled with 60 mL solution of various initial Hg(II) concentrations with solution conditions identical to dissolution reactions. The bottles were placed on a rotating shaker at 200 rpm for 24 hr which was observed to reach equilibrium in control experiments. The supernatant and particles were separated by centrifugation. The amount of Hg(II) adsorbed on cinnabar was determined from the difference between Hg(II) in initial solution and that remaining in the supernatant solution.

•OH produced by ultrasound was measured by TA dosimetry modified from the method of Mason et al. (*151*). Solution pH was controlled by a pH-stat autotitrator instead of phosphate buffer to avoid the formation of Hg(II)-phosphate complexes. pH 8 was chosen instead of pH 4 used in dissolution reactions to make sure that TA was present as terephthalate ion. Control experiments showed insignificant differences in cinnabar dissolution between pH 4 and pH 8 without TA. The product of TA reacting with •OH, 2-hydroxyterephthalic acid (HTA), was measured by a RF-5301 fluorescence spectrophotometer (Shimadzu) following the method of Frim et al. (*152*).

4.3.2 Analyses and characterization

Solution Hg(II) was analyzed by cold vapor atomic absorption spectroscopy (CVAAS) (SpectrAA 880Z, Varian). S(-II) was measured by a spectrophotometer (Thermo Spectronic) at 600 nm following the method of Ravichandran et al. (*12*). SO_4^{2-}, SO_3^{2-}, and $S_2O_3^{2-}$ were determined by ion chromatography (DX 500, Dionex). HA was measured by a Shimadzu TOC-5000A analyzer.

Surface area, IEP, XRD, and SEM were used to characterize cinnabar particle changes resulting from sonication. Surface areas were determined using BET N_2 with a surface area analyzer (Micromeritics® FlowSorb 2300). IEP was determined from ζ-pH curves. ζ was measured by a zeta potential analyzer (90 plus, BIC) at a cinnabar concentration of 1.67 g L^{-1} at different pH values. XRD analyses were conducted with an X-ray diffractometer (Philips Analytical). An SEM (Philips XL-30) operated at 12 kV was used to study particle size and morphology changes.

4.4 Results and Discussion

4.4.1 Sonochemical dissolution of cinnabar based on S_{ox} products

To investigate the dissolution of cinnabar, S oxidation products (S_{ox}) and Hg(II) released into solution from cinnabar were measured. No measurable S_{ox} or dissolved Hg(II) was detected by mechanical shaking indicating no dissolution of cinnabar under the experimental conditions without ultrasound. This was expected due to the extreme insolubility of cinnabar in the absence of ligands or oxidants. Ravichandran et al. (*12*) also found no measurable dissolution of Hg from cinnabar in distilled water. In a metacinnabar system, Barnett et al. (*27*) found dissolved Hg(II) in the presence of

bubbling air. However, Hg(II) levels observed were below the detection limit in this study (2.5 nM). Thus, our results are not inconsistent with previous results.

Next, the possibility of dissolution of cinnabar in the presence of ultrasound was examined. Figure 4.1 shows that SO_4^{2-} was the main S_{ox} product and production increased linearly with sonication time. With higher cinnabar concentration, higher SO_4^{2-} production was observed. The formation of intermediates (SO_3^{2-} and $S_2O_3^{2-}$) was only detected initially at a cinnabar concentration of 1.67 g L^{-1}. With longer sonication times, the concentrations of $SO_3^{2-}$and $S_2O_3^{2-}$ decreased and became nondetectable.

Sulfur in cinnabar is the only source of S_{ox} in the reactor; thus, the production of S_{ox} indicates that sonication dissolved cinnabar through oxidation reactions. Higher S_{ox} production with higher cinnabar concentration coupled with the observation that SO_3^{2-} and $S_2O_3^{2-}$ were produced at only high cinnabar concentration suggests that the availability of S from cinnabar reaction sites may be the reaction-limiting step. However, the dissolution rate decreased with the increase of cinnabar concentration (Table 4.1), indicating that the reaction-limiting step was not the availability of S from cinnabar, but the available oxidants generated from ultrasound.

•OH, HO_2•, H_2O_2 and/or thermolysis generated from ultrasonic cavitation bubbles (*68,71*) may be involved in the oxidation process of S in cinnabar to S_{ox}. As discussed above, these oxidizing species were the rate-limiting step under the three cinnabar concentrations in this study. SO_4^{2-} was the sole S_{ox} product at low and moderate cinnabar concentrations and the main S_{ox} product at high cinnabar concentration, indicating that the oxidizing species (•OH, HO_2•, etc.) reacted with S from cinnabar in series reactions, not parallel reactions. Therefore, certain oxidizing species initialized the dissolution

reactions followed by other oxidizing species to further oxidize the initial products into final product of SO_4^{2-}. The reaction-limiting step was the oxidizing species for the initial reaction, not the total available oxidizing species.

As a powerful oxidant, •OH is the major oxidizing species in sonicated aqueous systems. The mechanism of ultrasonic oxidation of S(-II) has been proposed to be initiated by •OH and further propagated by a free-radical chain reaction involving O_2 (*71*). The study of sonochemical oxidation of CS_2 (*153*) also showed the rate-determining step in the overall oxidation reaction to produce SO_4^{2-} depended on the availability of •OH. Similarly, sonochemical dissolution of cinnabar is expected to proceed via the initial reaction of •OH with S from cinnabar particles. The following simplified equation represents the overall reaction sequence

$$HgS / S(-II) \xrightarrow{\bullet OH} S^* \xrightarrow{O_2 / H\bullet / H_2O_2} SO_4^{2-} \qquad \text{(Equation 4.1)}$$

where S^* is the product from initial reaction with •OH, (e.g., HS• and HSOH•). The details of the chain reactions from S^* to SO_4^{2-} have been presented elsewhere (*71*,*153*). These chain reactions were adequate for the oxidation of S^*, resulting in SO_4^{2-} as the sole or main S_{ox} product. No dissolved S(-II) was detected (detection limit 0.6 μM) in this study. In the study by Kotronarou et al. (*71*), 200 μM initial S(-II) disappeared in 30 min of sonication following zero-order kinetics. Either there was no S(-II) formed or S(-II) produced was simultaneously oxidized into S^* during sonication. Thus, it was difficult to determine whether •OH initially reacted with S(-II) or S in cinnabar itself although this step was the rate-limiting step for the overall reaction.

To evaluate whether •OH was the limiting step in the overall dissolution reaction, TA was added to cinnabar systems to scavenge •OH. TA has been applied to measure sonochemically produced •OH and/or scavenge bulk •OH (*152*,*154*,*155*). As shown in Table 4.2, the •OH production rate in the presence of cinnabar was very close to that in the DI system, indicating that TA very effectively trapped •OH in cinnabar systems even though cinnabar competed for •OH. If •OH was the predominant species initiating the dissolution reaction, the S_{ox} production rates in the presence of TA were expected to be much slower than those in the absence of TA since TA scavenged 90% of •OH (0.29 of 0.31 μM min^{-1}). The presence of TA did decrease SO_4^{2-} production rates (Table 4.2), however, they were not 90% lower than those in the absence of TA.

Although SO_4^{2-} production rates were not reduced by 90% with more than 90% of bulk •OH scavenged by TA, the proposed dissolution mechanism may be valid. The high concentration of •OH, estimated to be 4 mM in the cavitation bubble interfacial region (*156*), may initiate the reaction to form S^* if cinnabar particles or S(-II) contacts this region. In addition, the presence of cinnabar particles may provide more nuclei for cavitation bubbles to generate more •OH (*84*). However, this effect was not expected to be significant because the •OH production rate (0.29 μM/min) did not increase with the increase of cinnabar concentration (Table 4.2).

In addition to the proposed dissolution mechanism initiated by •OH, there may be other reaction pathways responsible for dissolution. First of all, thermal decomposition of S(-II)/HgS by high temperatures at the interfacial region (2000 K) (*68*) of cavitation bubbles as well as that from interparticle collisions (3000 K) driven by shockwaves (*149*) may occur. At temperatures greater than 1700 K, thermal decomposition of H_2S produces

S_2 and SO_2 in the presence of O_2 (*78*). Kotronarou et al. (*71*) have proposed thermal decomposition of H_2S as an important pathway for ultrasonic oxidation of H_2S at pH ≤ 8.5. Next, the fact that SO_3^{2-} and $S_2O_3^{2-}$ were detected only at 1.67 g L^{-1} of cinnabar concentration may be due to the combined thermal and physical effects of ultrasound. Compared to low cinnabar concentrations, more cinnabar particles collide with each other (*157*) possibly generating S(-II) and/or contact the cavitation bubble interfacial region. SO_3^{2-} and $S_2O_3^{2-}$ may have been detected initially because there was not enough HO_2• and H_2O_2 to completely oxidize S^* in equation 1 and the thermally decomposed products. However, longer sonication fractured cinnabar particles reducing particle collisions with time, leading to decreases of S(-II) generated by physical effects due to fewer particle collisions with decreased particle size (*157*). Thus, SO_3^{2-} and $S_2O_3^{2-}$ decreased likely due to the accumulation of HO_2• and H_2O_2 at longer sonication time.

Furthermore, similar to that proposed by Sostaric et al. (*97*) with CdS particles, HO_2• and H_2O_2 generated from cavitation bubbles may directly react with S in cinnabar particles instead of S^* initiated by •OH. Additionally, dissolved oxygen (O_2) has been found to dissolve metacinnabar under a transport-controlled reaction (*26*,*27*). In this study, dissolved O_2 may have dissolved cinnabar directly and sonication may have synergistically enhanced O_2 oxidation dissolution by improving mass transfer.

Thus, based on S_{ox} formation, sonication dissolved cinnabar. •OH appeared to be the predominant factor in initiating the dissolution reaction followed by other oxidizing reactions (HO_2•, H_2O_2, O_2) to produce the final S_{ox} product, SO_4^{2-}. Thermal and physical effects of ultrasound may also play important roles in dissolution reactions.

4.4.2 Ultrasonic release of mercury

No matter what the dissolution mechanisms are, Hg released into aqueous solution is expected to equal S_{ox}. Surprisingly, dissolved Hg(II) concentrations (inset of Figure 4.1) were much lower than those of S_{ox}. In fact, at a cinnabar concentration of 1.67 g L^{-1}, there was no dissolved Hg(II) detected even though S_{ox} products were the highest of the three cinnabar concentrations.

One possibility for lower dissolved Hg(II) compared to S_{ox} is the volatilization of Hg (0) due to reduction reactions of Hg(II) (*4*). Hsieh et al. (*26*) observed volatilization of Hg(0) in a metacinnabar system. However, Hg(0) formed in their study was only a small amount of the dissolved Hg(II) and much lower than S_{ox} determined in this study. Therefore, the loss of Hg through volatilization does not account for the difference between S_{ox} production and dissolved Hg(II).

Previous studies have shown that a large portion of the Hg(II) dissolved from cinnabar or metacinnabar adsorbed onto HgS particles (*25*,*26*,*27*). Thus, the discrepancy between S_{ox} production and Hg(II) release in this study was hypothesized to be due to dissolved Hg(II) adsorbing back onto the remaining cinnabar particles. In order to test this hypothesis, given amounts of Hg(II) based on S_{ox} production were adsorbed onto 1.67 g L^{-1} cinnabar under identical solution conditions as those in sonochemical dissolution. The adsorption isotherm (data not shown) confirmed that Hg(II) was strongly adsorbed onto cinnabar particles with a maximum capacity of 7.5 μmol m^{-2}.

Given that S_{ox} was produced and no dissolved Hg(II) was detected at 1.67 g L^{-1} cinnabar, equivalent moles of Hg(II) adsorbed on cinnabar to S_{ox} produced were expected. Normalizing the amount of S_{ox} to the initial cinnabar surface area, the expected

Hg(II) concentration on the cinnabar surface after 3 hr sonication was nearly five times higher than the maximum adsorption capacity (inset of Figure 4.2). However, there was no dissolved Hg(II) detected in solution, indicating that cinnabar had a higher Hg(II) adsorption capacity under sonication.

4.4.3 Ultrasonic effects on cinnabar particles

To explore the reasons for higher Hg(II) adsorption under sonication than the maximum Hg(II) adsorption capacity of unsonicated cinnabar, particle characterization experiments were conducted to understand ultrasonic effects on cinnabar particle properties. First, SEM was used to look at the effect of ultrasound on the size and morphology of particles. As shown in Figure 4.3, without sonication, the majority of cinnabar particles were approximately 100 μm in diameter and had a smooth surface. There were also some small particles around 1 μm, mostly randomly attached to larger particles. After 3 hr sonication, the large cinnabar particles were completely broken down into smaller particles, which aggregated into clusters. High-speed interparticle collisions (hundreds of m s^{-1}) driven by shockwaves (*157*) break up large particles reducing particle size, fragment particles smoothing particle edges, and impinge on particles generating local surface erosion.

Based on the particle size and surface morphology changes observed in Figure 4.3, an increase in surface area was reasonably expected. Not surprisingly, significant increases in surface areas with sonication time were observed (Figure 4.2). Thus, the higher Hg(II) adsorption under sonication is attributed to newly formed reaction sites with higher surface area. It is obvious that after correcting for surface area increases,

Hg(II) adsorbed on the cinnabar surface, based on S_{ox} formation, became lower than the maximum sorption capacity (Inset of Figure 4.2). Apparently, this is why no dissolved Hg(II) was detected although high concentrations of S_{ox} were measured.

ζ potential increases in metal sulfides due to adsorption of metal ions, leading to surface IEP increases, have been observed in other studies (*158*,*159*,*160*). In our study, ultrasound increased the cinnabar IEP from around 3.9 without sonication to 4.6 after 3 hr sonication. The IEP measured for unsonicated cinnabar particles was close to previous reports, 4.0 determined by a ζ-pH curve (*12*) and 3.5 by the titration method (*159*). The observed increase in IEP with sonication may result from the adsorption of dissolved Hg(II). Hg(II) adsorption may result in a cinnabar surface functional group transition from ≡SH (with a lower acidity constant) to ≡HgOH (with a higher acidity constant), causing an increase in surface IEP. Thus, the increase in IEP of cinnabar after sonication indirectly supports the idea of dissolved Hg(II) adsorbing back onto cinnabar particles.

Alternatively, an IEP increase of cinnabar by ultrasound may be due to mineral phase transformations. Sonication has been found to induce phase transformations in Al_2O_3 (*128*,*138*). When the temperature is above 588 K, red cinnabar will transform to black metacinnabar (*148*,*161*). The high temperature in the cavitation bubble interfacial region (2000 K) (*68*) as well as that from interparticle collisions (3000 K) (*149*) may induce HgS phase transformations. Previous studies (*28*,*158*) have published IEP values for metacinnabar as 5.1 and 7.0, respectively, which are higher than the IEP of cinnabar. Therefore, the increase in IEP of cinnabar observed in this study may also implicate HgS mineral phase transformation. XRD analyses were conducted to examine the possible phase transformation. Similar to that found previously (*138*), no pronounced differences

were observed (data not shown) because XRD is a deep-penetrating technique, while any minor phase transformations are limited to a thin film at the particle surfaces. Since metacinnabar is more prone to dissolution than cinnabar (*161*), ultrasonic dissolution of cinnabar may become more effective with time if mineral phase transformations from cinnabar to metacinnabar occur with sonication.

4.4.4 Effects of humic acid

Dissolved HA was used to simulate DOM effects on ultrasonic dissolution of cinnabar. As shown in Figure 4.4 (a), Hg(II) dissolved in both sonication and mechanical shaking systems in the presence of HA. Dissolved Hg(II) concentrations were much higher by sonication than those by mechanical shaking.

Hg(II) dissolved by mechanical shaking showed that HA itself was able to dissolve cinnabar. One possible dissolution mechanism is ligand-promoted reactions (*162*). HA molecules adsorb onto cinnabar surfaces, complex with Hg, break the Hg-S bond, and detach Hg from cinnabar to generate new reaction surface. S_{ox} produced in the presence of HA (Figure 4.4 (b)) including SO_3^{2-} and SO_4^{2-} by mechanical shaking indicates that oxidation reactions between HA and S or S_{ox} from cinnabar occur. DOM has been known to participate in redox reactions due to electron-donating and electron-accepting properties by quinone moieties (*163*). In addition, HA may catalyze the reaction between O_2 and cinnabar to dissolve cinnabar. Higher total S_{ox} production compared to dissolved Hg(II) suggests that the adsorption of dissolved Hg(II) on the cinnabar surface still occurs. The other possible reason for lower dissolved Hg(II) than S_{ox} production may be due to the reduction of Hg(II) to Hg(0) by humic acid (*23*).

High dissolved Hg(II) produced by sonication is attributed to synergistic effects between ultrasound and HA. No matter whether the dissolution mechanism by HA is through ligand-promotion or oxidation reactions, HA needs to reach the cinnabar surface for dissolution to occur. Ravichandran et al. (*28*) found that mechanical stirring was necessary to bring about cinnabar dissolution by DOM. So, ultrasound may enhance HA dissolution of cinnabar by increasing the HA mass transfer rate. On the other hand, as described above, ultrasound itself dissolves cinnabar by oxidizing S from cinnabar, whereas dissolved Hg(II) adsorbs back onto cinnabar surfaces. The presence of dissolved HA may complex Hg(II) dissolved by ultrasound to keep it from adsorbing onto cinnabar, consequently enhancing dissolved Hg(II) concentrations.

Compared to in the absence of HA, the presence of HA inhibited the production of SO_4^{2-}, but greatly improved SO_3^{2-} production. Recalling that scavenging of bulk •OH by TA did not produce SO_3^{2-}, the primary production of SO_3^{2-} instead of SO_4^{2-} in the presence of HA indicates that HA affected not only •OH, but also other oxidation species, such as HO_2• and H_2O_2. Moreover, the total S_{ox} concentration was higher with HA than that without HA. This further supports the possibility that ultrasound accelerated HA dissolution of cinnabar through increasing the mass transfer rate. This accelerated dissolution also may be due to sonochemical oxidation of HA improving oxidation reactions between HA and cinnabar. In addition, the enhancement of cinnabar dissolution by HA may be due to increases in cinnabar particle surface area by ultrasound, providing more reaction sites for HA. However, surface area changes also lead to higher HA adsorption. Although no TOC reduction for HA was observed after 4 hr sonication without cinnabar (*115*), HA decreased by approximately 30% after 1 hr sonication

compared to 20% for mechanical shaking with cinnabar present, indicating more HA adsorption on cinnabar with sonication. This increased adsorption of HA under ultrasound may be a reason for lower dissolved Hg(II) than total S_{ox} products when HA is present.

In summary, ultrasound oxidizes S in cinnabar but Hg is not quantitatively released due to adsorption onto the remaining cinnabar particles. This effect is complicated by changes in particle surface area due to sonication. Dissolved HA enhances cinnabar dissolution, releases more Hg(II) into aqueous solution, and affects S_{ox} products formed by ultrasound. In natural systems, natural organic matter coated on cinnabar surfaces may reduce the ability of ultrasound to dissolve and release Hg(II) from cinnabar. Further, additional factors including pH, redox, and the presence of other minerals, other ligands, and microorganisms may also influence ultrasonic release of Hg(II) from cinnabar.

Acknowledgements

Funding from NOAA/Ohio Sea Grant College Program and the NSF Environmental Molecular Science Institute at The Ohio State University is gratefully acknowledged. The authors thank S. Jones and J. Bigham for their help with XRD and N_2 BET measurements.

Initial cinnabar concentrations (g HgS L^{-1})	Dissolution rate (μmol m^{-2} min^{-1}) [a]	R^2
0.0333	0.36	0.989
0.167	0.10	0.996
1.67	0.011	0.955

[a] Normalized to initial cinnabar surface area without considering cinnabar surface changes by ultrasound

Table 4.1 Dissolution rates of cinnabar based on S_{ox} production within 3 hr sonication

Experimental conditions [a]	Production rates ($\mu M\ min^{-1}$)		
	•OH (w/ TA)	SO_4^{2-} (w/o TA)	SO_4^{2-} (w/ TA)
DI	0.31	ND [b]	ND
0.0333 g HgS L^{-1}	0.29	0.16	0.14
0.167 g HgS L^{-1}	0.29	0.30	0.15
1.67 g HgS L^{-1}	0.29	0.37	0.22

[a] pH 8.0 [b] Not detected

Table 4.2 •OH and SO_4^{2-} production rates within 1 hr sonication

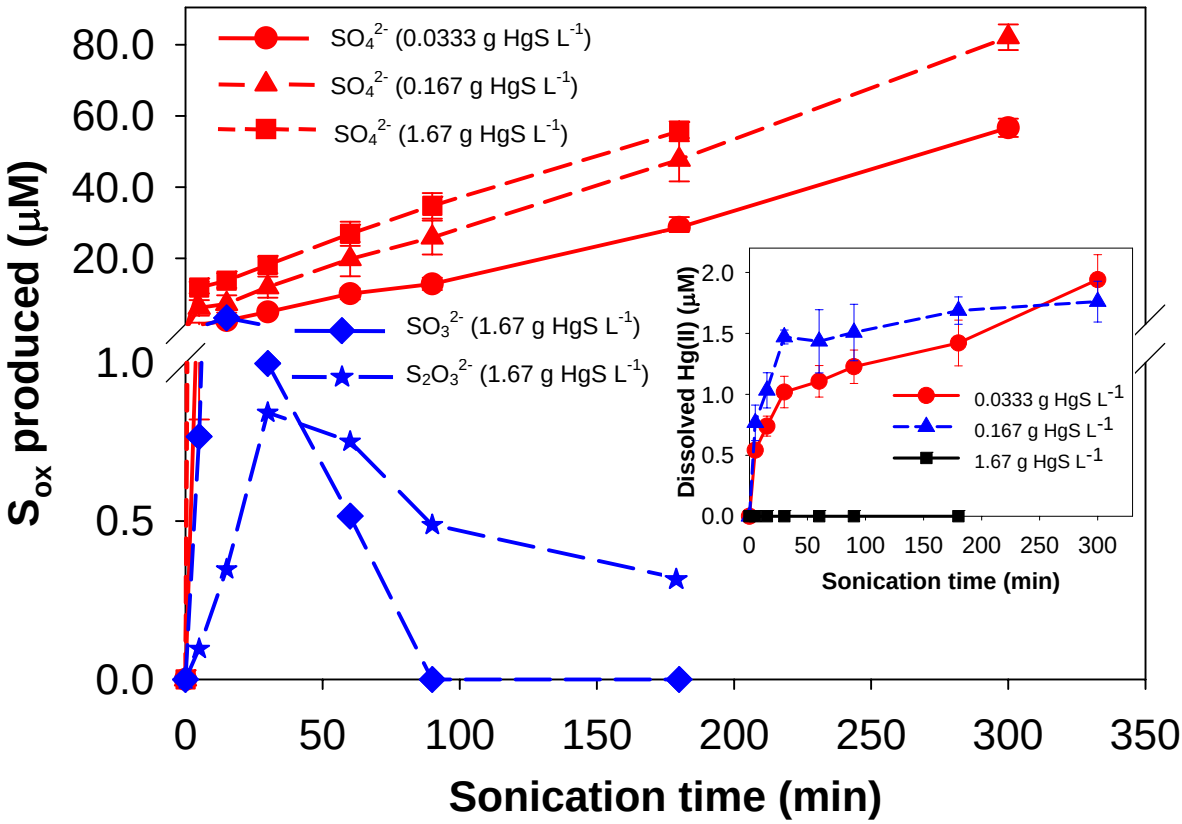

Figure 4.1 S_{ox} produced during sonication at three cinnabar concentrations (pH = 4.0, T = 20 °C, I = 0.01 M, sonication intensity 18 W cm^{-2}). Figure inset: dissolved Hg(II) formed during sonication at three cinnabar concentrations.

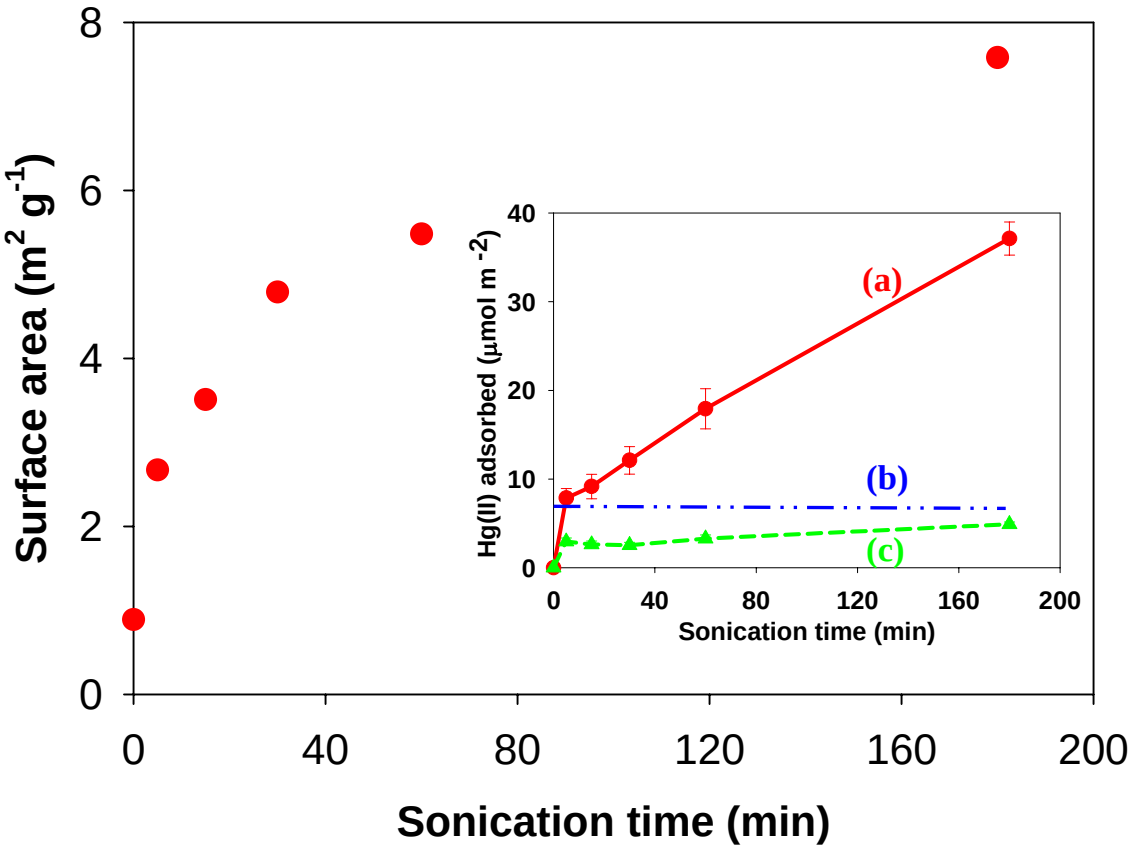

Figure 4.2 Cinnabar surface area during sonication (pH = 4.0, T = 20 °C, I = 0.01 M, [cinnabar] = 1.67 g L^{-1}, sonication intensity 18 W cm^{-2}). Figure inset: Hg(II) adsorbed on cinnabar (a) normalized Hg(II) content equivalent to S_{ox} based on initial surface area, (b) maximum Hg(II) adsorption capacity (7.5 μmol m^{-2}), (c) normalized Hg(II) content equivalent to S_{ox} correcting for surface area increases.

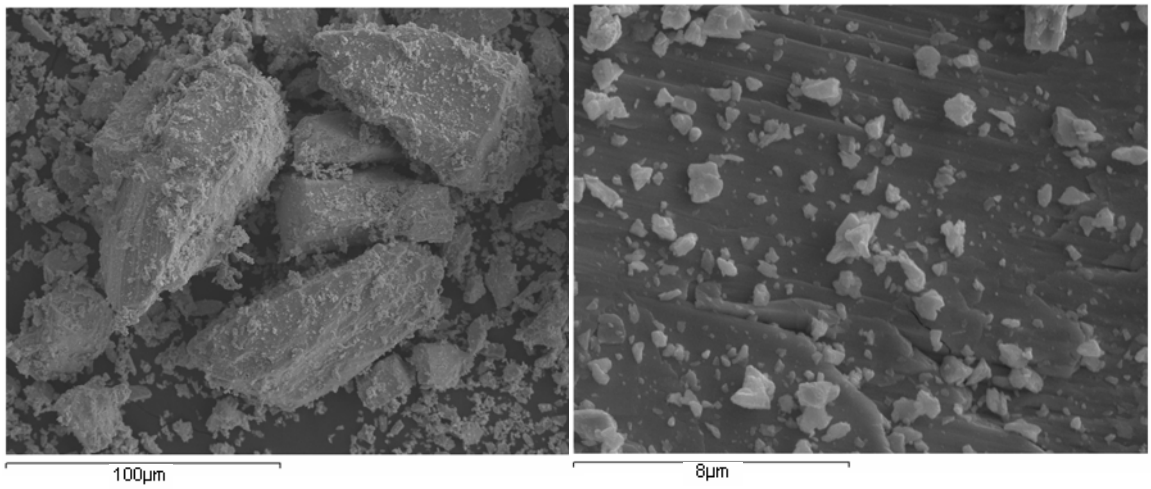

(a)

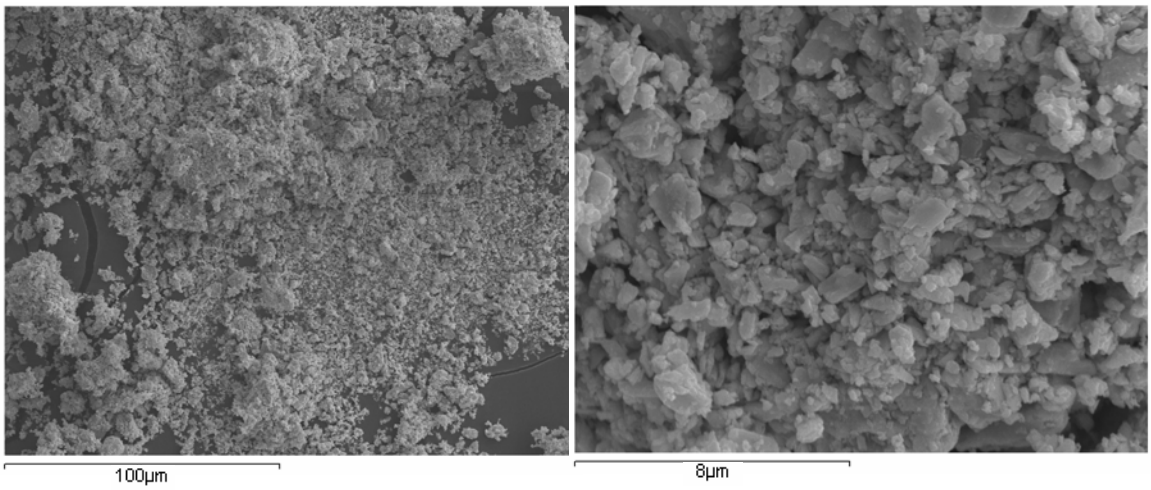

(b)

Figure 4.3 SEM images (a) before sonication, (b) after 3 hr sonication (pH = 4.0, T = 20 °C, I = 0.01 M, [cinnabar] = 1.67 g L^{-1}, sonication intensity 18 W cm^{-2}).

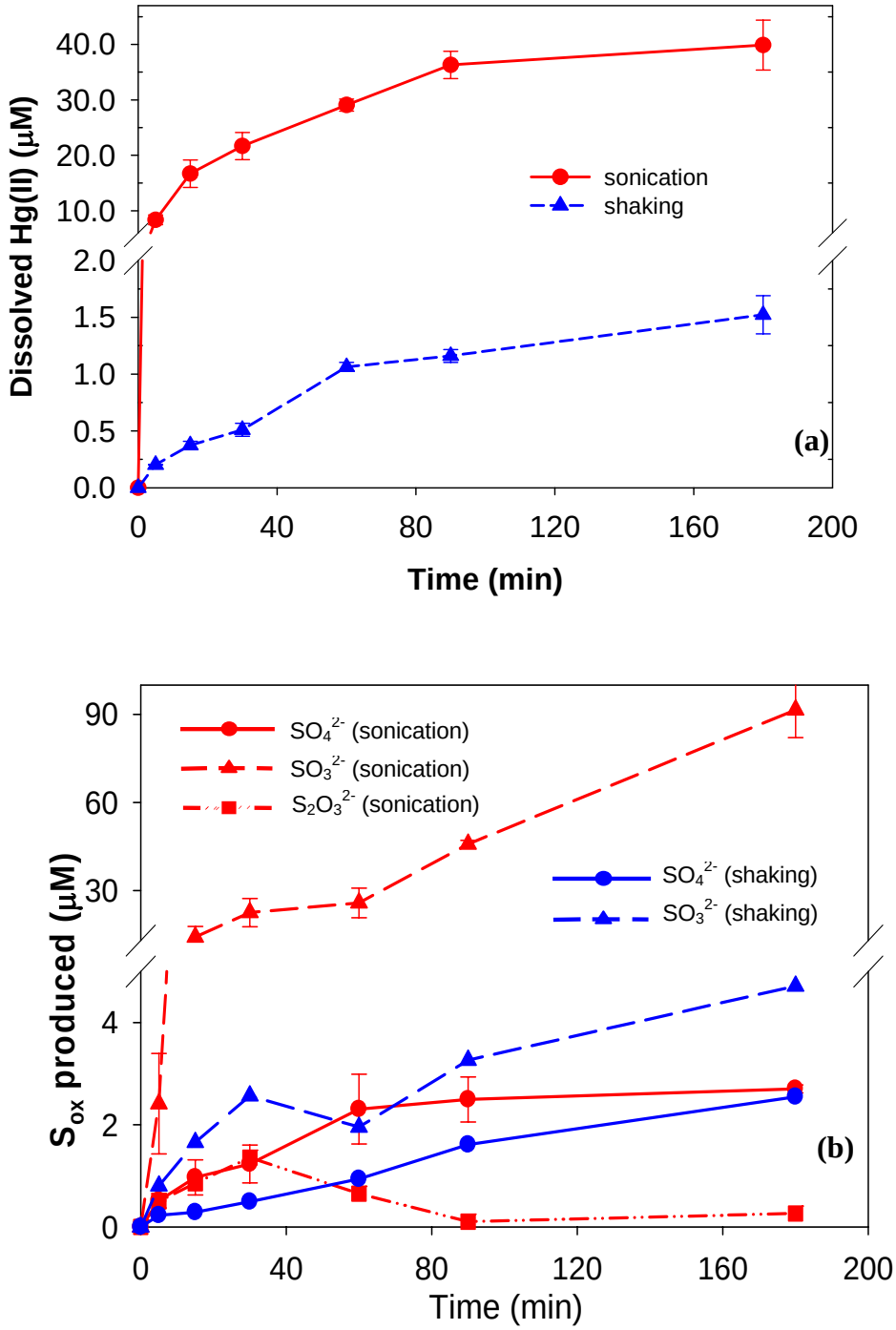

Figure 4.4 Dissolved Hg(II) formed (a) and S_{ox} produced (b) in the presence of humic acid (pH = 4.0, T = 20 °C, I = 0.01 M, [cinnabar] = 1.67 g L^{-1}, [HA] = 8.5 mg C L^{-1}, sonication intensity 18 W cm^{-2}).

CHAPTER 5

SONOLYTIC RELEASE OF METALS (Hg, Pb, Ni, Cr) FROM ALUMINUM OXIDE AND MARINE SEDIMENT

5.1 Abstract

Sonolytic release of Hg, Pb, Ni and Cr from Al_2O_3 and PACS-2 marine sediment was investigated to examine the ability of ultrasound to treat sediment contaminated with a series of metals. Results showed that sonication enhanced metal desorption from Al_2O_3 in acidic solution compared to hydrodynamic mixing. However, longer sonication times led to a decrease in Hg(II) and Pb(II) desorption while Ni(II) and Cr(III) desorption continued to increase. The net ultrasonic desorption of metals from Al_2O_3 was related to metal binding strength, ultrasonic conditions and metal water exchange rates. The release of the four metals from PACS-2 was far more complicated compared to Al_2O_3. The release patterns and rates were different for various metals and at different pH values. The different releases of Hg, Pb, Ni and Cr from PACS-2 were likely due to the differences in their affinity to different sediment components, metal speciation and oxidation state, and the effects of organic matter in the sediment. Hg release was likely

controlled by organic matter; Pb release was impacted by its affinity to organic matter and metal (hydr)oxides due to its high content; Ni release seemed to be affected by metal (hydr)oxides and silicate phases; whereas Cr release was influenced by its oxidation state.

5.2 Introduction

USEPA (*164*) has reported that metals are the dominant chemical class in contaminated sediment based on the total potential for adverse effects. Toxic metals (e.g., Hg, Pb, Cd, Cu, Ni, and Cr) pose a significant threat to the environment and public health because of their toxicity, accumulation in the food chain, and persistence. For example, Hg released from sediment into the aqueous phase provides a substrate for the synthesis of methylmercury, causing bioaccumulation in the food chain (*4*).

Although there exist many treatment techniques for metal-laden soils (*165*,*166*), much less is known for sediment control because of differences between soil and sediment properties (*48*,*49*). Currently, capping the sediments in place or extraction followed by landfilling are the most common methods of treatment. However, the long-term stability of metals after treatment is a major concern. To remove metals from sediments, metals must be released from the matrix into the aqueous phase. Subsequently, these dissolved metals can be concentrated or collected. Several types of techniques are applicable for the cleanup of dredged metal-contaminated sediments, including washing, chemical extraction, and biosorption treatment (*48*,*49*,*60*,*167*). However, besides costly excavation, all these techniques are time consuming due to slow and/or nonreversible desorption (*67*).

Sonochemistry has been widely applied for remediation (*68*). Ultrasound causes the formation of cavitation bubbles leading to high localized temperatures and pressures (in excess of 5000 K and 500 atm, respectively), which induce thermal and chemical reactions and the degradation of a range of organic pollutants in water (*68*,*73*,*75*,*115*). In addition, the collapse of cavitation bubbles results in a variety of physical and mechanical effects such as shock waves, microjets and microstreaming, which play important roles in heterogeneous systems. According to these effects, ultrasound-assisted extraction (*92*,*93*,*96*) and ultrasonic extraction (*94*,*95*,*137*,*138*) have been recently applied to accelerate the desorption of metals from soils and sediments.

Previous studies have focused on the release of one metal from either model or pretreated solids. Thus, to date little is known about ultrasonic remediation of sites contaminated by a mixture of metals.

The purpose of this study was to investigate the ability of sonochemical techniques to treat an array of metals (Hg, Pb, Ni and Cr) in contaminated sediment. Hg, Pb, Ni and Cr were chosen in this study based on their different binding strengths (*168*) and water exchange rates (*162*). Specifically, the desorption of Hg(II), Pb(II), Ni(II), and Cr(III) individually from Al_2O_3 model particles was demonstrated to examine sonolytic release of metals. Subsequently, PACS-2 marine sediment was used to evaluate the sonolytic ability to treat a series of metals in a real sediment matrix.

5.3 Experimental Section

5.3.1 Materials

$Hg(NO_3)_2$ (99.99+%, Sigma-Aldrich), $Pb(NO_3)_2$ (crystalline, Fisher Scientific), $Cr(NO_3)_3$ (99.99+%, Fisher Scientific), and $Ni(NO_3)_2{\cdot}6H_2O$ (crystalline, Fisher Scientific) were used without further purification. Ionic strength and pH were adjusted with NaOH, HNO_3 and $NaNO_3$ purchased from Fisher Scientific. Water used to prepare the solutions was from a Millipore system (R = 18.2 MΩ-cm). Aluminum oxide (adsorption grade Al_2O_3, 80-200 mesh particle size, density 4 g cm^{-3}) was purchased from Fisher Scientific. The particles had a surface area of 110 m^2 g^{-1} and an average diameter of 110 μm as tested by single-point N_2 BET surface area analysis and Malvern Mastersizer particle size analysis. PACS-2 marine sediment purchased from National Research Council (NRC) was used as a field contaminated sediment with a certified metal content (Hg = 3.04 ± 0.20 mg kg^{-1}, Pb = 183 ± 8 mg kg^{-1}, Ni = 39.5 ± 2.3 mg kg^{-1}, and Cr = 90.7 ± 4.6 mg kg^{-1}), which were confirmed in our labrotary (Hg = 3.61 ± 0.35 mg kg^{-1}, Pb = 201 ± 7 mg kg^{-1}, Ni = 40.1 ± 1.4 mg kg^{-1}, and Cr = 83.6 ± 1.8 mg kg^{-1}) by microwave digestion analysis.

5.3.2 Experimental procedures

Sorption samples were prepared by shaking 15 mL of metal stock solution of either 0.75 mM of Hg(II), 4 mM of Pb(II), 1.2 mM of Ni(II), or 6.7 mM of Cr(III (pH = 2.5, I = 0.1 M $NaNO_3$) with 2 g alumina particles in 60 mL polypropylene bottles on a rotating shaker at 350 rpm. After 2 hr mixing, the pH was adjusted to 7.0 with 0.1 M

HNO_3 or 0.1 M NaOH. After 24 hr the adsorption was observed to reach equilibrium, and the supernatant was separated from the particles by 15 min centrifugation at 1500 rpm. Supernatant was diluted with 5% HNO_3 for cold vapor atomic absorption spectroscopy (CVAAS) or inductively coupled plasma atomic emission spectroscopy (ICP-AES) analysis, and the metal-laden particles were used for sonication and hydrodynamic mixing desorption experiments. The amount of metal adsorbed on solids was determined from the difference between the stock solution and the supernatant solution.

For sonolytic desorption, 2 g of metal-laden Al_2O_3 particles or PACS-2 sediment were transferred to a glass rosette reactor with 60 mL of 0.1 M ionic strength solution. Batch desorptions were carried out at constant pH controlled with a pH-stat autotitrator using HNO_3 or NaOH. The desorption pH for different metals from Al_2O_3 were chosen based on metal pH dependent sorption curves (insets of Figure 5.1 to Figure 5.4). Two pH conditions (pH 3 and pH 8) were arbitrarily chosen for releases of metals from PACS-2 sediment. A 20 kHz ultrasonic probe system (550 Sonic Dismembrator, Fisher Scientific) was used for sonication experiments at a power input intensity of 36 W cm^{-2} as measured by calorimetry (*138*). The reactor was water-jacketed to control the reacting solution temperature at 20.0 ± 0.5 °C by a constant-temperature cooling bath. After selected times of sonication, samples were transferred to polypropylene centrifuge bottles and ultracentrifuged for 20 min at 17000 rpm using a centrifuge (Model J2-21, Beckman) to separate the supernatant and particle fractions. An aliquot of the supernatant was diluted with 5% HNO_3 for CVAAS and ICP-AES analyses. The particle pastes were freeze dried for later particle size, surface area, and X-ray diffraction (XRD) analyses.

For hydrodynamic mixing comparison experiments with Al_2O_3, 6 g of metal-laden Al_2O_3 particles and 180 mL 0.1 M ionic strength solution were transferred to another glass rosette reactor (with the same geometry as the sonication reactor), and mixed by circulation at a flow rate of 1.2 L min^{-1} driven by a peristaltic pump. All other conditions, such as pH and temperature, were the same as those used with sonolytic desorption. The amount of metal desorbed from the solid was calculated by analysis of the supernatant. Control experiments and selected experiments were performed in duplicate or triplicate to determine the data error and verify reproducibility.

Mechanical shaking was used for metal release in PACS-2 on a rotating shaker at 200 rpm under the same experimental conditions as those with sonication. In mechanical shaking, the pH was initially adjusted to pH 3 or pH 8 and no pH control was performed during shaking. pH measurements during and after mechanical shaking showed no obvious pH change.

Prior to Hg(II) analysis by CVAAS, solution samples were oxidized overnight with 5% BrCl followed by reduction with 30% $NH_2OH{\bullet}HCl$. Pb, Ni and Cr were measured by ICP-AES after acidifying by 5% HNO_3. Dissolved organic matter in PACS-2 marine sediment systems was measured by a Shimadzu TOC-5000A analyzer. Specific surface area was determined using single-point BET N_2 method (Micromeritics FlowSorb 2300).

5.4 Results and Discussion

5.4.1 Sonolytic desorption of metals from Al_2O_3

Desorption of metals from well-characterized model inorganic particles, Al_2O_3, was carried out first to examine the effects of ultrasound on metal desorption. No obvious desorptions of Hg(II) and Ni(II) at pH 8 were observed for either ultrasound or hydrodynamic mixing. These results are reasonable based on the pH dependent adsorption curves (insets of Figure 5.1 and 5.3).

Based on Hg(II), Pb(II), Ni(II), and Cr(III) sorption curve insets in Figure 5.1-4, desorption of metals was anticipated to occur at lower pH. The expected equilibrium desorption of Hg(II), Pb(II), Ni(II), and Cr(III) under experimental conditions (pH 4 for Hg(II) and Ni(II), and pH 3 for Pb(II) and Cr(III), respectively) was approximately 15%, 55%, 88% and 80%, respectively.

Figure 5.1-4 show the results of desorption of Hg(II), Pb(II), Ni(II), and Cr(III) from Al_2O_3 using sonication and hydrodynamic mixing. As expected, desorption of metals occurred and sonication enhanced the release of metals. The extent of desorption relative to the expected desorption based on sorption equilibrium varied with different metals. For hydrodynamic mixing, desorption of Hg(II) and Pb(II) at 1 hr were observed to approach equilibria (15% and 50% for Hg(II) and Pb(II), respectively, close to those expected based on sorption curves), Whereas desorption of Ni(II) (45%) and Cr(III) (6%) after 3 hrs were far from equilibria and much lower than 88% and 80% expected based on sorption curves. During the first few minutes, sonication accelerated desorptions of all four metals compared to hydrodynamic mixing. The enhancement of Hg(II) desorption was the most appreciable. Specifically, after 2 min desorption, 33% of Hg(II)

was released by ultrasound compared to 8% by hydrodynamic mixing. Prolonged sonication led to a decrease in desorption of Hg(II) and a slowdown in desorption of Pb(II) with very fast water exchange rates (Table 5.1) (*129*). At 60 min, less desorption occurred by sonication than that by hydrodynamic mixing, especially for 3% of Hg(II) desorption by sonication compared to 14% by hydrodynamic mixing . Comparatively, with Ni(II) and Cr(III), reduced desorption with longer sonication times was not observed even after 3 hr sonication.

The differences in the extent of approaching the expected desorption among different metals may be due to differences in water exchange rates (Table 5.1). The linear relationship between water exchange rate (k_{-H_2O}) and the adsorption rate (k_{ads}) is described by equation (5.1) (*162*):

$$\log k_{ads} = -2.42 + 0.92 \log(\frac{k_{-H_2O}}{55.6}) \qquad (5.1)$$

According to this equation, the slower the water exchange rate of a metal, the slower the sorption process. Therefore, for Hg(II) and Pb(II) which have very fast water exchange rates, the desorption approached equilibrium at 1 hr by hydrodynamic mixing. For Ni(II) and Cr(III) with slower water exchange kinetics, the desorption was still proceeding even at 3 hr. Another factor impacting metal desorption is slow intraparticle surface diffusion which usually determines the rate of desorption (67). Additionally, metal desorption is dependent on the nature of surface binding including inner-sphere complexation (Hg, Pb), mononuclear and polynuclear hydroxide formations (Cr), and coprecipitation (Ni) (*168*).

The enhanced initial desorption of metals by ultrasound may be attributed to chemical reaction, improved kinetics and an altered chemical equilibrium through physical and thermal effects generated by cavitation bubbles. First, shockwaves, microjets and thermal effects break chemical bonds between adsorbed metal and Al_2O_3. An example of this is the dissolution of metal oxides and metal sulfide by sonication (*84*,*137*,*138*). Second, the extreme agitation such as microstreaming improves mass transfer through intraparticle micropores, accelerating desorption (*124*). In addition, ultrasonic energy may shift the adsorption/desorption equilibrium. In this study, the desorption of Hg(II) by sonication reached 33% at 2 min was much higher than the 15% expected at pH 4 based on the adsorption curve, indicating that ultrasound altered the chemical equilibrium of Hg(II). Therefore, although the metals examined in this study form strong inner sphere surface complexes, polymerize, precipitate, or hydrotalcite-type coprecipitates (*168*), sonication improved the amount of and the rate of desorption for all metals. Similar results of ultrasonic effects on metal desorption (Cu, Mn, Hg, and Cr) from an activated carbon system have been reported (*169*).

The decrease in Hg(II) desorption with longer sonication was primarily due to occlusion by aluminum hydroxide precipitation induced by ultrasound (*138*,*170*). Ultrasound dissolved Al_2O_3 particles to produce a supersaturated Al solution which reprecipitated to cover the Al_2O_3 surface. Due to the fast sorption process, desorbed Hg(II) resorbed back onto Al_2O_3 particles and was buried by aluminum hydroxide precipitation. Pb(II) desorption by prolonged sonication became lower than that by hydrodynamic mixing. However, a dramatic decrease in Pb(II) was not observed even though the water exchange rate of Pb(II) is slightly higher than that of Hg(II). One reason

for this discrepancy is the different desorption pH values. At pH 3 for Pb(II) desorption, the polymeric aluminum hydroxide precipitates are smaller than those at pH 4 for Hg(II) desorption. Therefore, occlusion of Pb(II) was less than that observed with Hg(II). An alternative explanation for this difference may be due to the differences in Hg(II) and Pb(II) sorption modes. X-ray absorption fine structure (XAFS) results have suggested that Hg(II) forms monodentate and bidentate mononuclear complexes and Pb(II) forms mononuclear and polynuclear complexes on aluminum oxides (*33*,*171*). Mononuclear sorption of Hg(II) may be more subject to occlusion than polynuclear sorption of Pb(II). Without information of molecular study by XAFS in this study, it is difficult to determine the complexation effect.

Due to the relatively slow water exchange kinetic constants of Ni(II) and Cr(III) compared to Pb(II) and Hg(II), Ni(II) and Cr(III) desorption did not show a decreasing trend with longer sonication times. As shown in Figure 5.1-4, after 3 hr sonication, the highest net improved desorption (21%) was observed for Cr(III) with the slowest resorption rate. So, the net desorption amount by ultrasound may be kinetically determined by: i) ultrasonic desorption and ii) the resorption combined with the particle changes induced by ultrasound. However, without fast water exchange rates, the desorption of Ni(II) and Cr(III) was also slow even with sonication, the desorption is still far below expected equilibrium desorption (88% and 80%, respectively, for Ni(II) and Cr(III)). The other possibility for this observation is the strong binding between Ni(II) and Cr(III) and Al_2O_3. As XAFS studies have demonstrated, Ni(II) forms hydrotalcite-like coprecipitates with alumina (*168*) and Cr(III) polymerizes on the surface (*172*). These reported strong surface complexes may result in difficult desorption.

5.4.2 Sonolytic release of metals from PACS-2 marine sediment

To further test the effectiveness of ultrasonic release of metals, reference PACS-2 marine sediment (NRC, Canada) was chosen for field-contaminated sediment experiments.

Hg, Pb, Ni, and Cr release from PACS-2 (Figure 5.5-8) was much more complicated compared to the Al_2O_3 system (Figure 5.1-4). Overall, it is obvious that no two metals had similar release results from PACS-2. Hg was more prone to release at pH 8 than pH 3 and ultrasound increased Hg release compared to hydrodynamic mixing. There was more release of Pb, Ni and Cr at pH 3 than pH 8 by hydrodynamic mixing, while ultrasonic effects differed on their release. Specifically, ultrasonic release of Pb at pH 3 and pH 8 were similar; however, compared to hydrodynamic mixing it was faster than that at pH 8 and slower than that at pH 3. Ni release was enhanced by sonication at both pH conditions compared to hydrodynamic mixing and pH 3 resulted in greater release than pH 8.

At longer sonication times (1.5 hr), even though the release was higher than that by hydrodynamic mixing in all cases, the release of metals by sonication at pH 8 decreased with time as observed for Hg(II) desorption from Al_2O_3. In addition, under acidic conditions (pH 3), ultrasonic release of Pb decreased with sonication time after an initial release, while ultrasonic release of Hg, Ni and Cr seemed to approach equilibrium. The different release phenomena of various metals at different pH values may be due to the effects of natural organic matter (NOM) in sediment, the differences in metal speciation and content, and the properties of sediment.

The differences in Hg release between Al_2O_3 and PACS-2 systems may be attributed to the strong Hg-NOM complexes, which determine the behavior and distribution of Hg in sediments (*4*,*173*) and ultrasonic effects. The release of NOM at pH 3 and 8 in Figure 5. 9 was similar to those of Hg (Figure 5.5), suggesting that NOM controlled Hg release in the PACS-2 sediment. Release of dissolved NOM corresponded to Hg release. Yin et al. (*46*) demonstrated that both Hg adsorption and desorption rate coefficients were inversely correlated with soil organic C content. Thus, enhanced NOM desorption by sonication may explain improved Hg release by ultrasound. However, NOM desorption alone cannot account for higher Hg release by sonication at pH 3 than that by hydrodynamic mixing at pH 8 (Figure 5.5) given the higher NOM desorption at pH 8 by mixing than at pH 3 by sonication (Figure 5.9). Considering the low percent of Hg release, this discrepancy may be attributed to a small fraction of Hg binding to metal (hydr)oxides, which is prone to release under acidic conditions.

Sequential extraction (*173*) showed that Pb and Hg are in a group of elements displaying similar affinity to NOM in sediment. Hg release controlled by NOM desorption and totally different results for Pb release indicates that Pb speciation other than Pb-NOM is present in PACS-2 sediment. The higher Pb concentration compared to Hg in PACS-2 sediment supports this possibility. Some studies have reported that Pb sorbs on hydrous Fe(Mn)-oxides at high concentration (*174*,*175*,*176*). Similar to the Al_2O_3 system, Pb had more release at pH 3 than pH 8 by hydrodynamic mixing. Sonication did accelerate initial Pb release at pH 3 compared to hydrodynamic mixing. However, longer sonication may have exposed or created more Fe(Mn)-oxides surface sites through surfacial decoating of NOM and particle size reduction, leading to a

decrease in Pb release compared to hydrodynamic mixing. The fact that the highest release of Pb was not observed at pH 8 by sonication suggested that the Pb-NOM species was either lower than Pb on metal oxides or less mobile.

In comparison, similar release of Ni was observed as Pb, which was reasonable since Ni sorption on hydrous Fe(Mn)-oxides was also a major fraction (*176*). However, enhanced Ni release by sonication at pH 3 compared to hydrodynamic mixing and no decrease with prolonged sonication was intriguing. One reason for this phenomenon may be attributed to the slow resorption rate of Ni, resulting in Ni not re-associating with sediment similar to that observed with Al_2O_3. Additionally, instead of binding to Fe(Mn)-oxides, Ni complexation to silicates was found to be the least extractable and highest Ni fraction in several lake sediments (*173*). Thus, release of Ni from silicates during sonication may be another reason for this observation.

The Cr release pattern was dissimilar to the release of Ni although both Cr and Ni display a negative correlation with NOM and tend to sorb on hydrous metal oxides (*173*,*176*). The release of Cr is expected to be more complicated than Ni since it exists primarily in two oxidation states, Cr(III) and Cr(VI), which are stable and mobile, respectively, at high pH, and vice versa at low pH. Without sonication, the higher release of Cr at low pH than at high pH may indicate that more Cr(III) than Cr(VI) exists in PACS-2 sediment. Taking into account that Cr(VI) is very mobile in the environment, this observation is reasonable. Higher ultrasonic release of Cr at pH 8 than at pH 3 is apparently inconsistent with hydrodynamic mixing results. This is attributed to facile desorption of Cr(VI) because, presumably, more Cr(III) than Cr(VI) is present in PACS-2. Surface coatings of NOM may inhibit the desorption of Cr(VI), resulting in low

desorption by hydrodynamic mixing. After sonication removed a portion of the coated NOM (Figure 5.9), Cr(VI) release improved. On the other hand, sonication itself may accelerate Cr(VI) release. It should be noted that oxidation of Cr(III) to Cr(VI) may occur in PACS-2 system although sonication control experiments with Cr(III) in DI water did not result in detectable Cr(VI). This chemical transformation of Cr could influence its release by ultrasound, inhibiting Cr release at low pH and improving its release at high pH.

In summary, the release patterns and efficiencies were different for different metals from PACS-2 sediment likely due to the effects of NOM in sediment, the differences in metal affinity to different sediment compositions, metal content and oxidation state. Information obtained in this study will help to provide insight on the application of ultrasound to remediate metal contaminated sediments. For example, higher pH may result in more leaching of Hg and Cr, whereas lower pH may favor the release of Pb and Ni. Results obtained in this study may stimulate and identify new areas for further research. Particularly, the reason for the decrease in metal release at pH 8 by longer sonication times (1.5 hr) was expected to be due to re-association with sediment resulting from changes in sediment surface area. Sediment surface area measreuments (data not shown) did not show a significant increase after sonication, especially between 1 hr and 1.5 hr sonication. Therefore, the exact mechanisms for the decrease in metal release by longer sonication times are unclear in PACS-2 system and require further study to investigate effects of prolonged sonication. Furthermore, determination of metal speciation and oxidation by sequential chemical extraction and/or XAFS spectroscopy

may provide fundamental information for understanding the mechanism of metal sediment interaction in the presence of ultrasound.

Acknowledgements

Funding from NOAA/Ohio Sea Grant College Program and the NSF Environmental Molecular Science Institute at The Ohio State University is gratefully acknowledged. The authors thank S. Jones and J. Bigham for their help with BET N_2 and XRD measurements.

Metal Cation	Water Exchange Rate Constants k_{-H_2O} (s^{-1})
Hg(II)	2×10^{9}
Pb(II)	7×10^{9}
Ni(II)	3×10^{4}
Cr(III)	5×10^{-7}

Table 5.1 Metal water exchange rate constants [*129*]

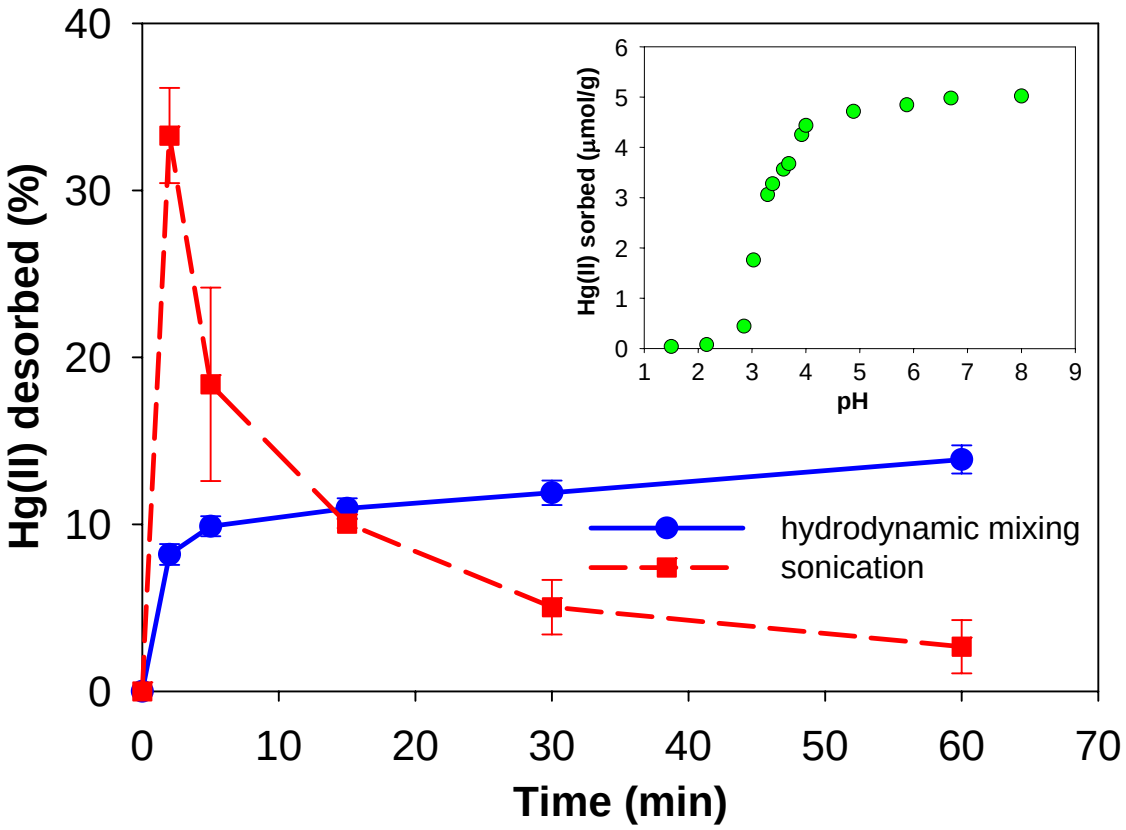

Figure 5.1 Desorption of Hg(II) from alumina particles (pH = 4.0, T = 20 °C, I = 0.1 M, [particle] = 33 g L^{-1}, $[Hg(II)]_{initial\ on\ particle}$ = 5.0 μmol g^{-1}, sonication intensity = 36 W cm^{-2}). Figure inset: pH dependent Hg(II) sorption curve.

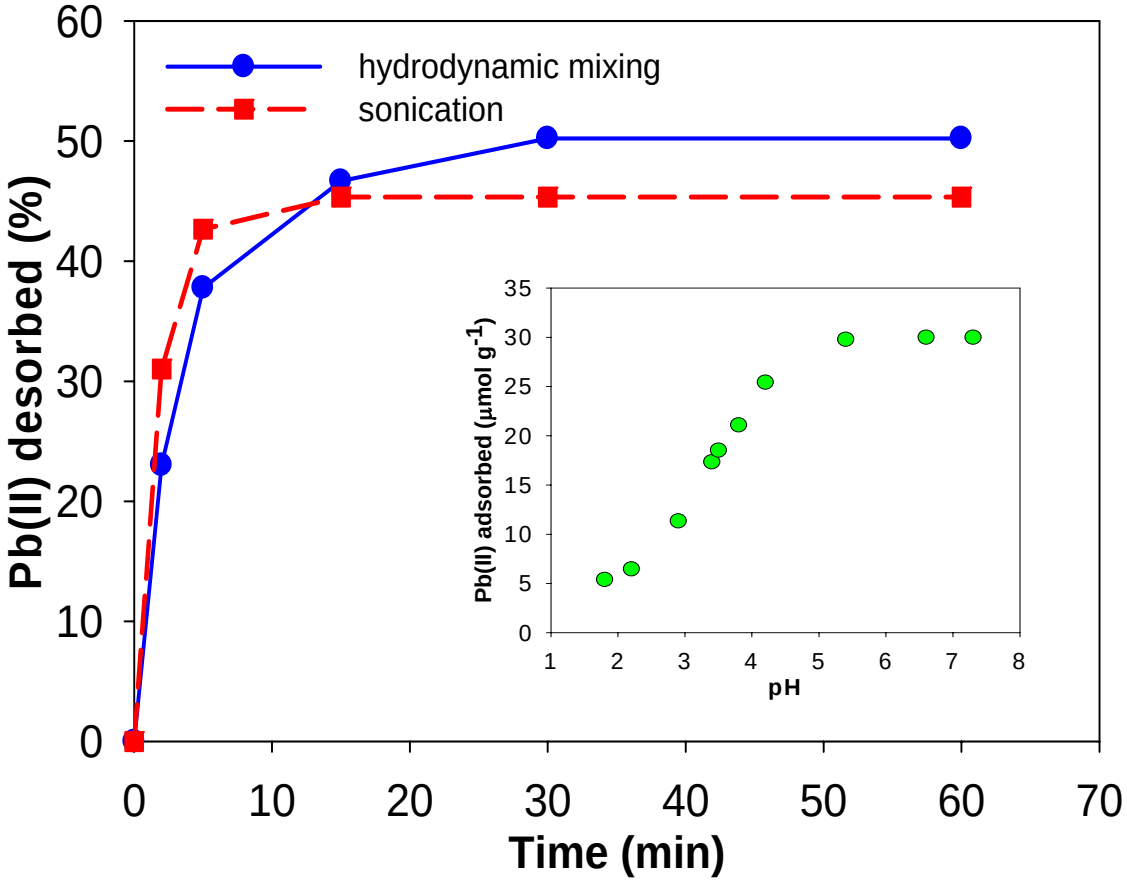

Figure 5.2 Desorption of Pb(II) from alumina particles (pH = 3.0, T = 20 °C, I = 0.1 M, [particle] = 33 g L^{-1}, $[Pb(II)]_{initial\ on\ particle}$ = 30 μmol g^{-1}, sonication intensity = 36 W cm^{-2}). Figure inset: pH dependent Pb(II) sorption curve.

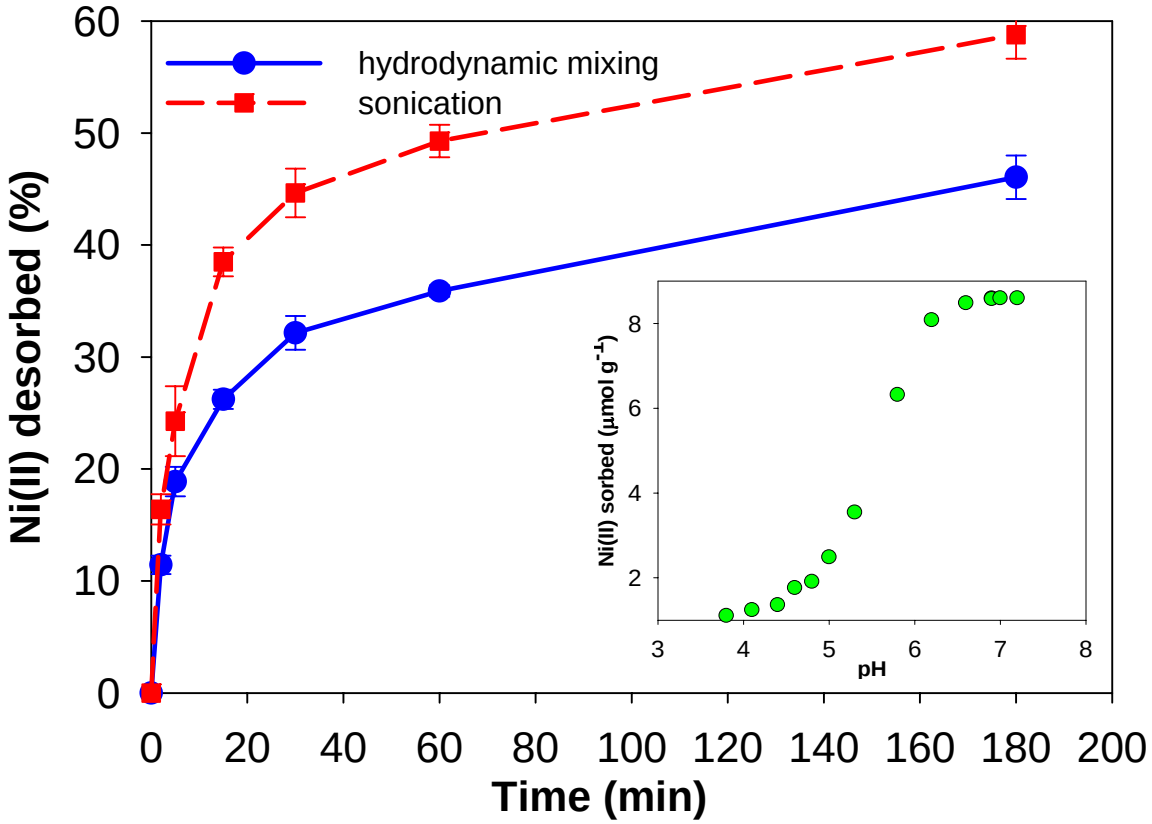

Figure 5.3 Desorption of Ni(II) from alumina particles (pH = 4.0, T = 20 °C, I = 0.1 M, [particle] = 33 g L^{-1}, $[Ni(II)]_{initial\ on\ particle}$ = 8.6 μmol g^{-1}, sonication intensity = 36 W cm^{-2}). Figure inset: pH dependent Ni(II) sorption curve.

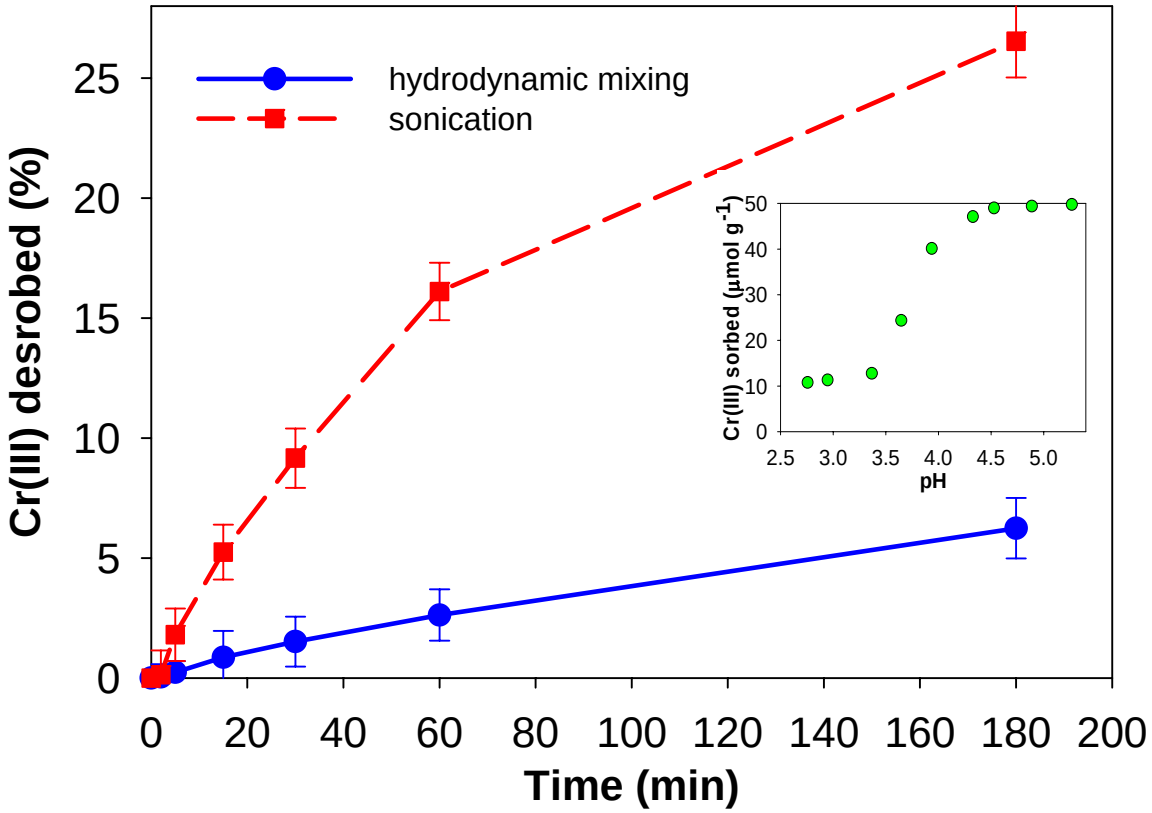

Figure 5.4 Desorption of Cr(III) from alumina particles (pH = 3.0, T = 20 °C, I = 0.1 M, [particle] = 33 g L^{-1}, $[Hg(II)]_{initial\ on\ particle}$ = 50 µmol g^{-1}, sonication intensity = 36 W cm^{-2}). Figure inset: pH dependent Cr(III) sorption curve.

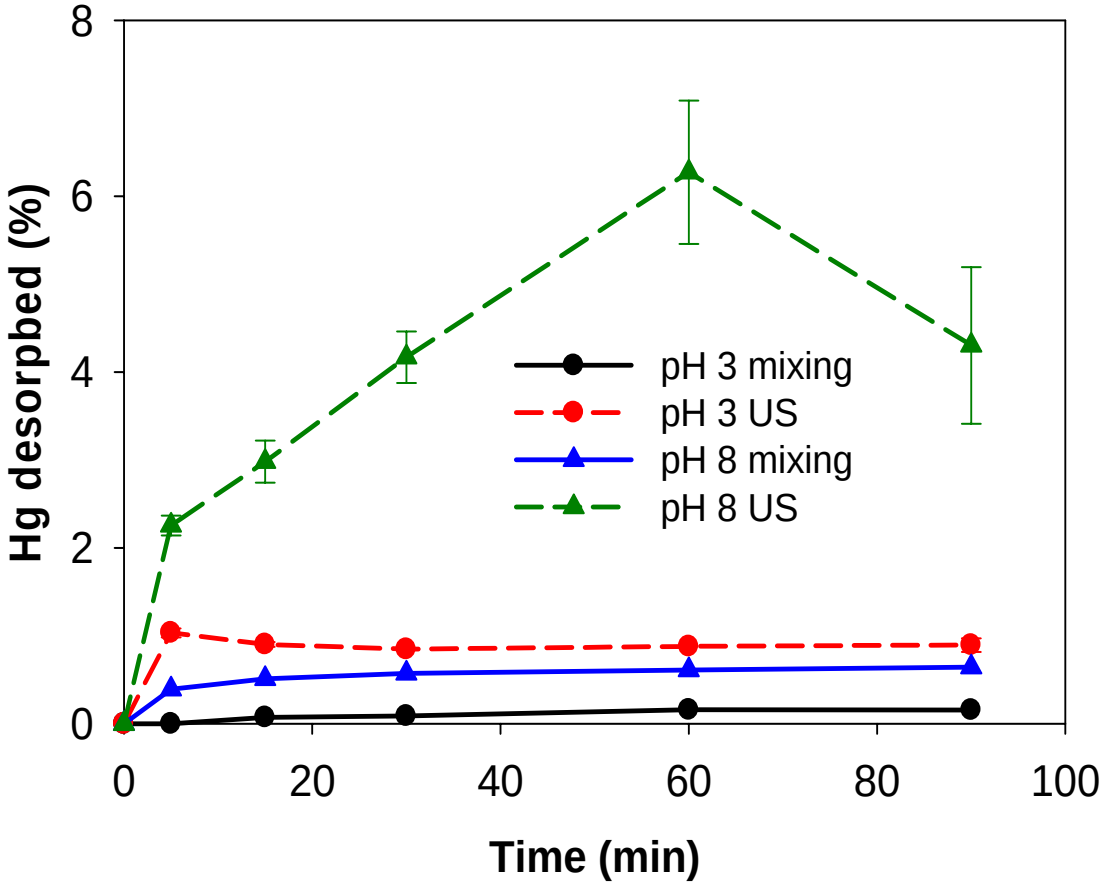

Figure 5.5 Release of Hg from PACS-2 marine sediment (T = 20 °C, I = 0.1 M $NaNO_3$, [particle] = 33 g L^{-1}, $[Hg]_{certified}$ = 3.04 ± 0.20 mg kg^{-1}, sonication intensity 36 W cm^{-2}).

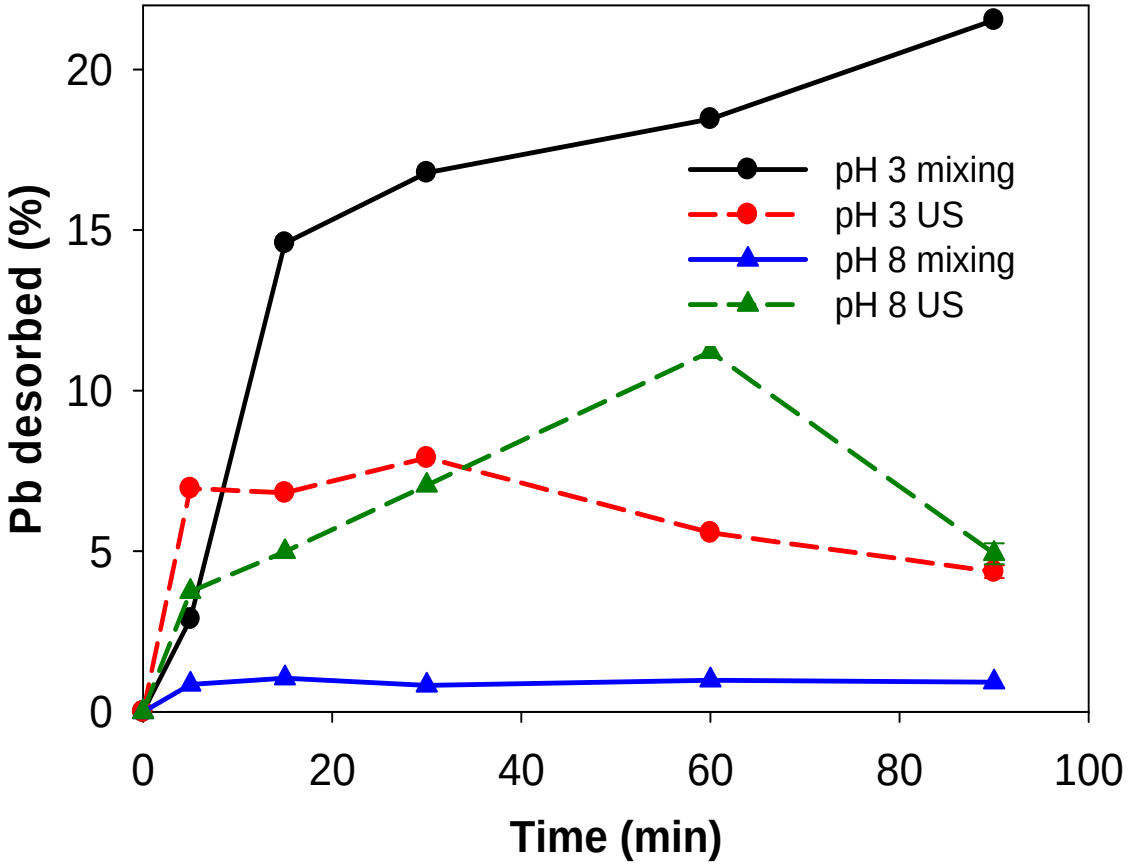

Figure 5.6 Release of Pb from PACS-2 marine sediment (T = 20 °C, I = 0.1 M $NaNO_3$, [particle] = 33 g L^{-1}, $[Pb]_{certified}$ = 183 ± 8 mg kg^{-1}, sonication intensity 36 W cm^{-2}).

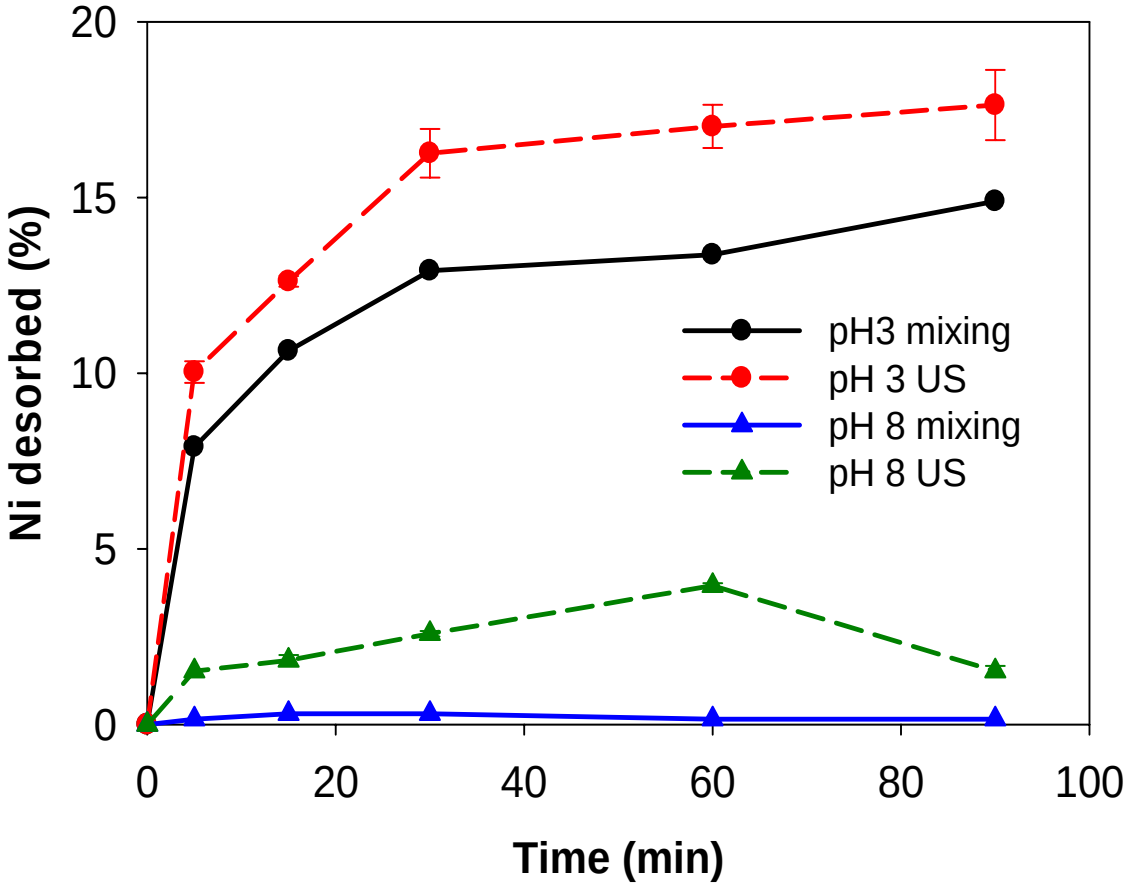

Figure 5.7 Release of Ni from PACS-2 marine sediment (T = 20 °C, I = 0.1 M $NaNO_3$, [particle] = 33 g L^{-1}, $[Ni]_{certified}$ = 39.5 ± 2.3 mg kg^{-1}, sonication intensity 36 W cm^{-2}).

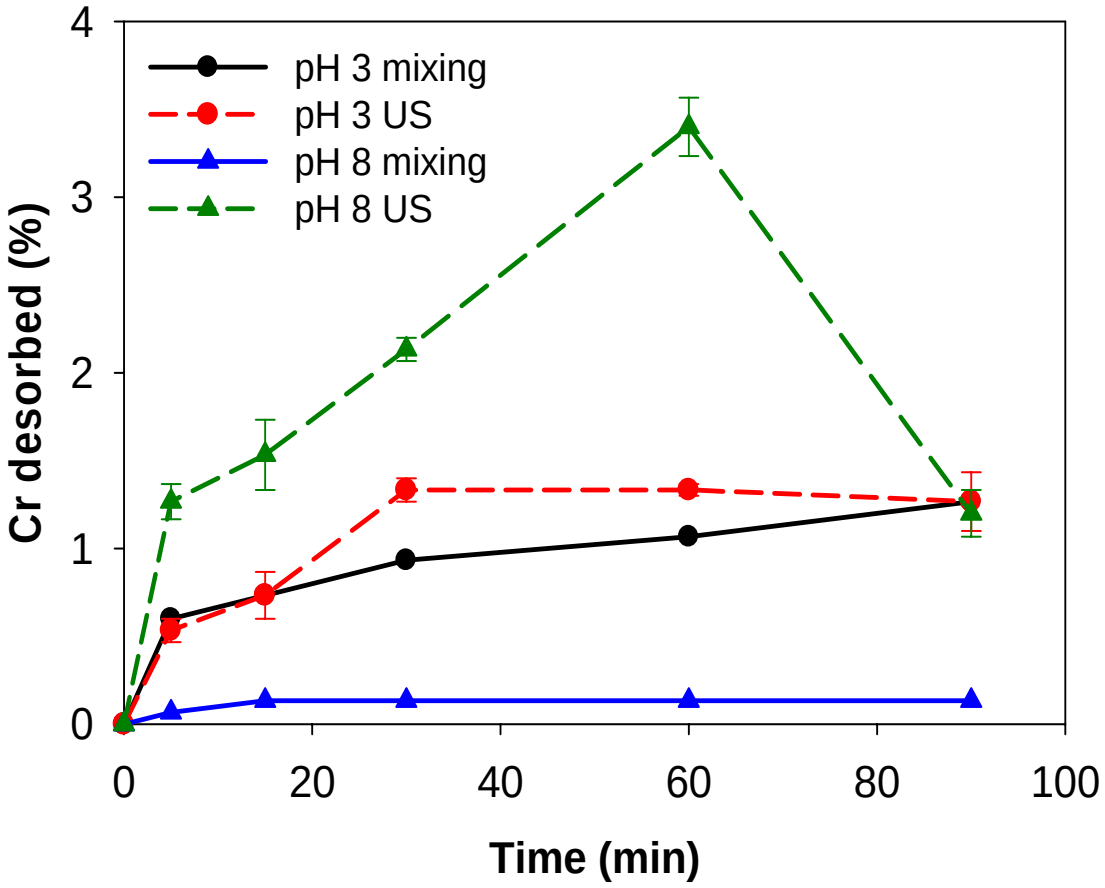

Figure 5.8 Release of Cr from PACS-2 marine sediment (T = 20 °C, I = 0.1 M $NaNO_3$, [particle] = 33 g L^{-1}, $[Cr]_{certified}$ = 90.7 ± 4.6 mg kg^{-1}, sonication intensity 36 W cm^{-2}).

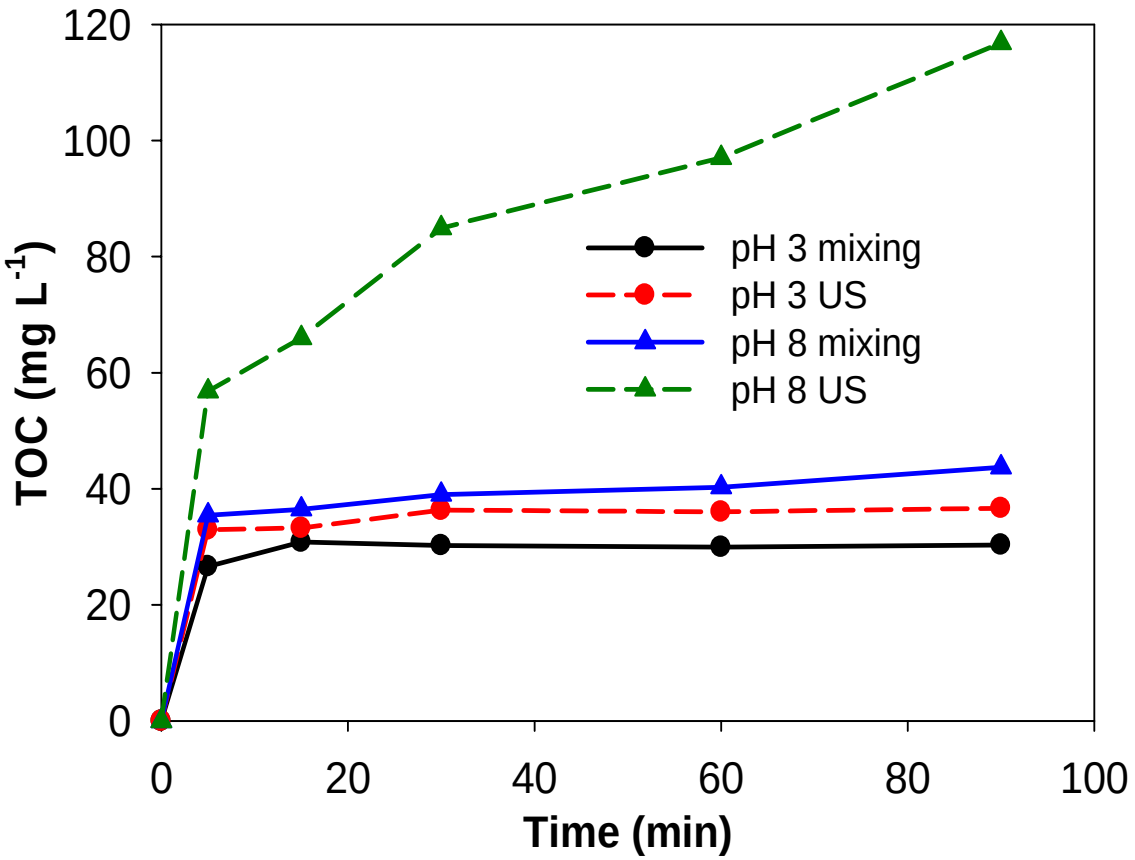

Figure 5.9 Dissolved organic matter released from PACS-2 marine sediment (T = 20 °C, I = 0.1 M $NaNO_3$, [particle] = 33 g L^{-1}, sonication intensity 36 W cm^{-2}).

CHAPTER 6

REMOVAL OF MERCURY FROM SEDIMENT BY ULTRASOUND COMBINED WITH BIOMASS (TRANSGENIC CHLAMYDOMONAS REINHARDTII)

(Submitted to *Environmental Science and Technology*, June 2006)

6.1 Abstract

As one of the most pervasive environmental problems, Hg pollution in sediment is particularly difficult to clean up because it cannot be decomposed. The application of ultrasound combined with biomass (transgenic *Chlamydomonas reinhardtii*, a green alga) for the removal of Hg from model and real sediments (Al_2O_3, α-HgS, and PACS-2 marine sediment) was investigated in this study. Ultrasound was found to effectively enhance Hg release from Al_2O_3, α-HgS, and PACS-2 marine sediment into the aqueous phase compared to mechanical shaking. A transgenic *Chlamydomonas reinhardtii* (2AMT-2) expressing a plasmamembrane-anchored metallothionein polymer effectively recovered Hg(II) released into the aqueous phase by sonication over a broad pH range from 2.0 to 9.0. The results showed that this combined technique of ultrasound and alga biomass (2AMT-2) engineered for enhanced metal recovery was effective to remove Hg

from solids and sediments, especially from Al_2O_3 and α-HgS with no natural organic matter. The results of this study are discussed with respect to the development of *in-situ* remediation techniques for Hg-contaminated sediments.

6.2 Introduction

In aquatic systems, the major fraction of mercury (Hg), inorganic mercury (Hg(II)), is stored in sediments by sorption and/or precipitation, which may be released into the aqueous phase providing a substrate for the synthesis of methylmercury, a serious threat to wildlife and human beings (*4*). Hg release from sediments can be facilitated by high Cl^- concentration, low acidity, or high dissolved organic matter (*44*,*45*,*46*). Therefore, it is necessary to treat and/or remove Hg from sediments to control the methylation and bioaccumulation of Hg in the biosphere.

Remediation options for metal-contaminated sediments can be categorized as (*48*,*166*): (i) isolation by "*in-situ*" and "*ex-situ*" capping; (ii) "*in-situ*" containment by solidification/stabilization, and (iii) dredging followed by "*ex-situ*" treatments. Capping and solidification/stabilization are relatively low-cost remediation techniques, but do not remove Hg from the contaminated site and thus have the potential for future Hg release. Several types of techniques may be applicable for the cleanup of dredged metal-contaminated sediments, including washing, chemical extraction, and biosorption treatment (*48*,*60*,*166*,*167*). However, besides costly excavation, all these techniques are time consuming due to slow and/or nonreversible desorption (*46*,*67*).

As an environmentally benign technology, sonochemistry has been widely applied in the environmental engineering field for remediation of contaminated substrates (*68*). The mechanisms of sonochemical techniques consist of thermal, chemical, and physical effects. Briefly, ultrasound will cause the formation of cavitation bubbles leading to high localized temperatures and pressures (in excess of 5000 K and 500 atm, respectively), which induce chemical reactions and the degradation of organic pollutants (*68*). Physical effects (shock waves, microjets, microstreaming, etc.) induced by ultrasound play an important role in heterogeneous systems (*149*). Ultrasound has been applied to desorb/leach contaminants from soils and sediments (*92*,*94*,*95*). In our previous studies, ultrasound was found to be effective in desorbing Hg(II) from Al_2O_3 (*138*) and releasing Hg(II) from HgS (*137*). Therefore, ultrasound may provide an alternative technology for Hg contaminated-sediment remediation, effectively releasing Hg from the sediment *in-situ* into aqueous phase. Once Hg is released by ultrasound it then must be recovered from aqueous solution by other techniques, such as activated carbon adsorption and biomass sorption.

As inexpensive biomass, algae (living or dead) have immense capacity to sorb metals and have been applied to treat wastewaters (*59*,*60*,99). *Chlamydomonas reinhardtii* (*C. reinhardtii*), a unicellular green alga, has been found to effectively adsorb or sequester dissolved metals such as Cd, Co, Cu, Ag, and Pb (*61*,*62*,*98*,*177*). Metallothionein (MT), a low molecular weight, cysteine-rich metal-binding protein, has been fused to biosorbents to enhance biomass tolerance and binding capacity to metals (*100*). Genetically engineered *E. coli* expressing MT was found to selectively bind Hg(II) over other metals and was resistant to changes in ambient conditions such as pH,

ionic strength, and common metal chelators (*64*). Transgenic *C. reinhardtii* expressing MT has been found to bind 2-5 fold more Cd relative to wild-type cells (*101,102*). Therefore, transgenic *C. reinhardtii* expressing MT is expected to selectively sequester Hg and to have a higher metal binding capacity than wild-type *C. reinhardtii*.

The purpose of this study was to investigate the application of ultrasound combined with biomass (*C. reinhardtii*) to remove Hg from sediments. Specifically, uptake of aqueous Hg(II) by transgenic *C. reinhardtii* was examined first to determine the binding capacity, kinetics and applicable pH range for metal binding. Subsequently, the removal of Hg from model and real sediments (Al_2O_3, α-HgS, and PACS-2 marine sediment) by ultrasound combined with transgenic *C. reinhardtii* was conducted.

6.3 Materials and Methods

6.3.1 Algae cell growth and harvest

Transgenic (2AMT-2) and wild-type (CC2137) strains of C. reinhardtii were cultured following the method of Siripornadulsil (*102*). Briefly, the cells were inoculated in 1 L tris-acetate phosphate (TAP) media with a 1% (v/v) inoculum shaking at 22-27 ^{o}C under continuous illumination from fluorescent tubes. After approximately 5 days, the cell density was monitored by measuring the absorbance at 750 nm using a UV-VIS spectrophotometer (Cary Eclipse, Varian) to determine the cell density. Cultures were harvested in the log phase of growth at a density < 1.0 A_{750nm} (= 1 x 10^6 cells mL^{-1}). The cells were collected by 10 min centrifugation at 5,000 rpm and washed twice with 1 L solution of 0.01 M ionic strength of $NaNO_3$ for use in the following experiments.

6.3.2 Hg(II) binding to algal cells

Hg(II)-cell binding isotherms were conducted in 60 mL polyethylene bottles. One mL of 5.0 A_{750nm} of cell suspension was added to each bottle filled with 30 mL solution of various initial Hg(II) concentrations ranging from 0 to 2.5 μM. The bottles were placed on a rotating shaker at 200 rpm for 24 hr which was observed to reach equilibrium in kinetic experiments. Solution pH was controlled initially at pH 6.0 ± 0.1 by manually adjusting with 0.1 M of NaOH and HNO_3. Samples were centrifuged to separate the supernatant and cells. The effect of pH on Hg(II) binding capacity and binding kinetics to 2AMT-2 transgenic cells were determined under similar conditions with initial [Hg(II)] = 1.33 μM which was observed to reach the maximum binding capacity. The amount of Hg(II) binding to cells was calculated from the difference between Hg(II) in the initial solution and that remaining in the supernatant solution.

6.3.3 Experimental procedures

Mercury (II) nitrate (99.99+%, Sigma-Aldrich) was used to make a dissolved Hg(II) solution without further purification. Ionic strength and pH were adjusted with NaOH, HNO_3 and $NaNO_3$ purchased from Fisher Scientific. Aluminum oxide (adsorption grade Al_2O_3, 80-200 mesh particle size, density 4 g cm^{-3}) and cinnabar (red HgS, 99.5%) purchased from Fisher Scientific were utilized as model sediments and PACS-2 marine sediment with a certified Hg content of 3.04 mg kg^{-1} purchased from National Research Council (NRC) was used as a comparison field contaminated sediment. Water used to prepare the solutions was from a Millipore system (R = 18.2 MΩ-cm).

At the start of an experiment, 1.0 g of Al_2O_3 sorbed with 5.0 μmol/g of Hg(II) (*138*), 0.002 g of cinnabar, or 0.5 g of PACS-2 marine sediment was transferred to a glass rosette reactor with 60 mL of 0.01 M of $NaNO_3$ solution. Batch reactions were carried out using a 20 kHz ultrasonic probe system (550 Sonic Dismembrator, Fisher Scientific) at a power input intensity of 20 Wcm^{-2}. In order to easily separate cells from sediments, concentrated algal cells were put inside dialysis bags (Spectro/Por regenerated cellulose biotech membrane, 3500 Da) and the dialysis bags were suspended in reaction solution around ultrasonic probe. The RCBT 3500 dialysis bags were chosen based on a previous study (*19*) and a control experiment showed no obvious Hg(II) loss due to the presence of dialysis bags. The reacting solution temperature was controlled at 20.0 ± 0.5 °C by a cooling bath. Solution pH was controlled with a pH-Stat autotitrator (PHM290, Radiometer Analytical). For comparison purposes, mechanical shaking experiments were also conducted on a rotating shaker at 200 rpm without sonication under the same experimental conditions as those with sonication. After selected times of reaction, the dialysis bags were taken out and rinsed with DI water. The cells were transferred to polypropylene tubes, recovered by 10 min centrifugation at 5,000 rpm, then digested with 20 mL of 70% HNO_3 using a nominal 630-watt system at 70% power and 80 psi for 60 min by microwave digestion (MDS 2100, CEM Co.). The supernatant and sediments were separated by centrifugation for 10 min at 5000 rpm. 0.1 g dried sediment was dissolved in 5 mL HNO_3, 1 mL HCl, and 10 mL HF using a nominal 630-watt system at 80% power and 150 psi for 60 min. All digested solutions and the supernatant samples were analyzed for Hg. Selected experiments were performed in duplicate or triplicate to determine data error and verify reproducibility.

6.3.4 Analyses

Prior to Hg(II) analysis, solution samples were oxidized overnight with 5% BrCl followed by reduction with 30% NH_2OH•HCl. All samples were analyzed by cold vapor atomic absorption spectroscopy (CVAAS) (SpectrAA 880Z, Varian, Australia) for Hg and inductively coupled plasma atomic emission spectroscopy (ICP-AES) (Vista Ax, Varian, Australia) for other metals. SO_4^{2-}, SO_3^{2-}, and $S_2O_3^{2-}$ in cinnabar systems were determined by ion chromatography (DX 500, Dionex) with an Ionpac® AS11 4mm anion-exchange column with 5 mM sodium hydroxide eluent. Dissolved organic matter in PACS-2 marine sediment systems was measured by a Shimadzu TOC-5000A analyzer.

6.4 Results and Discussion

6.4.1 Binding of aqueous Hg(II) to algal cells

To test the feasibility of algal cells to remove Hg from sediment combined with ultrasound, the uptake of aqueous Hg(II) by *C. reinhardtii* cells was conducted first. Figure 6.1 shows Hg(II) uptake isotherms for transgenic (2AMT-2) and wild-type (CC2137) *C. reinhardtii* cells versus dissolved Hg(II) concentrations. As we can see, transgenic *C. reinhardtii* cells have higher Hg(II) binding capacity than wild type. The enhancement is attributed to the expression of a plasma membrane-anchored metallothionein polymer and the observed enhancement of metal binding by fusing MT to the cell surface. This mechanism is consistent with the results obtained for Cd binding (*102*) and Hg binding by transgenic *E. coli* (*64*). However, the binding capacity by 2AMT-2 (6.0 nmol A_{750nm}^{-1}) was not several fold that of CC2137 as found with Cd (*102*). The difference may be due to differences in experimental conditions, such as harvested

cells versus growing cells and DI solution versus TAP media, or differences in protein expression between this and the previous study (*102*).

The Hg(II) uptake kinetics by transgenic cells at pH 6.0 is shown in Figure 6.2. A rapid initial uptake occurred in very short times and a pseudo-equilibrium (60% uptake) was reached. A slower uptake was observed after 1 hr and after 12 hr, a new equilibrium was approached (90% uptake). The results agreed with the binding processes of heavy metals by algae: an initial rapid (passive) uptake (few sec or min) followed by a much slower metabolism-dependent (active) uptake into the inside of the cells (*99*,*178*). Previous studies have reported similar sorption kinetics of metals to dead and living wild-type *C. reinhardtii* cells (*61*,*62*). In fact, the Hg(II) initial rapid uptake and the slower uptake by transgenic *C. reinhardtii* cells observed in this study were faster and slower, respectively, than those of other metals by wild-type cells (*61*,*62*). This observation was likely because of the presence of MT which has the sulfur-bearing cysteines. The high affinity of Hg for MT induced a faster initial uptake. On the other hand, the strong binding between Hg(II) and MT may inhibit Hg(II) diffusion into the algal cells, hindering the slow uptake phase.

The pH-dependent Hg(II) binding curve provides more support for the binding of heavy metals by MT in transgenic cells. Spectroscopic characterization and surface modeling studies have indicated that metal binding by wild-type algae is dominated by complexation to carboxylic functional groups in a pH-dependent manner (*61*,*62*,*98*,*178*). The uptake of metals increases with pH, reaching a maximum at an optimum pH value depending on metal concentrations, and then decreases at high pH values due to complexation by hydroxo species. However, changing pH (from 2 to 9) did not

significantly affect Hg(II) uptake by 2AMT-2 cells in this study (Inset in Figure 6.2). Ethylenediaminetetraacetic acid (EDTA) washing and extended X-ray absorption fine structure (EXAFS) have given information about the coordination of Cd by the MT cysteinyl sulfide (*102*). Similarly, Hg(II) is expected to form a stronger complex with the MT cysteinyl sulfide, which is stable over a broad pH range. The broad effective pH range under which transgenic algae sequester Hg(II) enhances its potential applicability to remove Hg from sediment once the Hg is released from sediment by ultrasonic treatment.

6.4.2 Removal of Hg(II) from Al_2O_3 and HgS by ultrasound combined with 2AMT-2

To test the ability of transgenic algae to recover Hg from substrates undergoing ultrasonic treatment, we exposed transgenic *C. reinhardtii* (2AMT-2) to Hg laden aluminum oxide (Al_2O_3) and mercury sulfide (HgS) during ultrasonic treatment. Al_2O_3 presorbed with Hg(II) was used to simulate sediment with low/no natural organic matter. Cinnabar (α-HgS) was used to model sulfidic and anoxic conditions where HgS is the major fraction of Hg in sediments.

As shown in Figure 6.3, the desorptions at pH 5.0 without algal cells by both ultrasound and mechanical shaking were very low (below 5%) although ultrasound enhanced the initial Hg(II) desorption. Based on the Hg(II) pH-dependent sorption curve to Al_2O_3 (*138*), Hg(II) has a sorption edge from pH 3.0 to pH 5.0. Thus, the low desorption rate without the presence of algal cells was due to 94% of the available Hg(II) sorbing to Al_2O_3 under equilibrium at pH 5.0 under our experimental conditions. Without changing the equilibrium condition by lowering pH or sequestration of Hg(II) from the

aqueous phase, a higher desorption rate cannot be achieved. As previously demonstrated (*138*), ultrasonic energy enhances initial Hg(II) desorption. However, longer sonication led to a decrease in Hg(II) desorption due to occlusion by aluminum hydroxide precipitation induced by ultrasound.

Although Hg(II) desorption was low at pH 5.0, the presence of 2AMT-2 cells facilitated the efficient removal of Hg(II) from Al_2O_3 (Figure 6.3). The combination of ultrasound and 2AMT-2 cells had a much faster removal rate compared to mechanical shaking with cells. After 30 min, the Hg(II) desorption by ultrasound with cells reached a plateau (28% removal efficiency). Hg(II) removal by mechanical shaking with cells increased with time indicating that the Hg(II) sorbed on Al_2O_3 was readily desorbed into the aqueous phase and sequestered by the algae. Strawn et al. (*179*) observed that 98% of sorbed Pb on Al_2O_3 was reversibly desorbed within 3 days at pH 6.5 using a cation-exchange resin as a sink for aqueous Pb. Gao et al. (*67*) also showed that 90% of freshly sorbed Pb and Cd were desorbed at pH 7-8 using EDTA to sequester aqueous Pb and Cd. Therefore, given long enough time and replacement of the algal cells, high Hg(II) removal from Al_2O_3 would be expected even at pH values above the sorption edge.

As shown in Figure 6.3, removal of Hg(II) by less than 15 min of ultrasonic treatment in the presence of cells achieved results equivalent to that observed for 60 min of mechanical shaking in the presence of cells. This is attributed to ultrasonic effects on Hg(II) desorption and an increase in the mass transfer rate. Ultrasonic enhanced release of Cu from brick and desorption of Hg(II) from Al_2O_3 have been observed previously (*94*, *138*). Oncel et al. (*92*) found that ultrasound combined with thiourea leached 98% of Ag from solid waste in 24 min. In this study, ultrasound improved Hg(II) desorption from

Al_2O_3 and increased Hg(II) transport through dialysis bags to reach the algal cells. The observed Hg(II) removal plateau after 30 min may be explained by saturation of algal cells with Hg(II) or occlusion of Hg(II) desorption by aluminum precipitation as observed with ultrasound (*138*). However, after 30 min of treatment, the normalized amount of Hg(II) on 2AMT-2 cells was approximately 6.5 nmol A_{750nm}^{-1} indicating saturation according to the binding capacity isotherm (Figure 6.1). Therefore, the removal plateau phenomenon observed appears to be due to saturation of algal cells limiting continued Hg(II) sequestration from the aqueous phase.

In the cinnabar system, ultrasound oxidizes sulfur (S) in HgS and releases Hg(II) into the aqueous phase. The concentrations of Hg(II) released into the aqueous phase are expected to be identical to the production of S oxidation products (SO_4^{2-}, SO_3^{2-}, $S_2O_3^{2-}$) since Hg and S are present in a 1:1 molar ratio in cinnabar. We observed that the primary S oxidation product was SO_4^{2-}. No S oxidation intermediates (SO_3^{2-} and $S_2O_3^{2-}$) were detected. Figure 6.4 shows the release of Hg(II) from cinnabar by ultrasound alone and by the combination of ultrasound with 2AMT-2 algal cells. Hg(II) release in the presence and absence of 2AMT-2 cells were substantially different. Without 2AMT-2 cells, dissolved Hg(II) was stoichiometrically less than SO_4^{2-}, whereas the release of Hg(II) in the presence of 2AMT-2 cells was substantially improved and was stiochiometrically higher than SO_4^{2-}.

Ultrasound dissolved cinnabar through oxidation reactions between S from cinnabar and the oxidizing species (•OH, HO_2•, H_2O_2, etc.) induced by ultrasound. The details of the dissolution mechanisms have been discussed elsewhere (*137*). Without the presence of algal cells, the majority of dissolved Hg(II) was adsorbed onto the remaining

cinnabar particles and ultrasonic effects on cinnabar particles led to higher Hg(II) adsorption. The presence of algal cells results in sequestration of dissolved Hg(II) released by ultrasound treatment keeping it from re-adsorbing onto cinnabar particles. However, unexpectedly, dissolved Hg(II) with the presence of algal cells was 2-fold higher than that equivalent to SO_4^{2-} production. One reason for this observation was that the algal cells may have actively transported SO_4^{2-} into the cells reducing the effective concentration in the solution.

The other interpretation for the observed higher [Hg(II)] than [SO_4^{2-}] was attributed to other S oxidation products. Although no SO_3^{2-} and $S_2O_3^{2-}$ were detected, they may be produced below the detection limits. However, these small amounts of intermediates are not attributed to the 2-fold difference between dissolved Hg(II) and SO_4^{2-}. One of the S oxidation products, colloidal elemental sulfur (S_x), was not measured in this study. The production of S_x from sulfide ion oxidation was observed and detected previously by H_2O_2 (*180*), shock waves (*181*), or ultrasonic treatment (*71*). In this study, physical effects of ultrasound may generate sulfide ion from cinnabar particles. Subsequently, thermal and chemical effects of ultrasound may produce SO_4^{2-} as well as S_x. Thus, Hg(II) sequestered by algal cells may be equivalent to the total of S_x and SO_4^{2-}, which would be higher than the SO_4^{2-} concentration.

Considering the results in Al_2O_3 and HgS systems (Figure 6.3 and Figure 6.4), the application of ultrasound combined with 2AMT-2 algal cells was demonstrated to be a very effective means to remove and recover Hg.

6.4.3 Removal of Hg from PACS-2 marine sediment by ultrasound combined with 2AMT-2

To further test the effectiveness of ultrasound combined with 2AMT-2 algal cells to remove Hg, the application of this combination was carried out with field-contaminated sediment. Reference PACS-2 marine sediment (NRC, Canada) was chosen for field-contaminated sediment experiments. The PACS-2 sediment has a certified Hg content of 3.04 ± 0.20 mg kg^{-1}, which was confirmed by microwave digestion analysis in our laboratory. Hg desorption and removal by ultrasound and 2AMT-2 algal cells were conducted at pH 4.0 and 8.0, respectively, to examine natural organic matter effects observed in other studies (*45*).

Figure 6.5 shows Hg desorption and removal by ultrasound with and without algal cells. Ultrasound released more Hg into the aqueous phase at pH 8.0 than at pH 4.0. At pH 4.0, Hg desorption was below 5% and increased slowly with sonication time. At pH 8.0, ultrasound greatly improved Hg desorption with 25% desorption at 60 min of sonication. This difference in Hg desorption at different pH values may be due to strong Hg complexation by natural organic matter (NOM), which determines the behavior and distribution of Hg in sediments (4). Xu et al. (*140*) found that at low pH, humic substances tended to adsorb and enhance the uptake of Hg(II) by alumina oxides from the solution phase. At high pH, the reverse effect was observed. Studies by Yin et al. (*45,46*) demonstrated that both Hg(II) adsorption and desorption rate coefficients were inversely correlated with the soil organic C content. The release of NOM at pH 4 and 8 in Figure 6.6 were similar to those of Hg, suggesting that NOM controlled Hg desorption in the

PACS-2 sediment system. Faster and greater NOM desorption at pH 8 led to fast and greater Hg desorption.

Hg sequestration by algal cells was not as high as expected. Relative to inorganic Al_2O_3 and HgS systems, where aqueous Hg was very low or nondetectable in the presence of algal cells, algal cells were less efficient at recovering Hg in the presence of sediments. At pH 8.0, only 5% of total Hg was sequestered by the algae while 25% of the total Hg was desorbed from sediments (Figure 6.5). As discussed above, NOM seemed to dominate Hg distribution in this system. In fact, aqueous Hg measured was just a few μg L^{-1} (data not shown), much lower compared to dissolved NOM as determined by TOC (Figure 6.6). The ratios of Hg to NOM were below 1 μg of Hg/mg of DOM, at which ratio strong Hg-thiol bonds have been observed to dominate Hg-NOM binding (*19*). Therefore, the strong NOM-Hg complexes may reduce the availability of free Hg ion, decreasing algal cell-Hg interactions. Indeed, it seems possible that at least some of the enhancement in sonication-induced removal of Hg at pH 8 vs 4 may have been due to the combined effect of pH and sonication on the dissolution/desorption of NOM from the sediments (Figure 6.5 and 6.6); with the latter happening due to the increased molecular charge associated with the dissociation of acidic functional groups on the organic moieties.

While enhanced solubilization of NOM likely controlled Hg-speciation, direct interactions between NOM and the algal biomass can not be ruled out. In the study by Lamelas et al. (*182*), Pb uptake by a green alga in the presence of NOM was higher than that predicted from measured free Pb^{2+} concentrations. They attributed this discrepancy to an effect of NOM on algae membrane permeability and surface ternary complexation.

In contrast to freely soluble NOM, the algae in our system are sequestered in a dialysis bag, limiting direct interactions with free Hg(II). Furthermore, there was no apparent diffusion of NOM into the dialysis bag. The expected MW of small NOM is less than the exclusion limit of the dialysis bag (3,500 Da). However, the effective MW of NOM may be increased, possibly, by aggregation mediated by bridging metal ions (*183*). Therefore, only a small amount of free Hg or Hg binding to small MW organic matter had the possibility to reach the algal cells inside the dialysis bags, leading to low Hg removal observed in real sediment.

In addition, the presence of cations (K^+, Ca^{2+}, Mg^{2+}, heavy metals) and other ligands (CO_3^{2-}, PO_4^{3-}, Cl^-) in complex solutions may inhibit or compete for Hg uptake by algal cells. Although Adhiya et al. (*62*) did not find inhibition of Cd uptake by lyophilized *C. reinhardtii* in the presence of equimolar levels of K^+ and Ca^{2+}, the K^+, Ca^{2+} and Mg^{2+} concentrations measured in this study were a thousand times higher than the Hg concentration. Besides NOM, other anion ligands may also lower Hg uptake by algal cells through complexation with Hg.

An implication of the results of this study is that the application of ultrasound and biomass (transgenic *C. reinhardtii*) has the potential for *in-situ* Hg removal from contaminated inorganic sediments. To effectively recover Hg from organic sediments, however, the competition for Hg binding between algae and NOM must be considered. The dialysis bag used in this study reduced the apparent effectiveness of this system. Another effective means for containing algal cells but allowing direct interaction of alga and Hg-NOM complexes would likely greatly improve algal uptake of Hg. To be applied as an *in-situ* remediation technique for Hg removal from natural sediments, efforts and

caution should be taken in reactor design. The criteria for reactor design should take into account not only how close the biomass should be to ultrasonic probe to trap released Hg, but also ultrasonic effects on biomass. The biomass should be immobilized on a stable matrix for easy collection and recovery of Hg. Further work is needed to determine parameters for optimum operations such as biomass replacement and sonication conditions.

Acknowledgements

Funding from NOAA/Ohio Sea Grant College Program and the NSF Environmental Molecular Science Institute at The Ohio State University is gratefully acknowledged. The authors also thank Zoee Gokhale for the growth of algal cells.

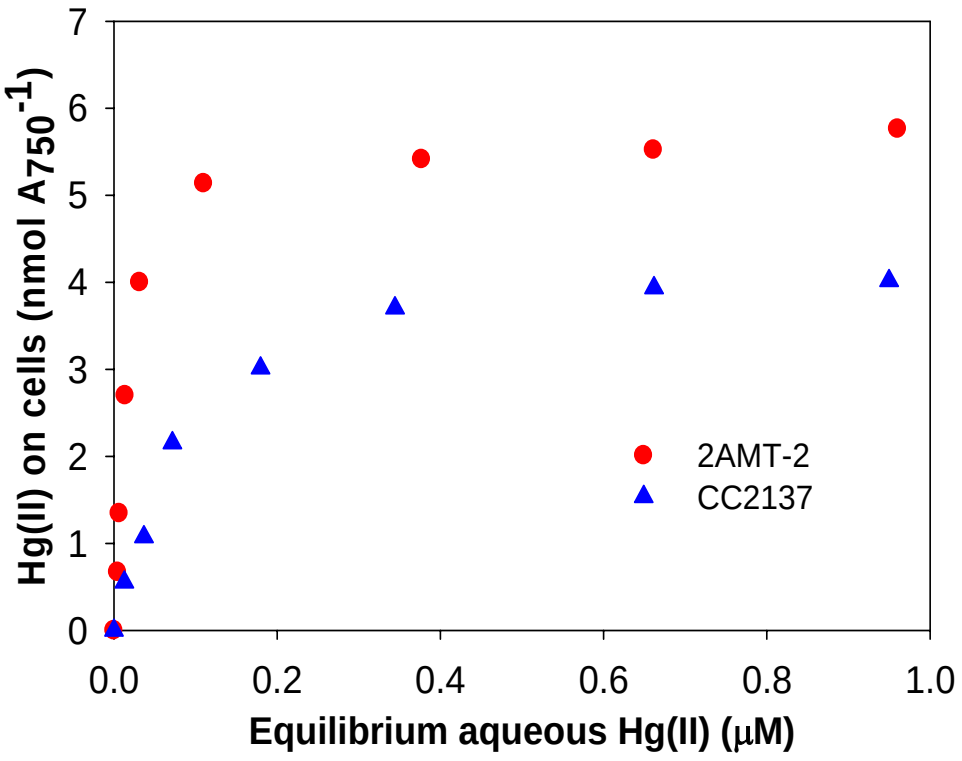

Figure 6.1 Binding of Hg(II) to transgenic (2AMT-2) and wild type (CC2137) of *C. reinhardtii* cells (pH = 6.0, I = 0.01 M $NaNO_3$, 1 mL of 5.0 A_{750nm} of cells in 30 mL solution with various Hg concentrations after sorption for 24 hr).

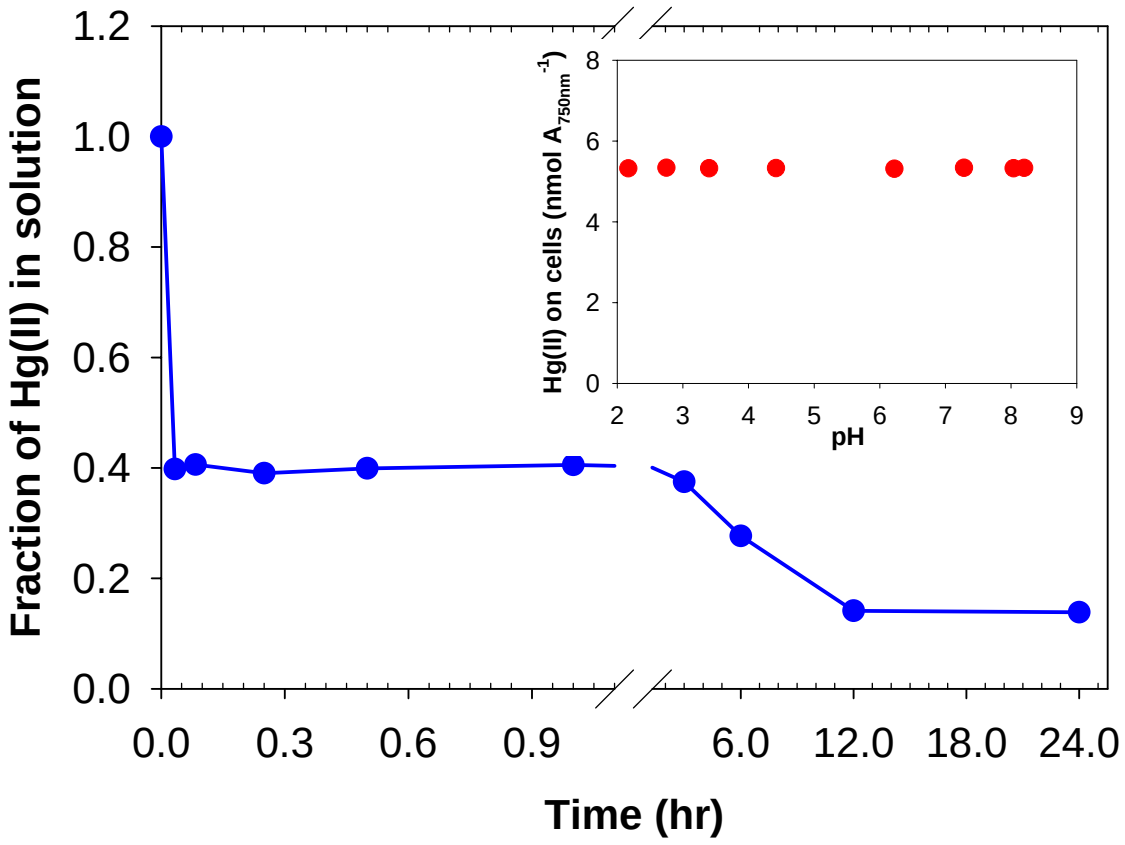

Figure 6.2 Hg(II) uptake kinetics by 2AMT-2 cells (pH = 6.0, I = 0.01 M $NaNO_3$, 1 mL of 6.4 A_{750nm} of cells in 30 mL with initial 1.33 μM Hg solution). Figure inset: pH dependent Hg(II) uptake by 2AMT-2 cells after sorption for 24 hr.

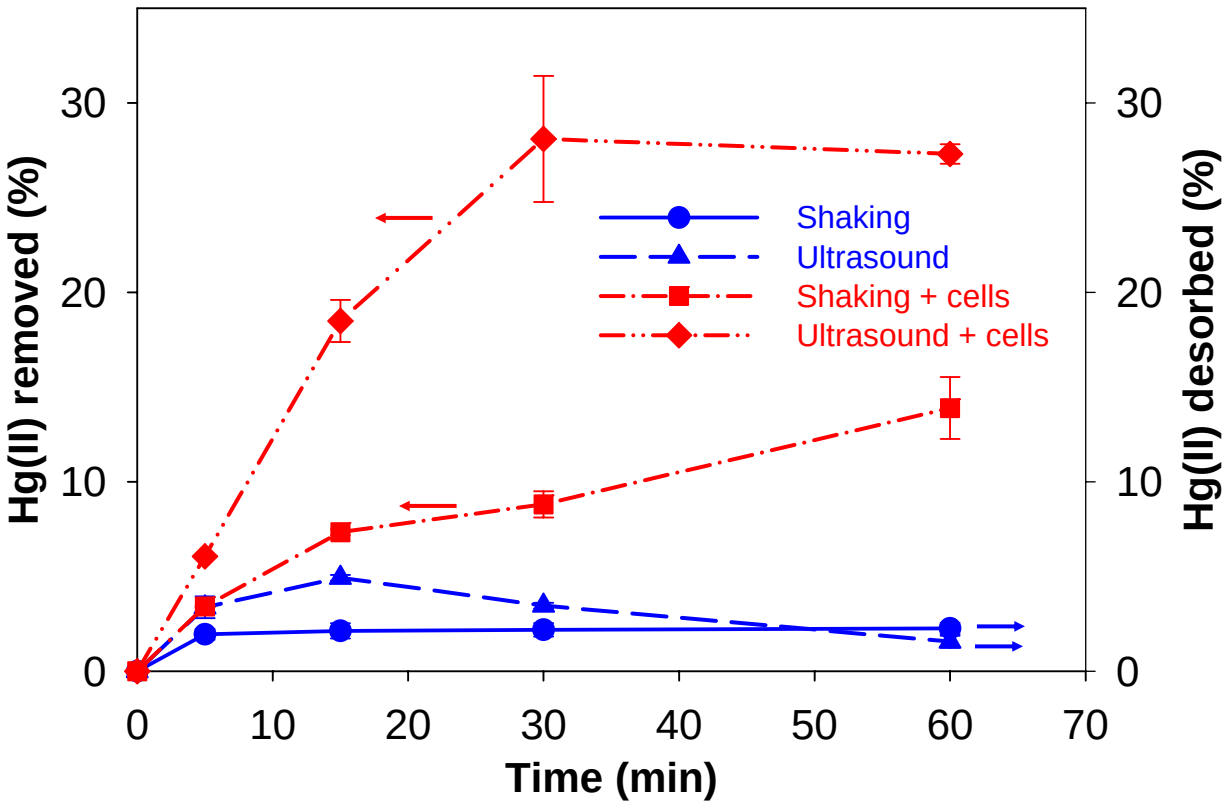

Figure 6.3 Removal of Hg(II) from Al_2O_3 with time (pH = 5.0, T = 20 °C, I = 0.01 M $NaNO_3$, [particle] = 16.7g L^{-1}, $[Hg(II)]_{initial\ on\ particle}$ = 5.0 μmol g^{-1}, 4 ml of 200 A_{750nm} of transgenic cells, sonication intensity 20 W cm^{-2}).

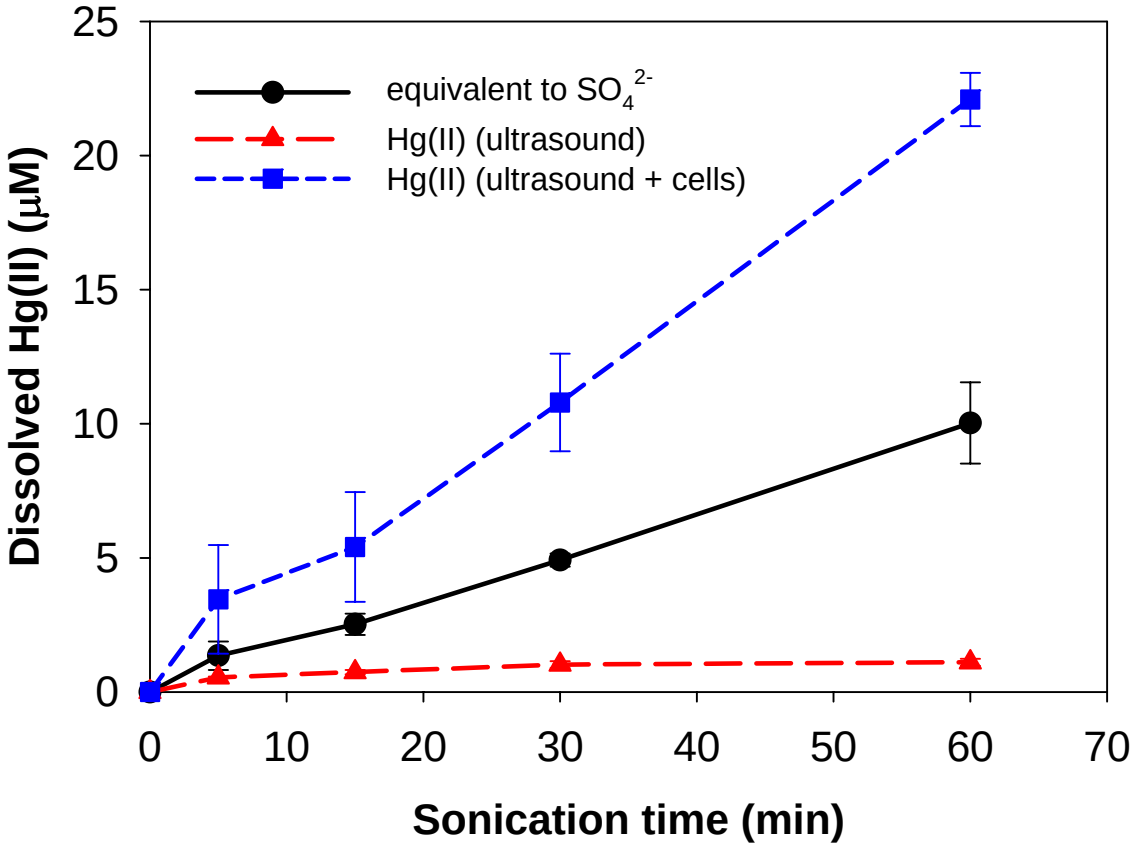

Figure 6.4 Release of Hg(II) from cinnabar by ultrasound and 2AMT-2 cells (pH = 4.0, T = 20 °C, I = 0.01 M $NaNO_3$, [cinnabar] = 0.0333 g L^{-1}, 4 ml of 200 A_{750nm} of transgenic cells, sonication intensity 20 W cm^{-2}, measured Hg(II) on algal cells by digestion was calculated as dissolved Hg(II)).

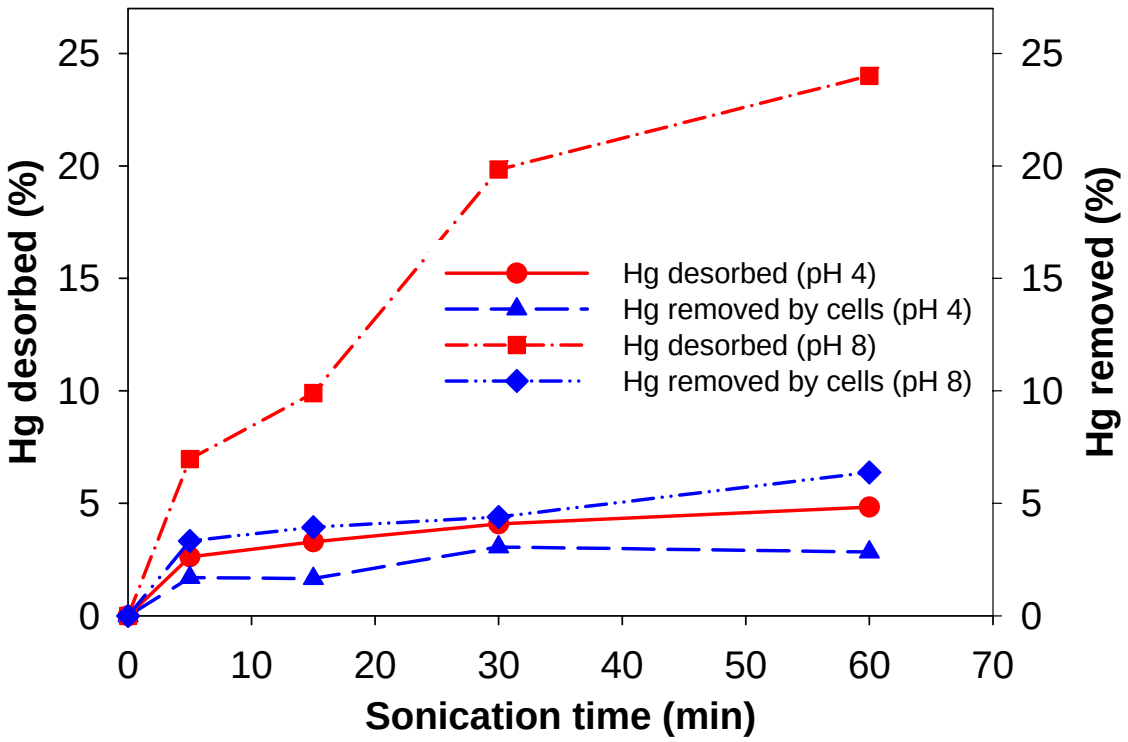

Figure 6.5 Removal of Hg from PACS-2 marine sediment with time (T = 20 °C, I = 0.01 M $NaNO_3$, [particle] = 8.3 g L^{-1}, $[Hg]_{certified}$ = 3.04 ± 0.20 mg kg^{-1}, 4 ml of 200 A_{750nm} of transgenic cells, sonication intensity 20 W cm^{-2}).

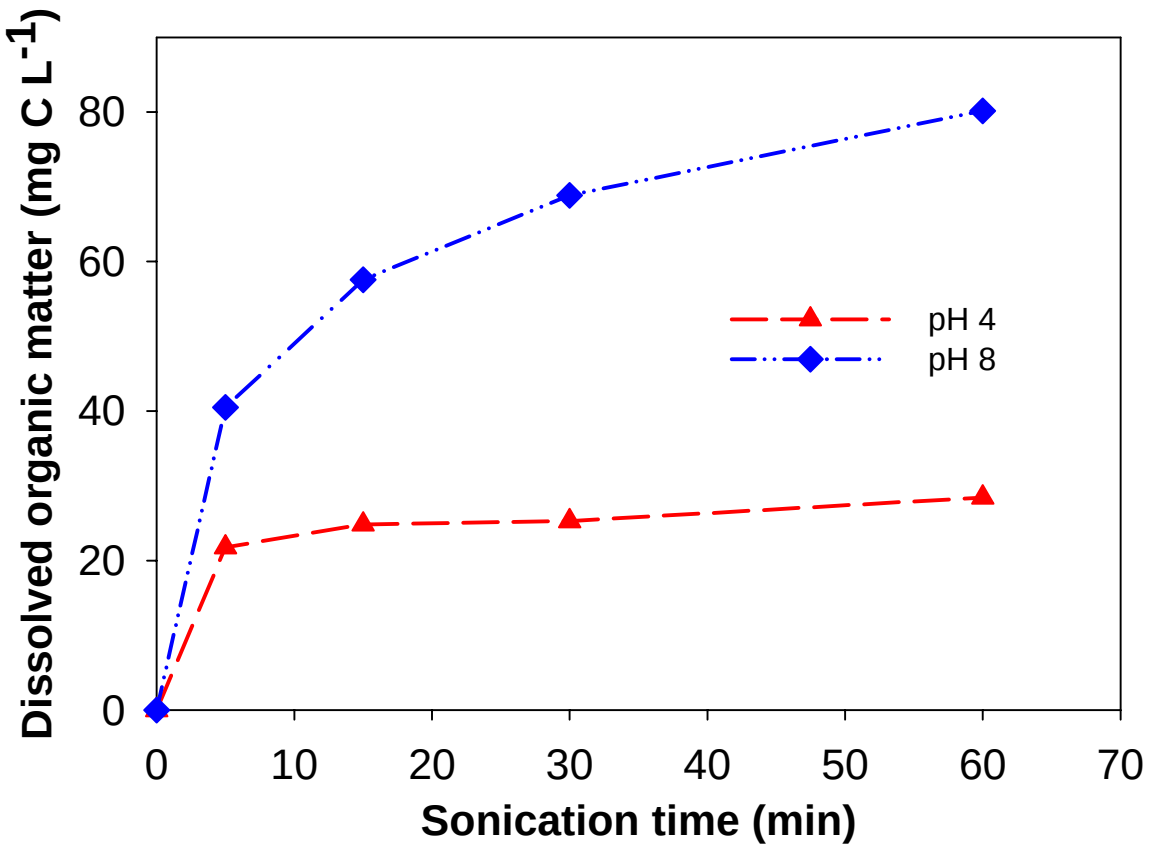

Figure 6.6 Dissolved organic matter released from PACS-2 marine sediment by sonication (T = 20 °C, I = 0.01 M $NaNO_3$, [particle] = 8.3 g L^{-1}, $[Hg]_{certified}$ = 3.04 ± 0.20 mg kg^{-1}, sonication intensity 20 W cm^{-2}).

CHAPTER 7

CONCLUSIONS AND FUTURE WORK

7.1 Conclusions

The investigation of sonication as a remediation technology of mercury contaminated sediments was conducted in this dissertation. The major observations from this study are the following.

First, ultrasound was found to be able to enhance mercury release from model and real sediments through its effects on desorption kinetics and equilibrium. In an Hg(II) doped Al_2O_3 system (Chapter 2), ultrasound enhanced initial Hg(II) release at pH 4.0 compared to hydrodynamic mixing suggesting that ultrasound accelerated the desorption kinetics. The desorption of Hg(II) by sonication at 2 min was higher than that expected based on the Hg(II) sorption curve indicating that ultrasound altered the chemical equilibrium of Hg(II). As shown in Chapter 4, ultrasound released Hg from cinnabar (HgS), the most stable form of Hg, into the aqueous phase through a series of oxidation reactions of S into sulfur oxidation products (S_{ox}) including $S_2O_3^{2-}$, SO_3^{2-} and SO_4^{2-}. Hydroxyl radical scavenging by terephthalic acid (TA) showed that •OH was the predominant oxidizing species in initiating the dissolution reaction, but not the only

pathway. Due to the adsorption of dissolved Hg(II) back onto the remaining cinnabar particles as Hg(II) adsorption isotherms indicated, Hg(II) release rates were much lower than those of S_{ox}. To validate the ability of ultrasound to release Hg, Hg release from certified PACS-2 marine sediment was examined in Chapter 5 and ultrasonic acceleration of Hg release compared to mechanical shaking was also observed at two different pH conditions.

Second, ultrasonic desorption/release of Hg was influenced by sediment matrix parameters including pH, chloride, and organic matter, and the power intensity and duration of sonication. In Chapter 3, sediment matrix parameters including pH, chloride, and organic matter were found to affect sonolytic desorption of Hg(II) from Al_2O_3. For example, low pH conditions and the presence of Cl^- facilitated sonolytic release of Hg(II); the behavior of humic acid desorption from Al_2O_3 dictated the release of Hg(II). As shown in Chapter 5 and 6, the difference in Hg release between pH 4 and 8 from PACS-2 sediment was attributed to the difference of dissolved natural organic matter at two pH values. Organic matter also affected Hg release from cinnabar (Chapter 4). Dissolved humic acid enhanced cinnabar dissolution, released more Hg(II) into aqueous solution, and affected S_{ox} products formed by ultrasound due to the synergistic effects of ultrasound and humic acid.

Besides sediment and solution condition effects, ultrasonic factors including power intensity and reaction time were observed to affect Hg desorption. As shown in Chapter 2 and 3, the higher the power intensity of sonication, the higher the desorption of Hg(II). Although ultrasound enhanced initial Hg desorption, decreases in Hg desorption occurred with prolonged sonication due to ultrasonic effects on the changes of sediment

particle properties. This observation suggested that caution should be taken with the duration of sonication when applying this technology to remediation of sediment to avoid re-association of desorbed Hg(II) with sediments.

Ultrasonic effects on the changes in particle properties were demonstrated in model Al_2O_3 (Chapter 2) and cinnabar (Chapter 4) systems. Ultrasound dramatically reduced Al_2O_3 particle size, changed surface morphology and decreased the point of zero charge (PZC) due to mineral phase transition. However, these observations were excluded as the primary mechanism for Hg(II) resorption with longer sonication times because no obvious surface area change occurred and XPS spectra showed different Hg(II) surface coverage before and after ultrasound. Based on the formation of supersaturated Al solution and similar Hg(II) desorption trends to pre-sonicated Al_2O_3 particles, Hg(II) occlusion by aluminum hydroxide re-precipitates was proposed as the primary reason for Hg(II) resorption with longer sonication times. However, in cinnabar system, ultrasound significantly reduced cinnabar particle size and increased surface area, leading to higher Hg(II) adsorption on HgS surfaces. In addition, sonication increased the cinnabar surface isoeletric point (IEP), indicating adsorption of Hg(II) and/or mineral phase transformation from cinnabar to metacinnabar.

Furthermore, the ability of ultrasound to release of a series of metals with different binding strengths and water exchange rates was investigated in Al_2O_3 and PACS-2 marine sediment (Chapter 5). Results showed that sonication was able to enhance Hg(II), Pb(II), Ni(II) and Cr(III) desorption from Al_2O_3 compared to hydrodynamic mixing. However, longer sonication times led to a decrease in Hg(II) and Pb(II) desorption while Ni(II) and Cr(III) desorption continued to increase due to the

difference in their water exchange rates which determined the resorption rates. The release patterns and efficiencies of metals from PACS-2 were different for various metals and at different pH conditions likely due to the differences in their affinity to different sediment compositions, metal speciation and oxidation state, and the effects of organic matter in sediment. Hg release was likely controlled by organic matter; Pb release was impacted by its affinity to organic matter and metal (hydr)oxides due to its high content; Ni release seemed to be affected by metal (hydr)oxides and silicates phases; whereas Cr release was influenced by its oxidation state.

Lastly, observing that ultrasound enhanced Hg desorption, the application of ultrasound combined with biomass sorption for the removal of Hg from model and real sediments (Al_2O_3, α-HgS, and PACS-2 marine sediment) was investigated (Chapter 6). A transgenic *C. reinhardtii* (2AMT-2) expressing a plasmamembrane-anchored metallothionein polymer was tested to quickly uptake Hg(II) from aqueous phase by higher binding capacity and broader pH range than wild type alga. The combined technique of ultrasound and 2AMT-2 was effective to remove Hg from solids and sediments, especially from Al_2O_3 and α-HgS with no natural organic matter. An implication of the results is that the application of ultrasound combined with biomass (transgenic *C. reinhardtii*) has the potential for Hg removal from contaminated sediments with the extreme ultrasonic phenomena (physical, chemical and thermal effects) to intensively release Hg from solid phase into aqueous phase followed by biomass sequestration and removal. The advantages of this approach include improved efficiency induced by ultrasound and high specific Hg affinity by the transgenic biomass.

7.2 Future Studies

Results of this research show that ultrasound is able to accelerate the release of Hg from sediment into aqueous phase. The combined system of ultrasound and biomass sorption is an effective means to remediate Hg contaminated sediments. However, further investigations are needed to address the following aspects before the application of this system to natural sediment.

(i) To expand the understanding of ultrasonic desorption mechanisms, first, more studies should be conducted on various model particles such as humin, Fe (hydr)oxides and clays because there are Hg sinks in a variety of different sediment compositions in addition to Al_2O_3 and cinnabar. The desorption patterns and mechanisms from different model systems will provide useful information for the application of ultrasound to a variety of Hg contaminated sites.

(ii) Methylmercury is the most toxic and bioaccumulative Hg species. Considering that methylmercury is a volatile compound, sonochemical treatment of methylmercury is worth testing to examine the fate of methylmercury during sonication. Thermal and chemical degradation of methylmercury to inorganic Hg will greatly reduce the toxicity of Hg, whereas physical effects of ultrasound may enhance the mobility and bioaccessibility of methylmercury.

(iii) Hg speciation measurements before and after sonication in sediment by sequential chemical extraction and/or XAFS spectroscopy may provide fundamental information for understanding the mechanisms of ultrasonic desorption of Hg from sediment. For example, will ultrasound be most effective at desorbing a particular Hg(II)

species? What sediment composition will control Hg(II) desorption from natural sediments by ultrasound?

(iv) Ultrasound enhanced initial Hg desorption from sediment. However, higher power density of ultrasound and longer sonication times leading to occlusion of Hg inside sediment particles was observed in this study, which may significantly decrease Hg bioavailability and greatly reduce its risk to aquatic life and humans. Therefore, it is necessary to explore the bioavailability of Hg after sonication.

(v) As shown in Al_2O_3 and cinnabar model systems, ultrasound dramatically reduced particle size possibly generating more colloidal particles. Previous studies have shown that colloidal Hg represents the majority of dissolved Hg and promotes Hg transport (*184,185*). Therefore, it is very important to investigate colloid transport and colloid-facilitated movement of Hg during sonochemical remediation.

(vi) As discussed in Chapter 6, high concentrations of dissolved organic matter and the utilization of a dialysis bag to contain algal cells seemed to decrease the apparent effectiveness of the combined system to remove Hg from real sediment. Direct interaction of alga and Hg-NOM complexes may greatly improve algal uptake of Hg. To effectively recover Hg from sediments with high organic carbon content, therefore, other effective means for containing algal cells but allowing direct contact of alga and Hg-NOM complexes are needed to improve the effectiveness of the combined system of ultrasound and biomass sorption. Additionally, to obtain a higher percentage of Hg removal, further studies are needed to determine parameters for optimum operation such as the amount of biomass, the effect of sediment to liquid ratio and sonication conditions.

(vii) The use of transgenic *C. reinhardtii* to remediate Hg in aquatic environments is not without risk. The application of transgenic microalgae for heavy metal bioremediation has risks as well as benefits that will require clever engineering and biological considerations to preclude the escape of transgenic organisms (*65*). The release of algae with enhanced Hg capacity could accelerate the biogeochemical cycling of Hg and its accumulation in food chains. In addition, the escape of transgenic biomass into environment may induce the growth of the transgenic algae or exchange of genetic material with non-transgenic algae. Therefore, efforts and caution should be taken in reactor design. The criteria for reactor design should take into account not only direct access of Hg to biomass but also secure barriers to preclude the release of live transgenic algae. An alternative strategy instead of using viable transgenic algae would be to use freeze dried dead cells.

APPENDIX A

SONOCHEMICAL REACTIONS OF DISSOLVED ORGANIC MATTER

(*Research on Chemical Intermediates*, **2004**, *30*, 735-753)

A.1 Abstract

Property changes of Aldrich and Pahokee peat dissolved organic matter (DOM) at different ultrasonic frequencies and energy densities were systematically investigated. Exposure of DOM to ultrasound resulted in decreases in TOC, $Color_{465}$, specific UV absorbance (SUVA), aromaticity, and molecular weight, while DOM acidity increased. Compared to 20 kHz ultrasound, greater sonochemical transformation of DOM occurred at 354 kHz and at higher energy density, due to greater •OH radical production. The changes to DOM properties suggest that ultrasound may significantly affect DOM-pollutant interactions (e.g., facilitate desorption of hydrophobic organics from DOM or promote complexation between metallic cations and DOM).

Keywords: natural organic matter, dissolved organic matter, ultrasound, ^{13}C NMR, oxidation, aromaticity, Aldrich, Pahokee

A.2 Introduction

Sonication has been explored as an oxidation technology for the treatment of refractory organic pollutants in water (*186,187*) and contaminated sediment (*75*,*138*), and for disinfection (*188*) and membrane cleaning (*80*,*189*) in drinking water applications. The presence of natural organic matter (NOM), however, may significantly influence the effectiveness of ultrasound in these systems. NOM is present in natural waters due to the degradation of plant and animal matter. The chemical structure of NOM is ill-defined (*190*), varies depending on the source, but typically includes aromatic, aliphatic, carboxylic, and phenolic functional groups (*191*). NOM can undergo a variety of reactions in natural and engineered systems and often interferes with treatment processes by binding organic and inorganic contaminants and scavenging reactive species (*75*,*192*). In addition, it plays an important role in particle coagulation, trace-metal cycling, and mobility of both inorganic and organic pollutants (*193*,*194*).

Sonochemical techniques involve the use of sonic or ultrasonic waves to produce a turbulent and/or oxidative environment via cavitation bubbles generated during the rarefaction phase of sound waves. During the compression cycle, when the cavitation bubble collapses, localized hot spots are formed which reach temperatures and pressures in excess of 5000 K and 1000 atm, respectively (*195*). These high temperatures result in the dissociation of chemical compounds including water (*68*), producing radical species including •OH radicals.

When polymers or other macromolecules (e.g., NOM) exist in the vicinity of cavitation bubbles, the solvent flow fields produced around cavitation bubbles serve to stretch and open the macromolecular coils, placing the chains under stress. These

macromolecules are then broken by shock waves resulting from the final collapse of cavitation bubbles (*196*). This is referred to as shear degradation of macromolecules by ultrasound. Breaking of these macromolecules (i.e., cleavage of a covalent bond) can occur in two ways: homolytically, resulting in one electron from the bond going to each fragment to produce radical species; or heterolytically, with both electrons associating with one fragment, leading to formation of an ion pair (*197*). Both of these possibilities have been observed during polymer degradation by ultrasound (*197,198,199,200*). In addition to shear degradation, macromolecules may be broken down by ultrasound due to the production of •OH radicals (*76,201*).

Studies of changes in NOM as a result of sonication are scarce (*76,201,202*). Previous studies focused on reducing disinfection by-products, and therefore, a detailed understanding of the influence of sonication on the chemical structure of NOM was not obtained. In the present work, dissolved organic matter (DOM) was characterized before and after sonication using a variety of analytical techniques. Two types of DOM were investigated: Aldrich and Pahokee peat DOM. Both have been studied previously, and are commonly used as model humic substances (*203,204*). The purpose of this study was to systematically characterize chemical changes to DOM with respect to different ultrasonic frequencies and energy densities, and to determine how DOM reactivity is altered by sonication.

A.3 Methodology

A.3.1 Preparation of DOM

Commercial Aldrich humic acid (sodium salt) was supplied by the Aldrich Chemical Company (Milwaukee, WI). Aldrich humic acid was purified according to procedures described by Chin et al. (*205*) followed by washing with 0.3 M HF and dialysis with 1000 Dalton (Da) molecular weight cut off (MWCO) membranes and freeze drying. DOM extracted from Pahokee peat purchased from the International Humic Substances Society (IHSS) was isolated using the IHSS standard method for soil (*206*), followed by dialysis with 1000 Da MWCO membranes and freeze drying. For both DOM, the dialysis was continued until the dialyzing water was free of chloride as determined with an $AgNO_3$ indicator.

A.3.2 Ultrasonic Units

Ultrasonic reactions of DOM were performed with two different ultrasonic reactors: a 20 kHz ultrasonic probe system (550 Sonic Dismembrator) from Fisher Scientific (Pittsburgh, PA) and a URS 1000 Ultrasonic Laboratory Reactor consisting of a USW 51-52 ultrasonic transducer operating at 354 kHz with an LVG 60 Radio Frequency Generator (L3 Communications ELAC Nautik). In both systems, experiments were run as batch reactors, and calorimetry was performed to measure the power output of ultrasound (207). Both reactors contained a water jacket connected to a cooling bath (Fisher Scientific 1006S Isotemp) to keep the reacting solution at 25 ^{o}C.

For the 20 kHz ultrasonic probe system, a 50 mL glass rosette reactor was used. The probe with replaceable titanium tip was immersed into the solution to a depth of 3.5

cm. The area of the tip was 1.26 cm^2. Before sonication, the titanium tip was polished with fine sand paper (220, 3M®) and tuned.

For the 354 kHz sonication system, sound waves were emitted from the bottom of the reactor. The emission area of the transducer was 23.7 cm^2. 100 or 500 mL solutions were sonicated to obtain different energy densities in solution.

A.3.3 Experimental Conditions

Water used was from a MilliQ water purification system (R=18.2 MΩ·cm). For all experiments, the TOC concentration of both DOM was 22.5 mg/L. All degradation experiments were run at an initial pH of 4.0. pH was adjusted manually by addition of 0.10 M nitric acid (Trace Metal Grade, Fisher Scientific) or 0.10 M sodium hydroxide (certified ACS, Fisher Scientific) to maintain the pH at 4.0. Additions did not exceed 1% of the original sonicated volume.

At specific times during sonication, samples were withdrawn from the batch reactors using a 5-mL pipette with Teflon tips. The total volume withdrawn during a single run never exceeded 5% of the total volume. Due to tip erosion in the 20 kHz probe system, samples from the probe system were centrifuged (Beckman centrifuge, Model J2-21) at 3500 rpm for 10 minutes to remove particles. For H_2O_2 detection in the probe system, samples were filtered with a 0.45 μm PTFE syringe filters. For the 354 kHz sonication system, samples were analyzed without centrifugation or filtration.

A.3.4 Sample Analysis

Total organic carbon (TOC) and dissolved organic carbon (DOC) were measured by a Shimadzu TOC-5000A analyzer operating in the non-purgable organic carbon mode. Determination of hydrogen peroxide was performed by the triiodide method (*208*). The UV absorbance of DOM at 254, 280, and 465 nm was measured by a UV-VIS spectrophotometer (UV-2401PC, Shimadzu). Potentiometric acidity titration of DOM was performed under a N_2 atmosphere following the procedures of Edwards et al. (*194*) using an Orion 960 Autochemistry System (Beverly, MA).

Molecular weight distributions of DOM before and after sonication were measured by high pressure size exclusion chromatography (HPSEC) (Waters Associates, Milford, MA) at 360 nm according to the method described by Chin et al. (*203*). A wavelength of 360 nm was chosen to minimize the interference of nitrate in analysis. The HPSEC was calibrated using sodium polystyrene sulfonates (Polysciences) with molecular weight of 18K, 8K, 4.6K, and 1.8K, respectively and acetone.

Cross Polarization Magic Angle Spinning (CPMAS) ^{13}C nuclear magnetic resonance (NMR) spectra were obtained using a Bruker DPX 300 MHZ NMR-spectrometer (Bruker Analytic GmbH, Germany). About 80 mg freeze-dried DOM samples before and after sonication were analyzed according to the details described by Dria et al. (*209*). The ^{13}C NMR spectra were integrated according to the following regions: 0-45 ppm, paraffinic carbons; 45-60 ppm, methoxyl; 60-90 ppm, carbohydrate carbons; 90-112 ppm, carbohydrate and proton-substituted aromatic carbons; 112-140 ppm, carbon-substituted aromatic carbons; 140-160 ppm, oxygen substituted aromatic carbons; 160-190 ppm, carboxyl and aliphatic amide carbons; 190-220 ppm, aldehyde

and ketone carbons (*209,210,211*). Total aromaticity was calculated by expressing aromatic C as a percentage of the aliphatic plus aromatic C (*209,212*).

A.4 Results

A.4.1 Initial Characterization of Aldrich and Pahokee Peat DOM

The chemical nature or structure of NOM is determined by its source materials and by biogeochemical processes that take place at the site of their formation (*213*). Aldrich humic acid is extracted from coal by base extraction by Aldrich Chemical Company (*214*). Generally, Aldrich humic acid is more aromatic and has a higher molecular weight than humic materials isolated from natural waters (*203*). Pahokee peat is a typical agricultural peat soil of the Florida Everglades. Pahokee series soils consist of very poorly drained soils that are 36 to 51 inches thick over limestone. Pahokee soils formed in organic deposits of freshwater marshes (*215*). It has been shown that soil and peat humic acids are generally less aliphatic and more aromatic than aquatic humic acids (*216*).

The properties of humic substances are important in complexation of trace metals, the solubilization and transport of relatively insoluble organic compounds, and biogeochemistry (*217*). Important characteristics of humic substances include concentration of organic carbon (measured by TOC), color (measured by $Color_{465}$, i.e., the UV-Vis absorbance at 465 nm), hydrophobicity (measured by specific UV absorbance (SUVA) at 254 nm), aromaticity (measured by SUVA at 280 nm and ^{13}C NMR), molecular weight (measured by HPSEC), and acidity (measured by potentiometric titration) (*217*). Of these parameters, color relates to chromophores in

DOM, including conjugated double bonds, aromatic rings, and phenolic functional groups. These groups serve as color centers in humic substances (*218*). SUVA ($m^{-1}L/mgC$) expressed by the ratio of UV absorbance at 254 or 280 nm over dissolved organic carbon concentration, increases with an increase in hydrophobicity and aromaticity of DOM, because π-π^* electron transitions occur at these wavelengths (*203*,*219*,*220*). Higher hydrophobicity, higher aromaticity, and greater molecular weight of humic substances results in stronger affinity to non-polar neutral organics (*221*), such as polycyclic aromatic hydrocarbons (PAHs) and polychlorinated biphenyls (PCBs) (*222*). Higher acidity of humic substances, on the other hand, facilitates increased complexation with metallic cations, mineral surfaces, and other positively charged species (*162*,*223*).

The characteristics of Aldrich and Pahokee peat DOM prior to sonication are shown in Table A.1. Aldrich DOM has higher aromaticity, color, SUVA, and total acidity than Pahokee peat DOM; while Pahokee peat DOM has a greater weight-averaged molecular weight (4200 Da) and number-averaged molecular weight (2500 Da) than Aldrich DOM (3200 and 2100 Da, respectively). Higher $Color_{465}$ of Aldrich DOM likely reflects the greater aromaticity of Aldrich DOM compared to the Pahokee peat DOM, because aromatic rings and phenolic functional groups are common chromophores in DOM (*218*). Higher SUVA values reflect the greater hydrophobicity and aromaticity of Aldrich DOM. Based on ^{13}C NMR analysis, Aldrich DOM has a higher percentage of carbon-substituted aromatic carbons and oxygen substituted aromatic carbons; while Pahokee peat DOM has a higher percentage of methoxyl and carbohydrate carbons (data not shown). Greater average molecular weight of Pahokee peat DOM suggests that its

carbohydrates are expected to be composed of significant amounts of long-chain carbons. The differences in the initial characteristics of these two DOM suggest that Aldrich DOM has a stronger affinity to non-polar neutral organics and has more complexation sites with metallic cations.

A.4.2 TOC Reduction of DOM

As shown in Figure A.1-2, no TOC reductions were observed for either DOM through 4 hours of sonication at 20 kHz with an energy density of 450 W/L. At 354 kHz with an energy density of 120 W/L, the TOC of Aldrich DOM decreased from 22.5 to 20.4 mg/L after 4 hours, while no obvious TOC reduction was observed with Pahokee peat DOM. When the sonolytic energy density was increased to 450 W/L at 354 kHz, the TOC of both DOM decreased significantly. TOC decreased from 22.5 mg/L to 15.0 and 18.2 mg/L after 4 hours for Aldrich and Pahokee peat DOM, respectively. These data demonstrate that Aldrich DOM was more readily mineralized than Pahokee peat DOM

A.4.3 Changes in $Color_{465}$

Although no TOC reduction was observed after 4 hours of sonication at 20 kHz, it is possible that the molecular structure of DOM changed through sonication. Figure A.3-4 shows that $Color_{465}$ (UV-Vis absorbance at 465 nm) of Aldrich and Pahokee peat DOM decreased with sonication at all frequencies and power densities. At 20 kHz after 4 hours, $Color_{465}$ decreased from 0.21 to 0.19 and from 0.17 to 0.14 for Aldrich and Pahokee peat DOM, respectively. Again, a significant decrease of $Color_{465}$ with increased sonication occurred at higher ultrasonic frequency and higher energy density. These

results indicate that sonication caused the destruction of chromophores in DOM, such as conjugated double bonds, aromatic rings, and phenolic functional groups (*218*). Figure A.3-4 indicates that a greater decline of $Color_{465}$ occurred with Pahokee peat DOM than Aldrich DOM at 20 kHz and at 354 kHz with 120 W/L. At 354 kHz and 450 W/L, similar reduction in $Color_{465}$ was observed for both Aldrich and Pahokee peat DOM.

A.4.4 SUVA Changes to DOM

Experimental results show that SUVA of Aldrich and Pahokee peat DOM decreased with sonication time at either 20 kHz or 354 kHz. For example, SUVA at 254 nm decreased from 6.65 to 5.99 and from 5.56 to 4.42 $m^{-1}L/mgC$ for Aldrich and Pahokee peat DOM, respectively over 4 hours of sonication at 20 kHz (see Figure A.5-6). A more significant decrease of SUVA at 254 nm was observed at 354 kHz and at the higher energy density. A similar trend was found for SUVA at 280 nm (see Figure A.7-8), which shows an increased loss of SUVA with sonication at higher ultrasonic frequency and energy density. Further, greater decrease of SUVA at 254 nm and 280 nm occurred with Pahokee peat DOM compared to Aldrich DOM at 20 kHz and at 354 kHz with 120 W/L. At 354 kHz with 450 W/L, a similar reduction in SUVA was observed for both Aldrich and Pahokee peat DOM. The decrease in SUVA at 254 and 280 nm suggests that the hydrophobicity and the aromaticity of DOM reduced through sonication.

A.4.5 ^{13}C NMR Changes to DOM

^{13}C NMR spectra (see Figure A.9-10) were used to directly determine changes in molecular structure of DOM as a result of sonication. Generally, the aromatic peak area

(determined from the spectra between 112~160 ppm) of Aldrich and Pahokee peat DOM decreased and the aliphatic peak area (determined from the spectra between 0~90 ppm) increased through sonication, particularly at 354 kHz. As shown in Table A.2, for both Aldrich and Pahokee peat DOM, sonication generally caused a decrease in the percentage of aromatic carbon, and an increase in the percentage of aliphatic carbon of the DOM. As a result, the aromaticity of DOM declined through sonication. For Pahokee peat DOM, its aromatic carbon decreased from 33.2% to 31.6%, its aliphatic carbon increased from 51.0% to 53.5%, and its aromaticity decreased from 39.4% to 37.1% after 4 hours of sonication at 354 kHz. Changes to the ^{13}C NMR spectra were not obvious with 20 kHz sonication. A more significant trend was observed with Aldrich DOM. The percentage of aromatic carbon declined from 43.4% to 40.3% and to 35.8%, and the aliphatic carbon increased from 40.5% to 44.1% and to 49.6% through 4 hours of sonication at 20 kHz and 354 kHz, respectively. As a result, the aromaticity of Aldrich DOM dropped from 51.7% to 47.8% through sonication at 20 kHz, and dropped to 41.9% through sonication at 354 kHz. With the decrease of aromaticity, the hydrophobicity of DOM is expected to decline with increased sonication. Therefore, ^{13}C NMR spectral analysis is consistent with the SUVA results that show a decrease in hydrophobicity and aromaticity of DOM through sonication.

A.4.6 Molecular Weight Changes to DOM

In addition to the molecular structural changes to DOM, the molecular weight was expected to decrease through sonication. Figure A.11-12 shows the spectra of HPSEC of DOM before and after sonication. Generally, the decline of the peak area suggests that

sonication destroys the chromophores of both Aldrich and Pahokee peat DOM molecules centered around 3000 Da. Sonication at 354 kHz resulted in a greater decrease in peak area than 20 kHz sonication. At 354 kHz, sonication reduced the peak more at the higher energy density than at the lower energy density. Comparing sonication at 20 kHz with 450 W/L (spectrum (2)) to 354 kHz with 120 W/L (spectrum (3)), we observed a broadening of the peak of spectrum (3) and a shifting of the peak of spectrum (2) to longer retention times for both Aldrich and Pahokee peat DOM. This result suggests that 20 kHz ultrasound preferentially transformed large molecules (larger than 6400 Da based on a retention time of 8.5 min).

The weight-averaged and number-averaged molecular weight of DOM before and after 4 hours of sonication are shown in Table A.3. For Aldrich DOM, the weight-averaged molecular weight decreased from 3200 to 2900 and to 2400, the number-averaged molecular weight decreased from 2100 to 2000 and to 1600 after sonication at 20 kHz and at 354 kHz with 450 W/L, respectively. A more apparent decrease in molecular weight occurred with Pahokee peat DOM. The weight-averaged molecular weight decreased from 4200 to 3400 and to 3100; the number-averaged molecular weight decreased from 2500 to 2100 and to 1800 after sonication at 20 kHz and at 354 kHz with 450 W/L, respectively. However, only a slight decrease in molecular weight was observed with Pahokee peat DOM, and no obvious decrease in molecular weight was found with Aldrich DOM at 354 kHz with 120 W/L. Generally, lower molecular weight DOM have lower hydrophobicity and lower aromaticity than higher molecular weight DOM (*224*). Thus, this result is contrary to the results of SUVA and ^{13}C NMR, which show a more significant decrease in the aromaticity of DOM at 354 kHz and 120 W/L

than at 20 kHz and 450 W/L. Nevertheless, the general trend shows a decrease in the average molecular weight of DOM, consistent with previous results indicating a decrease in aromaticity and hydrophobicity of DOM through sonication.

A.4.7 Total Acidity Measurement of DOM

Acidity is a fundamental characteristic of humic substances. It is believed that the acidity of humic substances is due primarily to the presence of carboxyl (strong acid) and phenolic (weak acid) functional groups (*223*). ^{13}C NMR spectra cannot conclusively distinguish these functional groups. Therefore, it is necessary to use potentiometric titration to determine the acidity of DOM upon exposure to sonication.

Previous studies have shown an increase in the total acidity of NOM compounds following ozonation (*225,226*). As illustrated in Table A.4, the result of acidity titrations indicates an increase in the total acidity of both Aldrich and Pahokee peat DOM after 4 hours of sonication, although no significant change was observed at 20 kHz ultrasound.

A.5 Discussion

A.5.1 Ultrasonic Factors Affecting Sonochemical Reactions of DOM

The experimental results of TOC, $Color_{465}$, SUVA, acidity titrations, ^{13}C NMR, and molecular weight distribution suggest that more significant ultrasonic effects occurred at 354 kHz than at 20 kHz ultrasound with the same energy density (450 W/L). At 354 kHz, the effect of sonication was more apparent at the energy density of 450 W/L

than 120 W/L. These results indicate that ultrasonic factors played an important role in the sonochemical reaction of these DOM.

Sonochemically generated •OH radical is important for the oxidation of chemical constituents by ultrasound (*68*). The detection of H_2O_2 formation is used to estimate relative quantities of •OH radical generated during sonication (*152*,*154*). •OH radical can self-recombine to form hydrogen peroxide:

$$2\ \bullet OH \rightarrow H_2O_2 \qquad (1)$$

The recombination rate constant measured in water under ambient conditions is 5.5×10^9 L mol^{-1} s^{-1} (*227*). Figure A.13 shows the concentration of H_2O_2 formed with sonication in the absence of DOM. The highest concentration of H_2O_2 (0.4 mM after 4 hours) was produced at 354 kHz with an energy density of 450 W/L. The second highest H_2O_2 concentration (0.3 mM after 4 hours) was generated at 354 kHz with an energy density of 120 W/L. However, the lowest concentration of H_2O_2 was formed at 20 kHz (0.07 mM after 4 hours), even though the energy density was higher than 120 W/L at 354 kHz. Higher •OH radical production has been observed at 354 kHz in other studies (*152*,*228*). As shown in Figure A.13, the trend of increasing H_2O_2 concentration is consistent with changes observed to DOM. Ultrasonic factors that produced more •OH radical also resulted in more significant changes in DOM properties, suggesting that •OH radical plays a dominant role in the sonochemical alteration of dissolved organic matter.

It is well known that •OH radical may cleave aromatic rings (*229,230,231*). The decrease in aromaticity determined from ^{13}C NMR spectra and SUVA correlates well with an increase in H_2O_2. Thus, the higher •OH radical concentrations at 354 kHz result in more cleavage of aromatic rings than at 20 kHz. Considering the relatively non-

selective nature of oxidation by •OH radicals (*220*), the aliphatic functional groups of DOM are also subject to degradation and consequently lead to partial mineralization of DOM. Therefore, a more obvious reduction in TOC and molecular weight occurred with higher •OH radical concentrations. It is reported that ozonation of NOM leads to the destruction of carbon-carbon double bonds and production of organic acid and aldehyde groups (*232*). Similarly, sonication of DOM is expected to produce organic acids through oxidation by •OH radicals, increasing the total acidity of DOM. Insignificant changes in the acidity of DOM at 20 kHz may be due to lower •OH radical production at this frequency.

In addition to •OH radical oxidation, dynamic shearing caused by cavitation bubbles may also play a role in breaking covalent bonds of macromolecules (*196, 233*). Table A.3 indicates that 20 kHz ultrasound had a more significant effect on the decrease in the molecular weight of DOM than 354 kHz with 120 W/L. Moreover, Figure A.11-12 shows that 20 kHz ultrasound effectively transformed DOM molecules greater than 6400 Da for both Aldrich and Pahokee peat DOM. Cavitation bubbles at 20 kHz ultrasound are thought to undergo more violent collapse and thus have stronger mechanical effects (for example, dynamic shearing) than at 354 kHz (*234*), although less •OH radicals were generated than at 354 kHz. Dynamic shearing is more effective in the degradation of polymers with higher molecular weight than lower molecular weight. In addition, there exists a limiting molecular weight of polymers, below which no further ultrasonic transformation occurs with time (*197*). This phenomenon is observed because when the molecule is small enough, the physical dimension of polymer will be too small to be impacted by shock waves. Based on these analyses, dynamic shearing of cavitation

bubbles likely contributed to the breakdown of Aldrich and Pahokee peat DOM macromolecules, especially at 20 kHz. H_2O_2 produced at 354 kHz with 120 W/L was more than four times that at 20 kHz. Thus, if the degradation of DOM solely depended on •OH radical and dynamic shearing did not play a role, we would not observe the more significant decrease in molecular weight at 20 kHz than at 354 kHz with 120 W/L (see Table A.3).

Finally, thermal pyrolysis cannot be ruled out as a transformation mechanism of DOM. When macromolecules composing DOM are degraded to smaller molecules, they may volatilize into the gaseous cavity of cavitation bubbles, and consequently are dissociated under high temperature during bubble collapse. These studies did not provide any evidence to support or refute this possibility.

A.5.2 Alterations to DOM through Sonication

For both Aldrich and Pahokee peat DOM, the experimental results indicated that $Color_{465}$, SUVA at 254 nm and 280 nm, aromaticity, and average molecular weight all decreased, while total acidity increased with sonication time. TOC reduction was observed at 354 kHz only. These results are consistent with previous studies which show a decrease in molecular weight (*76*), partial mineralization (*201*), and a decrease in UV absorbance at 254 nm (*201,202*) of NOM as a result of sonication.

In this study, the decrease of $Color_{465}$ suggests that sonication partially degraded chromophoric functional groups on DOM, which include conjugated double bonds, aromatic rings, and phenolic functional groups (*218*). As mentioned above, SUVA at 254 nm and 280 nm increase with higher hydrophobicity and higher aromaticity of DOM,

because π-π^* electron transitions occur at these wavelengths (*203,219,220*). The decrease of SUVA indicates that the DOM became less hydrophobic (i.e., more hydrophilic) and less aromatic as a result of sonication. The decrease of SUVA suggests that sonication changed the molecular structure of DOM, possibly by cleaving aromatic rings on the DOM. ^{13}C NMR verified this hypothesis by showing a decrease in the percentage of aromatic carbon and an increase in the percentage of aliphatic carbon through sonication. Also, an increase in the total acidity of DOM as a result of sonication implies more organic acids were produced. The HPSEC data indicates a decrease in the molecular weight of DOM through sonication. All these characteristic measurements show that the DOM became less hydrophobic, less aromatic, smaller in size, and had higher total acidity as a result of sonication. These results suggest that sonication changed the characteristics of both Aldrich and Pahokee peat DOM. The differences in changes to Aldrich and Pahokee peat DOM indicate that the degree of change depends on the source of DOM as well as ultrasonic factors.

Although Pahokee peat DOM was less readily mineralized than Aldrich DOM, a greater decrease in $Color_{465}$, SUVA at 254 and 280 nm, and molecular weight at 20 kHz and 354 kHz with 120 W/L was observed for the Pahokee peat DOM. This suggests that alterations to the molecular structure of Pahokee peat DOM were more pronounced than the changes for Aldrich DOM through sonication. Based on ^{13}C NMR and HPSEC analysis, Pahokee peat DOM has a higher percentage of carbohydrate carbons that have higher molecular weight and presumably are long-chain carbons, although its aromaticity is lower than Aldrich DOM. These carbohydrates are more difficult to mineralize but are readily modified. A reason for a greater decrease in the molecular weight of Pahokee peat

DOM through sonication is that these long-chain carbons are more readily cleaved by dynamic shearing of cavitation bubbles, since dynamic shearing preferentially causes breaks in the middle of a polymer chain (*197,235*), until the limiting molecular weight of the polymer has been reached.

However, similar effects of sonication on $Color_{465}$ and SUVA at 254 and 280 nm were observed at 354 kHz and 450 W/L for both Aldrich and Pahokee peat DOM. This may be due to the greater •OH radical production observed at 354 kHz and 450 W/L than at the other sonication conditions. The high •OH radical concentration allows for extensive oxidation of both DOM resulting in significant changes to their molecular structures.

A.5.3 Implications for Use of Sonolysis in Environmental Applications

This study shows that the aromaticity, the hydrophobicity, and the molecular weight of both Aldrich and Pahokee peat DOM decreased, while the acidity increased with sonication time. These trends were more significant with 354 kHz at a higher energy density. These characteristic changes to DOM have a significant impact on the behavior of DOM in the environment. A decrease in aromaticity and hydrophobicity of DOM is expected to weaken hydrophobic interactions between DOM and hydrophobic organic compounds (*236*) (for example, non-polar neutral organics (*221*) and bacteria (*237*)), and thus decrease the adsorptive affinity between them. Because DOM is ubiquitous in soil, sediment, and natural waters, these effects suggest that sonochemical techniques may reduce the interaction of hydrophobic organics with soil, sediment, or aqueous NOM. However, the affinity between DOM and bacteria is expected to be weaker. This effect

may influence biodegradation of DOM and adsorbed organic contaminants. In addition, in the presence of DOM, the oxidation rate of organic contaminants is decreased due to scavenging of •OH radicals by DOM (*75*).

Furthermore, an increase in acidity means an increase in the sum of carboxylic and phenolic functional groups on DOM. These functional groups are responsible for the negative charge of DOM (*238*); thus, DOM is expected to become more negatively charged through sonication. The charge of DOM affects the adsorption of metallic cations through outer-sphere complexation, colloid/particle coagulation, electrostatic interactions between colloids and DOM, and interactions between drinking water membranes and DOM (*162*,*239*,*240*). When both DOM and environmental components are negatively charged, sonication is expected to enhance charge repulsion between the components and reduce interaction. Conversely, if the component interacting with DOM is positively charged, the interaction will be increased upon sonication.

This study was performed with sonication at high intensity. In practice, the degree of the property change to DOM depends on the energy density of ultrasound as well as sonication time. For practical applications, if property changes to DOM are desired, higher frequency (354 kHz vs. 20 kHz), higher energy density, and longer contact times with ultrasound would be preferred. Otherwise, lower frequency, lower energy density, and limited contact time with ultrasound would be favored.

Acknowledgments

This project was funded by the Ohio Water Development Authority, National Oceanic and Atmospheric Administration through the Ohio Sea Grant College Program,

and the NSF Environmental Molecular Science Institute at The Ohio State University. The authors gratefully acknowledge William C. Hockaday for help with ^{13}C NMR analysis. The authors also thank Jerry M. Bigham and Sandy Jones for their help with freeze drying.

	Aromaticity (%)	$Color_{465}$	SUVA (at 254 nm) ($m^{-1}L/mgC$)	SUVA (at 280 nm) ($m^{-1}L/mgC$)	Total acidity (meq/g TOC)	Weight-averaged molecular weight (Da)	Number-averaged molecular weight (Da)
Aldrich DOM	51.7	0.21	6.46	6.19	12.7	3200	2100
Pahokee peat DOM	39.4	0.17	5.56	5.03	10.6	4200	2500

Table A. 1 Comparison of the initial characteristics of Aldrich and Pahokee peat DOM.

	Before sonication			20 kHz 450 W/L after 4 hours			354 kHz 120 W/L after 4 hours		
	aliphatic carbon (%)	aromatic carbon (%)	aroma-ticity (%)	aliphatic carbon (%)	aromatic carbon (%)	aroma-ticity (%)	aliphatic carbon (%)	aromatic carbon (%)	aroma-ticity (%)
Aldrich DOM	40.5	43.4	51.7	44.1	40.3	47.8	49.6	35.8	41.9
Pahokee peat DOM	51.0	33.2	39.4	50.5	34.1	40.3	53.5	31.6	37.1

Table A. 2 Comparison of the aromaticity of DOM as a result of sonication.

	Molecular weight (Da)	Before sonication	20 kHz (450 W/L)	354 kHz (120 W/L)	354 kHz (450 W/L)
Aldrich DOM	Number-averaged	2100	2000	2100	1600
	Weight-averaged	3200	2900	3150	2400
Pahokee peat DOM	Number-averaged	2500	2100	2300	1800
	Weight-averaged	4200	3400	4100	3100

Table A. 3 Molecular weight of DOM before and after 4 hours of sonication.

Total acidity (meq/g TOC)	Before sonication	20 kHz (450 W/L)	354 kHz (120 W/L)	354 kHz (450 W/L)
Aldrich DOM	12.7	11.0	17.5	61.5
Pahokee peat DOM	10.6	9.2	19.2	16.3

Table A. 4 Acidity of DOM before and after 4 hours of sonication.

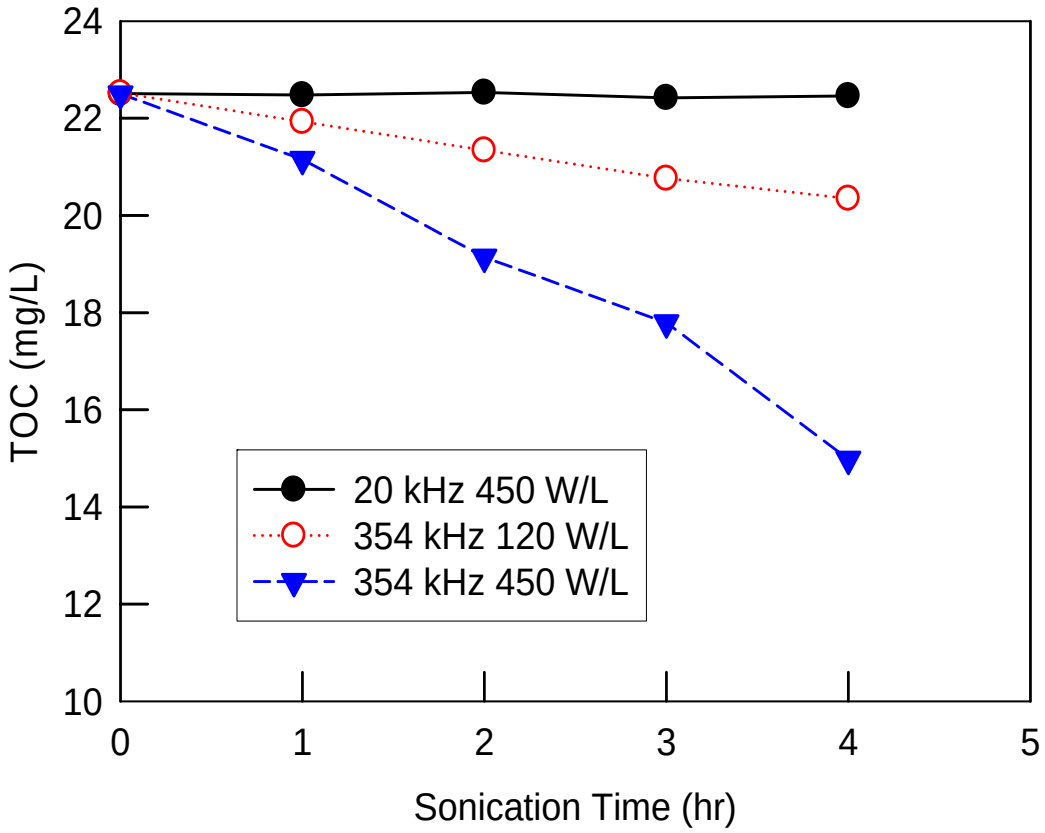

Figure A.1 TOC reduction of Aldrich DOM with sonication under different ultrasonic frequencies and energy densities.

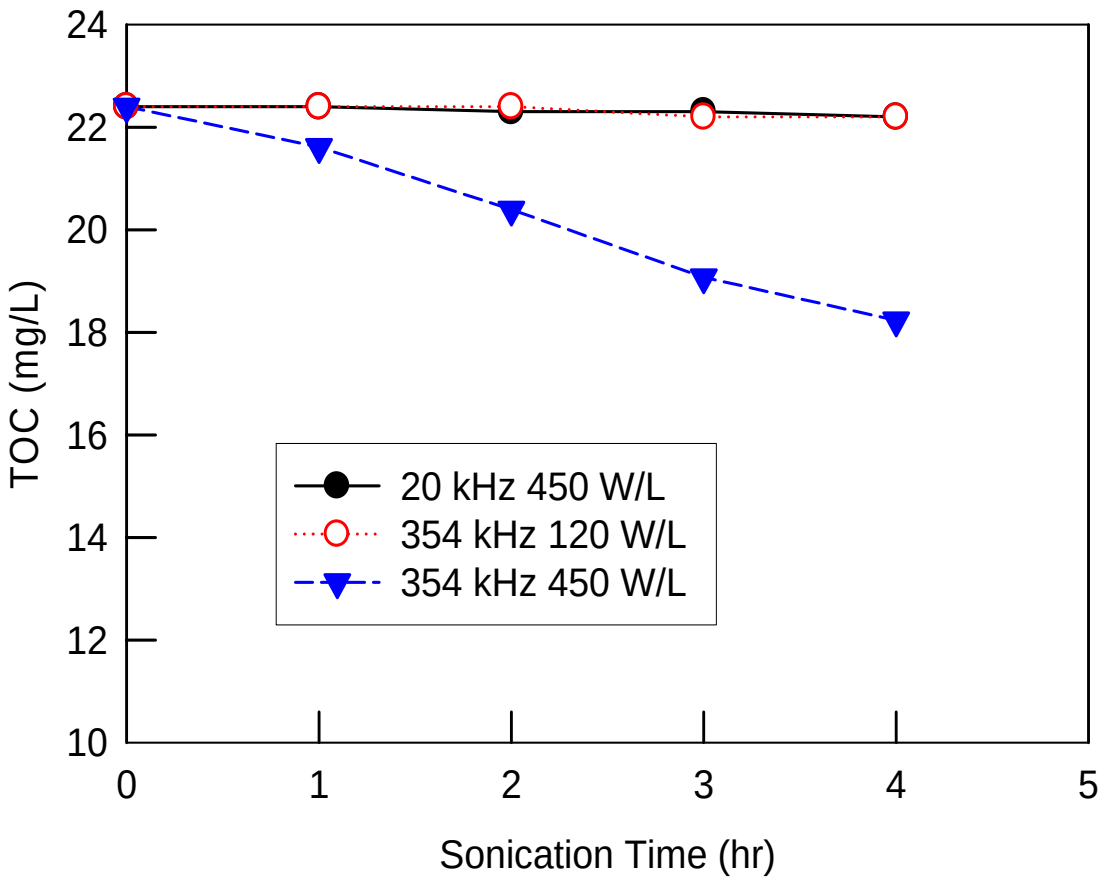

Figure A.2 TOC reduction of Pahokee peat DOM with sonication under different ultrasonic frequencies and energy densities.

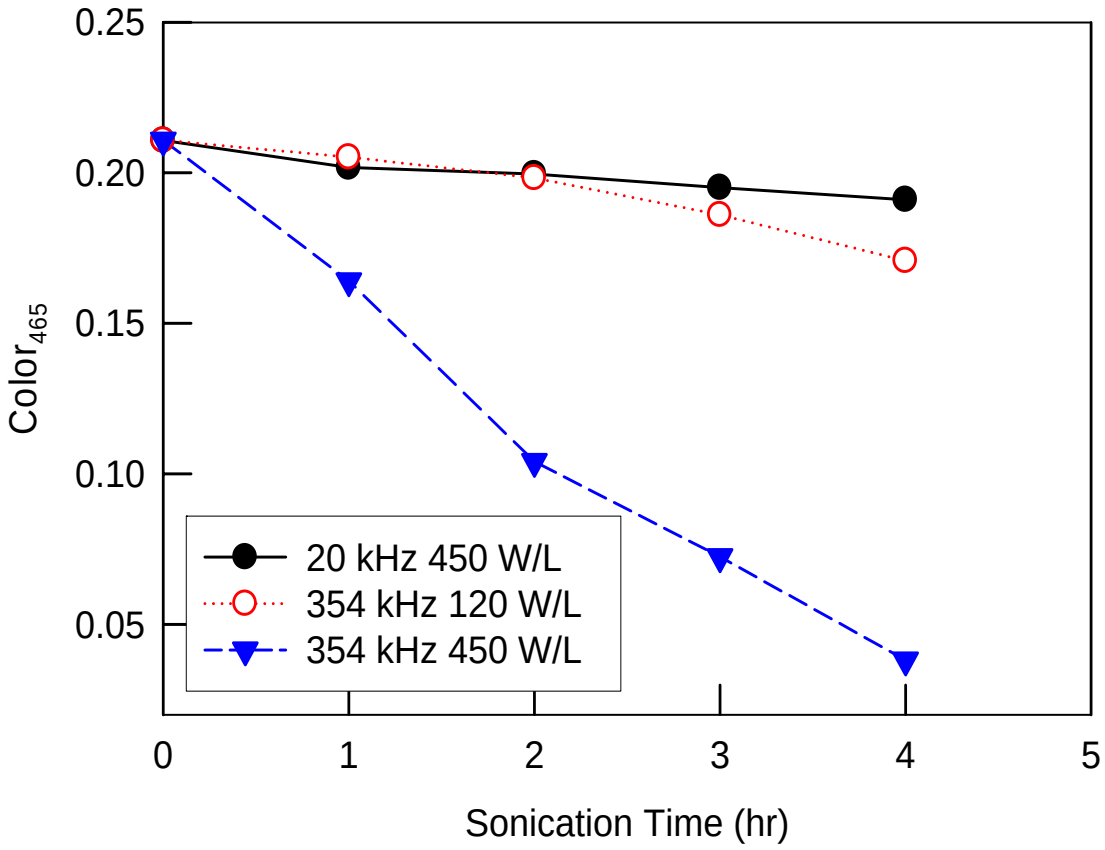

Figure A.3 $Color_{465}$ loss of Aldrich DOM with sonication under different ultrasonic frequencies and energy densities.

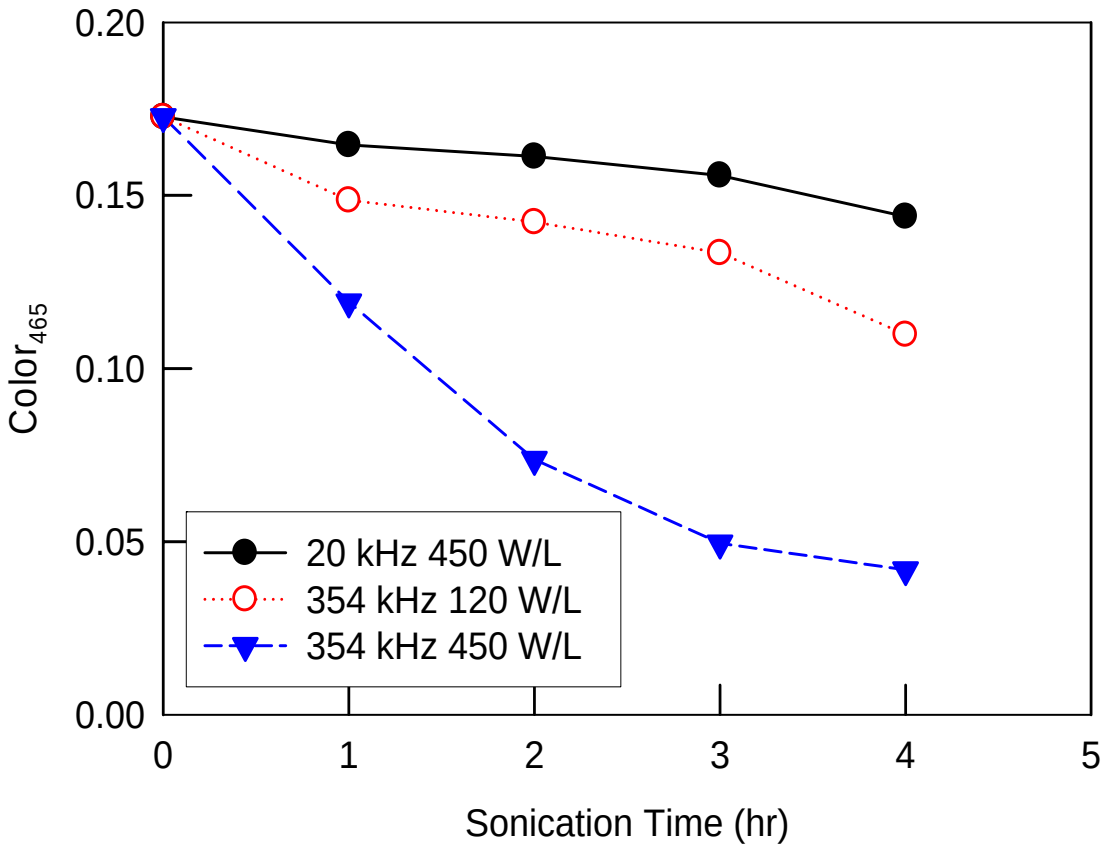

Figure A.4 Color$_{465}$ loss of Pahokee peat DOM with sonication under different ultrasonic frequencies and energy densities.

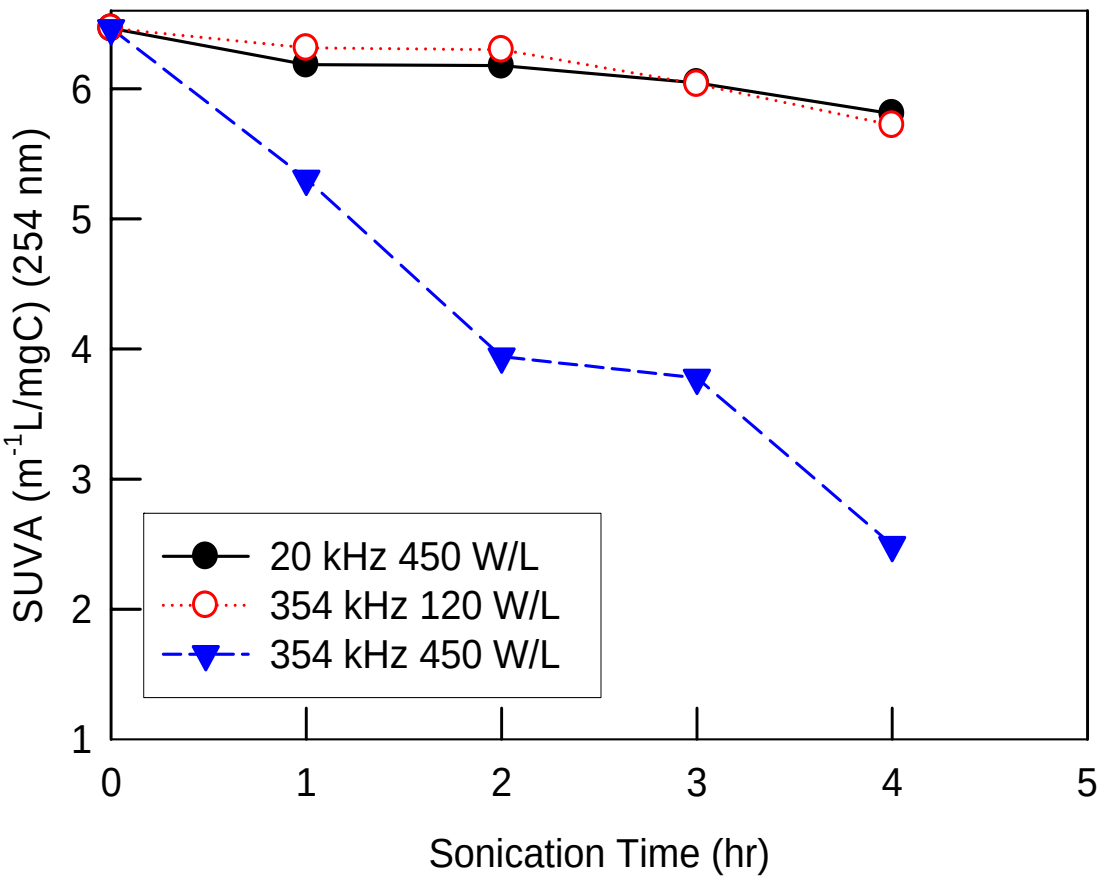

Figure A.5 SUVA at 254 nm decrease of Aldrich DOM with sonication under different ultrasonic frequencies and energy densities.

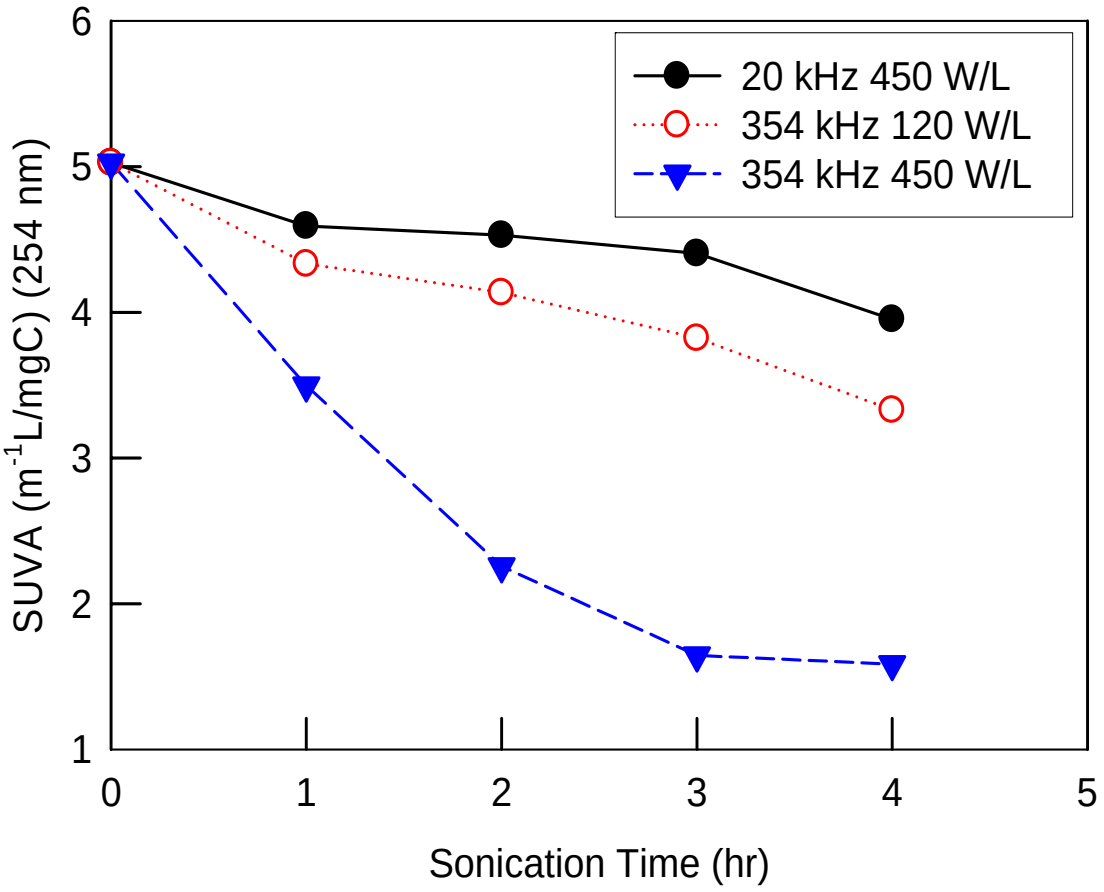

Figure A.6 SUVA at 254 nm decrease of Pahokee peat DOM with sonication under different ultrasonic frequencies and energy densities.

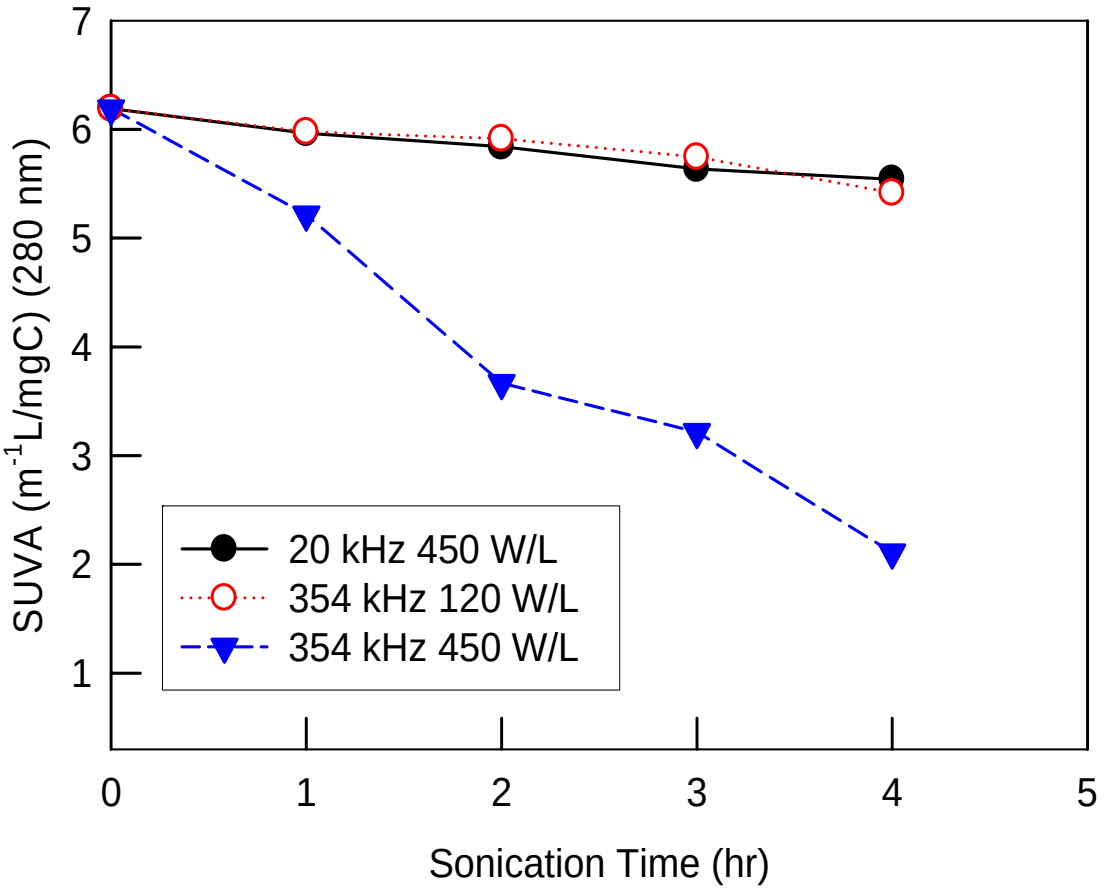

Figure A.7 SUVA at 280 nm of Aldrich DOM decrease with sonication under different ultrasonic frequencies and energy densities.

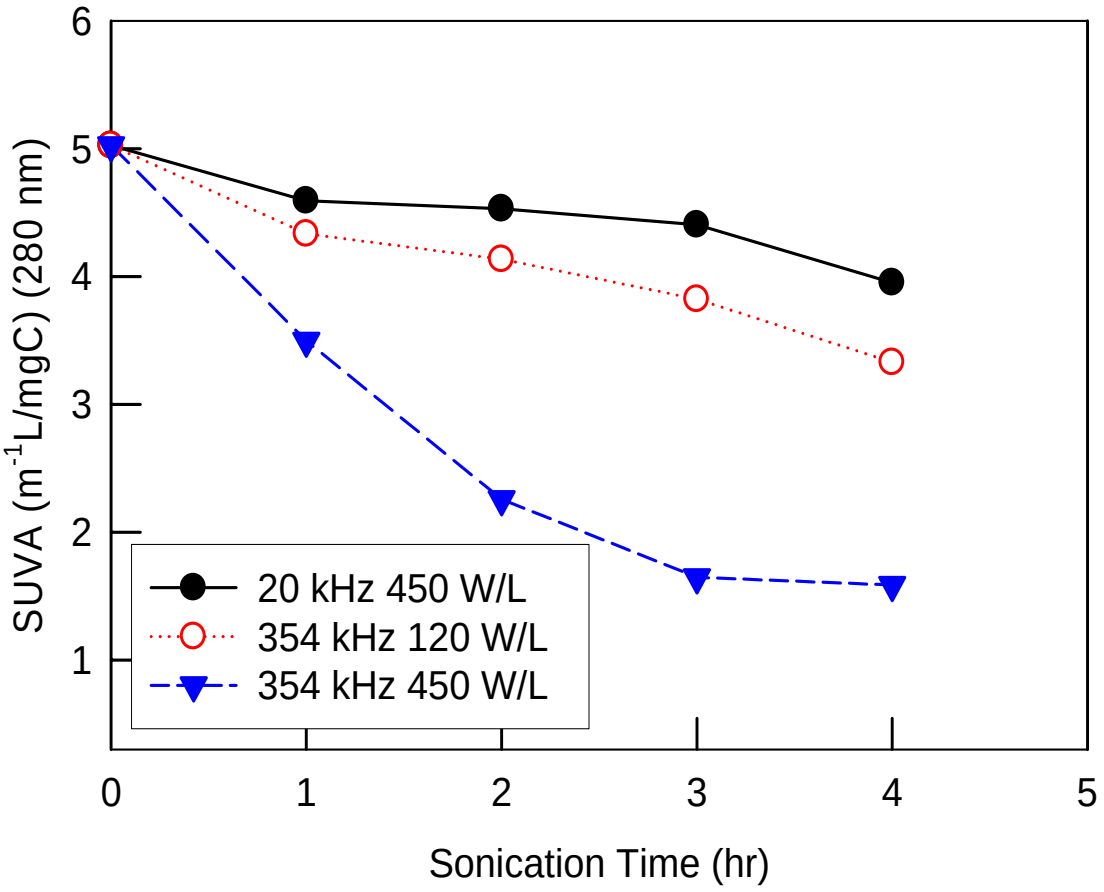

Figure A.8 SUVA at 280 nm decrease of Pahokee peat DOM with sonication under different ultrasonic frequencies and energy densities.

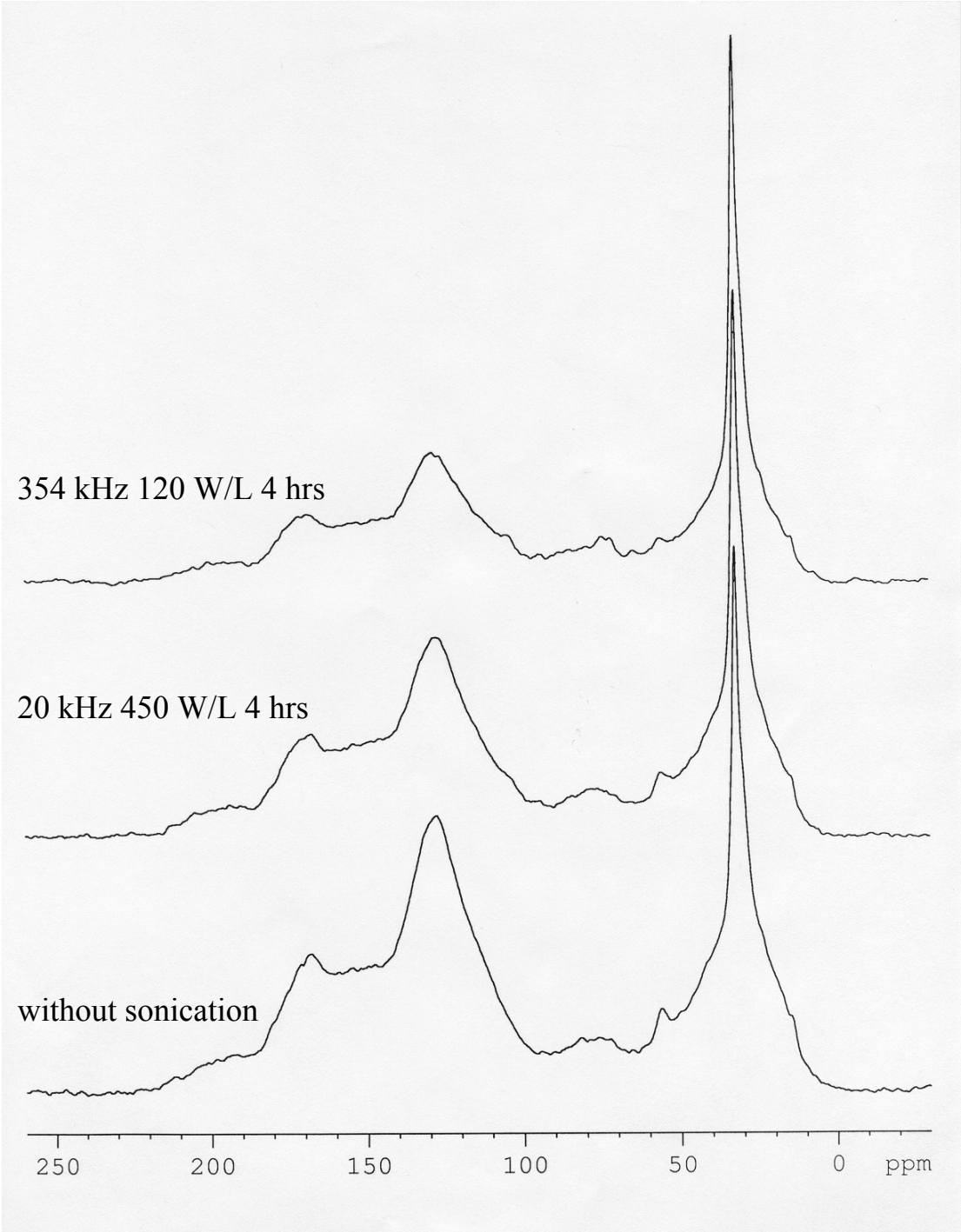

Figure A.9 ^{13}C NMR spectra of Aldrich DOM before and after 4 hours of sonication. Y-axis represents relatively intensity.

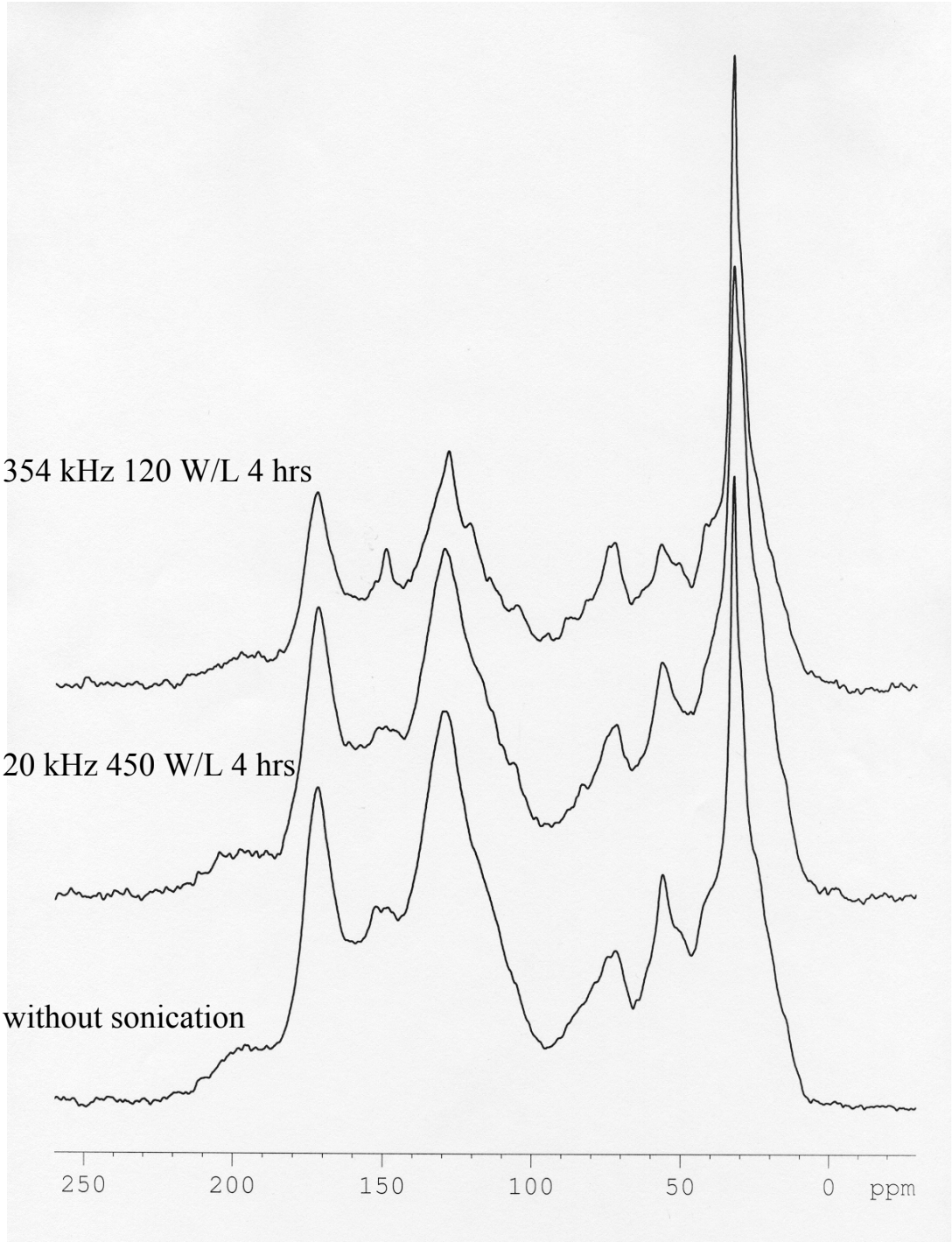

Figure A.10 ^{13}C NMR spectra of Pahokee peat DOM before and after 4 hours of sonication. Y-axis represents relatively intensity.

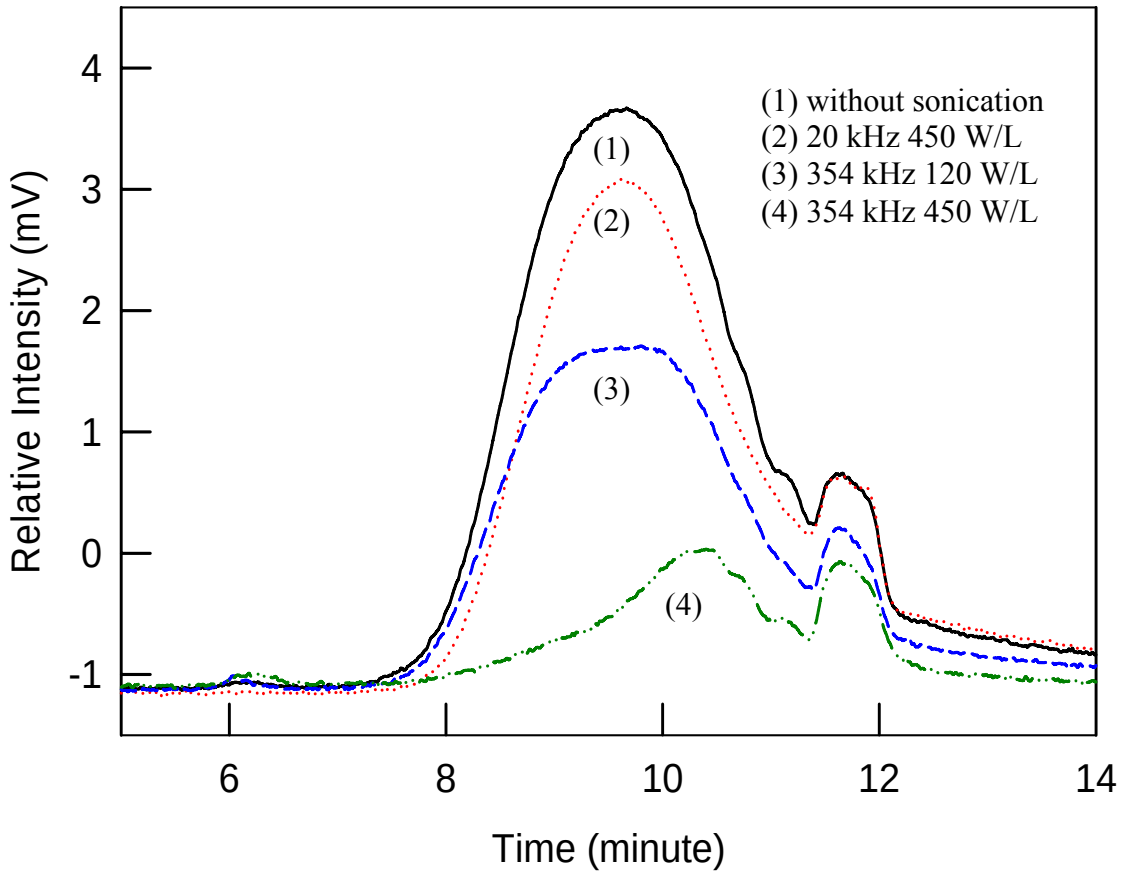

Figure A.11 HPSEC spectra of Aldrich DOM before and after 4 hours of sonication.

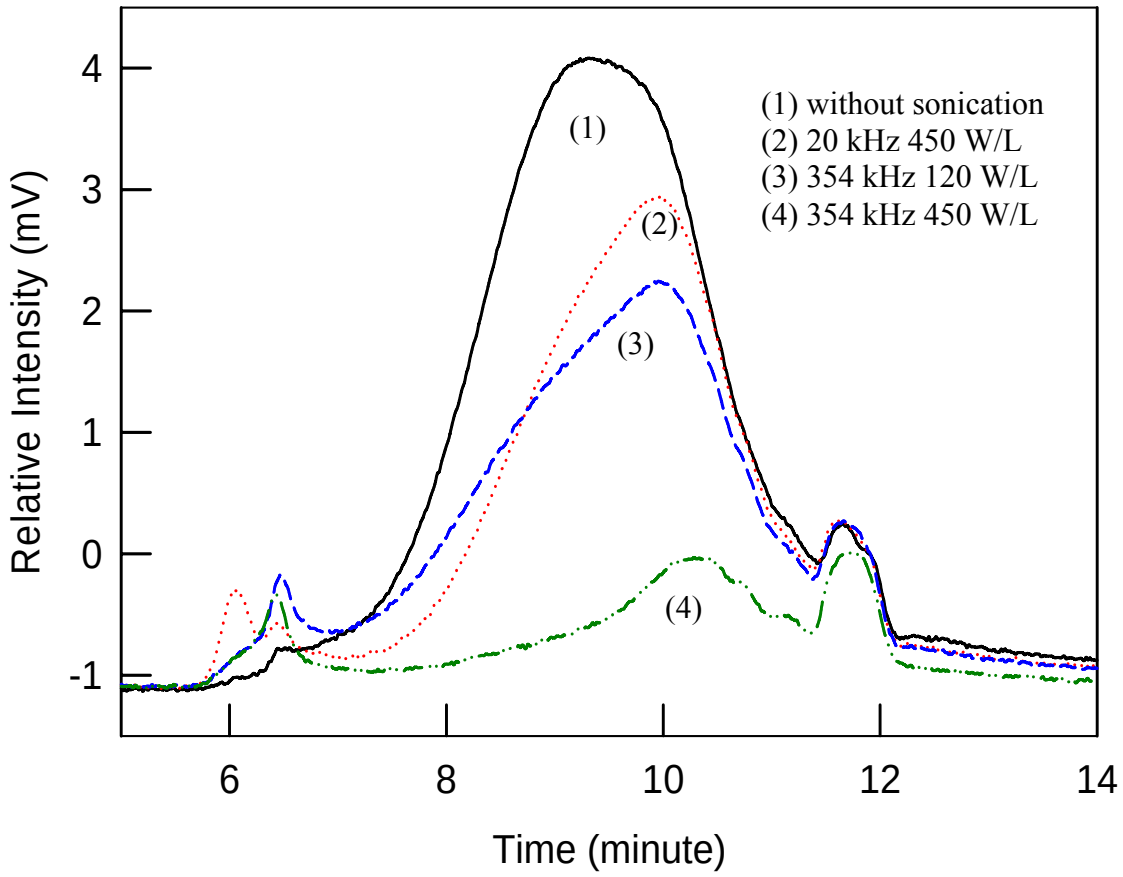

Figure A.12 HPSEC spectra of Pahokee peat DOM before and after 4 hours of sonication.

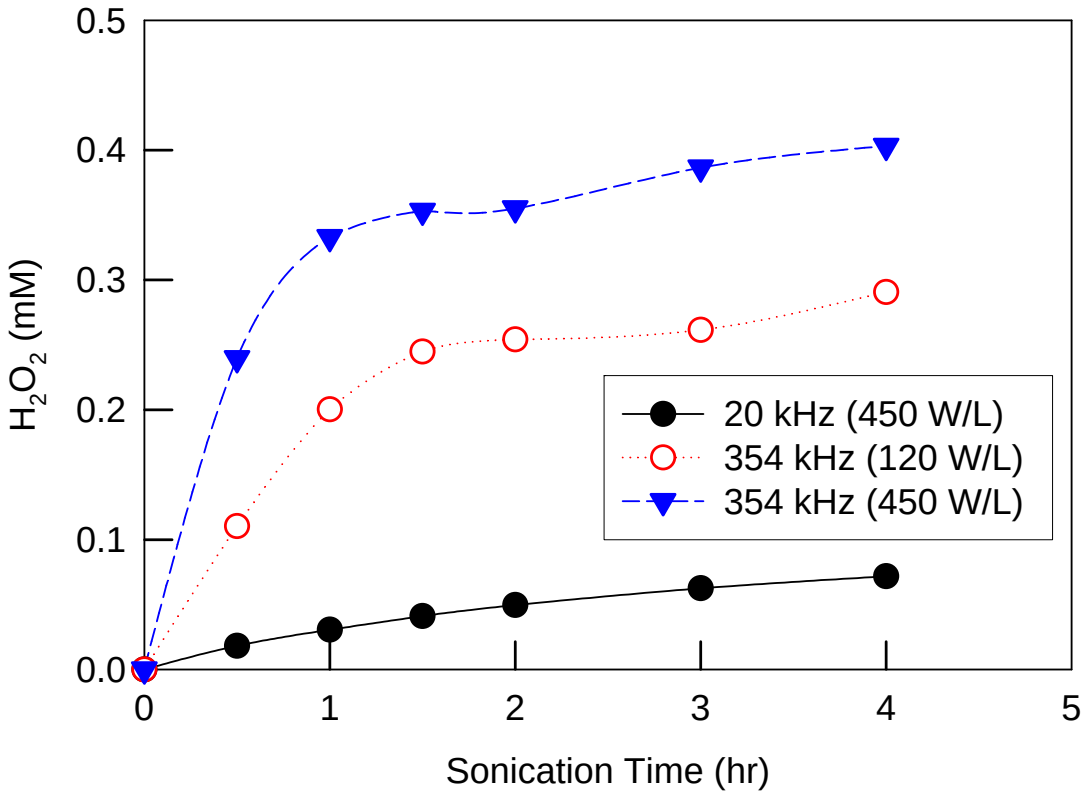

Figure A.13 The formation of H_2O_2 with sonication under different ultrasonic frequencies and energy densities.

BIBLIOGRAPHY

(1) Lindqvist, O., Johansson K., Aastrup M., Adersson A., Bringmark L., Hovsenius G., Hankanson L., Iverfeldt A., Meili M., Timm B. Mercury in the Swedish environment: recent research on causes, consequences and corrective methods. *Water Air Soil Pollu.* **1991**, *55*, 1-261.

(2) Downs, S.G.; Macleod, C. L.; Lester, J.N. Mercury in precipitation and its relationship to bioaccumulation in fish: a literature review. *Water Air Soil Poll.* **1998**, *108*, 149-187.

(3) Wang, Q.; Kim, D.; Dionysiou, D. D. Sources and remediation for mercury contamination in aquatic systems – a literature review. *Environ. Pollu*. **2004**, *131*, 323-336.

(4) Stein, E. D.; Cohen, Y.; Winer, A. M. Environmental distribution and transformation of mercury compounds. *Crit. Rev. Environ. Sci. Technol.* **1996**, *26*, 1-43.

(5) Pirrone, N., Keeler G.J., Nriagu J.O. Regional differences in worldwide emissions of mercury to the atmosphere. *Atmosph. Environ.* **1996**, *30*, 2981-2987.

(6) Pai, P., Niemi D., Powers B. A North Amercian inventory of anthropogenic mercury emissions. *Fuel Processing Technol.* **2000**, *65–66*, 101-115.

(7) Mason, R.P., Fitzgerald W.F., Morel M.M. The biogeochemical cycling of elemental mercury - anthropogenic influences. *Geochim. Cosmochim. Acta* **1994**, *58*, 3191-3198.

(8) US EPA. The Incidence and Severity of Sediment Contamination in Surface Waters of the United States Vol. 2. 1997, EPA 823-R-97-007.

(9) USGS, Mercury contamination of aquatic ecosystems. *Fact Sheet*, FS-215-95.

(10) Kotnik, J.; Horvat, M.; Jereb, V. Modelling of mercury geochemical cycle in Lake Velenje, Slovenia. *Environ. Modell. Softw.* **2002**, *17*, 593-611.

(11) Sigel, A. and H. Sigel. *Metal Ions in Biological Systems: Mercury and Its Effects on Environment and Biology*. **1997,** *34*.

(12) Ravichandran, M.; Aiken, G. R.; Reddy, M. M.; Ryan, J. N. Inhibition of precipitation and aggregation of metacinnabar (mercuric sulfide) by dissolved organic matter isolated from the Florida Everglades. *Environ. Sci. Technol.* **1999**, *33*, 1418-1423.

(13) Morel, F.M.M.; Kraepiel, A.M.L.; Amyot, M. The chemical cycle and bioaccumulation of mercury", Ann. Rev. Ecol. System. **1998**, *29*, 543-566.

(14) US EPA. Mercury study report to congress Vol. 3, fate and transport of mercury in the environment. 1997, EPA 452-R/97-005.

(15) Ullrich, S.M.; Tanton, T.W.; Abdrashitova, S.A. Mercury in the aquatic environment: A review of factors affecting methylation. *Crit. Rev. Environ. Sci. Technol.* **2001**, *31*, 241-293.

(16) Boszke, L.; Kowalski, A.; Glosiinska, G.; Szarek, R.; Siepak, J. Environmental factors affecting speciation of mercury in the bottom sediments; an overview. *Polish J. Environ. Stu.* **2003**, *12*, 5-13.

(17) Wang, W.X.; Stupakoff, I.; Gagnon, C.; Fisher, N.S. Bioavailability of inorganic and methylmercury to a marine deposit feeding polychaete. *Environ. Sci. Technol.* **1998**, *32*, 2564-2571.

(18) Ravichandran, M. Interactions between mercury and dissolved organic matter – a review. *Chemosphere* **2004**, *55*, 319-331.

(19) Haitzer, M.; Aiken, G. R.; Ryan, J. N. Binding of mercury(II) to dissolved organic matter: the role of the mercury-to-DOM concentration ratio. *Environ. Sci. Technol.* **2002**, *36*, 3564-3570.

(20) Xia, K.; Skyllberg, U.L.; Bleam, W.F.; Bloom, P.R.; Nater, E.A.; Helmke, P.A. X-ray Absorption Spectroscopic Evidence for the Complexation of Hg(II) by Reduced Sulfur in Soil Humic Substances. *Environ. Sci. Technol.* **1999**, *33***,** 257-261.

(21) Khwaja, A.R.; Bloom, P.R.; Brezonik, P.L. Binding constants of divalent mercury (Hg^{2+}) in soil humic acids and soil organic matter. *Environ. Sci. Technol.* **2006**, *40***,** 844-849.

(22) Kim, C. S.; Rytuba, J. J.; Brown, G. E. Jr. EXAFS study of mercury(II) sorption to Fe- and Al-(hydr)oxides II. Effects of chloride and sulfate. *J. Colloid. Interf. Sci.* **2004**, *270*, 9-20.

(23) Alberts, J. J.; Schindler, J. E.; Miller, R. W.; Nutter, D. E. Elemental mercury evolution mediated by humic acid. *Science*. **1974**, *184*, 895-897.

(24) Costa, M.; Liss P. Photoreduction and evolution of mercury from seawater. *Sci. Tot. Environ.* **2000**, *261*, 125-135.

(25) Burkstaller, J. E.; Mccarty, P. L.; Parks, G. A. Oxidation of cinnabar by Fe(III) in acid mine waters. *Environ. Sci. Technol.* **1975**, *9*, 676-678.

(26) Hsieh, Y. H.; Tokunaga, S.; Huang, C. P. Some chemical reactions at the HgS(s) – water interface as affected by photoirradiation. *Colloid. Surface.* **1991**, *53*, 257-274.

(27) Barnett, M. O.; Turner, R. R.; Singer, P. C. Oxidative dissolution of metacinnabar (β-HgS) by dissolved oxygen. *Appl. Geochem.* **2001**, *16*, 1499-1512.

(28) Ravichandran, M.; Aiken, G. R.; Reddy, M. M.; Ryan, J. N. Enhanced dissolution of cinnabar (mercuric sulfide) by dissolved organic matter isolated from the Florida Everglades. *Environ. Sci. Technol.* **1998,** *32*, 3305-3311.

(29) Waples, J. S.; Nagy, K. L.; Aiken, G. R.; Ryan, J. N. Dissolution of cinnabar (HgS) in the presence of natural organic matter. *Geochim. Cosmochim. Acta* **2005**, *69*, 1575-1588.

(30) Benoit, J. M.; Glimour, C. C.; Mason, R. P.; Heyes, A. Sulfide controls on mercury speciation and bioavailability to methylating bacteria in sediment pore waters. *Environ. Sci. Technol.* **1999**, *33*, 951-957.

(31) Suchanek, T.H.; Mullen, L.H.; Lamphere, B.A.; Richerson, P.J.; Woodmansee, C.E.; Slotton, D.G.; Harner, E.J.; Woodward, L.A. Redistribution of mercury from contaminated lake sediments of Clear Lake, Califonia. *Water Air Soil Pollu*. **1998**, *104*, 77-102.

(32) Sarkar, D.; Essington, M. E.; Misra, K. C. Adsorption of mercury(II) by variable charge surfaces of quartz and gibbsite. *Soil Sci. Soc. Am. J.* **1999**, *63*, 1626-1636.

(33) Kim, C. S.; Rytuba, J. J.; Brown, G. E. Jr. EXAFS study of mercury(II) sorption to Fe- and Al-(hydr)oxides I. Effects of pH. *J. Colloid. Interf. Sci.* **2004**, *271*, 1-15.

(34) Bonnissel-Gissinger, P.; Alnot, M.; Lickes, J. P.; Ehrhardt, J. J.; Behra, P. Modeling the adsorption of mercury(II) on (hydr)oxides II: alpha-FeOOH (goethite) and amorphous silica. *J. Colloid. Interf. Sci.* **1999**, *215*, 313-322.

(35) Collins, C. R.; Sherman, D. M.; Ragnarsdottir, K. V. Surface complexation of Hg^{2+} on goethite: Mechanism from EXAFS spectroscopy and density functional calculations. *J. Colloid. Interf. Sci.* **1999**, *219*, 345-350.

(36) Stumm, W.; Morgan, J. J. *Aquatic chemistry: chemical equilibria and rates in natural waters.* **1996**, John Wiley & Sons, New York.

(37) Wang, J. S.; Huang, P. M.; Liaw, W. K.; Hammer, U. T. The behavior of mercury in the soil with special emphasis on complexation and adsorption processes - a review of the literature. *Water Air Soil Poll.* **1991**, *56*, 533-542.

(38) Duarte, A.C.; Pereira, M.E. Oliveira, J.P. Hall, A. Mercury desorption from contaminated sediments. *Water Air Soil Poll.* **1991**, *56*, 77-82.

(39) Wallschlager, D.; Desaim, V.M.; Wilken, R.D. The role of humic substances in the aqueous mobilization of mercury from contaminated floodplain soils. *Water Air Soil Poll.* **1996**, *90*, 507-520.

(40) Barrow, N. J.; Cox, V. C. The effects of pH and chloride concentration on mercury sorption. I. by goethite. *J. Soil Sci*. **1992,** *43*, 295-304.

(41) Barrow, N. J.; Cox, V. C. The effects of pH and chloride concentration on mercury sorption. II. by a soil. *J. Soil Sci*. **1992,** *43*, 305-312.

(42) Compeau, G.; Bartha, R.; Effects of sea salt anions on the formation and stability of methylmercury. Bull. Environ. Contam. Toxicol. 1983, 31, 486-.493

(43) Yamamoto, m. Stimulation of elemental mercury oxidation in the presence of chloride ion in aquatic environments. *Chemosphere* **1996**, *32*. 1217-1224.

(44) Miskimmin, B. M. Effect of natural levels of dissolved organic-carbon (DOC) on methyl mercury formation and sediment water partitioning. *Bull. Environ. Contam. And Toxicol.* **1991**, *47*, 743-750.

(45) Yin, Y.; Allen, H. E.; Li, Y.; Huang, C. P.; Sanders, P. F. Adsorption of mercury(II) by soil: effects of pH, chloride, and organic matter. *J. Environ. Qual.* **1996**, *25*, 837-844.

(46) Yin, Y.; Allen, H. E.; Huang, C. P. Kinetics of mercury(II) adsorption and desorption on soil. *Environ. Sci. Technol*. **1997**, *31*, 496-503.

(47) US EPA. Capsule Report: Aqueous Mercury Treatment. **1997**, EPA/625/R-97/004

(48) Mulligan, C. N.; Yong, R. N.; Gibbs, B. F. An evaluation of technologies for the heavy metal remediation of dredged sediments. *J. Hazard. Mat.* **2001**, *85*, 145-163.

(49) Mulligan, C. N.; Yong, R. N.; Gibbs, B. F. Heavy metal removal from sediments by biosurfactants. *J. Hazard. Mat.* **2001**, *85*, 111-125.

(50) Palermo, M. R. Desigh considerations for *in-situ* capping of contaminated sediments. *Wat. Sci. Tech*. **1998**, *37*, 315-321.

(51) Moo-Young, H.; Myers, T.; Tardy, B.; Ledbetter, R.; Vanadit-Ellis, W.; Sellasie, K. Determination of the environmental impact of consolidation induced convective transport through capped sediment. *J. Hazard. Mater*. **2001**, *85*, 53-72.

(52) Azcue, J.M.; Zeman, A.J.; Mudroch, A.; Rosa, F.; Patterson, T. Assessment of sediment and porewater after one year of subaqueous capping of contaminated sediments in Hamilton Harbour, Canada. *Wat. Sci. Technol.* **1998**, *37*, 323-329.

(53) Randall, P.; Cgattopadhyay, S. Advances in encapsulation technologies for the management of mercury-contaminated hazardous wastes. *J. Hazard. Mater*. **2004**, *114*, 211-223.

(54) Liu, C.; Jay, J.A.; Ika, R.; Shine, J.P.; Ford, T.E. Capping efficiency for metal-contaminated marine sediment under conditions of submarine groundwater discharge. *Environ. Sci. Technol.* **2001**, *35*, 2334-2340.

(55) Wasay, S. A.; Arnfalk, P.; Tokunaga, S. Remediation of a soil polluted by mercury with acidic potassium iodide. *J. Hazard. Mater*. **1995**, *44*, 93-102.

(56) Wang, X.; Yolcubal, I.; Wang, W.; Artiola, J.; Maier, R.; Brusseau, M. Use of cyclodextrin and calcium chloride for enhanced removal of mercury from soil. *Environ. Toxicol. Chem*. **2004**, *23*, 1888-1892.

(57) Chang, T.C.; Yen, J.H. On-site mercury-contaminated soils remediation by using thermal desorption technology. *J. Hazard. Mater*. **2006**, *B128*, 208-217.

(58) Lloyd, J. R. Bioremediation of metals; the application of micro-organisms that make and break minerals. *Microbiology Today*, **2002**, *29*,67-69.

(59) Malik, A. Metal bioremediation through growing cells. *Environ. Int.* **2004**, *30*, 261-278.

(60) Gavrilescu, M. Removal of heavy metals from the environment by biosorptiom. *Eng. Life Sci*. **2004**, *4*, 219-232.

(61) Xue, H.; Stumm, W. Sigg, L. The binding of heavy metals to algal surfaces. *Wat. Res*. **1988**, *22*, 917-926.

(62) Adhiya, J.; Cai, X.; Sayre, R. T.; Traina, S. J. Binding of aqueous cadmium by the lyophilized biomass of *Chlamydomonas reinhardtii*. *Colloid Surface A*. **2002**, *210*, 1-11.

(63) He, L. M.; Tebo, B. M.; Surface charge properties of and Cu(II) adsorption by spores of the marine *Bacillus sp*. strain SG-1. *Appl. Environ. Microbial*. **1998**, *64*, 1123-1129.

(64) Chen, S.; Wilson, D. B. Genetic engineering of bacteria and their potential for Hg^{2+} remediation. *Biodegradation*. **1997**, *8*, 97-103.

(65) Rajamani, S.; Siripornadulsil, S.; Falcao, V.; Torres, M.; Colepicolo, P.; Sayre, R. Phycoremediation of heavy metals using transgenic microalgae. In: Transgenic Microalgae as Green Factories. Emilio Fernandes, Aurora Galvan, Rosa Leon, eds. Landes Press (submitted), **2006**.

(66) Mason, R. P.; Morel, F. M. M.; Hemond, H. F.The role of microorganisms in elemental mercury formation in natural waters. *Water Air Soil Pollu.* **1995**, *80*, 775-787.

(67) Gao, Y.; Kan, A. T.; Tomson, M. B. Critical evaluation of desorption phenomena of heavy metals from natural sediments. *Environ. Sci. Technol.* **2003**, *37*, 5566-5573.

(68) Adewuyi, Y. G. Sonochemistry: Environmental science and engineering applications. *Ind. Eng. Chem. Res.* **2001**, *40*. 4681-4715.

(69) Suslick, K. S.; Doktycz, J.; Flint, E. B. On the origin of sonoluminescence and sonochemistry. *Ultrasonics* **1990**, *28*, 280-290.

(70) Suslick, K. S. *Ultrasound: Its Chemical, Physical and Boilogical Effects*; VCH Publishers, Inc.: New York, 1988.

(71) Kotronarou, A.; Mills, G.; Hoffmann, M. R. Oxidation of hydrogen sulfide in aqueous solution. *Environ. Sci. Technol.* **1992,** *26*, 2420-2428.

(72) Hoffmann, M. R.; Hua, I.; Hochemer, R. Applications of ultrasonic irradiation for the degradation of chemical contaminants in water. *Ultrason. Sonochem.* **1996**, *3*, 163-172.

(73) Weavers, L. K.; Ling, F. H.; Hoffmann, M. R. Aromatic compound degradation in water using a combination of sonolysis and ozonolysis. *Environ. Sci. Technol.* **1998**, *32*, 2727-2733.

(74) Zhang, G. M.; Hua, I. Cavitation chemistry of polychlorinated biphenyls: Decomposition mechanisms and rates. *Environ. Sci. Technol.* **2000**, *34*, 1529-1534.

(75) Lu, Y.; Weavers, L. K. Sonochemical desorption and destruction of 4-chlorobiphenyl from synthetic sediments. *Environ. Sci. Technol.* **2002**, *36*, 232-237.

(76) Nagata, Y.; Hirai, K.; Bandow, H.; Maeda, Y. Decomposition of Hydroxybenzoic and Humic Acids in Water by Ultrasonic Irradiation. *Environ. Sci. Technol.* **1996**, *30*, 1133-1138.

(77) Doktycz, S. J.; Suslick, K. S. Interparticle collisions driven by ultrasound. *Science* **1990**, *247*, 1067-1039.

(78) Prozorov, T.; Prozorov, R.; Suslick, K. S. High velocity interparticle collisions driven by ultrasound. *J. Am. Chem. Soc.* **2004**, *126*, 13890-13891.

(79) Hammitt, F. G. *Cavitation and Multiphase Flow Phenomena*. 1980, New York, Mc Graw-Hill.

(80) Lamminen, M.O.; Walker H.W.; Weavers, L.K. Mechanisms and factors influencing the ultrasonic cleaning of particle-fouled ceramic membranes. *J. Membrane Sci.* **2004**, *237*, 213.

(81) Leighton, T.G. *The Acoustic Bubble*, Academic Press San Diego, **1994**.

(82) Thompson, L. H.; Doraiswamy, L. K. Sonochemistry: Science and engineering. *Ind. Eng. Chem. Res.* **1999**, *38*, 1215-1249.

(83) Tekin, T. Use of ultrasound in the dissolution kinetics of phosphate rock in HCl. *Hydrometallurgy* **2002**, *64*, 187-192.

(84) Lu, Y.; Riyanto, N.; Weavers, L. K. Sonolysis of synthetic sediment particles: particle characteristics affecting particle dissolution and size reduction. *Ultrason. Sonochem.* **2002**, *9*, 181-188.

(85) Verdan, S.; Burato, G.; Comet, M.; Reinert, L.; Fuzellier, H. Structural changes of metallic surfaces induced by ultrasound. *Ultrason. Sonochem.* **2003**, *10*, 291-295.

(86) Neppolian, B.; Jung, H.; Choi, H.; Lee, J. H.; Kang, J.-W. Sonolytic degradation of methyl *tert*-butyl ether: the role of coupled fenton process and persulphate ion. *Water Res.* **2002**, *36*, 4699-4708.

(87) Adewuyi, Y.G. Sonochemistry in environmental remediation. 1. Combinative and hybrid sonophotochemical oxidation processes for the treatment of pollutants in water. *Environ. Sci. Technol*. **2005**, *39*, 3409-3420.

(88) Adewuyi, Y.G. Sonochemistry in environmental remediation. 2. Heterogeneous sonophotocatalytic oxidation processes for the treatment of pollutants in water. *Environ. Sci. Technol*. **2005**, *39*, 8557-8570.

(89) Moriwaki, H.; Takagi, Y.; Tanaka, M.; Tsuruho, K.; Okitsu, K.; Maeda, Y. Sonochemical decomposition of perfluorooctane sulfonate and perfluorooctanoic acid. *Environ. Sci. Technol*. **2005**, *39*, 3388-3392.

(90) Kreller, D. I.; Turner, B.F.; Namjesnik-Dejanovic, K.; Maurice, P. A. Comparison of the Effects of Sonolysis and γ-Radiolysis on Dissolved Organic Matter. *Environ. Sci. Technol*. **2005**, *39*, 9732-9737.

(91) Mecozzi, M.; Amici, M.; Pietrantonio, E.; Tomanelli, G. An ultrasound assisted extraction of available humic substance from marine sediments. *Ultrason. Sonochem.* **2002**, *9*, 11-18.

(92) Oncel, M. S.; Ince M.; Bayramoglu, M. Leaching of silver from solid waste using ultrasound assisted thiourea method. *Ultrason. Sonochem.* **2005**, *12*, 237-242.

(93) Collasiol, A.; Pozebon, D.; Maia, S. M. Ultrasound assisted mercury extraction from soil and sediment. *Anal. Chim. Acta* **2004**, *518*, 157-164.

(94) Newman, A. P.; Lorimer, J. P.; Mason, T. J.; Hutt, K. R. An investigation into the ultrasonic treatment of polluted solids. *Ultrason. Sonochem.* **1997**, *4*, 153-156.

(95) Meegoda, J. N.; Perera, R. Ultrasound to decontaminate heavy metals in dredged sediments. *J. Hazard. Mater.* **2001**, *85*, 73-89.

(96) Kyllonen, H.; Pirkonen, P.; Hintikka, V.; Parvinen, P.; Gronroos, A.; Sekki, H. Ultrasonically aided mineral processing technique for remediation of soil contaminated by heavy metals. *Ultrason. Sonochem.* **2004**, *11*, 211-216.

(97) Sostaric, J. Z.; Caruso-Hobson, R. A.; Mulvaney, P.; Grieser, F. Ultrasound-induced formation and dissolution of colloidal CdS. *J. Chem. Soc. Faraday Trans.* **1997**, *93*, 1791-1795.

(98) Kola, H.; Wilkinson, K. J. Cadmium uptake by a green alga can be predicted by equilibrium modeling. *Environ. Sci. Technol.* **2005**, *39*, 3040-3047.

(99) Mehta, S. K.; Gaur, J. P. Use of algae for removing heavy metal ions from wastewater: progress and prospects. *Crit. Rev. Biotech*. **2005**, *25*, 113-152.

(100) Sayre, R. T.; Wagner, R. E. Method of making micro-algal-based animal foodstuff supplements, micro-algal-supplemented animal foodstuffs and method of animal nutrition. PCT Int. WO 2002056703 A1. **2002**, July 25.

(101) Cai, X.; Brown C.; Adhiya, J.; Traina, S. J.; Sayre, R. T. Growth and heavy metal binding properties of transgenic *Chlamydomonas* expressing a foreign metallothionein gen. *Int. J. Phytoremed*. **1999**, *1*, 53-65.

(102) Siripornadulsil, S. Molecular characterization of heavy metal metabolism in transgenic microalgae (*Chlamydomonas reinhardtii*). **2002,** Ph.D. Dissertation, The Ohio State University.

(103) Luthy, R. G.; Aiken, G. R.; Brusseau, M. L.; Cunningam, S. D.; Gschwend, P. M.; Pignatello, J. J.; Reinhard, M.; Traina, S. J.; Weber, W. J.; Westall, J. C. Sequestration of Hydrophobic Organic Contaminants by Geosorbents. *Environ. Sci. Technol.* **1997**, *31*, 3341-3347.

(104) Sarkar, D.; Essington, M. E.; Misra, K. C. Adsorption of mercury(II) by kaolinite. *Soil Sci. Soc. Am. J.* **2000**, *64*, 1968-1975.

(105) Biester, H.; Scholz, C. Determination of mercury binding forms in contaminated soils: Mercury pyrolysis versus sequential extractions. *Environ. Sci. Technol*. **1997**, *31*, 233-239.

(106) Bloom, N. S.; Preus, E.; Katon, J.; Hiltner, M. Selective extractions to assess the biogeochemically relevant fractionation of inorganic mercury in sediments and soils. *Anal. Chim. Acta* **2003**, *479*, 233-248.

(107) Behra, P.; Bonnissel-Gissinger, P.; Alnot, M.; Revel, R.; Ehrhardt, J. J. XPS and XAS study of the sorption of Hg(II) onto pyrite. *Langmuir* **2001**, *17*, 3970-3979.

(108) Ehrhardt, J. J.; Behra, P.; Bonnissel-Gissinger, P.; Alnot, M. XPS study of the sorption of Hg(II) onto pyrite FeS_2. *Surf. Interface anal.* **2000**, *30*, 269-272.

(109) Sposito, G. The Environmental Chemistry of Aluminum. Lewis Publishers, **1996**.

(110) Kasprzyk-Hordern, B. Chemistry of alumina, reactions in aqueous solution and its application in water treatment. *Adv. Colloid. Interfac*. **2004**, *110*, 19-48.

(111) Coston, J. A.; Fuller, C. C.; Davis, J. A. Pb^{2+} and Zn^{2+} adsorption by a natural aluminum-beraing and iron-bearing surface coating on an aquifer sand. *Geochim. Cosmochim. Acta* **1995**, *59*, 3535-3547.

(112) Trivedi, P.; Axe, L. Modeling Cd and Zn sorption to hydrous metal oxides. *Environ. Sci. Technol*. **2000**, *34*, 2215-2223.

(113) Trivedi, P.; Axe, L. Predicting divalent metal sorption to hydrous Al, Fe, and Mn oxides. *Environ. Sci. Technol*. **2001**, *35*, 1779-1784.

(114) Axe, L.; Trivedi, P. Intraparticle surface diffusion of metal contaminants and their attenuation in microporous amorphous Al, Fe, and Mn oxides. *J. Colloid. Interf. Sci.* **2002**, *247*, 259-265.

(115) Chen, D.; He, Z.; Weavers, L. K.; Chin, Y. P.; Walker, H. W.; Hatcher, P. G. Sonochemical reactions of dissolved organic matter. *Res. Chem. Intermed*. **2004**, *30*, 735-753.

(116) Breitbach, M.; Bathen, D. Influence of ultrasound on adsorption processes. *Ultrason. Sonochem.* **2001**, *8*, 277-283.

(117) Hamdaoui, O.; Naffrechoux, E.; Tifouti, L.; Petrier, C. Effects of ultrasound on adsorption-desorption of p-chlorophenol on granular activated carbon. *Ultrason. Sonochem.* **2003**, *10*, 109-114.

(118) Feng, D.; Aldrich, C. Sonochemical treatment of simulated soil contaminated with diesel. *Adv. Environ. Res.* **2000**, *4*, 103-112.

(119) Contamine, R. F.; Wilhelm, A. M.; Berlan, J.; Delmas, H. Power measurement in sonochemistry. *Ultrason. Sonochem.* **1995**, *2*, s43-s47.

(120) Cihacek, L. J.; Bremner, J. M. A simplified ethylene glycol monoethyl ether procedure for assessment of soil surface area. *Soil Sci. Soc. Am. J.* **1979**, *43*, 821-822.

(121) Bourikas, K.; Vakros, J.; Kordulis, C.; Lycourghiotis, A. Potentiometric mass titrations: Experimental and theoretical establishment of a new technique for determining the point of zero charge (PZC) of metal (hydr)oxides. *J. Phys. Chem. B* **2003**, *107*, 9441-9451.

(122) Bathen, D. Physical waves in adsorption technology - an overview. *Sep. Purif. Technol.* **2003**, *33*, 163-177.

(123) Li, Z.; Li, X.B.; Xi, H.X.; Hua, B. Effects of ultrasound on adsorption equilibrium of phenol on polymeric adsorption resin. *Chem. Eng. J.* **2002**, *86*, 375-379.

(124) Hagenson, L. C.; Doraiswamy, L. K. Comparison of the effects of ultrasound and mechanical agitation on a reacting solid-liquid system. *Chem. Eng. Sci.* **1998**, *53*, 131-148.

(125) Swamy, K. M.; Narayan, K. L. Intensification of leaching process by dual-frequency ultrasound. *Ultrason. Sonochem.* **2001**, *8*, 341-346.

(126) Goldberg, S.; Lebron, I.; Suarez, D. L.; Hinedi, Z. R. Surface characterization of amorphous aluminum oxides. *Soil Sci. Soc. Am. J.* **2001**, *65*, 78-86.

(127) Gregg. S. J.; Sing, K. S. W. *Adsorption, Surface Area and Porosity.* **1982**, Academic Press, London.

(128) Gasgnier, M.; Albert, L.; Derouet, J.; Beaury, L. Ultrasound effects on various oxides and ceramics – macroscopic and microscopic analyses. *J. Solid State Chem.* **1995**, *115*, 532-539.

(129) Stumm, W.; Morgan, J. J. *Aquatic Chemistry.* **1981**, 2nd, John Wiley. New York.

(130) Stack, A. G.; Higgins, S. R.; Eggleston, C. M. Point of zero charge of a corundum-water interface probed with optical Second Harmonic Generation (SHG) and Atomic Force Microscopy (AFM): New approaches to oxide surface charge. *Geochim. Cosmochim. Acta* **2001**, *65*, 3055-3063.

(131) Vanstraten, H. A.; Debruyn, P. L. Precipitation from supersaturated aluminate solutions .2. Role of temperature. *J. Colloid. Interf. Sci.* **1984**, *102*, 260-277.

(132) Dyer, C.; Hendra, P. J.; Forsling, W.; Ranheimer, J. Surface hydration of aqueous gamma-Al_2O_3 studied by Fourier-Transformation Raman and Infrared-Spectroscopy .1. Initial results. *Spectrochim. Acta A* **1993**, *49*, 691-705.

(133) Laiti, E.; Persson, P.; Ohman, L. O. Balance between surface complexation and surface phase transformation at the alumina/water interface. *Langmuir* **1998**, *14*, 825-831.

(134) Kosmulski, M. The pH-dependent surface charging and the points of zero charge. *J. Colloid. Interf. Sci.* **2002**, *253*, 77-87.

(135) Boland, J. J. Spatially resolved X-ray photoelectron-spectroscopy studies for device-type application. *J. Vac. Sci. Technol. B* **1986**, *4*, 1256-1258.

(136) Parthasarathy, N.; Buffle, J. Study of polymeric aluminum(III) hydroxide solutions for application in waste-water treatment - properties of the polymer and optimal conditions of preparation. *Water Res.* **1985**, *19*, 25-36.

(137) He, Z.; Traina, S. J.; Weavers, L. K. Release of mercury from cinnabar (HgS) by sonochemical dissolution. *Environ. Sci. Technol.* **2006**, (Submitted).

(138) He, Z.; Traina, S. J.; Bigham, J. M.; Weavers, L. K. Sonolytic desorption of mercury from aluminum oxide. *Environ. Sci. Technol.* **2005**, *39*, 1037-1044.

(139) Yardim, M. F.; Budinova, T.; Ekinci, E.; Petrov, N.; Razvigorova, M.; Minkova, V. Removal of mercury(II) from aqueous solution by activated carbon obtained from furfural. *Chemosphere* **2003**, *52*, 835-841.

(140) Xu, H.; Allard, B. Effects of a fulvic acid on the speciation and mobility of mercury in aqueous solutions. *Water Air Soil Poll.* **1991**, *56*, 709-717.

(141) Backstrom, M.; Dario, M.; Karlsson, S.; Allard, B. Effects of a fulvic acid on the adsorption of mercury and cadmium on goethite. *Sci. Total Environ*. **2003**, *304*, 257-268.

(142) Yin, Y.; Allen, H. E.; Huang, C. P.; Sanders, P. F. Adsorption/desorption isotherms of Hg(II) by soil. *Soil Sci.* **1997**, *162*, 35-45.

(143) Au, K. K.; Penisson, A. C.; Ynag, S. L.; O'Melia, C. R. Adsorption of aquatic humic substances on colloidal-size aluminum oxide particles: influence of solution chemistry. *Geochim. Cosmochim. Ac.* **1999**, *63*, 2903-2917.

(144) Naffrechoux, E.; Combet, E.; Fanget, B.; Petrier, C. Reduction of chloroform formation potential of humic acid by sonolysis and ultraviolet irradiation. *Wat. Res*. **2003**, *37*, 1948-1952.

(145) Dempsey, B.A.; Ganho, R.N.; O'Melia, C.R. The coagulation of humic substances by means of aluminum salts, *J. Am. Water Works Assoc.* **1984**, *74*, 141-150.

(146) Barnett, M. O.; Harris, L. A.; Turner, R. R.; Stevenson, R. J.; Henson, T. J.; Melton, R. C.; Hoffman, D. P. Formation of mercuric sulfide in soil. *Environ. Sci. Technol.* **1997**, *31*, 3037-3043.

(147) Kim, C. S.; Bloom, N. S.; Rytuba, J. J.; Brown, G. E. Mercury speciation by X-ray absorption fine structure spectroscopy and sequential chemical extractions: a comparison of speciation methods. *Environ. Sci. Technol.* **2003,** *37*, 5102-5108.

(148) Potter, R. W., II; Barnes, H. L. Phase relations in the binary Hg-S. *Am. Mineral.* **1978**, *63*, 1143-1152.

(149) Suslick, K. S.; Price, G. J. Applications of ultrasound to materials chemistry. *Annu. Rev. Mater. Sci.* **1999**, *29*, 295-326.

(150) Taylor, E.; Cook, B. B.; Tarr, M. A. Dissolved organic matter inhibition of sonochemical degradation of aqueous polycyclic aromatic hydrocarbons. *Ultrason. Sonochem.* **1999**, *6*, 175-183.

(151) Mason, T. J.; Lorimer, J. P.; Bates, D. M.; Zhao, Y. Dosimetry in sonochemistry: the use of aqueous terephthlate ion as a fluorescence monitor. *Ultrason. Sonochem.* **1994**, *1*, s91-s95.

(152) Frim, J. A.; Rathman, J. F.; Weavers, L. K. Sonochemical destruction of free and metal-binding ethylenediaminetetraacetic acid. *Water Res.* **2003**, *37*, 3155-3163.

(153) Adewuyi, Y. G.; Appaw, C. Sonochemical oxidation of carbon disulfide in aqueous solutions: reaction kinetics and pathways. *Ind. Eng. Chem. Res.* **2002**, *41*. 4957-4964.

(154) Hua, I.; Hoffmann, M. R. Optimization of ultrasonic irradiation as an advanced oxidation technology. *Environ. Sci. Technol.* **1997**, *31*, 2237-2243.

(155) Song, W.; Teshiba, T.; Rein, K.; O'shea, K. E. Ultrasonically induced degradation and detoxification of microcystin-LR (cyanobacterial toxin). *Environ. Sci. Technol.* **2005**, *39*, 6300-6305.

(156) Gutierrez, M.; Henglein, A.; Ibanez, F. Radical scavenging in the sonolysis of aqueous solutions of I-, Br-, and N3-. *J. Phys. Chem.* **1991**, *95*, 6044-6047.

(157) Prozorov, T.; Prozorov, R.; Suslick, K. S. High velocity interparticle collisions driven by ultrasound. *J. Am. Chem. Soc.* **2004**, *126*, 13890-13891.

(158) Bebie, J.; Schoonon, M. A. A.; Fuhrmann, M.; Strongin, D. R. Surface charge development on transition metal sulfides: an electrokinetic study. *Geochim. Cosmochim. Acta* **1998**, *62*, 632-642.

(159) Liu, J. C.; Huang, C. P. Eletrokinetic characteristics of some metal sulfide-water interfaces. *Langmuir* **1992**, *8*, 1851-1856.

(160) Nicolau, Y. F.; Menard, J. C. An electrokinetic study of ZnS and CdS surface chemistry. *J. Colloid. Interf. Sci.* **1992**, *148*, 551-570.

(161) Dickson, F. W.; Tunell, G. The stability relations of cinnabar and metacinnabar. *Am. Mineral.* **1959**, *44*, 471-487.

(162) Stumm, W. Chemistry of the solid-water interface. **1992**, John Wiley & Sons, Inc.

(163) Cory, R. M.; Mcknight, D. M. Fluorescence spectroscopy reveals ubiquitous presence of oxidized and reduced quinones in dissolved organic matter. *Environ. Sci. Technol.* **2005,** *39*, 8142-8149.

(164) US EPA. (1998) National conference on management and treatment of contaminated sediments. EPA/625/R-98/001.

(165) US EPA. (1996) Engineering bulletin: technology alternatives for the remediation of soils contaminated with arsenic, cadmium, chromium, mercury and lead. EPA/540/S-97/500.

(166) Mulligan, C. N.; Yong, R. N.; Gibbs, B. F. Remediation technologies for metal-contaminated soils and groundwater: an evaluation. *Engineering Geology*. **2001**, *60*, 193-207.

(167) Seidel, H.; Ondruschka, J.; Morgenstern, P.; Stottmeister, U. Bioleaching of heavy metals from contaminated aquatic sediments using indigenous sulfur-oxidizing bacteria: a feasibility study. *Wat. Sci. Tech*. **1998**, *37*, 387-394.

(168) Brown, G. E. Jr.; Parks, G. A. Sorption of trace elements on mineral surfaces: modern perspectives from spectroscopic studies, and comments on sorption in the marine environment. *Int. Geol. Rev*. **2001**, *43*, 963-1073.

(169) Hamdaoui, O.; Djeribi, R.; Naffrechoux, E. Desorption of metal ions from activated carbon in the presence of ultrasound. *Ind. Eng. Chem. Res*. **2005**, *44*, 4737-4744.

(170) He, Z.; Traina, S. J.; Weavers, L. K. Sonolytic desorption of mercury from aluminum oxide: effects of pH, chloride, and organic matter. *Environ. Sci. Technol.* **2006**, (Submitted).

(171) Barger, J. R.; Brown, G. E. Jr.; Parks, G. A. Surface complexation of Ph(II) at oxide-water interfaces: I. XAFS and bond-valence determination of mononuclear and polynuclear Pb(II) sorption products on aluminum oxides. *Geochim. Cosmochim. Ac.* **1997**, *61*, 2617-2637.

(172) Fitts, J. P.; Brown, G. E. Jr.; Parks, G. A. Structure evolution of Cr(III) polymeric species at the γ-Al2O3/water interface. *Environ. Sci. Technol.* **2000**, *34*, 5122-5128.

(173) El Bilali, L.; Rasmussen, P. E.; Hall, G.E.M.; Fortin, D. Role of sediment composition in trace metal distribution in lake sediments. *Appli. Geochem*. **2002**, *17*, 1171-1181.

(174) Gomez-Ariza, J. L.; Giraldez, I.; Sanchez-Rodas, D.; Morales, E. Optimization of a sequential extraction scheme for the characterization of heavy metal mobility in iron oxide rich sediments. *Int. J. Environ. Anal. Chem.* **1999**, *75*, 3-18.

(175) Ianni, C.; Magi, E.; Rivaro, P.; Ruggieri, N. Trace metals in Adriatic coastal sediments: distribution and speciation pattern. *Toxicol. Environ. Chem*. **2000**, *78*, 73-92.

(176) Savvides, C.; Papadopoulos, A.; Haralambous, K.J.; Loizidou, M. Sea sediments contaminated with heavy metals: metal speciation and removal. *Wat. Sci. Tech*. **1995**, *32*, 65-73.

(177) Pinheiro, J. P.; Galcern, J.; Leeuwen, H. P. V. Metal speciation dynamics and bioavailability: bulk depletion effects. *Environ. Sci. Technol.* **2004**, *38*, 2397-2405.

(178) Crist, R. H.; Oberholser, K.; Schwartz, D.; Marzoff, J.; Ryder, D.; Crist, D. R. Interactions of metals and protons with algae. *Environ. Sci. Technol.* **1988**, *22*, 755-760.

(179) Strawn, D. G.; Scheidegger, A. M.; Sparks, D. L. Kinetics and mechanisms of Pb(II) sorption and desorption at the aluminum oxide – water interface. *Environ. Sci. Technol.* **1998**, *32*, 2596-2601.

(180) Hoffmann, M. R. Kinetics and mechanism of oxidation of hydrogen sulfide by hydrogen peroxide in acidic solution. *Environ. Sci. Technol.* **1977**, *11*, 61-66.

(181) Bradley, J. N.; Dobson, D. C. Oxidation of hydrogen sulfide in shock waves. I. Absorption studies of OH and SO_2 in hydrogen sulfide-oxygen-argon mixtures. *J. Chem. Phys.* **1967**, *46*, 2865-2871.

(182) Lamelas, C.; Wilkinson, K. J.; Slaveykova, V. I. Influence of the composition of natural organic matter on Pb bioavailability to microalgae. *Environ. Sci. Technol.* **2005,** *39*, 6109-6116.

(183) Wrobel, K.; Sadi, Baki B. M.; Wrobel, K.; Castillo, J. R.; Caruso, J. A. Effect of metal ions on the molecular weight distribution of humic substances derived from municipal compost: ultrafiltration and size exclusion chromatography with spectrophotometric and inductively coupled plasma-MS detection. *Anal. Chem*. **2003,** *75*, 761-767.

(184) Guentzel, J.L.; Powell, R.T.; Landing, W.M.; Mason, R.P. Mercury associated with colloidal material in an estuarine and an open-ocean environment. *Marine Chemistry*. **1996**, *55*(1-2), 177-199.

(185) Slowey, A.J.; Johnson, S.B.; Rytuba, J.J.; Brown, G.E. Role of Organic Acids in Promoting Colloidal Transport of Mercury from Mine Tailings. *Environ. Sci. Technol.* **2005**, *39*, 7869-7874.

(186) Berlan, J.; Trabelsi, F.; Delmas, H.; Wilhelm A.; Petrignani, J. Oxidative-degradation of phenol in aqueous-media using ultrasound. *Ultrason. Sonochem.* **1994**, *1*, S97-S102.

(187) Sakai, Y.; Sadaoka Y.; Takamaru, Y. Decomposition of chloral hydrate in aqueous solution by the action of ultrasound. *J. Phys. Chem.* **1977**, *81*, 509-511.

(188) Joyce, E.; Mason, T.J.; Phull S.S.; Lorimer, J.P. The development and evaluation of electrolysis in conjunction with power ultrasound for the disinfection of bacterial suspensions. *Ultrason. Sonochem.* **2003**, *10*(4-5), 231-234.

(189) Chen, D.; Weavers L.K.; Walker, H.W. Ultrasonic control of ceramic membrane fouling: Effect of particle characteristics. submitted to *Wat. Res.* (2004).

(190) Aiken G.R.; Malcolm, R.L. Molecular-weight of aquatic fulvic-acids by vapor-pressure osmometry. *Geochim. Cosmochim. Ac.* **1987**, *51*, 2177-2184.

(191) Stevenson, F.J. *Humus Chemistry. Genesis, Composition, Reactions.* John Wiley & Sons, New York, **1994**, p.212.

(192) Kitis, M.; Karanfil, T.; Wigton A.; Kilduff, J.E. Probing reactivity of dissolved organic matter for disinfection by-product formation using XAD-8 resin adsorption and ultrafiltration fractionation. *Wat. Res.* **2002**, *36*, 3834-3848.

(193) Meier, M.; Dejanovic, K.N.; Maurice, P.A.; Chin Y.P.; Aiken, G.R. Fractionation of aquatic natural organic matter upon sorption to goethite and kaolinite. *Chem. Geol.* **1999**, *157*, 275-284.

(194) Edwards, M.; Benjamin M.M.; Ryan, J.N. Role of organic acidity in sorption of natural organic matter (NOM) to oxide surfaces. *Colloids and Surfaces A: Physicochem. Eng. Aspects* **1996**, *107*, 297-307.

(195) Flint E.B.; Suslick, K.S. The temperature of cavitation. *Science* **1991**, *253*, 1397-1399.

(196) Basedow A.M.; Ebert, K.H. Ultrasonic degradation of polymers in solution. *Adv. Polym. Sci.* **1977**, *22*, 83-148.

(197) Price, G.J. The use of ultrasound for the controlled degradation of polymer solutions. *Adv. Sonochem.* **1990**, *1*, 231-287.

(198) Melville, H.W.; Murray, A.J. Photopolymerization of vinylidene chloride. I. *J. Trans. Faraday Soc.* **1950**, *46*, 976-996.

(199) Henglein, A. The reaction of 2,2-diphenyl-1-picrylhydrazyl with long-chain free radicals produced from ultrasonic degradation of polymethyl methacrylate. *Makromol. Chem.* **1955**, *15*, 188-210.

(200) Thomas, J.R.; de Vries, D.L. Sonically induced heterolytic cleavage of poly(methyl siloxane). *J. Phys. Chem.* **1959**, *63*, 254-256.

(201) Chemat, F.; Teunissen, P.G.M.; Chemat S.; Bartels, P.V. Sono-oxidation treatment of humic substances in drinking water**.** *Ultrason. Sonochem.***2001**, *8*, 247-250.

(202) Naffrechoux, E.; Combet, E.; Fanget B.; Petrier, C. Reduction of chloroform formation potential of humic acid by sonolysis and ultraviolet irradiation. *Wat. Res.* **2003**, *37*, 1948-1952.

(203) Chin, Y.P.; Aiken G.; O'Loughlin, E. Molecular-weight, polydispersity, and spectroscopic properties of aquatic humic substances. *Environ. Sci. Technol.* **1994**, *28*, 1853-1858.

(204) Borisover M.; Graber, E.R. Classifying NOM−organic sorbate interactions using compound transfer from an inert solvent to the hydrated sorbent. *Environ. Sci. Technol.* **2003**, *37*, 5657-5664.

(205) Chin Y.P.; Gschwend, P.M. The abundance, distribution, and configuration of porewater organic colloids in recent sediments. *Geochim. Cosmochim. Ac.* **1991**, *55*, 1309-1317.

(206) Swift R.S. in Sparks D.L. et al. (Ed.), *Methods of Soil Analysis. Part 3. Chemical Methods*, Soil Science Society of America, Madison, WI, **1996**, p.1018.

(207) Mason T.J.; Lorimer, J.P. *Sonochemistry: Theory, Applications and Uses of Ultrasound in Chemistry*, Ellis Horwood Ltd., Chichester, **1988**.

(208) Klassen V.D.; McGowan, H.C.E. H_2O_2 Determination by the I^{3-} Method and by $KMnO_4$ Titration. *Anal. Chem.* **1994**, *66*, 2921-2925.

(209) Dria, K.J.; Sachleben J.R.; Hatcher, P.G. Solid-state carbon-13 nuclear magnetic resonance of humic acids at high magnetic field strengths. *J. Environ. Qual.* **2002**, *31*, 393-401.

(210) Knicker H.; Lüdemann, H.D. N-15 and C-13 CPMAS and solution NMR-studies of N-15 enriched plant-materail during 600 days of microbial-degradation. *Org. Geochem.* **1995**, *23*, 329-341.

(211) Chefetz, B.; Deshmukh A.P.; Hatcher, P.G. Pyrene sorption by natural organic matter. *Environ. Sci. Technol.* **2000**, *34*, 2925-2930.

(212) Hatcher, P.G.; Schnitzer, M.; Dennis L.W.; Maciel, G.E. Aromaticity of humic substances in soils. *Soil Sci. Soc. Am. J.* **1981**, *45*, 1089-1094.

(213) Aiken G.; Cotsaris, E. Soil and hydrology – their effect on NOM. *J. Am. Water Works Assoc.* **1995**, *87*, 36-45.

(214) Bob M.M.; Walker, H.W. Effect of natural organic coatings on the polymer-induced coagulation of colloidal particles. *Colloids and Surfaces A: Physicochem. Eng. Aspects* **2001**, *77*, 215-222.

(215) IHSS. http://www.ihss.gatech.edu/.

(216) Hatcher, P.G.; Rowan R.; Mattingly, M.A. 1H and 13C NMR of marine humic acids. *Org. Geochem.* **1980**, *2*, 77-85.

(217) Thurman E.M. in Aiken G.R. et al. (Ed.) *Humic Substances in Soil, Sediment, and Water. Geochemistry, Isolation, and Characterization.* John Wiley & Sons, New York, **1985**.

(218) Schnitzer M.; Khan, S.U. *Humic Substances in the Environment*, Marcel Dekker, New York, **1972**, p.327.

(219) Croue, J.P.; Violleau, D.; Bodaire C.; Legube, B. Removal of hydrophobic and hydrophilic constituents by anion exchange resin. *Wat. Sci. Technol.* **1999**, *40*, 207-214.

(220) Westerhoff, P.; Aiken, G.; Amy G.; Debroux, J. Relationships between the structure of natural organic matter and its reactivity towards molecular ozone and hydroxyl radicals. *Wat. Res.* **1999**, *33*, 2265-2276.

(221) Chin, Y.P.; Aiken G.R.; Danielsen, K.M. Binding of pyrene to aquatic and commercial humic substances: The role of molecular weight and aromaticity. *Environ. Sci. Technol.* **1997**, *31*, 1630-1635.

(222) Schwarzenbach, R.P.; Gschwend P.M.; Imboden, D.M. *Environmental Organic Chemistry*, John Wiley & Sons, New York, **1993**, p.131.

(223) Bowles, E.C.; Antweiler R.C.; MacCarthy P. in Averett R.C.et al. (Ed.), *Humic Substances in the Suwannee River, Georgia: Interactions, Properties, and Proposed Structures,* U.S. Geological Survey, Washington DC, **1994**, p.115.

(224) Cabaniss, S.E.; Zhou, Q.; Maurice, P.A.; Chin Y.P.; Aiken, G.R**.** A log-normal distribution model for the molecular weight of aquatic fulvic acids. *Environ. Sci. Technol.* **2000**, *34*, 1103-1109.

(225) Edwards M.; Benjamin, M.M. Transformation of NOM by ozone and its effect in iron and aluminum solubility. *J. Am. Water Works Assoc.* **1992**, *84*(6), 56-66.

(226) Carlson G.; Silverstein, J. Effect of ozonation on sorption of natural organic matter by biofilm. *Wat. Res.* **1997**, *31*, 2467-2478.

(227) Buxton, G.V.; Greenstock, C.L.; Helman W.P.; Ross, A.B. Critical-review of rate constants for reactions of hydrated electrons, hydrogen-atoms and hydroxyl radicals ($^{\cdot}OH/^{\cdot}O^{-}$) in aqueous-solution. *J. Phys. Chem. Ref. Data* **1988**, *17*, 513-886.

(228) Beckett M.A.; Hua, I. Impact of ultrasonic frequency on aqueous sonoluminescence and sonochemistry. *J. Phys. Chem. A* **2001**, *105*, 3796-3802.

(229) Park, J.K.; Hong S.W.; Chang, W.S. Degradation of polycyclic aromatic hydrocarbons by ultrasonic irradiation. *Environ. Technol.* **2000**, *21*, 1317-1323.

(230) Darnall, K.R.; Atkinson R.; Pitts, J.N. Observation of biacetyl from the reaction of OH radicals with o-xylene. Evidence for ring cleavage. *J. Phys. Chem.* **1979**, *83*, 1943-1946.

(231) Tuazon, E.C.; Macleod, H.; Atkinson R.; Carter, W.P.L. α-dicarbnyl yields from the NOx-air photooxidations of a series of aromatic-hydrocarbons in air. *Environ. Sci. Technol.* **1986**, *20*, 383-387.

(232) Maggiolo A. in Rice R.G. et al. (Ed.), *Ozone/Chlorine Dioxide Oxidation Products of Organic Materials,* Ozone Press International, Cleveland, Ohio, **1978**, p.59.

(233) Price, G.J. The use of ultrasound for the controlled degradation of polymer solutions. *Adv. Sonochem.* **1990**, *1*, 231-287.

(234) Crum, L.A. Comments on the evolving field of sonochemistry by a cavitation physcist. *Ultrason. Sonochem.* **1995**, *2*, S147-S152.

9235) Gooberman, G. Ultrasonic degradation of polystyrene. I. A proposed mechanism for degradation. *J. Polym. Sci.* **1960**, *42*, 25-33.

(236) Khan S.U.; Schnitzer, M. Retention of hydrophobic organic compounds by humic acid. *Geochim. Cosmochim. Ac.* **1972**, *36*(7), 745-754.

(237) Fein, J.B.; Boily, J.F.; Guclu K.; Kaulbach, E. Experimental study of humic acid adsorption onto bacteria and Al-oxide mineral surfaces. *Chem. Geol.* **1999**,*162*(1), 33-45.

(238) Cornel, P.K.; Summers R.S.; Roberts, P.V. Diffusion of humic-acid in dilute aqueous –solution. *J. Colloid Interface Sci.* **1986**, *110*, 149-164.

(239) Fan, L.; Harris, J.L.; Roddick F.A.; Booker, N.A. Influence of the characteristics of natural organic matter on the fouling of microfiltration membranes. *Wat. Res.* **2001**, *35*, 4455-4463.

(240) Hong S.; Elimelech, M. Chemical and physical aspects of natural organic matter (NOM) fouling of nanofiltration membranes. *J. Membrane Sci.* **1997**, *132*, 159-181.